LABORATORY OF NUCLEAR, ATOMIC, MOLECULAR PHYSICS, AND BIOPHYSICS

Nonlinear Dynamics of Fractional Blood Flow in a Viscoelastic Tube of Rotating Nanofluid with the Effects of Nanoparticles, Magnetic Field, Heat Transfer, Thermal Radiation and Chemical Reactions

THESIS

Submitted and defended in fulfillment of the requirements for the award of the Degree of **Doctorat/Ph.D. in Physics**

Specialty: ATOMIC, MOLECULAR PHYSICS, AND BIOPHYSICS

By:

NDJAWA YOMI Pavel Arnold

Registration number: 12W0309
Master of Science in Physics

Under the supervision of
MOHAMADOU ALIDOU

Professor
University of Maroua

YEAR : 2023

UNIVERSITE DE YAOUNDE I
UNIVERSITY OF YAOUNDE I

FACULTE DES SCIENCES
FACULTY OF SCIENCE

DEPARTEMENT DE PHYSIQUE
DEPARTMENT OF PHYSICS

ATTESTATION DE CORRECTION DE LA THESE DE DOCTORAT/Ph.D

Nous, Professeurs, **ZEKENG Serge Sylvain**, **DJUIDJE KENMOE Germaine**, **THIODJIO SENDJA Bridinette**, et Professeur **NDJAKA Jean-Marie Bienvenu**, respectivement Examinateurs et Président du jury de la thèse de Doctorat/Ph.D de Monsieur **NDJAWA YOMI Pavel Arnold** Matricule **12W0309**, preparée sous la direction du Professeur **MOHAMADOU Alidou** intitulée: « NONLINEAR DYNAMICS OF FRACTIONAL BLOOD FLOW IN A VISCOELASTIC TUBE OF ROTATING NANOFLUID WITH THE EFFECTS OF NANOPARTICLES, MAGNETIC FIELD, HEAT TRANSFER, THERMAL RADIATION AND CHEMICAL REACTIONS », soutenue le **Mercredi, 17 Mai 2023**, en vue de l'obtention du grade de Docteur/Ph.D en Physique, Spécialité **Physique Atomique, Moléculaire et Biophysique**, attestons que toutes les corrections demandées par le Jury de soutenance ont été effectuées.

En foi de quoi, la présente attestation lui est delivrée pour servir et valoir ce que de droit.

Fait à Yaoundé le, **18 JUIN 2023**

Examinateurs

Président du Jury

Pr. ZEKENG Serge Sylvain   Pr. DJUJDJE KENMOE Germaine   Pr. NDJAKA Jean-Marie B.

Pr. THIODJIO SENDJA Bridinette

Le Chef de Département de Physique

Ndjaka Jean-Marie Bienvenu
Professeur

Nonlinear dynamics of fractional blood flow in a viscoelastic tube of rotating nanofluid with the effects of nanoparticles, magnetic field, heat transfer, thermal radiation and chemical reactions

Laboratory of Nuclear, Atomic, Molecular Physics and Biophysics

THESIS

Submitted and defended in fulfillment of the requirements for the award of the Degree of

Doctorat/Ph.D in Physics

Option: Atomic, Molecular Physics and Biophysics

By

NDJAWA YOMI Pavel Arnold

Registration number: 12W0309

Master of Science in Physics

Under the supervision of

MOHAMADOU ALIDOU

Professor

University of Maroua (UMa)

June 16, 2023

Dedication

✠ My first and foremost dedication is devoted to our Almighty **God** who takes care of us every day and guides us on the straight way.

✠ To my late parents **Mrs TALSA NJEUKAM Clémentine** and **Mr YOMI Maurice** who have left us, may their souls rest in peace and may our Almighty God welcome them in his great mercy.

✠ To my Grand-mother **Mrs NGUETBAM Lisette**, my tutor **Mrs & Mr NKWUAMUO**, my **Uncles** and **Aunts** for their encouragement and support.

✠ To my brothers **NJEUKAM YOMI Jaurès** and **MBIANKWA YOMI Boris Virnie** for their precious advice, encouragement and permanent support.

Acknowledgements

At the end of this doctoral journey, I am deeply grateful for the opportunity to have learned from and worked with so many brilliant teachers, collaborators and students. I am happy to express my sincere gratitude to all those who have accompanied me during these doctoral years and have directly or indirectly contributed to the completion of this document. Nevertheless, I will do my best to condense my thoughts on this subject.

★ First of all, I would like to express my sincere gratitude to Almighty **God** who gave me the life, the opportunity and the knowledge to reach and finish with the PhD level of study.

★ I have furthermore to thank the persons responsible of the Faculty of Sciences, and the Research and postgraduate training unit for physics and applications who gave and confirmed the permission to go ahead with my thesis.

★ I would like to express my sincere gratitude to my supervisor **Prof. A. MOHAMADOU** who, despite his multiple academic, administrative and family occupations, accepted to supervise this thesis. I want to thank him for all his teachings and advices he has provided me.

★ I would like to deeply thanks the honorable **members of the Jury**, who agreed to put aside their multitude occupations so as to evaluate this work. I express to them all my greatest respect.

★ I would like to deeply thanks **Prof. C. B. TABI** who, despite his multiple occupations, accepted to give his constructive comments to this thesis. I want to thank him for all his teachings and advices he has provided me.

★ I am very grateful to **Prof. H. P. EKOBENA FOUDA** Director of the laboratory of Molecular Physics and Biophysics for his advices and constructive discussions.

★ I would like to thank **Prof. J. M. B. NDJAKA**, Head of the Department of Physics. I am very grateful for his administrative contribution and encouragement.

★ I would like to thank **Prof. T. C. KOFANE**, Head of the Laboratory of Mechanics, Materials and Structures. I am very grateful for the quality of his teaching and for his constructive comments.

★ I am grateful to **Prof. P. WOAFO**, Chairman of the Cameroon Physical Society for his teaching specially in numerical methods.

Contents

Résumé

Dans cette thèse, nous étudions la propagation de nanoparticules à travers un débit fraction-naire sanguin dans un tube viscoélastique. Pour cela, nous nous sommes attardés à l'influence de la présence de particules magnétiques dans un écoulement sanguin magnétohydrodynamique à travers un cylindre. Le fluide à l'intérieur du tube est soumis à un gradient de pression oscillant et à un champ magnétique externe constant. La température du sang est supposée changer avec les vitesses du sang et des particules. Egalement, la présence de nanoparticules magnétiques est considérée ainsi que les effets de l'énergie d'activation, des radiations thermiques et d'effets vibrants. Toute l'étude est basée sur des modèles mathématiques qui incluent des dérivés d'ordre fractionnaire selon Caputo. Les solutions proposées pour les vitesses de particules, de sang sont assimilées au mouvement brownien et à la thermophorèse pour la plupart, qui sont associées à celles des distributions de température et concentration du sang qui sont tous obtenues par la combinaison des méthodes de transformation de Laplace et de Hankel. Puis numériquement, nous utilisons les méthodes de différences finies et la méthode de l'algorithme L_1. Les résultats montrent que le champ magnétique appliqué et les effets du paramètre d'ordre fractionnaire réduisent la vitesse du nanofluide et des nanoparticules, ce qui affecte considérablement la température et la concentration du fluide sanguin, pour les intervalles de temps courts et longs. Cependant, dans le cas d'intervalles de temps longs, les particules semblent être accélérées. Il en découle que, le nanofluide à l'intérieur du tube est activé par l'effet de rotation des particules chargées, un champ magnétique externe constant et l'énergie d'activation. Il est également trouvé que la forme des particules et les paramètres de dérivée fractionnaire influencent significative-ment les vitesses et le transfert de chaleur. Dans le cas de la super diffusion, la température réagit fortement pour des valeurs élevées du paramètre fractionnaire montrant l'existence d'un seuil critique, et une compréhension claire de l'évolution des températures et des vitesses dans les différentes zones du tube. Ceci permettra à une meilleure observation de la dynamique des dommages au niveau des tissus dus aux vibrations à travers les flux comme dans le cas des coagulations et du ciblage des zones cancérigènes par les nano éléments.

Mots clés: *Ecoulement sanguin, Viscosité du sang, Nanofluidique, Nanoparticules, Magnétohy-drodynamique, Transfert de chaleur, Effets vibrants, Méthode de l'algorithme L_1 .*

Abstract

In this thesis, we study the propagation of nanoparticles through a fractionated blood flow in a viscoelastic tube. For this purpose, we focused on the influence of the presence of magnetic particles in a magnetohydrodynamic blood flow through a cylinder. The fluid inside the tube is subjected to an oscillating pressure gradient and a constant external magnetic field. The temperature of the blood is assumed to change with the velocities of the blood and the particles. Also, the presence of magnetic nanoparticles is considered as well as the effects of activation energy, thermal radiation and vibrational effects. The whole study is based on mathematical models that include fractional order derivatives according to Caputo. The proposed solutions for particle velocities, blood velocities are assimilated to Brownian motion and thermophores for the most part, which are associated with those of the temperature and concentration distributions of the blood, all of which are obtained by the combination of Laplace and Hankel transformation methods. Then numerically, we use the finite difference methods and the L_1 algorithm method. The results show that the applied magnetic field and fractional order parameter effects reduce the velocity of the nanofluid and nanoparticles, which significantly affects the temperature and concentration of the blood fluid, for both short and long time intervals. However, in the case of long time intervals, the particles seem to be accelerated. It follows that the nanofluid inside the tube is activated by the spin effect of the charged particles, a constant external magnetic field and the activation energy. It is also found that the shape of the particles and the fractional derivative parameters significantly affects the velocities and heat transfer. In the case of super diffusion, the temperature reacts strongly for high values of the fractional parameter showing the existence of a critical threshold, and a clear understanding of the evolution of temperatures and velocities in the different zones of the tube. This will allow a better observation of the dynamics of tissue damage due to vibrations through the flows as in the case of coagulations and the targeting of carcinogenic areas by nano elements.

Keywords: *Blood flow, Blood viscosity, Nanofluidics, Magnetic Nanoparticles, Magnetohydrodynamics, Heat transfer, Vibrating effects, L_1-algorithm method .*

List of Abbreviations

AVK	:	Antivitamins K
BFD	:	Biomagnetic Fluid Dynamics
COVID-19	:	Coronavirus Disease
DNA	:	Deoxyribonucleic Acid
DOA	:	Direct Oral Anticoagulants
EG	:	Ethylene Glycol
ENMs	:	Engineering Nanomaterials
FDM	:	Finite Difference Method
FHD	:	Ferrohydrodynamics
GaNNTs	:	Gallium Nitride Nanotubes
MHD	:	Magnetohydrodynamics
MWCNTs	:	Multi-Wall-Carbon Nanotubes
NRGs	:	Nanoribbon Graphenes
NPs	:	Nanoparticles
ODEs	:	Ordinary Differential Equations
PDEs	:	Partial Differential Equations
RBCs	:	Red Blood Cells
RK	:	Runge-Kutta
RK2	:	Runge-Kutta in 2nd order approximation
RK4	:	Runge-Kutta in 4th order approximation
SARS-Co-V-2	:	Severe Acute Respiratory Syndrome Coronavirus 2
SWCNTs	:	Single-Wall-Carbon Nanotubes
WHO	:	World Health Organization

List of Tables

List of Figures

General Introduction

Nanotechnology is an ancient science that humans are constantly impacting and innovating, it was first introduced long before the term nanotechnology was used by the American physicist and Nobel Prize winner: Richard Feynman in 1959 [1]. The concept of nanotechnology will become more and more important in the research community, impacting several industrial sectors: Pharmacology, Petroleum, Communication, Astronomy etc. [2]. In the same vein, several studies have been directed towards Bio-nanotechnology, which is a new research direction combining natural sciences and medicine. Nanoscience studies the structure of matter at the molecular level with the aim of innovating in the fields of manufacturing new materials, products and prototypes in the nanometer range (10^{-9} m) [3]. These feats allow researchers to better interpret molecular metabolisms in the context of the diagnosis, treatment, and prognosis of diseases and recently the coronavirus (COVID-19). The development of nanotechnologies is therefore a challenge for the years to come. The presence of nanoparticles in a fluid referring to the term nanofluid was first used by Choi *et al.* [4], which is a study of nanoparticles in the form of metals: Cu, Ag; metal nitrides such as SiN and AlN; oxide ceramics and PbO and CuO. Throughout our work, the basic fluid will be blood and the interaction of the non-linear dynamics between blood and particles will be understood through the study of the present interaction parameters of the medium. This will enable the advancement of the resolution of cardiovascular diseases, cancer, tumour and emerging diseases by radiation, under the action of nanoelements. These technological advances have made it possible to obtain solid particles of nanometric size, which reduces the risks of erosion and agglomeration in the bloodstream. This allows the treatment of cardiovascular diseases (thrombosis, stenosis, atherosclerosis, aneurysm...), cancers and tumours, which are diseases with a high mortality rate and whose causes and treatment are still little known. The aim of this study is to propose and present blood flow models that will allow a better understanding of the heat transfer, propagation velocity and concentration of nanoparticles based on the thermophysical properties of the base fluid (blood) and the nanoparticles. It appeared that nanofluids have thermal properties, which have been studied by several researchers such as Aaiza *et al.* [5] and Lomascolo *et al.* [6], who experimentally demonstrated the link between thermal conductivity, concentration of the medium, shape and size of the nanoparticles: the smaller they are, the

more damage they can cause in the form of inhalation by humans.

Blood is one of the channels to reach the cellular tissues, the understanding of its speed, temperature and concentration plays a very important role in some medical procedures especially in the treatment of myalgia, fibromyalgia, contracture, as indicated by the experimental studies of Inoue *et al.* [7] and Kobu [8] on the effects of infrared and ultrasonic radiations through the blood stream.

Blood is also a fluid with electrical properties that allow it to conduct current and have a magnetohydrodynamic aspect. In the presence of a magnetic field, its velocity tends to decrease due to the existence of the Lorentz force, which is the product of the interaction between electric and magnetic field [9]. This provides to the blood, the role of a Biomagnetic fluid, because the strong presence of erythrocytes acting as magnetic particles and plasma as a carrier liquid. The erythrocytes, or red blood cells (RBCs), carry a negative charge, which creates a magnetic field on the vessel wall, able to influence the pulsatile character of the blood flowing inside the vessel [10,11]. This type of fluid was studied in these decades by Kolin [12] and later by Korchevskii [13], and also the work of Shit and Roy [14], Ogulu [15], Sankar and Hemalatha [16], Mandal [17] and Vajravelu *et al.* [18], which focused on the pulsatile flow of blood through the imposition of an external magnetic field. The contribution of Sharma *et al.* [19] was an example in the case of stenosis. Furthermore, the magnetization of blood can be increased by adding artificially created nanoparticles to the flow, as is usually the case for targeted drug delivery. Specifically, this implies that biofluids can behave as ferromagnetic fluids, this is why most of the magnetic particles frequently used in biomedicine are manganese ferrites ($MnFe_2O_4$), iron oxides (Fe_2O_3 or Fe_2O_4) and iron oxide particles [20], to name a few. One of the first models to address this aspect of BFD was proposed by Haik *et al.* [21], who carried out a comparative study between mathematical models of BFD and Ferrohydrodynamics (FHD). Some numerical models have also been used to stimulate these radiation effects as the case of human breast tumours [22,23]. Other researchers, following the example of Szasz [24], have proposed a coupling of electromagnetic radiation and radiative heat transfer effects on cancerous tissues. These techniques allow a slowing down of blood velocity through the use of the magnetohydrodynamic principle based on the Lorentz force [25], and Sharma *et al.* [26] investigated this magnetohydrodynamic effect for the case of an artery in the presence of stenosis. Ogulu and Bestman [15] addressed theoretically how to treat some diseases by using the thermal radiation therapy and these heat effects. Mekheiner and Kot [27], Majee and Shit [9], Craciunescu and Clegg [28] and Horng *et al.* [29] studied the behavior of arteries during thermal therapy under the pulsatile blood flow effects. The presence of Erythrocytes makes the blood to be a biomagnetic fluid, creates a magnetic field on the vessel wall [30,31]. Studies on blood flow through porous vessels are receiving growing attention of researchers, owing to the observation that appreciable changes occur in blood flow behaviour and also due to the porosity of blood vessels. Khalid and Vafai [32] studied the role of porosity on blood flow and its impact on temperature distribution in living biological tissues during hyperthermic treatment. Kandasamy *et*

al. [33] investigated a single-walled carbon nanotube (SWCNT), alumina (*Al2O3*), and copper (Cu) nanoparticles on convective mass transfer in the presence of base fluid (water) over a horizontal plate. S. Pramanik [34] in his turn looked the effect of thermal radiation, Casson fluid and heat transfer through an exponentially porous stretching surface. Hari R. Kataria *et al.* [35], Hamid Khan *et al.* [36] introduce the effects of magneto-hydrodynamics through a porous medium. In 2018, S. Rama Mohan *et al.* [37] have combined those ideas to come out with some results. Until now several works done on fractional order derivative have been proposed to solve different problems in applied mathematics, Sciences, engineering and industry. See for instance [38–40]. Bansi *et al.* [41] proposed the fractional blood flow in oscillatory arteries with thermal radiation and magnetic field effects. Zhao *et al.* [42,43] formulated and derived new equations governing the fractional boundary layer, which are nonlinear coupled equations with a mixed derivative of space-time in convection terms.

In chapter 1, we would be presenting the general theory and some ideas that are basic to our current understanding of nanoscience and nanotechnology in blood flow. A brief summary of nanostructure, thermophysical characteristics of nanofluids and the fluid flow modeling, including the description of diseases encountered in the vessels.

Chapter 2, describes the methodology, mathematical background and the fractional models in the fluid flows mechanism. In this light, would be presenting the conservation laws used to derive the continuity equation, the equations of fluid motion, and the equations describing the dynamics in elastic vessels under the influence of magnetic field, thermal radiation, chemical reactions and nanoparticles through the introduction of fractional order derivative models in Caputo's sense for the incompressible fluid case. In mathematical frame work, we present the special function, Laplace and the Hankel method transform. Also are presented some numerical method such as, the finite difference method (FDM), the fourth-order Runge-Kutta scheme, and the L_1-algorithm method given by the finite difference approximations of Caputo differentiation that have been used to numerically integrate different model equations used in this thesis.

In chapter 3, we present the main results of this thesis. By generating the Navier-Stock equation for the fluid velocity, temperature and concentration distributions. We have applied the Laplace and Hankel method analytically by constructing many families of analytical solutions. Then, numerically by using the finite difference method (FDM) and the FDM approximation of Caputo differentiation for the incompressible flow in an elastic tube. We discuss the numerical analysis, where the flow parameters and fractional order effects are comprehensively addressed in the blood viscosity, external magnetic field, radiation and the presence of nanoparticles in the rotating nanofluid on the waveforms of the velocity, temperature and concentration distributions of the blood. This thesis ends with a general conclusion and provides some future directions that could be investigated.

Chapter 1

Generality on Nanoscience and Nanotechnology in Blood Flow

1.1 Introduction

Blood flow occurs through a well-structured system called the cardiovascular system, of which the heart is the major organ for blood transport. The movement of blood is moved through elastic vessels such as veins, arteries, capillaries lymphatic vessels. Blood is a liquid that is made up of more than 50% plasma, 1% leukocytes and 40% red blood cells that allow the transport of nutrients, oxygen and many other elements that allow the proper functioning of other organs. This composition of the blood presents many nano-elements, so multiple researches have been directed towards the application of Biomedicine, in particular the design of nanoparticles (NPs) which are an asset for the treatment and imaging of several diseases through the development of new materials and processes which are for the most part in the trial phase.

In this chapter, we will firstly introduce the different structures and materials of nanoscience and nanotechnology. Secondly, their role on blood flow and disease patterns in vessels will be presented. Finally, the modelling of blood flow in the presence of nano-elements, will be described taken the case of the human body.

1.2 Different structures and materials in nanoscience and nanotechnology

1.2.1 Nanostructures and Nanoparticules

In recent years, the nanostructure materials have been used in different disciplines allowing the advancement of nanotechnology and the understanding of researchers on physical, chemical, mechanical and electronic properties. Leading to introduce disciplines such as nanoelectronics, nano-medicine, nanomachinery to name a few. In the case of nano-medicine, it allows the design of biocompatible tunneling nanotubes that can help deliver drugs to specific targets and monitor patients' health. Nanostructure field is also part of the creation of organic nanostructural components or organic functional syntheses of medical devices such as pacemakers, implants, artificial joints etc.

The nature is full of many nano-sized particles such as blood proteins and blood cells etc., which are around 100 nanometres in size as shown in figure (1.1).
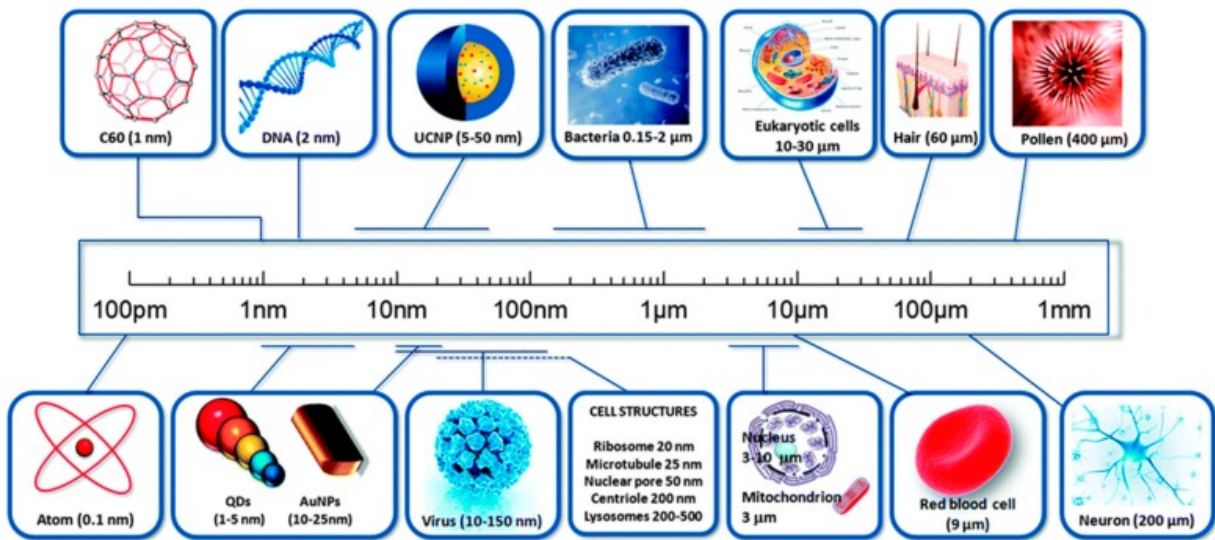
Figure 1.1: Cell size in meters [44].

This implies that the nanomaterials produced, must be of the same scale as the organisms studied Jeevanandam *et al.* [45] indicate that the interaction of nanodevices such as nanoparticles with cells and tissues are able to perform specific tasks.

1.2.2 Nanomaterials

Nanoparticles are nanostructured materials with a dimension on the nanometer scale, such as quantum dots with quantum effects, nanorods and nanowires, thin films and bulk materials. According to [45], we can classify them into two categories depending on their origin: natural and synthetic.

★ Natural Nanomaterials

Their production occurs naturally either in anthropogenic activities or in biological species, allowing a classification of organic and inorganic natural origin as nanomaterials. For organic nanomaterials, we can mention the wax crystals covering a lotus, the scales of a butter wing, blood proteins, lipids in blood, body fat illustrated in figure (1.2).
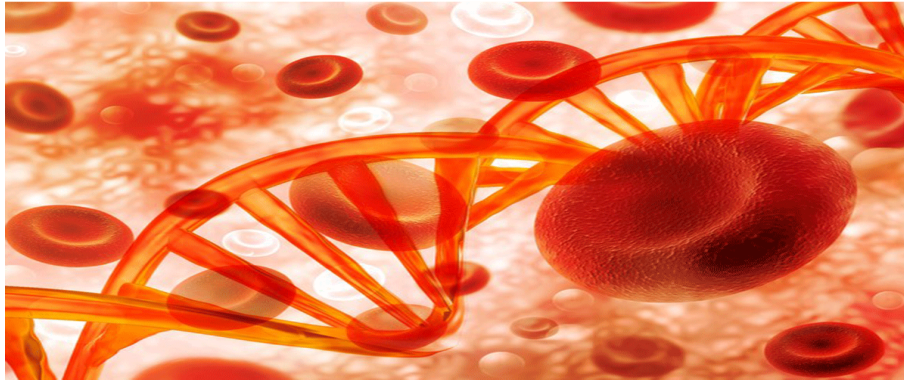
Figure 1.2: Nanostructural components in living beings: red blood cell DNA [46].

For inorganic cases, we have among others interplanetary dust that falls on the earth about thousands of tons per year, and also viruses, atmospheric dust. As an example of a virus, we have the SARS-Co-V-2 strain of the current Covid-19 virus, which is currently causing a lot of damage in the world.

★ Synthetic Nanomaterials

They are found in engine exhaust, smoke, even in mechanical grinding and also in physical, chemical and biological or hybrid methods. Also, in process engineering nanomaterials (ENMs) for commercial use. These include sunscreens, cosmetics, tyres, and electronic items. These nanomaterials are also used in medical diagnostics and imaging. The evolution of nanomaterial synthesis started with the discovery of fullerene by Buckminster Fuller and continued with the graphene-based nanomaterials described below.

a) Buckminsterfullerene

The philosopher scientist Buckminster Fuller discovered a phenomenal structure called Buckminsterfullerene or fullerene, which has the soccer ball shape and this was the beginning of the evolution of nano-scale materials. The new form of carbon (C_{60}: buckminsterfullerene) was discovered in 1985 when the mechanism of long chain carbon molecules was understood in an experimental way, where 60 carbon atoms were produced by Kroto et al. [47]. Thus, from the pure carbon atom, the C_{60} particle in the form of a soccer ball like molecule was made, having a polygonal shape with 60 vertices and 32 faces.

Figure 1.3: Buckminsterfullerene molecule [48]

b) Nanotubes

♦ Case of carbon nanotube

In June 1991, Sumio Iijima discovered an extremely thin needle-like material by examining carbon materials under an electron microscope [49]. The basic structure of these materials is graphite and they present a tubular of sheets of carbon atoms, of dimension lower than a few nanometers and gave the name of carbon nanotubes. Those materials will attract a large number of researchers in both the academic and industrial worlds, enabling the promotion of future technologies and nanotechnology. Iijima [49], reports for the first time a carbon nanotube composed of multi-walled carbon nanotubes (MWCNTs) in the form of a honeycomb network of carbon atoms, called graphene, which is seamlessly wound into a tubular shape. Much later, in 1993, Iijima *et al.* [50] discovered a single-walled carbon nanotube (SWCNTs), whose structure has not yet been found in nature and was therefore a new type of artificially created solid. This nanotube has a diameter of the size of a single molecule of the order of a nanometer and a length of a few micrometers, figure (1.4) and has both solid, molecular and hybrid behavior with unique physicochemical properties.
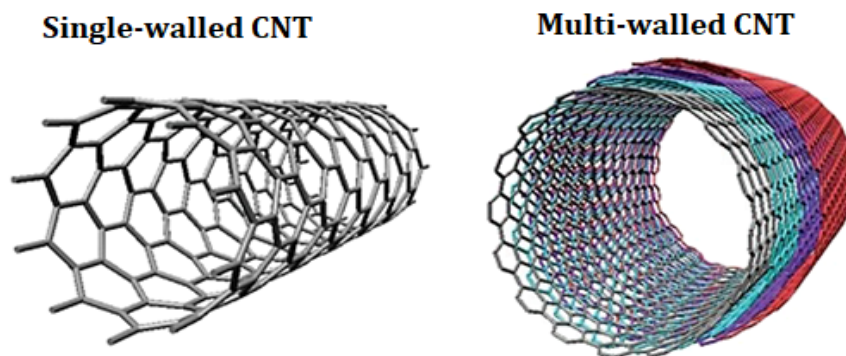
Figure 1.4: Carbon nanotubes single and multiple walled [51].

Carbon nanotubes exhibit remarkable electrical conductivity [52,53] while others are semiconductors and have exceptional thermal conductivity due to their structure and bond strength between atoms.

♦ Case of Gallium

Goldberger *et al.* [54] reported for the first time a nanomaterial initially synthesised with nanowires from pure zinc oxide crystals on a sapphire wafer, using a process giving rise to single-crystal gallium nitride nanotubes that he and his colleagues have dubbed "epitaxial flow". Developed by chemical vapour deposition, they are a much more stable material than zinc oxide. Gallium nitride nanotubes are 2 to 5 micrometres long and 30 to 200 micrometres in diameter. GaNNTs also differ in the way the tubes are rolled up as shown in figure (1.5).
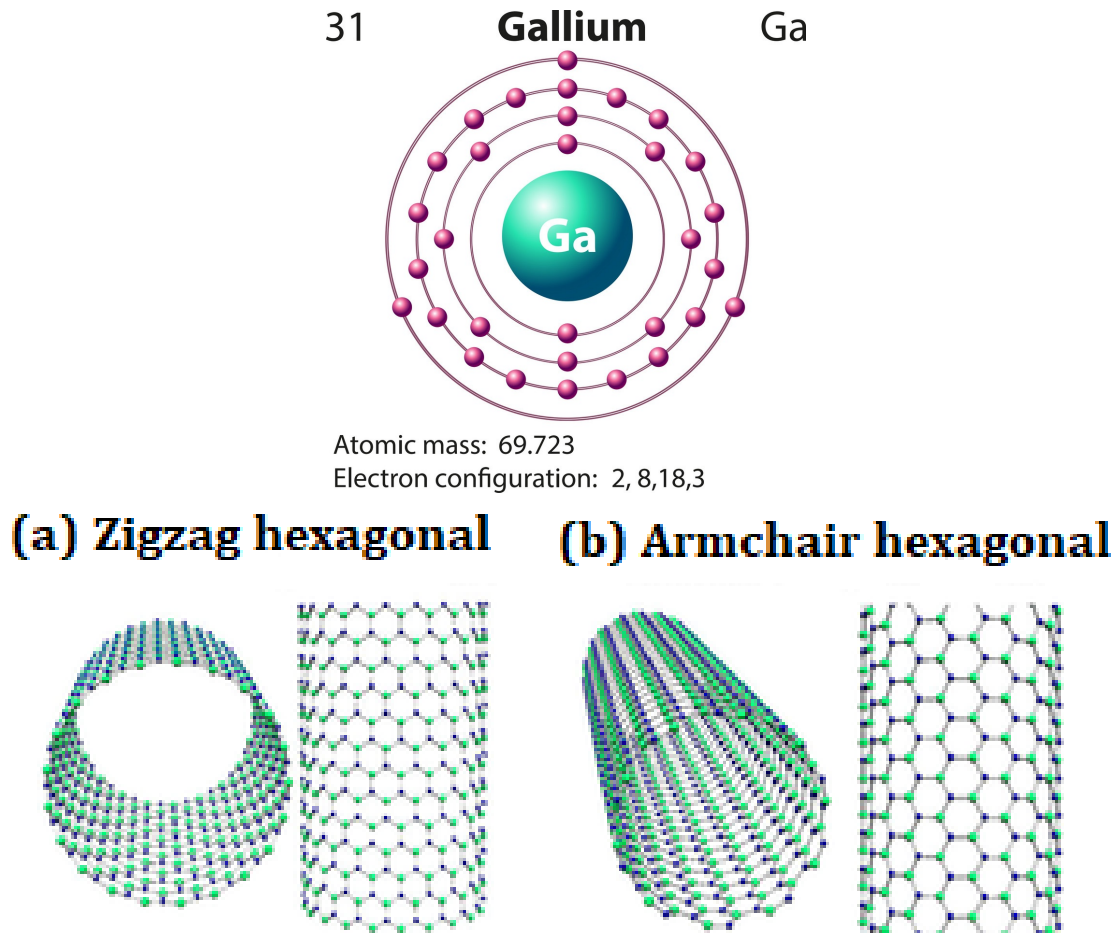
Figure 1.5:   Diagram of gallium nanotube chirality [55, 56].

♦ **Case of Silicon**

Emerging around the year 2000 [58], these nanoparticles with a tubular structure from silicon atoms possess unusual physical properties that differ fundamentally from those of bulk silicon [59]. The formation process is still based on chemical vapour deposition [60], where the smallest inner diameter is limited to tens of nanometres [61]. This formation is done by two methods, the most common of which uses germanium, carbon or zinc oxide nanowires as matrix. Silicon, usually from silane or silicon tetrachloride gas, is deposited on the nanowires and the core is dissolved leaving a silicon tube [62].

c) Graphene-based nanomaterials

Graphene is an allotrope of carbon consisting of a single layer of atoms arranged in a two-dimensional honeycomb lattice [63], as reported by Novoselov *et al.* [64] in a micromechanical cleavage method carried out for the exfoliation of highly oriented pyrolyzed graphite. It is found to be an excellent conductor of heat and electricity along its plane [65], and exhibits large quantum oscillations and significant non-linear diamagnetism. Graphene strongly absorbs light of all visible wavelengths [66], hence its black graphite colour. More to that, a single sheet of graphene is almost transparent due to its thinness, and is about 100 times stronger than the strongest steel of the same thickness [67, 68]. Thanks to the work of pioneers such as Andre Geim and K. Novoselov, who won the 2010 Nobel Prize in Physics for revealing the exceptional physical properties of graphene, whose 2D monolayer structure makes it possible to obtain several carbon allotropes that can be wound in a 0D network (fullerenes) or in 1D nanotube or stacked in 3D graphite, as shown in figure (1.6).
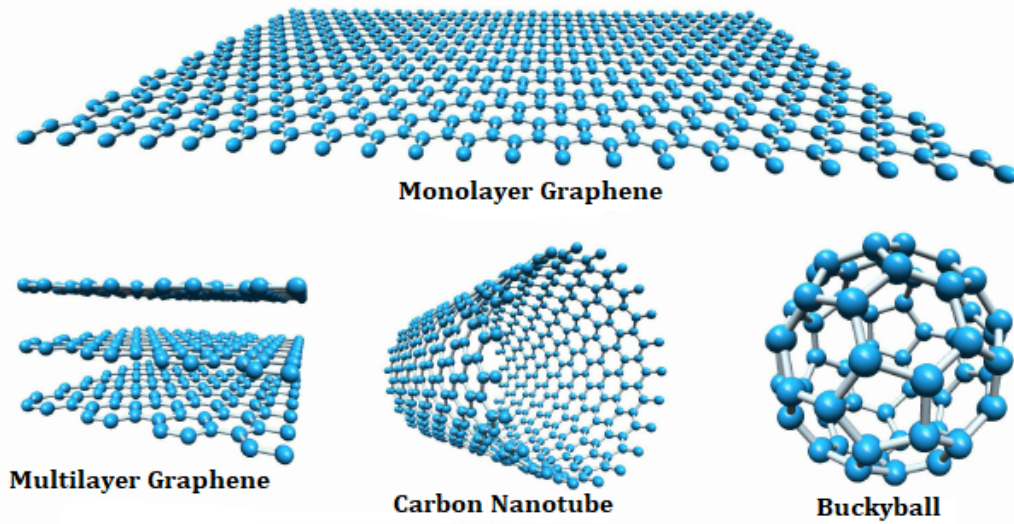
Figure 1.6: Diffrent conformation of Graphene [69].

As a category of graphene, we have nanoribbon graphenes (NRGs) and nanographene. Graphenes are promising candidates for various future applications in electronics, energy storage and conservation, also in biological labelling.

1.3 Nanofluid.

Heat transfer in fluids leads to many practical and industrial applications, including transport, energy, air conditioning, electronics and even medicine. The advent of nanoscale materials with specific properties has led to a great advance in the nanosciences, sparking many fields of study in many laboratories and also to the development of fluids with novel properties. Our work on these will be focused on nanofluids, the basic fluid of which is blood.

1.3.1 Nanoparticles and carrier fluids

We can say that a nanofluid is a fluid carrying nanoparticles. Nanoparticles are located at the borders between the microscopic world and the atomic or molecular world, and are being studied a lot nowadays in both fundamental and applied science. Physicists and chemists are synthesising them and others are trying to understand the physics of these nanometric objects, while biologists are using them as cell markers. Thus, the most commonly used of nanoparticles to obtain nanofluids are: aluminium oxide, aluminium, copper, copper oxide, gold, silver, carbon nanotubes, silicon, titanium dioxide. The most commonly used base liquids are also: water, ethylene glycol EG, oils, toluene [70, 71].

As mentioned above the term nanofluid was first proposed by Choi [4] who investigated on the effective conductivity of water-Al_2O_3 mixture which increases by 20% for (1-5)% volume concentration of Al_2O_3. For low concentrations of 1%, a volume of carbon nanotubes increases by 150% [72], and that of copper nanoparticles by 40% [73]. Thus, several studies have been carried out to develop a new class of nanofluids with better mechanisms and also to develop more efficient heat transfer fluids. Using heat exchange to improve their performance, Keblinski [74] has shown that adding nanoparticles to a liquid increases the viscosity and therefore the pressure drop Yang [75]. The fabrication of nanofluids requires different types of nanoparticles, namely: oxide-based nanofluids, metal nanoparticles and those containing carbon nanotubes.

1.3.2 Oxide-based nanofluids

We can mention among others: aluminium oxide, copper oxide and titanium dioxide nanoparticles. Massuda et $al.$ [76] were the pioners to work on the improvement of thermal conductivity using aluminium oxide of diameter 13 nm in water. They found a 30% improvement in conductivity at a volume fraction of 4.3%. This study was continued by Eastman et $al.$ [77], who used a volume fraction of 5% in water and obtained a 30% improvement in the thermal conductivity of (Al_2O_3) nanoparticles of size 33 ηm and for (CuO) of diameter 36 nm the conductivity was improved by 60%, twice than that of Al_2O_3.

Lee et $al.$ [78] used copper oxide (CuO) and aluminium oxide (Al_2O_3) on the base liquids: water and ethylene glycol. The results show a 10% improvement for the nanofluid (water+Al_2O_3) at a volume fraction of 4.3% and a 20% improvement for (glycol+Al_2O_3) at a fraction of 5%. For CuO of diameter 18.6 ηm in water or glycol the improvement of the thermal conductivity increases linearly with the volume fraction of the nanoparticles. The increase temperature of 34.7 °C pure water corresponding to a volume fraction of 10% was observed for Al_2O_3 nanoparticles of diameter 36 ηm [79]. The authors revealed a 30% improvement in conductivity and proposed a relationship to calculate it (water+Al_2O_3). For the case of copper oxide of diameter 29 ηm under the same conditions,

they obtained a 52% improvement in thermal conductivity and also proposed a relationship for the nanofluid (water+CuO).

Al_2O_3 and CuO nanoparticles were the most studied and easy to find in the early days of nanofluid research. Pack and Choi [80] introduced an oxide nanoparticle: Tin dioxide (TiO_2) with a diameter of 27 ηm into water and obtained an improvement of 10.7% in thermal conductivity for 4.35% in volume fraction. This result is lower than that obtained in the case of (water+Al_2O_3) under the same conditions. Tin dioxide (TiO_2) nanoparticles were also studied by Murshed *et al.* [81], where the nanoparticles had spherical and cylindrical shapes. It was found that spherical nanoparticles of 15 ηm lead to a small improvement in thermal conductivity compared to cylindrical nanoparticles of 40 ηm, for volume fractions of 5% [82, 71].

1.3.3   Metal nanoparticles

Metal nanoparticles such as copper (Cu), gold (Au) and silver (Ag) have higher thermal conductivities than the corresponding metal oxides. Thus, in the case of copper at room temperature, its thermal conductivity is 700 times greater than that of (oil+Cu). Theoretical studies of Xuan *et al.* [83] have shown that the Hamilton-Crosser model can be used to reconcile this with experimental results. It is found that the thermal conductivity of the nanofluid (water+Cu) increases by 75% and that of the nanofluid (oil+Cu) increases by 45% for volume fractions between 2.5% and 7.5%. For gold and silver, for diameters of 10-20 ηm and 60-80 ηm respectively, the studies of Pater *et al.* [84] showed for the nanofluid (Au-thiolate+Toluene) at 60°C an improvement of 8.8% for 0.011% volume fraction. For the nanofluid (Ag+water), the thermal conductivity is lower than that for the nanofluid (gold+water), although silver is more thermally conductive than gold. This result could be due to the size of gold nanoparticles which are 3 to 8 times smaller than silver, Kumar *et al.* [85] observed for a nanofluid (gold+water) an improvement of 20% for a volume fraction of 0.00013%.

1.4   Thermophysical characteristics of nanofluids

1.4.1   Density

The density ρ_{nf} of a homogeneous nanofluid (good dispersion of nanoparticles in the fluid) is given by the following expression:

$$\rho_{nf} = \left(\frac{m}{V} \right)_{nf} = \frac{m_f + m_s}{V_f + V_s} = \frac{\rho_f V_f + \rho_s V_s}{V_f + V_s}, \qquad (1.1)$$

where ρ is a density, m is a mass, V_s is a volume, nf is the nanofluid index, f is the base fluid index, s is the solid nanoparticles index. The volume fraction noted ψ, represents the ratio of the volume of

nanoparticles to the total volume (fluid + solid) at a given temperature T.

$$\psi = \frac{\text{Solid volume}}{\text{Volume of nanofluid}} = \frac{V_s}{V_s + V_f}. \tag{1.2}$$

The density of the nanofluid is therefore given as a function of the volume fraction as follows:

$$\rho_{nf} = (1 - \psi)\rho_f + \psi\rho_s, \tag{1.3}$$

1.4.2 Specific heat capacity

The mass heat capacity, formerly called mass heat or specific heat, is the heat capacity of a material relative to its mass. It is a quantity that has the capacity to accumulate energy in the form of heat, for a given mass, during a temperature increase. A large heat capacity means that a large amount of energy can be stored for a relatively small temperature increase [86]. Specific heat is the heat capacity per unit mass of a substance or a homogeneous system $C_P = dQ/mdT$.

The specific heat of a nanofluid has been given by several researchers such as Pak *et al.* [80] and Xuan *et al.* [87]. Throughout this study we have considered the one given by Xuan and Roetzel [87].

$$\begin{aligned}
(\rho C_P)_{nf} = \rho_{nf}(C_P)_{nf} &= \rho_{nf}\frac{Q_f + Q_s}{(m_f + m_s)\Delta T} \\
&= \frac{\rho_f V_f + \rho_s V_s}{V_f + V_s}\frac{(mC_P)_f\Delta T + (mC_P)_s\Delta T}{(m_f + m_s)\Delta T} \\
&= \frac{\rho_f V_f + \rho_s V_s}{V_f + V_s}\frac{(\rho V C_P)_f + (\rho V C_P)_s}{(\rho V)_f + (\rho V)_s} \\
&= (\rho C_P)_f\frac{V_f}{V_f + V_s} + (\rho C_P)_s\frac{V_s}{V_f + V_s} \\
&= (1 - \psi)(\rho C_P)_f + \psi(\rho C_P)_s
\end{aligned}$$

Thus the nanofluid specific heat is given by:

$$(\rho C_P)_{nf} = (1 - \psi)(\rho C_P)_f + \psi(\rho C_P)_s, \tag{1.4}$$

where $(C_P)_{nf}, (C_P)_f$ and $(C_P)_s$ represent the heat capacities of the nanofluid, the base fluid and the nanoparticle respectively.

1.4.3 Thermal expansion

Thermal expansion is the variation of shape, surface area, volume and density through a change in temperature without including phase transitions [86]. This variation is characterised by the coefficient of thermal expansion $\beta = -\frac{1}{\rho}\left(\frac{\partial\rho}{\partial T}\right)_P$, also known as the coefficient of dilatability. The subscript 'P' of the derivative indicates that the pressure is kept constant during the expansion. In order to find the expression of this coefficient in the context of nanofluids, many researchers have used the relation given in Eq.(1.3), which led to the following expression:

$$(\rho\beta)_{nf} = (1 - \psi)(\rho\beta)_f + \psi(\rho\beta)_s \tag{1.5}$$

1.4.4 Viscosity of nanofluids

Several models for the viscosity of nanofluids have been proposed in the literature, among them the fundamental formulation of Albert Einstein in 1906, based on the assumption that energy has a linear dependence on viscosity. Since this result is the combination of energy and work, it can be used to determine the dissipation of this energy around a single particle in a fluid [88]. Thus, the expression of the viscosity was found for a fluid with particles for a mixture containing dilute suspensions of fine spherical and rigid particles.

$$\nu_{nf} = \nu_f(1 + 2.5\psi), \tag{1.6}$$

where ψ is the volume fraction of the nanoparticles and ν_f the dynamic viscosity. This formulation remains true for a low nanoparticle concentration of approximately 3% [89]. This study carried out by Einstein has undergone many improvements among those proposed by Brinkman in 1952 [90],

$$\nu_{nf} = \frac{\nu_f}{(1 - \psi)^{2.5}}. \tag{1.7}$$

It can be seen that for low volume fractions, Brinkman's relation leads exactly to Einstein's relation. These relations do not include the effects of Brownian motion or of particle size.

Frankel and Acrivos' etablished the relation of viscocity:

$$\nu_{nf} = \nu_f \frac{9}{8} \left(\frac{\left(\frac{\psi}{\psi_m}\right)^{1/3}}{1 - \left(\frac{\psi}{\psi_m}\right)^{1/3}} \right), \tag{1.8}$$

where ψ_m is the maximum concentration to be determined experimentally.

Furthermore, Lundgren 1972 proposed a formulation based on the expansion of the concentration using the Taylor series

$$\nu_{nf} = \nu_f[1 + 2.5\psi + \frac{25}{4}\psi^2 + O(\psi^3)]. \tag{1.9}$$

In our study we only used the one given by Brinkman (see Eq.(1.7)).

1.4.5 Thermal conductivity

Quantifying the increase in the thermal conductivity of nanofluids is a major scope in the study of nanofluids, making it possible to obtain the ratio of the thermal conductivity of the nanofluid to that of the carrier fluid, while including the characteristics related to the size and shape of the nanoparticles. Thus, several thermal conductivity models have been developed, namely : Maxwell, Hamilton-Crosser, Yu and Choi, Bruggeman [91].

★ **Maxwell model**

Maxwell was interested in estimating the thermal conductivity of a fluid containing spherical particles in suspension. He assumed that the particles have the same diameter, and the distance

between them is relatively small, thus cancelling out the effect of mutual interaction between them making the medium highly dilated [92]. This formulation is given by :

$$\frac{k_{nf}}{k_f} = \frac{k_s + 2k_f - 2(k_f - k_s)\psi}{k_s + 2k_f + (k_f - k_s)\psi}, \tag{1.10}$$

where, k_{nf}, k_f and k_s are respectively the thermal conductivities of the nanofluid, the base fluid and the solid particles.

★ **Hamilton-Crosser model**

This model is an extension of Maxwell, considering particles of various sizes. To achieve this, Hamilton introduces a geometric factor called sphericity (ϕ), which is the ratio of the surface of the sphere having the same volume as the nanoparticles to the surface of a nanoparticle [93]. This leads to the following expression for the thermal conductivity:

$$\frac{k_{nf}}{k_f} = \frac{k_s + (n-1)k_f - (n-1)(k_f - k_s)\psi}{k_s + (n-1)k_f + (k_f - k_s)\psi}, \tag{1.11}$$

where n is a factor given by: $n = 3/\phi$.

★ **Yu and Choi model**

Their formulation is also based on Maxwell's, whose considerations are based on solid particles, which are separated by a nanoscale layer. This layer acts as a thermal bridge between the base fluid and the nanoparticles [94]. Its expression is given as :

$$\frac{k_{nf}}{k_f} = \frac{k_s + 2k_f - 2(k_f - k_s)(1 + \beta)^3\psi}{k_s + 2k_f + (k_f - k_s)(1 + \beta)^3\psi}, \tag{1.12}$$

where β is the ratio of the thickness of the nanoscale layer to the radius of the particles.

1.4.6 Electrical conductivity

Electrical conductivity can be defined as a physical phenomenon related to the capacity of a material or an electrolyte solution to let electric charges pass freely through a body, solid or liquid. It is expressed in Siemens per metre $(S.m^{-1})$, the higher its value, the more freely the current passes and the more interesting it is. According to the Nernst-Einstein law, the mathematical relationship of the electrical conductivity of a liquid or solid material is given by:

$$\sigma = \frac{Dz^2e^2C}{KT}, \tag{1.13}$$

where, D is the diffusion coefficient of the material, z is the number of charges carried by the material, e is the elementary charge, C is the concentration of the material, K is the Boltzmann constant, T is the absolute temperature [95]. Conductivity is also given as a function of electrical resistivity: $\sigma = 1/\rho$, with $\rho = \frac{RA}{L}$, R being the electrical resistance, A the cross-sectional area and L is the length of the material.

When the temperature is lowered, the electrical conductivity increases in a metallic conductor. Below a certain critical temperature, the electrical current could flow through a loop of superconducting wire with no applied power, when resistance drops to zero. Metals and plasma are materials with high electrical conductivity, like: silver, copper, gold, aluminium, zinc, nickel, brass. One of the best electrical conductor is silver (a metal) and for poor electrical conductivity, we have glass and pure water [95].

The electrical conductivity of a nanofluid is given by the expression:

$$\sigma_{nf} = \sigma_f \left[1 + \frac{3\left(\frac{\sigma_p}{\sigma_f} - 1\right)\psi}{\left(\frac{\sigma_p}{\sigma_f} + 2\right) - \psi\left(\frac{\sigma_p}{\sigma_f} - 1\right)} \right],$$

(1.14)

with σ_p the electrical conductivity of the particles and σ_f for the base fluid.

1.5 Summary table of thermophysical characteristics values.

Numerical value of the sphericity η for different shapes of nanoparticles.

Model	Platelets	Blades	Cylinders	Bricks
ψ	0.36	0.52	0.62	0.81

Table 1.1: Sphericity η for diferent shapes of nanoparticles.

Physical properties	$\rho\ (kg/m^3)$	$C_p\ (J/kgK)$	$k\ (W/mK)$	$\sigma\ (s/m)$	$\beta \times 10^{-5}(1/K)$
Blood/base fluid	1080	3500	0.59	0.6	0.18
SWCNTs	2600	425	6600	$10^6 - 10^7$	27
MWCNTs	1600	796	3000	50×10^6	27
Al_2O_3**(Alumina)**	3970	765	40	35×10^6	0.85
TiO_2**(Tin)**	4250	686.2	8.953	2.6×10^6	0.9
Fe_2O_3**(Iron Oxide)**	5180	670	9.7	35×10^6	0.5
Cu**(Copper)**	8933	385	401	59.5×10^6	1.67
CuO**(Copper Oxide)**	6320	531.8	76.5	58.8×10^6	18

Table 1.2: Thermo-physical properties of Blood and nanoparticles.

1.6 Nanoparticles in blood flow and the diseases encountered.

Blood is a living tissue made up of liquids and solids. The liquid part called plasma is made up of water, mineral salts, and proteins. More than half of the blood is plasma. The solid part of blood contains red blood cells, white blood cells and platelets. The blood moves through vessels such as arteries, veins and capillaries.
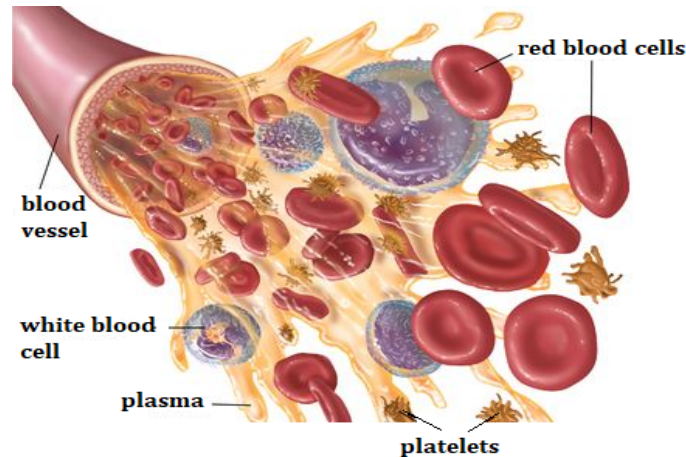
Figure 1.7: Blood cells [96].

1.6.1 Blood system and vessel elasticity.

Veins are blood vessels in which blood flows through the body towards the heart. They are so-called capacitive vessels. This means that one of the main functions of the veins, apart from returning blood to the heart, is also to regulate the volume of blood. In contrast to arteries, veins have valves and they are dark red in colour. In the case of capillaries, these are vessels of very small diameter (about 5 to 30 cm), located inside the organs in very large quantities (about 5 billion). They constitute a real heat transfer surface, since it is at this level that exchanges take place between the blood and the internal environment. A small artery is a blood vessel that connects and branches off from an artery into the capillaries. Small arteries have large muscular walls and are the main site of vascular resistance. The lymphatics, which contain lymph rather than blood, are produced directly in the tissues before entering the venous network. Particular attention will be paid to the arteries and veins, as they are the most essential element.
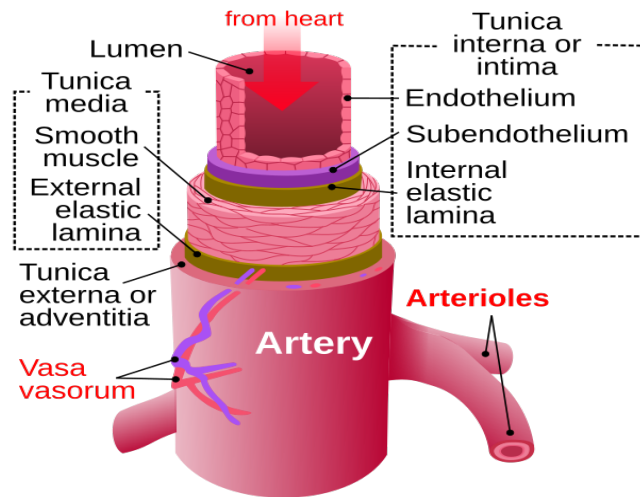
Figure 1.8: Different parts of artery [97].

The blood system is made up of vessels that can be assimilated to elastic tubes containing several sub-layers illustrated in figure (1.8) and of which the deposition of atheroma takes place. This leads to the creation of the structural deformations in the vessels which will favour an increase or decrease in pressure depending on the case of anomaly: stenosis and aneurysm [98].

★ **Stenosis**

Inadequate secretion of insulin (the hormone that regulates blood sugar levels) in the pancreas results in insulin deficiency, which can cause diabetic ketoacidosis. Diabetic ketoacidosis results from the mechanism by which the penetration of glucose into the cells is prevented by a lack (insufficiency) of insulin in the bloodstream. This results in the use of fats to obtain the fuel needed for cells functioning. Unused glucose will accumulate in the bloodstream, causing fat to be deposited in the vessel walls, resulting in stenosis. Stenosis is an abnormality related to the narrowing of blood vessels or other organ or tubular structure such as foramina and ducts. In most cases, it is due to narrowing caused by lesions that reduce the space of the lumen, as is the case of atherosclerosis illustrated in the figure (1.9), whose causes are not yet well known, but the risk factors are abnormal overproduction of cholesterol, increased levels of inflammatory markers, high pressure, diabetes, smoking, obesity, genetic and unhealthy Diet.

Common Carotid Stenosis

Facial artery
External carotid artery
Lingual artery
Superior thyroid artery
Common carotid artery
Blood flow
Internal carotid artery
Athersclerotic plaque

x
L
2d
R(x)
L
Ro
Ro
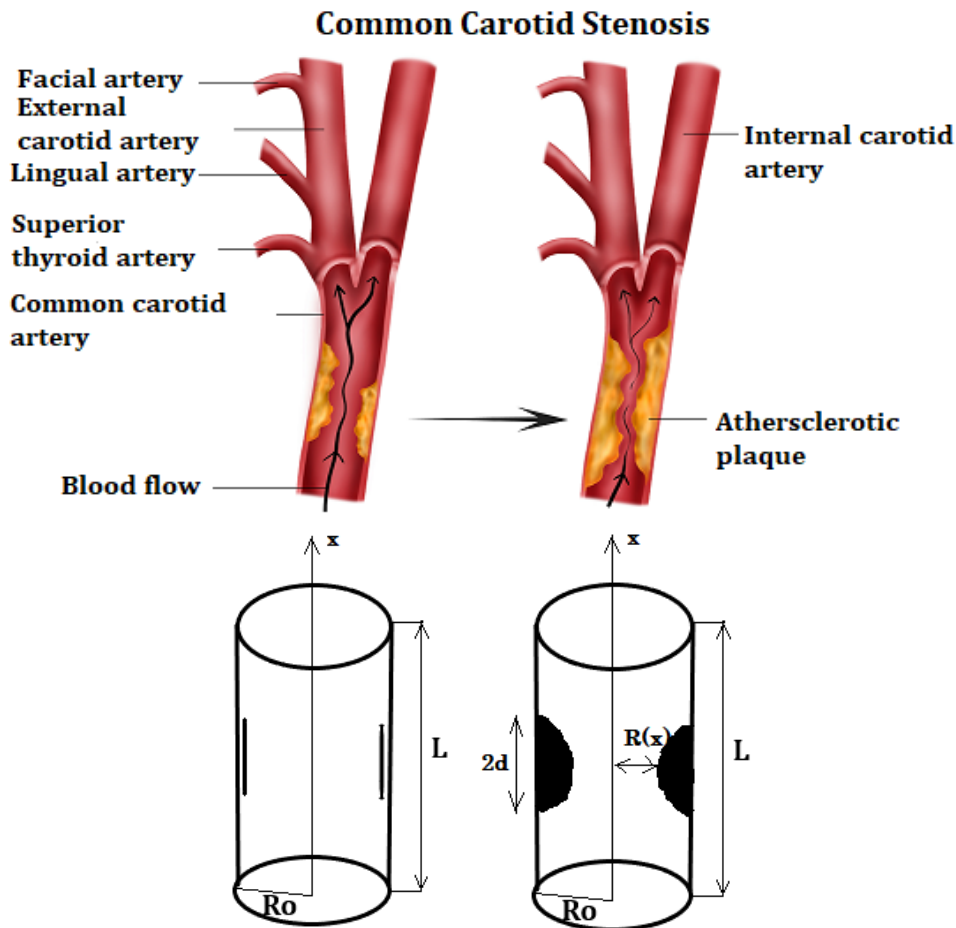
Figure 1.9: Stenosis [99].

★ **Aneurysm**

The aneurysm is an anomaly of the large arteries of the body which receive oxygen-rich blood from the left ventricle and distribute it throughout the body, except to the lungs which are connected to the right ventricle. Blood pressure tends to push out the arterial walls. The best known aneurysm is the abdominal aortic aneurysm (AAA). The aneurysm can also be located towards the base of the brain (ampullary aneurysm), or towards the thorax (thoracic aneurysm). The constitution of the artery at the exit of the heart has several small branches of arteries. Along its path from the heart to the abdomen appears a subdivision of the aorta into two arteries for the legs. The aneurysm is part of the aortic disorder in the weak area of the aortic walls. If left untreated, it can tear up and cause pain and internal bleeding. It can also develop in other arteries, namely: peripheral, popliteal, femoral, carotid, cerebral and coronary arteries. Aortic aneurysms occur most often in the abdomen and in the elderly people. The areas where the arteries bifurcate are the areas at risk. According to World Health Organization (WHO), 2-13% of men in 65 years old or greater and 6% of women on the same age can have an abdominal aortic aneurysm, which is rare for people under 60 years old. Ascending aortic aneurysms and ampullary aneurysms have a hereditary component, but the genes responsible have not yet been found in humans but rather in mice. These ascending aneurysms are

18

known as Marfan syndrome [100].
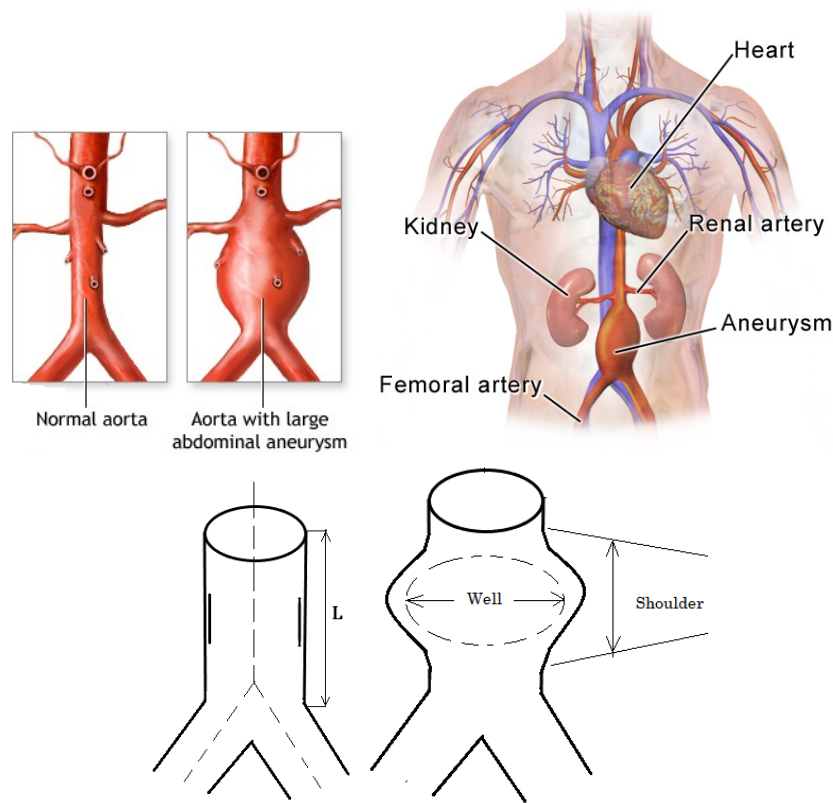
Figure 1.10: Aneurysm [101].

1.6.2 Description and resolution of diseases encountered

For its proper functioning the body needs glucose (in the blood we speak of a blood sugar level between 0.8-1.15 g/L of blood; that is to say between 4.5-6.4 μmol/L of blood). This glucose molecule is produced in the digestive tract and constitutes the first source of energy for the body which circulates in the blood. When the blood is rich in oxygen, the glucose is broken down into energy that can be used by the muscles, brain, cells etc. On the other hand, if the blood is not rich enough in oxygen, the glucose is degraded into lactic acid which is not only harmful but also important for the kidneys, the heart and the liver for their functioning. High energy consumption by the body leads to the production of lactic acid, which is a natural acid molecule that occurs after heavy muscular effort. It is generated by the muscles when they have used up all the energy, they had to carry out the movements and also occurs when oxygen tends to be lacking in the red blood cells, kidneys, and skin.

Poor diet and stress are major factors in the increase of heart rate and blood pressure, thus causing vessel-related diseases called cardiovascular diseases. It is one of the leading causes of premature death in the world.

The deposition of lipids in the arteries or atherosclerotic plaque causes a reduction in the diam-

eter of the artery. This leading to an arterial disease called atherosclerosis, which is different from arteriosclerosis. The latter is an ageing of the artery without the deposition of atherosclerotic plaque and is very common in the elderly people. Atherosclerosis is characterized by a progressive and silent deposit of bad cholesterol narrowing the artery lumen and whose symptoms are chest pain, sweating, shortness of breath, intense headaches in case of stroke. The most common causes are smoking, high blood pressure, diabetes, age and high cholesterol. It can be treated by physical activity or by anti-platelet agents (which can also be used for thrombus).
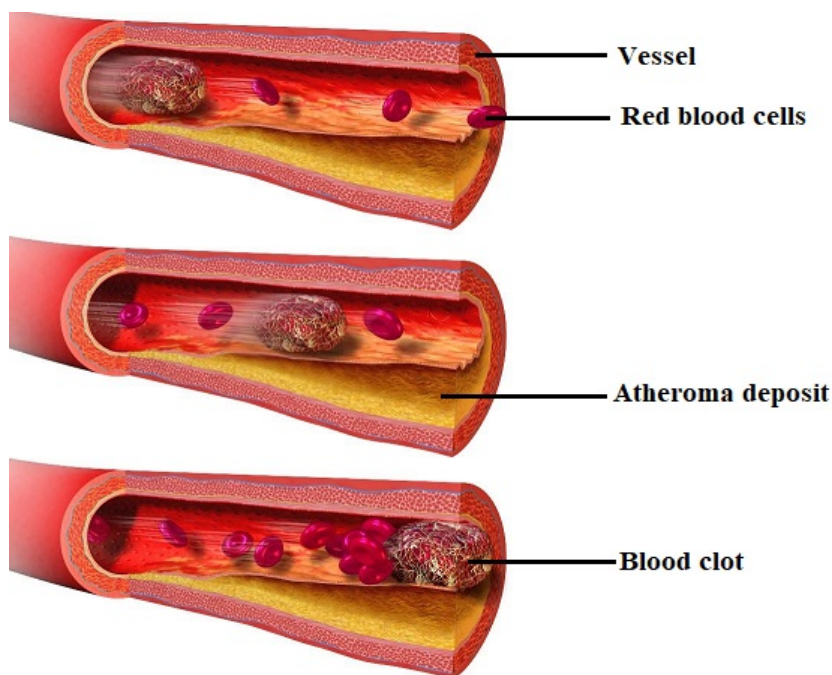
Figure 1.11: Blood clot motion [102].

Thrombosis is the abnormal presence of thrombus (blood clot) (figure (1.11)) leading to partial or total occlusion of a vein (venous thrombosis) or an artery (infarction, stroke). One of the best-known thromboses is phlebitis, which forms in a vein leg, arm, brain, etc. and is caused by poor blood clotting. It migrates to the pulmonary artery and causes a pulmonary embolism for example. This embolism prevents the lung from being sufficiently perfused and the blood from being poorly oxygenated [103]. This is why oral anticoagulations like antivitamins K (AVK) and direct-acting non-vitamin K oral anticoagulants (DOA): (edoxaban, dabigatran, apixaban...) are applied to patients to prevent any complications.

Proper functioning genes reflect proper cell development and division as the body replaces aging or damaged cells. Gene failure can lead to the proliferation of cancer cells, turning normal cells into cancer cells due to, for example, exposure to ultraviolet light from the sun, smoking, alcohol and many others. These cancer cells have the particularity to grow and divide in a disorderly way without dying when they were supposed to. They remain immature and do not mature like normal cells,

evade the immune system, spread to other parts of the body through the blood or lymphatic system, invade and damage tissues and organs. They also have the ability to obtain oxygen and nutrients to function, and the more these cells divide, the more tumors are formed. When the tumor grows to a certain size, it produces new blood vessels for the additional supply of oxygen and nutrients. This self-growth is called angiogenesis, and facilitates the migration of cancer cells to other parts of the body through the bloodstream forming metastases as shown in figure (1.12).
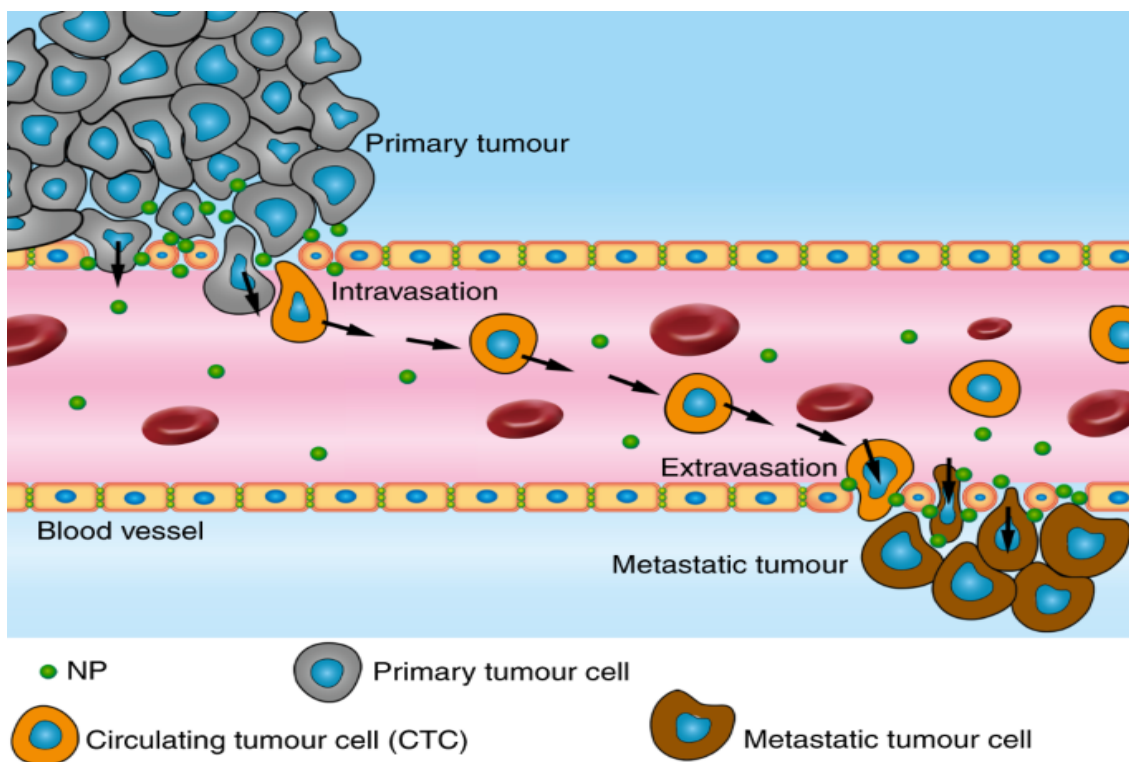
Figure 1.12: Action of nanoparticles in the vessel fighting against a carcinogenic proliferation [104].

Thus, one of the treatments proposed is surgery for the primary tumors, plus chemotherapy for the metastases. This treatment is called adjuvant treatment. It is done in order to prevent a recurrence of the cancer cells. In cases of recurrence, certain genetic mutations make the cancer cells resistant to chemotherapy and other treatments. One of the approaches recently tested is the use of nanoparticles either orally or intravenously. This approach is still in experimental mode on laboratory to better understand the behavior of nanoparticles on cancer cells [105].

Many blood disorders are caused by genes and the most common diseases among others are anemia, hemophilia, hemopathy, dyslipidemia, leukemia, ischemia to name a few. The cause of most leukemias is unknown. It may be due to certain radiation exposure to chemotherapy, and also to chemicals that increase the risk of occurrence. In some cases, it is due to hereditary diseases, anemia and chromosome abnormalities. The production of white blood cells by the bone marrow during the gradual differentiation (or maturation) of stem cells can be abnormal and parts of chromosomes are rearranged. These abnormal chromosomes disrupt normal cell division, so that the affected

cells multiply uncontrollably or become resistant to normal cell death, leading to the development of leukemia. It is subdivided into four main types: acute lymphocytic leukemia, acute myeloid leukemia, chronic lymphocytic leukemia and chronic myeloid leukemia. Their resolution requires surgical intervations, radiation exposure and injections in most cases.

1.7   Conclusion.

In this chapter, we focused on the generalities of nanoscience and nanotechnology in blood flows by presenting the different structures of nanoparticles both natural and artificial. Also, on their presence in a basic fluid mainly the case of water. The thermo-physical characteristics of some nanoelements were listed and defined. Finally, we presented some diseases encountered in the vessels and the role that these nano-elements play in the blood flow. The next chapter will focus on the description of different methods used to investigate the dynamics of these nanoparticles in the case of an incompressible fluid subjected to thermal radiation, magnetic fields, chemical reactions and nanofluid rotation.

Chapter 2

Methodology and Fractional Models

2.1 Introduction

In this chapter, we will first of all give a brief introduction to the Navier-Stockes equations which has been considered in this thesis, because of its ability to better understand 1 to 3 dimensional microfluidic behaviour. Then, we will present the different magnetohydrodynamic models used. Finally, we will describe the analytical and numerical methods applied to these models. Fluid mechanics is a branch of physics that studies fluids (liquid, gas and plasma) and the forces that apply to them. In the reminder, we will use terms statics fluid, kinematic fluid and dynamic fluid respectively, for a study of fluid at rest, fluid in motion and fluid flow.

2.2 Conservation law

Many researchers have worked to understand this branch of physics. Among them, Leonardo Da Vinci (1452-1519) [106], was the first to visualise the movement of particles in fluid flow. Isaac Newton (1642-1727) [107], brought his many contributions to fluid mechanics, in particular through his work entitled 'PRINCIPIA'. He introduced the notion of Newtonian fluids which is an increase in viscous stresses coming from the flow at each point and which is linearly proportional to the local strain rate [108, 109]. Furthermore, in a Newtonian fluid the internal forces are proportional to the change ratios of the fluid velocity at each point in space. The study of the fluid is based on the properties related to the compressibility, which reflects a change in pressure or temperature leading to a change in the density. Thus, any fluid is compressible to some extent. However, in many situations the change in the density can be neglected for very small pressures and temperatures. So in this case, the flow can be modelled as an incompressible flow [110, 111] as is the case in this thesis. As another property, we have the viscosity which is the measure of the resistance of a fluid to deformation at

a given velocity. It is also the internal frictional force between the fluid layers. For example, if a viscous fluid is flowing along a tube, the velocity near the axis of the tube is higher than near the walls. The steady and unsteady flow are considered as properties of fluid. For steady-state flow the condition of fluid properties at a point in the system do not change over time. In the opposite case, we speak of unsteady, also called transient. The assumptions of continuity, of the laws of conservation of physics allow us to derive mathematical formulations from the partial differential equations of the fluid. In a microscopic medium the molecules perform random movements varied on positions and times to be considered. The physical properties most observed in these movements are density, pressure, temperature, concentration and velocity. All this in Euler and Lagrange coordinate systems describing the motion of the fluid. To derive the equations of fluid dynamics, we consider the effect of mass, momentum and conservative energy. This allows us to derive the mathematical formulations of the conservation laws for a control volume V in a domain D, where the Eulerian coordinate system is taken as fixed in space and time.

2.2.1   Fondamental relation

Let us study the control domain D, through a volume V and of surface Σ in a continuous medium Ω. Over time the motion of an elementary fluid particle M in D and of volume dV will be observed. We will define f a function which is continuous on D. A material domain is a space where the points in the fluid domain have a velocity equal to that of the fluid at each instant. The material derivative of a quantity f integrated over a material domain through a volume V depending on time is given by:

$$\frac{d}{dt}\int_D f dV = \int_D \frac{\partial f}{\partial t} dV + \int_\Sigma f\vec{u}\cdot\vec{n}d\Sigma, \tag{2.1}$$

where $\vec{u}$ is a local velocity of the control surface, $\vec{n}$ is the outgoing normal volume, $\frac{d}{dt}$ is the derivative along the D domain of the fluid in motion.

Using the Green-Ostrogradsky theorem or divergence theorem, the second term of (2.1) can still be written as :

$$\int_\Sigma f\vec{u}.\vec{n}d\Sigma = \int_D \vec{\nabla}\cdot(f\vec{u})dV. \tag{2.2}$$

(2.1) and (2.2), allows us to bring out the Leibnitz rule or the transport theorem:

$$\frac{d}{dt}\int_D f dV = \int_D \left[\frac{\partial f}{\partial t} + \vec{\nabla}\cdot(f\vec{u})\right]dV. \tag{2.3}$$

2.2.2   Mass Conservation

★ The Equation of Continuity

We consider a fixed volume of fluid V, whose mass is:

$$m = \int_V \rho dV. \tag{2.4}$$

The variation of mass through time is given by the mass flux density $\rho \vec{u}$ crossing the surface (S) bounding the volume (V).
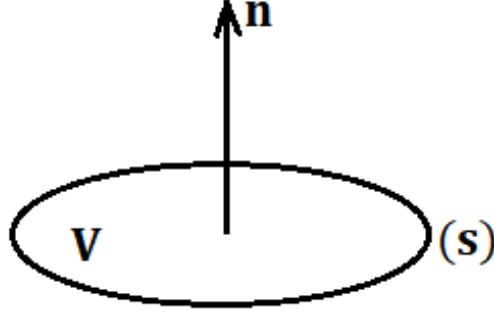
Figure 2.1: Representation of an area.

Let $d\vec{S}$ be the surface element oriented by the external normal $\vec{n}$ so that $d\vec{S} = \vec{n}dS$. Hence

$$\frac{dm}{dt} = - \oint \rho \vec{v} \cdot d\vec{S}. \tag{2.5}$$

The negative sign comes from the orientation of the surface (S): when $\vec{u}$ is parallel to $d\vec{S}$ the mass m decreases. The increase rate of the mass in V is $\frac{d}{dt}(\int_V \rho dV)$ and, as V is fixed in space, one deduces that

$$\frac{d}{dt} \int_V \rho dV = \int_V \frac{\partial \rho}{\partial t} dV. \tag{2.6}$$

Considering the conservation of mass

$$\int_V \frac{\partial \rho}{\partial t} dV = - \oint \rho \vec{u} \cdot d\vec{S}, \quad \Rightarrow \quad \int_V \frac{\partial \rho}{\partial t} dV + \int_S \rho \vec{u} \cdot \vec{n} dS = 0, \tag{2.7}$$

which is the conservation equation in integral form. By using the divergence theorem (2.2), the above equation takes the form:

$$\int_V \left[\frac{\partial \rho}{\partial t} + \vec{\nabla} \cdot (\rho \vec{u}) \right] dV = 0. \tag{2.8}$$

For any volume V, (2.8) is true and the equation of continuity in the differential form is:

$$\frac{\partial \rho}{\partial t} + \vec{\nabla} \cdot (\rho \vec{u}) = 0. \tag{2.9}$$

Considering the Euler Lagrangian formalism, given by:

$$\frac{D\rho}{Dt} = \frac{\partial \rho}{\partial t} + \vec{u} \cdot \vec{\nabla} \rho, \tag{2.10}$$

One may also write it using the material derivative of ρ, namely

$$\frac{D\rho}{Dt} = -\rho \vec{\nabla} \cdot \vec{u}, \tag{2.11}$$

which shows that the density of a fluid element varies because of its volume variation expressed by $\vec{\nabla} \cdot \vec{u}$, since its mass is constant. Therefore, for a particle with constant density during it motion (2.11) reduced to

$$\vec{\nabla} \cdot \vec{u} = 0, \tag{2.12}$$

which is the equation of continuity for an incompressible fluid.

★ Incompressible fluid

Let us consider a fluid whose volume is constant whatever the pressure and any fluid being in reality sensitive to the pressure. The mass flux is the mass of flow per unit time from figure (2.2), we observe that at section 1 the flux is $\rho v_1 S_1$ which is equal to that of section 2 $\rho v_2 S_2$, and we observe no accumulation of fluid between the two sections. Hence vS is a constant along an elementary stream tube.
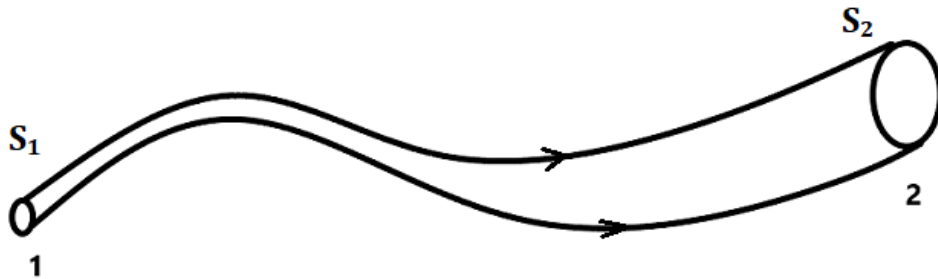
Figure 2.2: Diagram of continuity in the incompressible fluid.

It is observed that where the streamlines contract the velocity increases, and where they expand the velocity decreases.

2.2.3   Momentum Conservation

The momentum of the fluid contained in a volume V is given by:

$$\vec{p} = \int_V \rho \vec{u} dV. \tag{2.13}$$

Using the fundamental principle of dynamics, the time variation of the momentum of the fluid contained in a volume V, is equal to the sum of the external forces applied to it. This is expressed as:

$$\frac{d}{dt} \left(\int_V \rho \vec{u} dV \right) = \int_V \vec{f} dV + \int_S \vec{T} dS, \tag{2.14}$$

where dS is an element of surface of normal $\vec{n}$, $\vec{f}$ is the force exerted per unit of volume, the stress vector: $\vec{T} = \bar{\bar{\sigma}} \cdot \vec{n}$, with $\bar{\bar{\sigma}}$ the stress tensor given by the expanded expression in i-component:

$$\sigma_{ij} = -P\delta_{ij} + \tau_{ij}, \tag{2.15}$$

where P is the static pressure: that is, minus the normal stress acting in any direction and τ_{ij} is a shear stresses, and also has diagonal components whose sum is zero,implie that $\tau_{ii} = 0$. Equation (2.14) is in the form of Lagrangian derivative depending on time and it is possible to write it, in i-component: $\int_V \frac{d(\rho u_i)}{dt} dV$. Using the theorem of Ostrogradsky, the integral of the force of surface can be written as: $\int_V (F_i + \frac{\partial \sigma_{ij}}{\partial x_j}) dV$. Therefore, due to the fact that volume V is non-time-varying, we can write

$$\frac{\partial(\rho u_i)}{\partial t} + \frac{\partial(\rho u_i u_j)}{\partial x_j} = F_i + \frac{\partial \sigma_{ij}}{\partial x_j}. \tag{2.16}$$

By developing the derivatives, and rearranging, we obtain

$$\left(\frac{\partial \rho}{\partial t} + u_j \frac{\partial \rho}{\partial x_j} + \rho \frac{\partial u_j}{\partial x_j} \right) u_i + \rho \left(\frac{\partial u_i}{\partial t} + u_j \frac{\partial u_i}{\partial x_j} \right) = F_i + \frac{\partial \sigma_{ij}}{\partial x_j}. \tag{2.17}$$

In tensor notation, the contunity equation is

$$\left(\frac{\partial \rho}{\partial t} + u_j \frac{\partial \rho}{\partial x_j} + \rho \frac{\partial u_j}{\partial x_j} \right) = 0 \tag{2.18}$$

So, the fluid equation of motion is written

$$\rho \left(\frac{\partial u_i}{\partial t} + u_j \frac{\partial u_i}{\partial x_j} \right) = F_i + \frac{\partial \sigma_{ij}}{\partial x_j}. \tag{2.19}$$

Another form is given by

$$\rho \frac{Du_i}{Dt} = F_i + \frac{\partial \sigma_{ij}}{\partial x_j}. \tag{2.20}$$

2.2.4 Energy Conservation

Conservation of energy is a physical principle in which the total energy of an isolated system is invariant over time [115]. Based on the first principle of thermophysics where the variation with respect to time of the total energy per unit volume is equal to the sum of the powers of the forces across a surface (S), in a continuous medium Ω.

$$\frac{dE}{dt} = \sum P_{F_{ext}} \iff \frac{d(E_c + U_{in})}{dt} = P_e + \dot{Q}, \tag{2.21}$$

where $\dot{Q}$ is the calorific power, P_e is the power of the external forces, E_c is the kinetic energy: $E_c = \frac{\rho V^2}{2}$, U_{in} the internal energy: $U_{in} = \rho e$, where e is the energy per unit mass .

Considering the kinetic energy theorem which states that the variation over time of the kinetic energy of a particle follows the movement of the fluid which is equal to the sum of the powers of the external and internal forces acting in this medium.

$$\frac{d(E_c)}{dt} = P_e + P_i. \tag{2.22}$$

By applying (2.22) in (2.21), we obtain the balance on the internal energy U_{in}:

$$\frac{dU_{in}}{dt} = \dot{Q} - P_i, \tag{2.23}$$

where $U_{in} = \int_D \rho e dV$, $\dot{Q} = \int_\Sigma q(\vec{X}, t, \vec{n})d\Sigma + \int_D r(\vec{X}, t)dV$, $q = -\vec{q} \cdot \vec{n}$ represents the surface density of the heat flow collected by conduction and where r represents the power density dissipated locally in the form of heat (radiative, nuclear, electromagnetic). And finally, $P_i = -\int_D (\bar{\bar{\sigma}} : \vec{\nabla} \cdot \vec{u})dV$, where $(\bar{\bar{\sigma}} : \vec{\nabla} \cdot \vec{u}) = \sigma_{ik}U_{ik} = -P\vec{\nabla} \cdot \vec{U} + (\bar{\bar{\tau}} : \vec{\nabla} \cdot \vec{u})$. (2.23) is reduced to:

$$\frac{d}{dt}\int_D \rho e dV = \int_\Sigma q(X, t, n)d\Sigma + \int_D r(X, t)dV - \int_D P(\vec{\nabla} \cdot \vec{U})dV + \int_D (\bar{\bar{\tau}} : \vec{\nabla} \cdot \vec{U})dV. \qquad (2.24)$$

By applying the divergence theorem given in equation (2.2) and the transport theorem given in equation (2.3), we arrive at:

$$\rho \frac{de}{dt} = -\vec{\nabla} \cdot \vec{q} + r - P\vec{\nabla} \cdot \vec{U} + (\bar{\bar{\tau}} : \vec{\nabla} \cdot \vec{U}). \qquad (2.25)$$

According to Fourier's law, the conductive heat flux density vector $\vec{q}$ is proportional to the temperature gradient. And the proportionality coefficient K is the thermal conductivity of the fluid or nanofluid under study. So, we have the conservation of energy equation:

$$\rho \frac{de}{dt} = -\vec{\nabla} \cdot (-K\vec{\nabla}T) + r - P\vec{\nabla} \cdot \vec{U} + (\bar{\bar{\tau}} : \vec{\nabla} \cdot \vec{U}). \qquad (2.26)$$

The conservation of energy of most systems is described as a function of temperature and heat capacity, compared to that given by the internal mass energy. This leads us to express e as a function of T and P. To do this, we introduce the enthalpy of mass: $h = e + \frac{P}{\rho}$ which is expressed as follows:

$$dh = C_p dT + \frac{1}{\rho}(1 - \beta_T T)dP, \qquad (2.27)$$

where $\beta_T = \beta = -\frac{1}{\rho}\left(\frac{\partial \rho}{\partial T}\right)_P$ which is the coefficient of thermal expansion, $C_p = \left(\frac{\partial h}{\partial T}\right)_P$ which is the specific heat per unit mass at constant pressure. By deriving (2.27) with respect to time we obtain the final expression of (2.26) in the form:

$$\rho C_p \frac{dT}{dt} - \beta_T T \frac{dP}{dt} = \vec{\nabla} \cdot (K\vec{\nabla}T) + r + (\bar{\bar{\tau}} : \vec{\nabla} \cdot \vec{U}), \qquad (2.28)$$

which marks the conservation of energy equation of an incompressible fluid, the one considered in our study through precise approximations. As an approximation, we have the Boussinesq approximation, attributed to Boussinesq [112] and first presented by Oberbeck [113]. In this approximation, it is supposed that the fluid has a constant heat capacity per unit volume ρC_p; then, $\rho C_p \frac{dT}{dt}$ is equal to the rate of heating per unit volume of a fluid particle. Lorentz used it in 1881 [114] to establish a correlation in natural convection. According to this approximation the different thermo-physical properties of the fluid are independent of temperature and pressure. In addition, the incompressible fluid is assumed to be dilatable with a constant density equal to its mean value ρ_0. Hence we have the expression of the density ρ by first order Taylor expansion depending on the temperature:

$$\rho = \rho_0[1 - \beta_T(T - T_0)], \qquad (2.29)$$

with T the temperature of the fluid at a point in the system, T_0 the average temperature of the system. By considering this last relation in equation (2.28); the power density linked to the pressure variations $\beta_T(\frac{d\rho}{dt})$ and the viscous dissipation $(\bar{\bar{\tau}} : \vec{\nabla} \cdot \vec{U})$ are negligible in comparison with the diffusive term $K\Delta T$.

2.2.5 Navier-Stokes Equation

Equation (2.15) expresses the stress tensor in i-component, due to the fact that σ_{ij} and δ_{ij} are both symmetric tensors, it follows that τ_{ij} is also symmetric

$$\tau_{ij} = \tau_{ji}. \tag{2.30}$$

Let the $u_i(r,t)$ be the Cartesian components of the fluid velocity at point r and time t. The various velocity gradients within the fluid take the form $\partial u_i / \partial x_j$, the components of the deviatoric stress tensor are linear functions of these velocity gradients: that is,

$$\tau_{ij} = A_{ijkl} \frac{\partial u_k}{\partial x_l}. \tag{2.31}$$

The most general expression for an isotropic fourth-order tensor is

$$A_{ijkl} = \alpha \, \delta_{ij} \, \delta_{kl} + \beta \, \delta_{ik} \, \delta_{jl} + \gamma \, \delta_{il} \, \delta_{jk}, \tag{2.32}$$

where α, β and γ are arbitrary scalars. By combining (2.31) and (2.32), we have:

$$\tau_{ij} = \alpha \, \frac{\partial u_k}{\partial x_k} \, \delta_{ij} + \beta \frac{\partial u_i}{\partial x_j} + \gamma \frac{\partial u_j}{\partial x_i}. \tag{2.33}$$

According to (2.30), τ_{ij} is a symmetric tensor which implies that $\beta = \gamma$, then

$$\tau_{ij} = \alpha \, e_{kk} \, \delta_{ij} + 2\, \beta \, e_{ij}, \tag{2.34}$$

with

$$e_{ij} = \frac{1}{2} \left(\frac{\partial u_i}{\partial x_j} + \frac{\partial u_j}{\partial x_i} \right), \tag{2.35}$$

where, e_{ij} is called rate of strain tensor, β is the dynamic viscosity coefficient, α the volume viscosity coefficient. So, for $\tau_{ii} = 0$, τ_{ij} is a traceless tensor, which yields $3\alpha = -2\beta$ and

$$\tau_{ij} = 2\, \mu \left(e_{ij} - \frac{1}{3} \, e_{kk} \, \delta_{ij} \right). \tag{2.36}$$

In addition, with $\mu = \beta$, the general expression for the stress tensor in an isotropic Newtonian fluid is

$$\sigma_{ij} = -P\, \delta_{ij} + 2\, \mu \left(e_{ij} - \frac{1}{3} \, e_{kk} \, \delta_{ij} \right). \tag{2.37}$$

By applying equations (2.35) and (2.37), the derivative term of the stress tensor giving by (2.20) is

$$\frac{\partial \sigma_{ij}}{\partial x_j} = -\frac{\partial P}{\partial x_i} + \frac{\partial}{\partial x_j} \left[\mu \left(\frac{\partial u_i}{\partial x_j} + \frac{\partial u_j}{\partial x_i} \right) \right] - \left(\frac{2}{3} \, \mu \frac{\partial u_j}{\partial x_j} \right). \tag{2.38}$$

29

By expanding and grouping the terms, then replacing in the equation (2.20), we arrive at the one proposed by Claude-Louis Navier and George Gabriel Stokes, named Navier-Stokes equation which is a good approximation to treat viscosity as a spatially uniform quantity. It is given by

$$\rho \frac{Du_i}{Dt} = F_i - \frac{\partial P}{\partial x_i} + \mu \left(\frac{\partial^2 u_i}{\partial x_i \partial x_j} + \frac{1}{3} \frac{\partial^2 u_j}{\partial x_i \partial x_j} \right). \tag{2.39}$$

The vector form of the previous expression becomes

$$\rho \frac{Du}{Dt} \equiv \rho \left[\frac{\partial u}{\partial t} + (u.\nabla)u \right] = f - \nabla P + \mu \left[\nabla^2 u + \frac{1}{3} \nabla(\nabla \cdot u) \right]. \tag{2.40}$$

Finally, in the incompressible fluid with $\nabla \cdot v = 0$ the Navier-Stokes equation becomes

$$\rho \frac{Du}{Dt} \equiv \rho \left[\frac{\partial u}{\partial t} + (u.\nabla)u \right] = f - \nabla P + \mu \nabla^2 u. \tag{2.41}$$

★ **Cartesian coordinates**

We derive the basic equations governing the motion of a thin elastic tube filled with an incompressible and viscous fluid. In order to elucidate the main aspects of the fluid of arterial blood, we chose to study the motion of this tube in a simple form.

According to what precedes in (2.41), the differential vector operator nabla ∇ can be put in the cartesian coordinates (x, y, z) form $\nabla \equiv (\frac{\partial}{\partial x}, \frac{\partial}{\partial y}, \frac{\partial}{\partial z})$. Consider the velocity components $u \equiv (u_x, u_y, u_z)$, the external force $f \equiv (f_x, f_y, f_z)$ and the laplacian $\Delta = \nabla^2 \equiv (\frac{\partial^2}{\partial x^2}, \frac{\partial^2}{\partial y^2}, \frac{\partial^2}{\partial z^2})$. We consider the one-dimensional fields of longitudinal flow-velocity u_z, fluid pressure P and radial displacement of the arterial wall u_x. Then, the continuity and the Navier-Stokes equation becomes

$$\frac{\partial u_z}{\partial z} = 0,$$
$$\frac{\partial u_z}{\partial t} + u_z \frac{\partial u_z}{\partial z} = -\frac{1}{\rho} \frac{\partial P}{\partial z} + \nu \left(\frac{\partial^2 u_z}{\partial z^2} \right) + \frac{1}{\rho} f_z \tag{2.42}$$

If the fluid is non ideal we can approximate the surface forces at $f_z \approx -8\nu \frac{u_z}{u_x^2}$, with $\nu = \mu/\rho$ is the kinematic viscosity.

$$\frac{\partial u_z}{\partial t} + u_z \frac{\partial u_z}{\partial z} + \frac{1}{\rho} \frac{\partial P}{\partial z} = 0,$$
$$\frac{\partial u_z}{\partial t} + u_z \frac{\partial u_z}{\partial z} + \frac{1}{\rho} \frac{\partial P}{\partial z} = \nu \left(-8 \frac{u_z}{u_x^2} + \frac{\partial^2 u_z}{\partial z^2} \right). \tag{2.43}$$

(2.43) show the Navier-Stokes equations of motion relevant to the longitudinal flow, respectively, not dissipation and with dissipation.

★ **Cylindrical coordinates**

In our study we consider an incompressible, non-Newtonian fluid such as blood, in rotational symmetry hence the choice of cylindrical coordinates (r, θ, z), and the flow velocity does not change much with the radial coordinate. However, during fluid flow in an elastic tube, the viscous flow near

the tube shifts towards the central region of the tube, so that the haematocrit rate becomes quite low near the artery. Also, due to the high shear rate near the venous walls, the viscosity is further reduced. On the other hand, for large vessels, blood can be considered as a Newtonian fluid, and the hematocrit rate is high but the shear rate is quite low. Therefore, in the study of flow problems in arteries, blood near the arterial wall can be treated as an incompressible and inviscid fluid, while blood in the central region can be considered as an incompressible Newtonian fluid, with the assumption that the field variables do not change with the radial coordinate. The continuity equation $\nabla \cdot u = 0$ for an incompressible fluid in cylindrical coordinates (r, θ, z) is

$$\frac{1}{r}\frac{\partial}{\partial r}(ru_r) + \frac{1}{r}\frac{\partial u_\theta}{\partial \theta} + \frac{\partial u_z}{\partial z} = 0. \tag{2.44}$$

By considering an ideal incompressible and non-viscous fluid, the surface forces will be neglected and the Navier-Stokes equation of motion is given as

$$\begin{aligned}
\frac{\partial u_r}{\partial t} + u.\nabla u_r - \frac{u_\theta^2}{r} + \frac{1}{\rho}\frac{\partial P}{\partial r} &= 0, \\
\frac{\partial u_\theta}{\partial t} + u.\nabla u_\theta + \frac{u_r u_\theta}{r} + \frac{1}{\rho r}\frac{\partial P}{\partial \theta} &= 0, \\
\frac{\partial u_z}{\partial t} + u.\nabla u_z + \frac{1}{\rho}\frac{\partial P}{\partial z} &= 0.
\end{aligned} \tag{2.45}$$

If the fluid is non ideal, the problem into consideration involves Navier-Stokes equations describing the fluid flow. The Navier-Stokes equations of motion for an incompressible fluid of constant dynamic viscosity μ, and density ρ, in cylindrical coordinates (r, θ, z) are

$$\begin{aligned}
\rho\left[\frac{Du_r}{Dt} - \frac{u_\theta^2}{r}\right] &= -\frac{\partial P}{\partial r} + f_r + \mu\left(\nabla^2 u_r - \frac{u_r}{r^2} - \frac{2}{r^2}\frac{\partial v_\theta}{\partial \theta}\right), \\
\rho\left[\frac{Du_\theta}{Dt} + \frac{u_\theta u_r}{r}\right] &= -\frac{\partial P}{\partial \theta} + f_\theta + \mu\left(\nabla^2 u_\theta - \frac{u_\theta}{r^2} - \frac{2}{r^2}\frac{\partial u_r}{\partial \theta}\right), \\
\rho\frac{Du_z}{Dt} &= -\frac{\partial P}{\partial z} + f_z + \mu\nabla^2 u_z,
\end{aligned} \tag{2.46}$$

where u_r, u_θ, u_z are the velocities in the r, θ, z cylindrical coordinate directions, P is the pressure and f_r, f_θ, f_z are the body force components in the r, θ, z directions and the operators D/Dt and ∇^2 are

$$\begin{aligned}
\frac{D}{Dt} &= \frac{\partial}{\partial t} + u_r\frac{\partial}{\partial r} + \frac{u_\theta}{r}\frac{\partial}{\partial \theta} + u_z\frac{\partial}{\partial z}, \\
\nabla^2 &= \frac{\partial^2}{\partial r^2} + \frac{1}{r}\frac{\partial}{\partial r} + \frac{1}{r^2}\frac{\partial}{\partial \theta^2} + \frac{\partial}{\partial z^2}.
\end{aligned} \tag{2.47}$$

Blood is polarised, i.e. has electrical charges due to the presence of ions illustrated in figure (2.3). Blood is then a biomagnetic fluid (BFD), which brings into play the elements of magnetohydrodynamics, in particular the study of the magnetic field. If a magnetic material flows in a magnetic field, it experiences an electromotive force which results in an electric current flowing. By applying a magnetic field to an electrically conductive fluid such as blood, an electromagnetic force is generated due to the interaction of the current with the magnetic field.
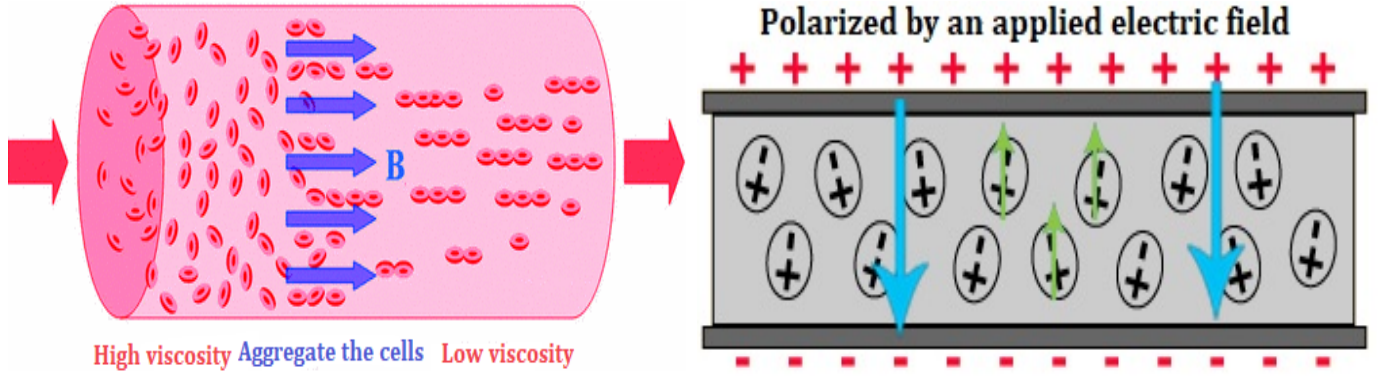
Figure 2.3: Polarisation in the vessel [116, 117].

This study of the influence of the magnetic field in an elastic tube takes into account Maxwell's second law of Newton's law for moving particles which is given by

$$\nabla.\overrightarrow{B} = 0, \quad \nabla \times \overrightarrow{B} = \mu_0 \overrightarrow{J}, \quad \nabla \times \overrightarrow{E} = -\frac{\partial \overrightarrow{B}}{\partial t}, \tag{2.48}$$

where B is the magnetic flux intensity, μ_0 is the magnetic permeability, E is the electric field intensity and J is the current density given by $\overrightarrow{J} = \sigma(\overrightarrow{E} + \overrightarrow{U} \times \overrightarrow{B})$. σ being the electrical conductivity and U the velocity field. The electromagnetic force F_{em} is given by

$$\begin{aligned}
\overrightarrow{F_{em}} &= \overrightarrow{J} \times \overrightarrow{B}, = \sigma(\overrightarrow{E} + \overrightarrow{U} \times \overrightarrow{B}) \times \overrightarrow{B}, = \sigma[\overrightarrow{E} \times \overrightarrow{B} + (\overrightarrow{U}.\overrightarrow{B})\overrightarrow{B} - B^2\overrightarrow{U}], \\
&= \sigma B_0^2 U(r,t) \overrightarrow{k},
\end{aligned} \tag{2.49}$$

where k is the unit vector in the z-direction and $\overrightarrow{U} = U(r,t)\overrightarrow{k}$ is the axial velocity of the blood. The force F_{em} will be included in the momentum equations. We can write the Navier-Stokes equations of motion in the cylindrical coordinates in the form

$$\begin{aligned}
\frac{\partial u_r}{\partial t} + u.\nabla u_r - \frac{u_\theta^2}{r} + \frac{1}{\rho}\frac{\partial p}{\partial r} &= \nu\left[\Delta u_r - \frac{u_r}{r^2} - \frac{2}{r^2}\frac{\partial u_\theta}{\partial \theta}\right] - \frac{\sigma B_0^2 u_r}{\rho}, \\
\frac{\partial u_\theta}{\partial t} + u.\nabla u_\theta + \frac{u_r u_\theta}{r} + \frac{1}{\rho r}\frac{\partial p}{\partial \theta} &= \nu\left[\Delta u_\theta - \frac{u_\theta}{r^2} + \frac{2}{r^2}\frac{\partial u_r}{\partial \theta}\right] - \frac{\sigma B_0^2 u_\theta}{\rho}, \\
\frac{\partial u_z}{\partial t} + u.\nabla u_z + \frac{1}{\rho}\frac{\partial p}{\partial z} &= \nu\Delta u_z - \frac{\sigma B_0^2 u_z}{\rho}.
\end{aligned} \tag{2.50}$$

Under the gradient effect of pressure, the dense fluid is moving slowly than the light fluid.

2.3 Flow in rotating fluids.

In this part, we would be talking about the dynamics of fluid in rotating systems, which is an interesting subject to researchers as it enables them understand the application of fluid dynamics in a number of important problems.

The theory of rotating fluids has brought out several inventive ideas, the characteristics of which are the constraint on fluid motion imposed by the control of rotational forces; the uniqueness of oscillatory motions, inertial oscillations and inertial waves; and a viscous boundary layer produced by the rotational forces. This field thus contains two main branches, namely:

- Inertial waves that describe the motion of an inviscid fluid in a rotating system.

- Convective instabilities which are reflected in the convective motion in thermal buoyancy.

These problems are governed by the Poincaré equations, and several systems were discussed by Greenspan in (1968) [118] and by Chandrasekhar in (1961) [119] on the formulation of their different geometries. Their studies have brought together these theories of inertial waves, thermal convections and precessions or librationally driven oscillations in rotating fluids. These studies were carried out experimentally in different geometries: an annular channel, a circular cylinder, and a spherical shell. For liquids without free surface effects, we can cite among others Malkus (1968) [120], Davies-Jones and Gilman (1971) [121], Benton and Clark (1974) [122] etc. .

In order to better observe the rotary motion of blood fluid in the presence of nanoelements, these theories will be implemented in our models to observe their interactions and the role they play in the cardiovascular system.

2.3.1 Rotating coordinates.

Let $U = U_x \hat{x} + U_y \hat{y} + U_z \hat{z}$ any vector in a rotating frame, where (U_x, U_y, U_z) are the components of U in the rotating coordinates and $(\hat{x}, \hat{y}, \hat{z})$ the unit vectors. Considering the velocity $\vec{u} = \Omega \times \vec{r}$ shows in figure (2.4), it is equivalent to $\frac{D\mathbf{r}}{Dt} = \Omega \times \mathbf{r}$. In rotating frame,

$$\left(\frac{DU}{Dt}\right)_R = \hat{x}\frac{DU_x}{Dt} + \hat{y}\frac{DU_y}{Dt} + \hat{z}\frac{DU_z}{Dt}. \tag{2.51}$$

Hence, the derivation of U in the inertial frame of reference is given by:

$$\begin{aligned}
\left(\frac{DU}{Dt}\right)_I &= \hat{x}\frac{DU_x}{Dt} + \hat{y}\frac{DU_y}{Dt} + \hat{z}\frac{DU_z}{Dt} + \frac{D\hat{x}}{Dt}U_x + \frac{D\hat{y}}{Dt}U_y + \frac{D\hat{z}}{Dt}U_z \\
&= \hat{x}\frac{DU_x}{Dt} + \hat{y}\frac{DU_y}{Dt} + \hat{z}\frac{DU_z}{Dt} + \Omega \times (\hat{x}U_x + \hat{y}U_y + \hat{z}U_z) \\
&= \left(\frac{DU}{Dt}\right)_R + \Omega \times U.
\end{aligned} \tag{2.52}$$

2.3.2 Equation of motions in rotating system.

The formulations observed above have led us to consider conditions that will be given through terms with a rotating structure. Thus the equations of motion and Navier-Stockes given in (2.40), will
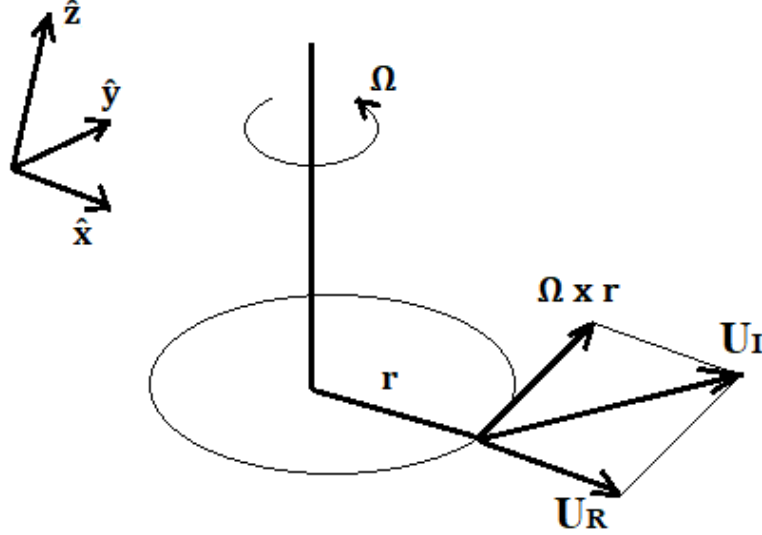
Figure 2.4: Illustrative diagram of a rotating system.

be modified by taking into account the nature of the fluid and the rotations in a boundary domain from the angular velocity, hence the expression for the velocity which is given by:

$$u_I = u_R + \Omega \times \mathbf{r}, \tag{2.53}$$

with $\mathbf{r}$ the position vector of the fluide in the rotating frame, I and R refer to inertial and rotaing frames of references. Then, the acceleration in the rotating frame is given by:

$$
\begin{aligned}
\frac{Du_I}{Dt} &= \left[\left(\frac{D}{Dt} \right)_R + \Omega \times \right] (u_R + \Omega \times \mathbf{r}), \\
&= \left(\frac{Du_R}{Dt} \right)_R + \Omega \times \frac{D\mathbf{r}}{Dt} + \Omega \times u_R + \Omega \times (\Omega \times \mathbf{r}) + \left(\frac{D\Omega}{Dt} \right)_R \times \mathbf{r}, \\
&= \frac{Du_R}{Dt} + 2\Omega \times u_R + \Omega \times (\Omega \times \mathbf{r}) + \left(\frac{D\Omega}{Dt} \right)_R \times \mathbf{r},
\end{aligned}
\tag{2.54}
$$

with $2\Omega \times u_R$ characterizing the Coriolis force, $\Omega \times (\Omega \times \mathbf{r})$ denoting the centrifugal force, and $\left(\frac{D\Omega}{Dt} \right)_R \times \mathbf{r}$ relating to the Eulerian force.

In the uniformly rotating frames, the Eulerian force is zero: $\frac{D\Omega}{Dt} = 0$. This leads us to derive the acceleration in the rotating frame as a function of the inertial acceleration, predefined in equation (2.40). We have:

$$\frac{\partial u_R}{\partial t} + (u \cdot \nabla)u = f - \nabla P + \mu \left[\nabla^2 u_R + \frac{1}{3} \nabla(\nabla \cdot u) \right] - 2\Omega \times u_R + \Omega \times (\Omega \times r) \tag{2.55}$$

Considering (2.41) for an incompressible fluid with the presence of an external force and removing the subscript R, the modified Navier-Stockes equation in a rotating system can be put into the form:

$$
\begin{aligned}
&\nabla u = 0 \\
&\frac{\partial u}{\partial t} + (u \cdot \nabla)u + 2\Omega \times v + \Omega \times (\Omega \times r) = f - \nabla P + \mu [\nabla^2 u].
\end{aligned}
\tag{2.56}
$$

2.4 Models used in the thesis

2.4.1 Fractional model with external magnetic field and thermal radiations.

In the first model, we are interested in the effect of the magnetic field for heat distributions, which was not the case in the studies conducted by Ali *et al.* [126]. This first model also complements the studies carried out by Bansi *et al.* [41]. The effect of the coupling between temperature and velocity via haemoglobin and particle acceleration forces according to Newton's second law will be taken into account in this modified model. Blood considering as a non Newtonian fluid, is assumed to flow in a cylindrical vessel of radius R_0, together with magnetic particles (see figure (2.6)).
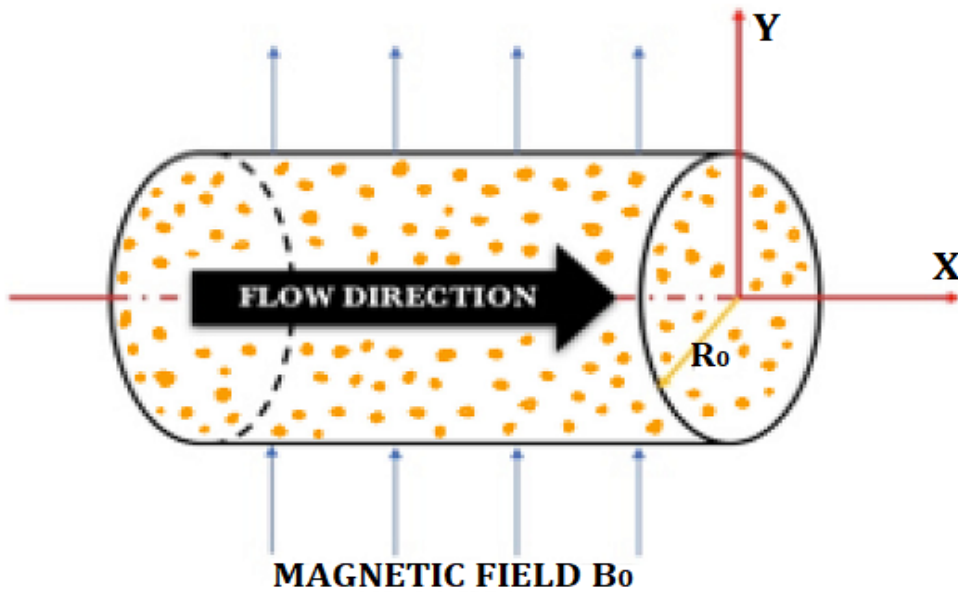
Figure 2.5: Schematic representation of the geometry model with orange spots being the magnetic particles.

This makes a two-phase mixture, with a solid phase consisting of magnetic particles and a liquid phase being the blood. We consider the magnetic particles to be uniformly distributed in the blood, while the ensemble flows in the axial direction x of the vessel. The magnetic field acts perpendicular to the vessel and the induced magnetic field is neglected because of the smallness of the magnetic Reynold's number [123]. The particles, the tube and the blood inside are supposed to be at rest at t = 0. Particles are subjected to an electromotive force resulting from the interaction of current with the magnetic field. Its expression can be found in Refs. [20, 124, 125] in the form

$$\vec{f}em = -\sigma B_0^2 U(r,t)\vec{i} \tag{2.57}$$

with $\vec{i}$ being the unit vector in the x-direction and $U(r,t)$, the axial velocity of the blood. B_0 is a uniform magnetic field and σ the electrical conductivity. The equation describing the motion of

magnetic particles is governed by the Newton's second law and is given in the form [20, 124, 125]

$$m\frac{\partial V}{\partial t} = K(U - V) \tag{2.58}$$

where K is the Stokes constant, m is the average mass of the magnetic particles and V is the velocity of the particles. The unsteady pulsatile flow of blood in an axisymmetric cylindrical blood vessel of radius R, considered to be affected by a uniform transverse magnetic field B_0 is governed by the following momentum equation in polar coordinates [11, 41]

$$\rho\frac{\partial U}{\partial t} = -\frac{\partial P}{\partial x} + \frac{1}{r}\frac{\partial}{\partial r}\left(r\mu\frac{\partial U}{\partial r}\right) + KN(V - U) - \sigma B_0^2 U \tag{2.59}$$

where P is the blood pressure. μ, σ and ρ are the dynamic coefficient of viscosity, the electrical conductivity and the density of blood, respectively. N is the number of magnetic particles per unit volume. The first three terms on the right-hand side of Eq. (2.59) represent the pressure gradient, the viscosity and the force generated by the relative motion between the fluid and the particle. The last term stands for the Lorentz force brought by the magnetic field. The oscillating pressure gradient $\frac{\partial P}{\partial x}$ is given by

$$-\frac{\partial P}{\partial x} = b_0 + b_1\cos(\omega t), \quad t > 0. \tag{2.60}$$

where b_0 and b_1 are the amplitude of the systolic and diastolic pressure gradient, respectively [124, 41, 127], with ω being the frequency. Eq. (2.59) can also be rewritten, by introducing the kinematic viscosity $\hat{\mu} = \mu/\rho$, as

$$\frac{\partial U}{\partial t} = -\frac{1}{\rho}\frac{\partial P}{\partial x} + \frac{1}{r}\frac{\partial}{\partial r}\left(r\hat{\mu}\frac{\partial U}{\partial r}\right) + \frac{KN}{\rho}(V - U) - \frac{\sigma B_0^2 U}{\rho} \tag{2.61}$$

The energy equation, related to thermal radiation is given by [4,5]

$$\rho C_p\frac{\partial T}{\partial t} = \kappa\frac{1}{r}\frac{\partial}{\partial r}\left(r\frac{\partial T}{\partial r}\right) - \frac{\partial q_r}{\partial r} + \mu\left(\frac{\partial U}{\partial r}\right)^2, \quad t > 0, \ r \in [0, R_0], \tag{2.62}$$

where the term $\mu\left(\frac{\partial U}{\partial r}\right)^2$ in (2.62) represents the viscous dissipation due to the assumption of the unidirectional flow. C_p and κ represent the specific heat at constant pressure and thermal conductivity. The radiative flux q_r p is written assuming that blood is an optically thin fluid with a relatively low density and heat absorption coefficient. q_r can then be simplified as proposed by Cogley et al. [128] in the form

$$\begin{aligned}
\frac{\partial q_r}{\partial r} &= 4\alpha^2(T - T_\infty), \\
\frac{\partial U}{\partial z} &= 0, \quad T = T_\infty \quad on \quad r = 0 \\
U &= 0, \quad T = T_w \quad on \quad r = R_0
\end{aligned} \tag{2.63}$$

where $\alpha^2 = \int_0^\infty \phi\chi\frac{\partial B}{\partial T}$ is the linear Planck mean absorption coefficient, with B and ϕ being respectively the Planck's constant and radiation absorption coefficient, and χ being the frequency. The above formulated models equations correspond to the initial and boundary conditions

$$U(r,0) = 0, \quad V(r,0) = 0, \quad T(r,0) = T_\infty, \quad r \in [0, R_0];$$
$$U(R_0,t) = 0, \quad V(R_0,t) = 0, \quad T(R_0,t) = T_w, \quad t > 0. \tag{2.64}$$

The set of model Eqs. (2.58), (2.59) and (2.62) can be generalized to their time-fractional versions by multiplying each of them by $\lambda = \sqrt{\frac{R_0\rho}{b_0}}$. This leads to the fractional-order equations

$$\lambda^a D_t^a U = \frac{\lambda}{\rho}[b_0 + b_1\cos(\omega t)] + \lambda\widehat{\mu}\left[\frac{\partial^2 U}{\partial r^2} + \frac{1}{r}\frac{\partial U}{\partial r}\right] - \frac{\lambda KN}{\rho}(V - U) - \frac{\lambda\sigma B_0^2}{\rho}U,$$

$$\lambda^a D_t^a V = \frac{\lambda K}{m}(U - V), \tag{2.65}$$

$$-\lambda^a D_t^a T = -\frac{\kappa}{\rho C_p}\left(\frac{\partial^2 T}{\partial r^2} - \frac{1}{r}\frac{\partial T}{\partial r}\right) + \frac{4\alpha^2}{\rho C_p}(T - T_\infty) + \frac{\mu}{\rho C_p}\left(\frac{\partial U}{\partial r}\right)^2,$$

where

$$D_t^a f(r,t) = \frac{1}{\Gamma(1-a)}\int_0^t \frac{1}{(t-\tau)^a}\frac{\partial f(r,\tau)}{\partial\tau}d\tau, \tag{2.66}$$

is the Caputo fractional derivative of order a [129–132]. In the meantime, recent works have developed new directions in fractional derivative operators and using Mittag-Leffler functions. For example, a new definition of fractional derivative, with a smooth kernel which considers two different representations for the temporal and spatial variable, was proposed in [133]. Operators including the Atangana-Beleanu derivative and the Caputo-Fabrizio derivative, respectively related to the Mittag-Leffler law and the exponential law were applied to the non-linear Kaup-Kupershmidt equation [134]. Making use of the traditional Caputo derivative and Caputo-Fabrizio derivative with fractional order and no singular kernel, the nonlinear Kaup-Kupershmidt was extended to the span of fractional calculus by Atangana and Doungmo [135]. Moreover, further relationship and new results of Atangana-Baleanu derivative, with some integral transform operators, were obtained from a simple nonlinear system [136]. Another important feature of the non-local and non-singular kernel operator was pointed out and applied to chaotic models whose the bifurcation, period doubling dynamics and chaotic behaviors were discussed [137, 138]. In addition, the Atangana-Baleanu fractional derivative with non-singular kernel and non-local kernel was applied to chaotic processes with two-parameter derivative, including non-singular and non-local kernel based on the one-parameter Mittag-Leffler function [137, 138]. To further proceed, the following dimensionless variables can be introduced

$$r = \frac{r^*}{R_0}, \quad t^* = \frac{t}{\lambda}, \quad U = \frac{U^*}{U_0}, \quad V = \frac{V^*}{U_0}, \quad b_0^* = \frac{\lambda b_0}{\rho U_0}, \quad b_1^* = \frac{\lambda b_1}{\rho U_0}, \quad \omega^* = \lambda\omega, \quad T^* = \frac{T - T_\infty}{T_w - T_\infty}. \tag{2.67}$$

Considering all the above and dropping the (∗) notation, we get the following fractionalized set of

equations

$$D_t^a U = [b_0 + b_1 \cos(\omega t)] + \frac{1}{R_e}\left[\frac{\partial^2 U}{\partial r^2} + \frac{1}{r}\frac{\partial u}{\partial r}\right] - R(V - U) - \mathcal{H}^2 U,$$

$$G.D_t^a V = U - V \tag{2.68}$$

$$- D_t^\alpha T + \frac{k}{\rho C_p}\left(\frac{\partial^2 T}{\partial r^2} + \frac{1}{r}\frac{\partial T}{\partial r}\right) - \frac{4\alpha^2}{\rho C_p}T = -\frac{\hat{\mu}}{\rho C_p}\left(\frac{\partial U}{\partial r}\right)^2$$

where $R_e = \frac{R_0^2}{\lambda\hat{\mu}}$ is a Reynold number, $R = \frac{KN\lambda}{\rho}$ is a particle concentration parameter, $\mathcal{H}^2 = B_0^2 R_0\sqrt{\frac{\sigma}{\hat{\mu}}}$ is a magnetic parameter or Hartmann number, $G = \frac{m}{K\lambda}$ is the particle mass parameter. The initial and boundary conditions are

$$U(r,0) = 0, \quad V(r,0) = 0, \quad T(r,0) = 0, \quad r \in [0,1];$$

$$U(1,t) = 0, \quad V(1,t) = 0, \quad T(1,t) = 0, \quad t > 0. \tag{2.69}$$

2.4.2 Modelling of fractional blood flow in the presence of nano elements.

The second model of our study contributes to the previous model [139], by observing in a more precise way the behaviour of the magnetized particles through their different thermo-physical properties and also through the geometrical form they may have. This observation will be done for an ensemble (fluid + particles) in a rotating system allowing to highlight the influence of microrotations on the blood dynamics. We consider an unstable viscous transient one-dimensional MHD blood and incompressible nanofluid flow on an extended sheet with a rotating frame. The structure has an oscillatory movement on time t and frequency n with velocity $u(0,t)$, which is given by $\bar{u}(0,\bar{t}) = U_0\sin(\bar{n}\bar{t})$, with U_0 a space-dependent Gaussian form [140]. Physically, we assume that the whole frame is at rest in time $t < 0$, however for $t = 0$ ($\bar{u}(0,0) = 0$), the sheet is stretched along the x direction at $r = 0$ with angular velocity (Ω). The viscoelastic liquid model is created through types of species that incorporate chemical reactions and Arrhenius activating energy. B_0 is a uniform (magnetic field) and applied with direction r, which is taken normal to $y-$ axis and crossing an exponential accelerated infinite vertical plate in $x-$ axis. Initially, at $t \leq 0$, the fluid and plate are stable, with temperature and concentration being constant. When $t > 0$, the plate is exponentially accelerated with $u = U_0\sin wt$; the surface temperature and concentration are raised to T_w and C_w, from their respective equilibrium values C_∞ and T_∞. The schematic representation of the configuration, with the coordinate system related to the problem, is given in Fig. 2.6.

Figure 2.6: Schematic representation of the physical system.

The modified model proposed in this work is inspired by the seminal contributions from Refs. [3, 41, 141, 142]. In fact, we make use of the usual approximation, and propose the flow to be governed by the following equations:

$$\frac{\partial w^*}{\partial r^*} = 0$$

$$\frac{\partial u^*}{\partial t^*} + w^* \frac{\partial u^*}{\partial r^*} - 2\Omega v^* = \frac{1}{\rho_{nf}} \left[\nu_{nf} \frac{\partial^2 u^*}{\partial r^{*2}} - \frac{\nu_{nf}}{k^*} u^* - (\sigma_{nf} B_0^2) u^* + g\rho_{nf}(\beta_T)_{nf}(T^* - T_\infty^*) \right.$$

$$\left. + g\rho_{nf}(\beta_C)_{nf}(C^* - C_\infty^*) \right],$$

$$\frac{\partial v^*}{\partial t^*} + w^* \frac{\partial v^*}{\partial r^*} + 2\Omega u^* = \frac{1}{\rho_{nf}} \left[\nu_{nf} \frac{\partial^2 v^*}{\partial r^{*2}} - \frac{\nu_{nf}}{k^*} v^* - (\sigma_{nf} B_0^2) v^* \right],$$

$$\frac{\partial T^*}{\partial t^*} + w^* \frac{\partial T^*}{\partial r^*} = \frac{k_{nf}}{(\rho C_t)_{nf}} \frac{\partial^2 T^*}{\partial r^{*2}} - \frac{1}{(\rho C_t)_{nf}} \frac{\partial q_r}{\partial r^*} - \frac{Q_H}{(\rho C_t)_{nf}}(T^* - T_\infty^*),$$

$$\frac{\partial C^*}{\partial t^*} + w^* \frac{\partial C^*}{\partial r^*} = D_B \frac{\partial^2 C^*}{\partial r^{*2}} + \frac{D_T}{T_\infty} \frac{\partial^2 T^*}{\partial r^{*2}} - K_r^2(C^* - C_\infty^*) \left(\frac{T^*}{T_\infty^*} \right)^m \exp\left(\frac{-E_a}{K_B T^*} \right),$$

(2.70)

where u^* represents the axial velocity, T^* and C^* are the temperature and concentration of the solute, B_0 is the applied magnetic field, g, σ_{nf} and ρ_{nf} are, respectively, the acceleration due to the gravity, electrical conductivity and Density of blood, $C_{t_{nf}}$, k_{nf}, and ν_{nf} represent, respectively, the specific heat at constant pressure, thermal conductivity and dynamic viscosity of nanofluid, D_B is the molecular diffusivity, k^* is the permeability of the porous medium, K_r^2 is the reaction rate, m is a fitted rate constant, k_{tnf} is the thermal diffusion ratio of nanofluid, k_{cnf} is the chemical reaction

parameter of nanofluid and T_m is the mean fluid temperature, w^* is a velocity component along z axe, v^* is a velocity component along y axe, D_T is the thermal diffusivity.

Table 1.1, shows us the contribution of the shape of different nanoparticles representing by sphericity ψ in Refs [5, 144, 146]. In this study, the base fluid is a blood, with $SWCNTs$, Al_2O_3, T_iO_2 and Cu based nanoparticles. The thermophysical properties of the nanofluids are presented in Table 1.2 [5, 145, 146]. The coefficient of thermal expansion and the density of nanofluid are taken to be [143, 147]

$$(\rho\beta)_{nf} = (1-\psi)(\rho\beta)_f + \psi(\rho\beta)_p, \quad \rho_{nf} = (1-\psi)\rho_f + \psi\rho_p, \quad (\rho C_t)_{nf} = (1-\psi)(\rho C_t)_f + \psi(\rho C_t)_p,$$

$$\nu_{nf} = \frac{\nu_f}{(1-\psi)^{2.5}}, \quad \frac{\sigma_{nf}}{\sigma_f} = 1 + \frac{3\left(\frac{\sigma_p}{\sigma_f}-1\right)\psi}{\left(\frac{\sigma_p}{\sigma_f}+2\right)-\psi\left(\frac{\sigma_p}{\sigma_f}-1\right)}, \quad \frac{k_{nf}}{k_f} = \frac{(k_p+(m-1)k_f)-(m-1)\psi(k_f-k_p)}{(k_p+(m-1)k_f)+\psi(k_f-k_p)},$$

$$(2.71)$$

where ψ is the solid volume fraction. The indexes nf, f, p denote, respectively, the nanofluid, fluid and nanosolid particles. The initial and boundary conditions for the problem are:

$$t^* < 0: \quad u^* = 0, \quad v^* = 0, \quad T^* = T_w^* + (T_w^* - T_\infty^*),$$
$$C^* = C_w^* + (C_w^* - C_\infty^*), \quad \text{at} \quad \text{for all} \quad r^*;$$
$$t^* \geq 0: \quad u^* = 0, \quad v^* = 0, \quad T^* = T_w^*, \quad C^* = C_w^*, \quad \text{at} \quad r^* = 0; \qquad (2.72)$$
$$t^* > 0: \quad u^* \longrightarrow 0, \quad v^* \longrightarrow 0, \quad T^* \longrightarrow T_\infty^*,$$
$$C^* \longrightarrow C_\infty^* \quad \text{as} \quad r^* \longrightarrow \infty.$$

Using the Rosseland approximation for radiation [3, 141], the radiative heat flux is simplified as $q_r = -\dfrac{4\sigma^*}{3\beta_R}\dfrac{\partial T^{*'4}}{\partial r^*}$, where σ^* is the Stefan-Boltzman fluid constant and β_R is the coefficient of mean absorption.

It is assumed that: $T^{*'4} = 4T_\infty^{*3}T^* - 3T_\infty^{*4}$ then, $\dfrac{\partial q_r}{\partial r^*} = -\dfrac{16\sigma^* T_\infty^{*3}}{3\beta_R}\dfrac{\partial^2 T^*}{\partial r^{*2}}$.

Substituting the above into the equation of temperature in system (2.70), we obtain

$$\frac{\partial T^*}{\partial t^*} + w^*\frac{\partial T^*}{\partial r^*} = \frac{k_{nf}}{(\rho C_t)_{nf}}\frac{\partial^2 T^*}{\partial r^{*2}} + \frac{16\sigma_{nf}^* T_\infty^{*3}}{3(\rho C_t)_{nf}\beta_R}\frac{\partial^2 T^*}{\partial r^{*2}} - \frac{Q_H(T^* - T_\infty^*)}{(\rho C_t)_{nf}}. \qquad (2.73)$$

Our study will mainly focus on velocities perpendicular to the applied magnetic field, then we consider the solution of the first equation of (2.70) as: $w^* = -w_0$. We introduce the following dimensionless variables and parameters:

$$r = \frac{r^* U_0}{\nu_f}, \quad t = \frac{U_0^2 t^*}{\nu_f \rho_f}, \quad u = \frac{u^*}{U_0 \rho_f^2}, \quad v = \frac{v^*}{U_0 \rho_f^2}, \quad n = n^*\frac{\nu_f \rho_f}{U_0^2}, \quad \theta = \frac{T^* - T_\infty^*}{T_w^* - T_\infty^*}, \quad \phi = \frac{C^* - C_\infty^*}{C_w^* - C_\infty^*}. \qquad (2.74)$$

These equations and conditions are obtained after the transformations

$$\frac{\partial u}{\partial t} - S\frac{\partial u}{\partial r} - Rv = \frac{1}{E_1 E_3}\frac{\partial^2 u}{\partial r^2} - \frac{K_p}{E_1 E_3}u - \frac{E_6 M^2}{E_3}u + \frac{E_4 G_r}{E_3}\theta + \frac{E_7 G_m}{E_3}\phi,$$

$$\frac{\partial v}{\partial t} - S\frac{\partial v}{\partial r} + Ru = \frac{1}{E_1 E_3}\frac{\partial^2 v}{\partial r^2} - \frac{K_p}{E_1 E_3}v - \frac{E_6 M^2}{E_3}v,$$

$$\frac{\partial \theta}{\partial t} - S\frac{\partial \theta}{\partial r} = \frac{1}{P_r}\left[\frac{E_2}{E_5}\frac{\partial^2 \theta}{\partial r^2} - \frac{Q}{E_5}\theta\right],$$

$$\frac{\partial \phi}{\partial t} - S\frac{\partial \phi}{\partial r} = \frac{1}{L_e}\left[\frac{\partial^2 \phi}{\partial r^2} + \frac{N_t}{N_b}\frac{\partial^2 \theta}{\partial r^2}\right] - Le\lambda^*(1+\gamma\theta)^m \exp\left(\frac{-EE}{1+\gamma\theta}\right)\phi,$$

(2.75)

where $\lambda^* = \Omega^* D_B$ is the chemical reaction rate, with $\Omega^* = \frac{K_r^2 \rho_f^2}{U_0^2}$, a function of reaction rate K_r^2,

$P_r = \frac{(C_t)_f \nu_f}{k_f}$ is the Prandtl number, $S = \frac{w_0 \rho_f}{U_0}$ is the suction parameter, $M = \sqrt{\frac{\sigma_f B_0^2 \nu_f}{U_0^2}}$ is the

magnetic parameter, $R_e = \frac{U_0^2}{\nu_f \rho_f}$ is the Reynold number, $R = \frac{2\Omega}{Re}$ is the rotating parameter, $G_r =$

$\frac{g(\beta_T)_f \nu_f (T_w^* - T_\infty^*)}{U_0^3 \rho_f}$ is the thermal Grashof number, $G_m = \frac{g(\beta_C)_f \nu_f (C_w^* - C_\infty^*)}{U_0^3 \rho_f}$ is the mass Grashof

number, $Q = \frac{Q_H \nu_f^2}{k_f U_0^2}$ is the heat source, $Le = \frac{\nu_f}{D_B \rho_f}$ is the Lewis number, $N_b = \frac{\tau D_B(C_w^* - C_\infty^*)}{\nu_f C_\infty^*}$ is

the Brownian motion, $N_t = \frac{\tau D_T(T_w^* - T_\infty^*)}{\nu_f T_\infty^*}$ is the thermophoresis parameter, $\gamma = \frac{T_w^* - T_\infty^*}{T_\infty^*}$ is the

thermal relaxation parameter, $EE = \frac{E_a}{K_B T_\infty^*}$ is an activation energy, $K_p = \frac{\nu_f^2}{k^* U_0^2}$ is the porosity

parameter, $F = \frac{4\sigma^* T_\infty^{*3}}{\beta_R k_f}$ is the radiation parameter, $(\beta_T)_f$ is the thermal expansion of fluid for the

case of temperature, $(\beta_C)_f$ is the thermal expansion of fluid for the case of concentration, $(\rho C_t)_f$ is

the product of density and the specific heat for the case of base fluid, ρ_f is the density of base fluid,

$(C_t)_f$ is the specific heat for the case of base fluid, T_∞^* is temperature of the ambient fluid, C_∞^* is

concentration of the ambient fluid, with

$$E_1 = (1-\psi)^{2.5}, \; E_2 = \frac{k_{nf}}{k_f} + \frac{4F}{3}, \; E_3 = 1 - \psi + \psi\left(\frac{\rho_p}{\rho_f}\right), \; E_4 = 1 - \psi + \psi\left(\frac{(\rho\beta_T)_p}{(\rho\beta_T)_f}\right),$$

$$E_5 = 1 - \psi + \psi\left(\frac{(\rho C_t)_p}{(\rho C_t)_f}\right), \; E_6 = 1 + \frac{3\left(\frac{\sigma_p}{\sigma_f}-1\right)\psi}{\left(\frac{\sigma_p}{\sigma_f}+2\right) - \psi\left(\frac{\sigma_p}{\sigma_f}-1\right)}, \; E_7 = 1 - \psi + \psi\left(\frac{(\rho\beta_C)_p}{(\rho\beta_C)_f}\right).$$

(2.76)

$(\beta_T)_{nf}, (\beta_T)_f, (\beta_C)_{nf}, (\beta_C)_f$ are notations of the thermal expansion to distinguish the Grashof case temperature and concentration in the system, for reasons of transformations and equivalence. But thereafter, they are taken identical in the numerical program since a particle has a unique β, the values of the parameter $(\beta_C)_p$ not being given in the literature.

To generalize (2.75), we have applied the definition of Caputo fractional derivate operator. Then,

the corresponding fractional model is formulated as

$$
\begin{aligned}
_cD_t^\alpha u =& \frac{1}{E_1 E_3}\frac{\partial^2 u}{\partial r^2} - \frac{K_p}{E_1 E_3}u - \frac{E_6 M^2}{E_3}u + \frac{E_4 G_r}{E_3}\theta + \frac{E_7 G_m}{E_3}\phi + S\frac{\partial u}{\partial r} + Rv,\\
_cD_t^\alpha v =& \frac{1}{E_1 E_3}\frac{\partial^2 v}{\partial r^2} - \frac{K_p}{E_1 E_3}v - \frac{E_6 M^2}{E_3}v + S\frac{\partial v}{\partial r} - Ru,\\
_cD_t^\alpha \theta =& \frac{1}{P_r}\left[\frac{E_2}{E_5}\frac{\partial^2 \theta}{\partial r^2} - \frac{Q}{E_5}\theta\right] + S\frac{\partial \theta}{\partial r},\\
_cD_t^\alpha \phi =& \frac{1}{L_e}\left[\frac{\partial^2 \phi}{\partial r^2} + \frac{N_t}{N_b}\frac{\partial^2 \theta}{\partial r^2}\right] - Le\lambda^*(1+\gamma\theta)^m \exp\left(\frac{-EE}{1+\gamma\theta}\right)\phi + S\frac{\partial \phi}{\partial r},
\end{aligned}
\tag{2.77}
$$

where

$$
D_t^\alpha f(r,t) = \frac{1}{\Gamma(1-\alpha)}\int_0^t \frac{1}{(t-\tau)^\alpha}\frac{\partial f(r,\tau)}{\partial \tau}d\tau, \quad 0 < \alpha < 1,
\tag{2.78}
$$

is the Caputo fractional derivative operator of order $0 < \alpha \leq 1$ [148, 149, 151]. The corresponding boundary conditions become:

$$
\begin{aligned}
t < 0 : & \quad u = 0, \quad v = 0, \quad \theta = 0, \quad \phi = 0, \quad \text{at} \quad r \geq 0,\\
t \geq 0 : & \quad u = 0, \quad v = 0, \quad \theta = 1, \quad \phi = 1, \quad \text{at} \quad r = 0,\\
t > 0 : & \quad u \longrightarrow 0, \quad v \longrightarrow 0, \quad \theta \longrightarrow 0, \quad \phi \longrightarrow 0 \quad \text{as} \quad r \longrightarrow \infty.
\end{aligned}
\tag{2.79}
$$

2.4.3 Fractional model with superdiffusive effect in the medium.

After being interested in the influence of microrotations in the previous model, the interest in better understanding these rotational actions on the temperature in the vessels has captured our attention. We are now in the situation where the blood flow dynamics have strong and very varied fluctuations, under the presence of nano-elements and to have an observation on their behavior in a super diffusive medium. So, we are looking for the behaviour of nano hybrids in a highly diffusive medium in micro dimensional motions. The diagram of the configuration with the coordinate system of the developed problem is sketched in figure (2.7).
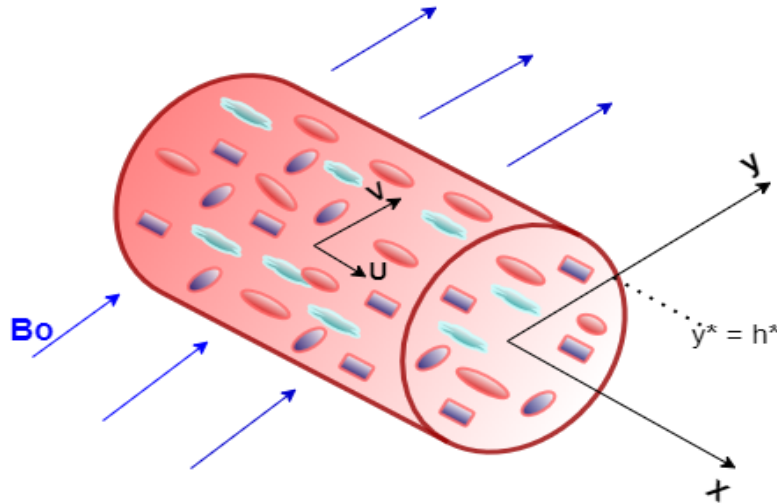
Figure 2.7: Schematic diagram of the physical system.

The proposed model is inspired by Misra *et al.* [150], with some usual approximations. The flow is governed by the following equations:

$$\begin{cases} \dfrac{\partial v^*}{\partial y^*} = 0 \\[2mm] \dfrac{\partial u^*}{\partial t^*} + v^* \dfrac{\partial u^*}{\partial y^*} = -\dfrac{1}{\rho_{nf}} \dfrac{\partial p^*}{\partial x^*} + \nu_{nf} \dfrac{\partial^2 u^*}{\partial y^{*2}} - \dfrac{\eta_1}{\rho_{nf}} \dfrac{\partial^4 u^*}{\partial y^{*4}} + g(\beta_T)_{nf}(T^* - T_\infty^*), \\[2mm] \dfrac{\partial T^*}{\partial t^*} + v^* \dfrac{\partial T^*}{\partial y^*} = \dfrac{(k_0)_{nf}}{(\rho C_p)_{nf}} \dfrac{\partial^2 T^*}{\partial y^{*2}} - \dfrac{(k_1)_{nf}}{(\rho C_p)_{nf}} \dfrac{\partial T^4}{\partial y^{*4}} + \dfrac{(\mu + k)_{nf}}{(\rho C_p)_{nf}} \left(\dfrac{\partial u^*}{\partial y^*} \right)^2 + \dfrac{\sigma_{nf} B_0^2 u^{*2}}{(\rho C_p)_{nf}}, \end{cases}$$ (2.80)

where u^* represents axial velocity, T^* is the temperature of the solute, B_0 being the applied magnetic field, g, σ_{nf} and ρ_{nf} are acceleration due to the gravity, electrical conductivity and Density of blood, C_p is the specific heat at constant pressure, k_0 is a thermal conductivity, η_1 is a constant associated with the couple stress tensor, k_1 is a thermal conductivity associated with the stress tensor, k is a rotational viscosity, T_∞ is a blood reference temperature.

In order to specify our problem, it is necessary to prescribe that, for $t > 0$, the pressure gradient $\frac{\partial P}{\partial z}$, which determines the nature of the flow has the expression of the form

$$-\dfrac{\partial p^*}{\partial x^*} = A_0^* + A_1^* \cos(\omega^* t^*).$$ (2.81)

where A_0^* is the constant amplitude of pressure gradient, A_1^* the amplitude of pulsatile component gives rise to systolic and diastolic pressure, and ω the frequency. Table 1.1, shows the contribution of the shape of the different nanoparticles represented by the sphericity ψ in References [5, 144, 146]. In this study, the base fluid is blood, with the consideration of $SWCNTs$, $MWCNTs$, Fe_2O_3, T_iO_2 and CuO nanoparticles. Their thermophysical properties are used as shown in Table 1.2, and we consider the same expressions for the nanofluid properties given by (2.71).

The initial and boundary conditions for the problem are:

$$\begin{aligned} &\dfrac{\partial u^*}{\partial x^*} = 0, T^* = T_\infty^*, \quad \text{at} \quad y^* = R(x^*); \\ &u^* = 0, T^* = T_w^*, \quad \text{at} \quad y^* = 0; \\ &u^* \longrightarrow 0, T^* \longrightarrow T_\infty^*, \quad \text{as} \quad r^* \longrightarrow \infty, \end{aligned}$$ (2.82)

To consider the time-fractional model, we firstly multiply Eqs.(1) by $\lambda = \sqrt{\frac{R_0 \rho}{b_0}}$ which has the dimension of time. The corresponding transformation model, has recently introduiced by Shah *et al.* [182], used by Tabi *et al.* [139]. The governing equations of the time-fractional are

$$\lambda^\alpha D_t^\alpha u^* = \dfrac{\lambda}{\rho_{nf}}[A_0^* + A_1^* \cos(\omega^* t^*)] - \lambda v^* \dfrac{\partial u^*}{\partial y^*} + \lambda \nu_{nf} \dfrac{\partial^2 u^*}{\partial y^{*2}} - \dfrac{\lambda \eta_1}{\rho_{nf}} \dfrac{\partial^4 u^*}{\partial y^{*4}} + \lambda g(\beta_T)_{nf}(T^* - T_\infty^*),$$

$$\lambda^\alpha D_t^\alpha T^* = \dfrac{\lambda k_0}{(\rho C_p)_{nf}} \dfrac{\partial^2 T^*}{\partial y^{*2}} - \dfrac{\lambda k_1}{(\rho C_p)_{nf}} \dfrac{\partial T^{*4}}{\partial y^{*4}} - \lambda v^* \dfrac{\partial T^*}{\partial y^*} + \dfrac{\lambda(\mu + k)_{nf}}{(\rho C_p)_{nf}} \left(\dfrac{\partial u^*}{\partial y^*} \right)^2 + \dfrac{\lambda \sigma_{nf} B_0^2 u^{*2}}{(\rho C_p)_{nf}},$$ (2.83)

where the derivative operator is defined from the fractional order parameter of Caputo "α". We introduce the following dimensionless variables and parameters:

$$y = \frac{y^*}{R_0}, \ t = \frac{t^*}{\lambda}, \ u = \frac{u^*}{u_0}, \ v = \frac{v^*}{v_0}, \ A_0 = \frac{\lambda A_0^*}{\rho_f u_0}, A_1 = \frac{\lambda A_1^*}{\rho_f u_0}, \omega = \lambda \omega^*, \ T = \frac{T^* - T_\infty^*}{T_w^* - T_\infty^*}. \tag{2.84}$$

The boundary conditions are:

$$
\begin{aligned}
&t \leq 0 : u^*(y^*, 0) = 0, \ T^*(y^*, 0) = 0, \quad \text{at} \quad y^* \in [0, R_0], \\
&t > 0 : u^*(R_0, t^*) = 0, \ T^*(R_0, t^*) = 0,
\end{aligned}
\tag{2.85}
$$

Introducing the above (2.84) into (2.83) the whole problem reduced to its dimensionless form as follow:

$$
\begin{aligned}
&\lambda^\alpha D_t^\alpha u = \frac{1}{E_3}[A_0 + A_1 \cos(\omega t)] - Pv\frac{\partial u}{\partial y} + \frac{1}{E_1 E_3 Re}\frac{\partial^2 u}{\partial y^2} - \frac{R}{E_3}\frac{\partial^4 u}{\partial y^4} + \frac{E_4}{E_3}GrT, \\
&\lambda^\alpha D_t^\alpha T = \frac{E_2}{E_5 P_e}\frac{\partial^2 T}{\partial y^2} - \frac{E_2}{E_5 P_{e1}}\frac{\partial T^4}{\partial y^4} - P_1 v\frac{\partial T}{\partial y} + \frac{Da}{E_1 E_5 Q}\left(\frac{\partial u}{\partial y}\right)^2 + \frac{E_6 M^2 u^2}{E_5 Q},
\end{aligned}
\tag{2.86}
$$

with

$$E_1 = (1 - \psi)^{2.5}, \ E_2 = \frac{k_{nf}}{k_f}, \ E_3 = 1 - \psi + \psi\left(\frac{\rho_p}{\rho_f}\right), E_4 = 1 - \psi + \psi\left(\frac{(\rho\beta)_p}{(\rho\beta)_f}\right),$$

$$E_5 = 1 - \psi + \psi\left(\frac{(\rho C_p)_p}{(\rho C_p)_f}\right), E_6 = 1 + \frac{3\left(\dfrac{\sigma_p}{\sigma_f} - 1\right)\psi}{\left(\dfrac{\sigma_p}{\sigma_f} + 2\right) - \psi\left(\dfrac{\sigma_p}{\sigma_f} - 1\right)}.$$

The corresponding boundary and initial conditions are:

$$
\begin{aligned}
&t \leq 0 : u(y, 0) = 0, \ T(y, 0) = 0, \quad \text{at} \quad y \in [0, 1], \\
&t > 0 : u(1, t) = 0, \ T(1, t) = 0,
\end{aligned}
\tag{2.87}
$$

where $P_e = \frac{(\rho C_p)_f R_0^2}{\lambda k_0}$ is the Peclet number, $P_{e1} = \frac{(\rho C_p)_f R_0^4}{\lambda k_1}$ is the Peclet number modified, $M = B_0 R_0 \sqrt{\frac{\lambda \sigma_f u_0}{\rho_f}}$ is the magnetic parameter, $R_e = \frac{R_0^2}{\lambda \nu}$ is the Reynold number, $R = \frac{\lambda \eta_1}{\rho_f R_0^4}$ is the rotating parameter, $G_r = \frac{\lambda g \beta(T_w^* - T_\infty^*)}{u_0}$ is the thermal Grashof number, $Q = \frac{R_0^2 C_{p_f}(T_w^* - T_\infty^*)}{u_0}$ is the metabolic heat source, $D_a = \frac{(\mu + k E_1 E_2)u_0}{\rho_f}$ is the porosity parameter, $P = \frac{\lambda v_0}{R_0}$ is the radiation parameter.

2.5   Special Functions and Analytical Methods

To understand the definition and the use of fractional calculus, we will give some simple mathematical definitions and concepts of special functions, such as gamma function, Mittag-Leffler function, beta function and Laplace transform just to mention a few. Some general forms and the ways to solve them will be presented in the next section.

2.5.1 The Gamma Function

Gamma function or simply the Euler integral equation of the second kind is the most important function using in the fractional calculus. Assume z is a complex number with $\mathbf{Re}(z) > 0$, the integral is definied as

$$\Gamma(z) = \int_0^\infty t^{z-1} e^{-t} dt \tag{2.88}$$

The generalization of this function can be put in factorial form

$$\Gamma(n) = (n-1)! \text{ with } n \in \mathbb{N}^+, \tag{2.89}$$

where $\Gamma(1) = 1$. By considering the integration by parts technique, we can reach to the basic property of the next value

$$\Gamma(z+1) = z\Gamma(z), \quad z \in \mathbb{N}^+. \tag{2.90}$$

2.5.2 The Bessel Function

Daniel Bernoulli was the first to define a Bessel function and Friedrich Bessel generalize to the canonical solutions $y(x)$ of Bessel's differential equation [152]:

$$x^2 \frac{d^2 y}{dx^2} + x \frac{dy}{dx} + \left(x^2 - \alpha^2\right) y = 0. \tag{2.91}$$

where α is an arbitrary complex number and the order of the Bessel function. The same differential equation is obtained using α or $-\alpha$, and it is conventional to define different Bessel functions for these two values in such a way that the Bessel functions are mostly smooth functions of α [152].

★ **Bessel functions of the first kind** : J_α

$J_\alpha(x)$ denoted the Bessel functions of the first kind, are taken as solutions of Bessel's differential equation. For positive integer α, Bessel functions of the first kind are finite at the origin $(x = 0)$; while for negative non-integer α, they diverge as x approaches zero. It is possible to define the function by its series expansion around $x = 0$.

$$J_\alpha(x) = \sum_{m=0}^\infty \frac{(-1)^m}{m! \Gamma(m+\alpha+1)} \left(\frac{x}{2}\right)^{2m+\alpha}, \tag{2.92}$$

where $\Gamma(z)$ is the gamma function, a shifted generalization of the factorial function to non-integer values.

★ **Bessel functions of the second kind** : J_α

The Bessel functions of the second kind, denoted by $Y_\alpha(x)$, occasionally denoted instead by $N_\alpha(x)$, are solutions of the Bessel differential equation that have a singularity at the origin $(x = 0)$ and are multivalued. These are sometimes called Weber functions, as they were introduced by H. M. Weber

in 1873 [152], and also Neumann functions after Carl Neumann [153]. For non-integer α, $Y_\alpha(x)$ is related to $J_\alpha(x)$ by

$$Y_\alpha(x) = \frac{J_\alpha(x)\cos(\alpha\pi) - J_{-\alpha}(x)}{\sin(\alpha\pi)}. \tag{2.93}$$

2.5.3 The Mittag-Leffler function

The Mittag-Leffler function E_α, β is a special function and a complex function which depends on two complex parameters α and β. It may be defined by the following series when the real part of α is strictly positive

$$E_{\alpha,\beta}(z) = \sum_{k=0}^{\infty} \frac{z^k}{\Gamma(\alpha k + \beta)}, \ \alpha > 0, \ \beta > 0, \ \alpha, \beta \in \mathbb{R}, \ z \in \mathbb{C}, \tag{2.94}$$

where $\Gamma(x)$ is the gamma function. When $\beta = 1$, it is abbreviated as $E_\alpha(z) = E_{\alpha,1}(z)$. For $\alpha = 0$, the series above equals the Taylor expansion of the geometric series and consequently $E_{0,\beta}(z) = \frac{1}{\Gamma(\beta)} \frac{1}{1-z}$.

2.5.4 The Laplace Transform

In mathematics, the Laplace transform is an integral transformation of a function with real variable t (often time) to a function of a complex variables (complex frequency). This transformation has many applications in engineering and science [154]. Pierre-Simon Laplace used a similar transform in his work on probability theory. The definition of a function $f(t)$ using the Laplace transform, for all real numbers $(t \geqslant 0)$, is the function $F(s)$, which is a unilateral transform defined by

$$F(s) = \int_0^\infty f(t)e^{-st}dt, \tag{2.95}$$

where s is a complex number. The integral exists when the condition in f must be locally integrable on $[0, \infty)$. The inverse Laplace transform is given by Mellin's inverse formula:

$$f(t) = \mathcal{L}^{-1}\{F(s)\}(t) = \frac{1}{2\pi i} \lim_{T \to \infty} \int_{\gamma-iT}^{\gamma+iT} e^{st}F(s)ds, \tag{2.96}$$

where $\gamma = \mathbf{Re}(s)$. If the singularities are in the left half-plane or $F(s)$ is an entire function, then γ can be set to zero and the inverse Fourier transform becomes as same as the inverse integral formula above.

By solving partial differential equations. The transformation is defined by:

$$\mathcal{L}(u(x,t))(s) = U(x,s) = \int_0^\infty u(x,t)e^{-st}dt, \tag{2.97}$$

where $u(x,t)$ is a function with respect to variable x and t. We can get the relations [155]:

$$\mathcal{L}\left(\frac{\partial u}{\partial t}\right) = sU(x,s) - u(x,0), \tag{2.98}$$

$$\mathcal{L}\left(\frac{\partial^2 u}{\partial x^2}\right) = \frac{d^2 U}{dx^2}(x,s). \tag{2.99}$$

★ Convolution

The Laplace convolution is given by

$$f(t) * g(t) = \int_0^t f(t - \tau)g(\tau)d\tau = g(t) * f(t). \tag{2.100}$$

The convolution of two functions in the domain of t is somewhat complicated to solve, however, the convolution leads to simple function multiplication in the Laplace domain, that is,

$$\mathcal{L}(f(t) * g(t)) = F(s)G(s). \tag{2.101}$$

The Laplace transform of a derivative of integer order q of the function $f(t)$, is defined by

$$\mathcal{L}\{f^{(q)}(t)\} = s^q F(s) - \sum_{j=0}^{q-1} s^{q-j-1} f^{(j)}(0) = s^q F(s) - \sum_{j=0}^{q-1} s^q f^{(q-j-1)}(0). \tag{2.102}$$

The summarized forms given by Magin [156], Podlubny [157], of a few Laplace transform for some Mittag-Leffler function are

$$\mathcal{L}\{E_\alpha(-\lambda t^\alpha)\} = \frac{s^{\alpha-1}}{s^\alpha + \lambda}, \ \ \mathcal{L}\{t^{\alpha-1}E_{\alpha,\alpha}(-\lambda t^\alpha)\} = \frac{1}{s^\alpha + \lambda} \tag{2.103}$$

$$\mathcal{L}\{t^{\beta-1}E_{\alpha,\beta}(-\lambda t^\alpha)\} = \frac{s^{\alpha-\beta}}{s^\alpha + \beta}, \ \ \mathcal{L}\{\varepsilon_k(t, \pm\lambda; \alpha, \beta)\} = \frac{k! s^{\alpha-\beta}}{(s^\alpha \pm \lambda)^{k+1}} \tag{2.104}$$

2.5.5   Hankel Transform

The Hankel transform is an integral transformation like the Laplace transform. It is a transformation with respect to the space and the expression for any given function $f(r)$ depends on the weighted sum of an infinite number of Bessel functions of the first kind $J_\nu(kr)$. This transform is more appropriate in solving differential equations with boundary conditions in which there is axial symmetry. To deal with the problems formulated in the finite domain, finite-integral transforms are introduced. The finite Hankel transform $(F_\nu(k))$ of the function $f(r)$ was first introduced by Sneddon in 1946 [158]. For the Bessel functions, all the sums have the same order ν but differ in a scaling factor k along the r axis. Then, for any coefficient F_ν of each Bessel function, we can have a function with respect to the scale that constitutes the transformed function. It is also known as the Fourier-Bessel transform. Just as the Fourier transform for an infinite interval is related to the Fourier series over a finite interval, so the Hankel transform over an infinite interval is related to the Fourier-Bessel series over a finite interval [159]. We have

$$F_\nu(k) = \int_0^\infty r f(r) J_\nu(kr) dr, \tag{2.105}$$

where ν is the order of the Hankel transform of $f(r)$, and the inverse Hankel transform is given by:

$$f(r) = \int_0^\infty k F_\nu(k) J_\nu(kr) dk. \tag{2.106}$$

The formula is valid for $\nu > -1/2$.

★ **Properties of Hankel transforms**

Hankel transforms have the following properties. Define

$$\Delta_\nu = \frac{d^2}{dr^2} + \frac{1}{r}\frac{d}{dr} - \frac{\nu^2}{r^2}. \tag{2.107}$$

Let $f(r)$ be an arbitrary function with the property that $\lim\limits_{r \to +\infty} f(r) = 0$. The term $\frac{\nu^2}{r^2}$ can be neglected. Then, we have [169, 172]:

$$\begin{aligned}
\mathcal{H}_\nu[\Delta_\nu f(r)] &= -k^2 F_\nu(k), \\
\mathcal{H}_\nu[f'(r)] &= \frac{k}{2\nu}[(\nu+1)F_{\nu-1}(k) - (\nu-1)F_{\nu+1}(k)], \\
\mathcal{H}_\nu\left[\frac{1}{r}f(r)\right] &= \frac{k}{2\nu}[F_{\nu-1}(k) + F_{\nu+1}(k)].
\end{aligned} \tag{2.108}$$

2.5.6 Caputo Fractional Derivative

Fractional calculus is a branch of mathematical analysis that studies the several different possibilities of defining real number powers or complex number powers of the differentiation operator D

$$Df(x) = \frac{d}{dx}f(x), \tag{2.109}$$

and of the integration operator

$$Jf(x) = \int_0^x f(s)\,ds, \tag{2.110}$$

Fractional order operators are mathematical tools that are nowadays widely used by researchers in many disciplines of engineering sciences to solve real life problems. One of the properties of this operator is its ability to produce and reveal with precision some chaotic problems. Their resolution in an analytical way is usually very complex and sometimes impossible to obtain, so many researchers turn to numerical methods to solve it [170]. Fractional derivative and Riemann-Liouville integral for analytic functions we have the following definitions

$$_aI^\alpha f(x) = \frac{1}{\Gamma(\alpha)}\int_a^x f(t)(x-t)^{\alpha-1}\,dt, \quad a \in \mathbb{R}. \tag{2.111}$$

The fundamental relations hold

$$\frac{d}{dx}I^{\alpha+1}f(x) = I^\alpha f(x), \quad I^\alpha(I^\beta f) = I^{\alpha+\beta}f, \tag{2.112}$$

So, the generalize Riemann-Liouville form is given

$$D_x^\alpha f(x) = \begin{cases} \frac{d^q}{dx^q}I^{q-\alpha}f(x) & \alpha > 0 \\ f(x) & \alpha = 0 \\ I^{-\alpha}f(x) & \alpha < 0. \end{cases} \tag{2.113}$$

48

with $q = \bar{\alpha} + 1$. In 1967, Caputo was the first to intrduce a good alternative method of the Riemann-Liouville for computing fractional derivative. Caputo's definition is illustrated as follows, where again $n = \alpha$:

$$
{}^{C}_{a}D^{\alpha}_{t}f(t) = \frac{1}{\Gamma(q-\alpha)} \int_{a}^{t} \frac{f^{(q)}(\tau)\,d\tau}{(t-\tau)^{\alpha+1-q}}. \tag{2.114}
$$

The Caputo definition of fractional derivatives with operator of order "α" can be written [160]

$$
{}_{a}D^{\alpha}f(t) = \frac{1}{\Gamma(q-\alpha)} \int_{a}^{t} (t-\tau)^{(q-\alpha-1)} f^{(q)}(\tau)d\tau, \qquad (q-1) < \alpha < q. \tag{2.115}
$$

Let us denote the Riemann-Liouville fractional derivative by ${}^{RL}_{a}D^{\alpha}_{t}f(t)$ and the Caputo defnition by ${}^{C}_{a}D^{\alpha}_{t}f(t)$, then the relationship between them is:

$$
{}^{RL}_{a}D^{\alpha}_{t}f(t) = {}^{C}_{a}D^{\alpha}_{t}f(t) + \sum_{k=0}^{q-1} \frac{t^{k-\alpha}}{\Gamma(k-\alpha+1)} f^{(k)}(a) \tag{2.116}
$$

2.5.7 Atangana-Baleanu Fractional Derivative

The generalized Mittag-Leffler function is given by (2.94) which is the solution of the equation: $\frac{d^{\alpha}u}{dx^{\alpha}} = au$; which is the function allowing to solve analytically the Riemann-Liouville definition given by (2.111), which was the first operator, followed by the Caputo operator (2.114). Considering, the Taylor series at a point t of the exponential decay law:

$$
\exp[-(t-\tau)] = \sum_{s=0}^{\infty} \frac{[-a(t-\tau)]^{s}}{s!}, \tag{2.117}
$$

we end up at the definition of Caputo and Fabrizio:

$$
{}^{CF}D^{\alpha}_{t}[f(t)] = \frac{M(\alpha)}{1-\alpha} \int_{0}^{t} \frac{df(\tau)}{d\tau} \exp[-(t-\tau)]d\tau, \quad \text{with } 0 < \alpha < 1. \tag{2.118}
$$

By taking, $a = \frac{a}{1-\alpha}$ and replacing (2.117) in (2.118), we obtain:

$$
{}^{CF}_{a}D^{\alpha}_{t}[f(t)] = \frac{M(\alpha)}{1-\alpha} \sum_{s=0}^{\infty} \frac{(-a)^{s}}{s!} \int_{a}^{t} \frac{df(\tau)}{d\tau} [(t-\tau)]^{s}d\tau. \tag{2.119}
$$

Then by replacing $s!$ by $\Gamma(\alpha s + 1)$ and $(t-\tau)^{s}$ by $(t-\tau)^{\alpha s}$, we have:

$$
{}^{CF}_{a}D^{\alpha}_{t}[f(t)] = \frac{M(\alpha)}{1-\alpha} \sum_{s=0}^{\infty} \frac{(-a)^{s}}{\Gamma(\alpha s + 1)} \int_{a}^{t} \frac{df(\tau)}{d\tau} [(t-\tau)]^{\alpha s}d\tau. \tag{2.120}
$$

Moreover, Abdon Atangana and Dumitru Baleanu have proposed a new kernel on the generalized Mittag-Leffler function [170],

$$
{}^{ABC}_{0}D^{\alpha}_{t}[f(t)] = \frac{M(\alpha)}{1-\alpha} \int_{0}^{t} f'(\tau)E_{\alpha}\left[-\alpha \frac{(t-\tau)^{\alpha}}{1-\alpha}\right]d\tau, \tag{2.121}
$$

$$
{}^{ABR}_{0}D^{\alpha}_{t}[f(t)] = \frac{M(\alpha)}{1-\alpha} \frac{d}{dt} \int_{0}^{t} f(\tau)E_{\alpha}\left[-\alpha \frac{(t-\tau)^{\alpha}}{1-\alpha}\right]d\tau. \tag{2.122}
$$

By applying the Laplace transforms (2.102), we arrive at:

$$\mathcal{L}\{^{ABR}_0 D^\alpha_t[f(t)]\}(q) = \frac{M(\alpha)}{1-\alpha}\frac{q^\alpha \mathcal{L}\{f(t)\}(q)}{q^\alpha + \frac{\alpha}{1-\alpha}},\tag{2.123}$$

and

$$\mathcal{L}\{^{ABC}_0 D^\alpha_t[f(t)]\}(q) = \frac{M(\alpha)}{1-\alpha}\frac{q^\alpha \mathcal{L}\{f(t)\}(q)}{q^\alpha + \frac{\alpha}{1-\alpha}} - \frac{q^{\alpha-1}f(0)}{q^\alpha + \frac{\alpha}{1-\alpha}}\frac{M(\alpha)}{(1-\alpha)}.\tag{2.124}$$

By replacing (2.123) in (2.124), and to inverse the transformation we obtain the Atangana-Baleanu relation [171]:

$$^{ABC}_0 D^\alpha_t[f(t)] =^{ABR}_0 D^\alpha_t[f(t)] - \frac{M(\alpha)}{1-\alpha}f(0)E_\alpha\left(-\frac{\alpha}{1-\alpha}t^\alpha\right).\tag{2.125}$$

The Atangana-Baleanu fractional integral of a continuous function is defined as:

$$^{AB}_a I^\alpha_t f(t) = \frac{1-\alpha}{AB(\alpha)}f(t) + \frac{\alpha}{AB(\alpha)\Gamma(\alpha)}\int_a^t (t-\tau)^{\alpha-1}f(\tau)\,d\tau\tag{2.126}$$

2.6 Numerical Methods

The numerical solution of ordinary differential equations (ODEs) or partial differential equations (PDEs) works by replacing the region over which the independent variables are defined with a finite grid (also called mesh) of points over which the dependent variable is approximated. Using Taylor's theorem the derivatives of the ODE at each point on the grid are approximated from neighbouring values.

2.6.1 Finite difference method

Finite-difference methods (FDM) are a class of numerical techniques for solving differential equations by approximating derivatives with finite differences. The discretisation is carried out over a domain of space and time which is divided into a finite number of steps and whose solution value at these discrete points is approximated by solving algebraic equations containing finite differences and values from nearby points [161].

Let $v(x,y,z,t)$ a function of space and time. The derivation is given by:

$$\frac{\partial v}{\partial x} = \lim_{\Delta x \to O}\frac{v(x+\Delta x,y,z,t) - v(x,y,z,t)}{\Delta x},\tag{2.127}$$

if Δx is small, then the Taylor expansion of $v(x+\Delta x,y,z,t)$ in the neighborhood of x gives:

$$v(x+\Delta x,y,z,t) = v(x,y,z,t)+\Delta x\frac{\partial v}{\partial x}(x,y,z,t)+\frac{\Delta x^2}{2}\frac{\partial^2 v}{\partial x^2}(x,y,z,t)+\frac{\Delta x^3}{3!}\frac{\partial^3 v}{\partial x^3}(x,y,z,t)+...\tag{2.128}$$

By truncating the series to first order in Δx, we have:

$$\frac{v(x+\Delta x,y,z,t) - v(x,y,z,t)}{\Delta x} = \frac{\partial v}{\partial x}(x,y,z,t) + O(\Delta x).\tag{2.129}$$

So, the approximation of the derivative $\frac{\partial v}{\partial x}(x)$ is for order 1, indicating that the truncation error $O(\Delta x)$ tends to zero as the first power of Δx.

We consider a mesh (or calculation grid) composed of $N + 1$ points x_i for $i = 0, ..., N$ regularly spaced with a step Δx. The points $x_i = i\Delta x$ are called the nodes of the mesh. Let v_i be the discrete value of $v(x)$ at point x_i, i.e. $v_i = v(x_i)$. The first-order finite difference scheme presented above in (2.129) is written in index notation as:

$$\left(\frac{\partial v}{\partial x}\right)_i = \frac{v_{i+1} - v_i}{\Delta x} + O(\Delta x), \tag{2.130}$$

this scheme is called forward or off-centre forward or upwind.

In addition, we have first-order scheme, called backward:

$$\left(\frac{\partial v}{\partial x}\right)_i = \frac{v_i - v_{i-1}}{\Delta x} + O(\Delta x). \tag{2.131}$$

To construct the higher order finite difference schemes, we will have to manipulate the Taylor expansion in the neighbourhood of x_i, which gives us:

$$
\begin{aligned}
v_{i+1} &= v(x_i + \Delta x) = v_i + \Delta x \left(\frac{\partial v}{\partial x}\right)_i + \frac{\Delta x^2}{2}\left(\frac{\partial^2 v}{\partial x^2}\right)_i + O(\Delta x^3) \\
v_{i-1} &= v(x_i - \Delta x) = v_i - \Delta x \left(\frac{\partial v}{\partial x}\right)_i + \frac{\Delta x^2}{2}\left(\frac{\partial^2 v}{\partial x^2}\right)_i + O(\Delta x^3)
\end{aligned}
\tag{2.132}
$$

By subtracting these two relationships, we have:

$$\left(\frac{\partial v}{\partial x}\right)_i = \frac{v_{i+1} - v_{i-1}}{2\Delta x} + O(\Delta x^2), \tag{2.133}$$

called 'centered approximation' of the first derivative of v in the second order scheme. So, to approximte the second derivative, we applyied the same approaches like previously in second order scheme by adding the next term of the Taylor expansion. We reach to the centered approximation:

$$\left(\frac{\partial^2 v}{\partial x^2}\right)_i = \frac{v_{i+1} - 2v_i + v_{i-1}}{\Delta x^2} + O(\Delta x^2). \tag{2.134}$$

As an example, consider the normalized heat equation in one dimension, with homogeneous Dirichlet boundary conditions

$$
\begin{aligned}
V_t &= V_{xx} \\
V(0,t) = V(1,t) &= 0 \quad \text{(boundary condition)} \\
V(x,0) &= V_0(x) \quad \text{(initial condition)}
\end{aligned}
\tag{2.135}
$$

Solving this equation is to approximate all the derivatives by finite differences methods. Then, to do so, we partition the domain in space using a mesh $x_0, ..., x_I$ and in time using a mesh $t_0, ..., t_N$. We assume a uniform partition both in space and in time, so the difference between two consecutive

space points will be h and between two consecutive time points will be k. Then, we have the points $u(x_j, t_n) = u_j^n$.

★ Explicit method

By using a forward difference at time t_n and a second-order central difference for the space derivative at position x_i, we get the recurrence equation:

$$\frac{v_i^{n+1} - v_i^n}{k} = \frac{v_{i+1}^n - 2v_i^n + v_{i-1}^n}{h^2}. \tag{2.136}$$

From the above result, we can write:

$$v_i^{n+1} = (1 - 2r)v_i^n + rv_{i-1}^n + rv_{i+1}^n, \quad \text{where} \quad r = k/h^2. \tag{2.137}$$

★ Implicit method

The Implicit method is the use of backward difference at time t_{n+1} and for the space derivative at position x_i, the second-order central difference is used:

$$\frac{v_i^{n+1} - v_i^n}{k} = \frac{v_{i+1}^{n+1} - 2v_i^{n+1} + v_{i-1}^{n+1}}{h^2}. \tag{2.138}$$

We obtain,

$$(1 + 2r)v_i^{n+1} - rv_{i-1}^{n+1} - rv_{i+1}^{n+1} = v_i^n, \quad \text{where} \quad r = k/h^2. \tag{2.139}$$

★ Crank-Nicolson method

It use the central difference at time $t_{n+1/2}$ and a second-order central difference for the space derivative at position x_i, we get to

$$\frac{v_i^{n+1} - v_i^n}{k} = \frac{1}{2}\left(\frac{v_{i+1}^{n+1} - 2v_i^{n+1} + v_{i-1}^{n+1}}{h^2} + \frac{v_{i+1}^n - 2v_i^n + v_{i-1}^n}{h^2}\right). \tag{2.140}$$

We can obtain v_i^{n+1} from solving a system of linear equations:

$$(2 + 2r)v_i^{n+1} - rv_{i-1}^{n+1} - rv_{i+1}^{n+1} = (2 - 2r)v_i^n + rv_{i-1}^n + rv_{i+1}^n, \quad \text{where} \quad r = k/h^2. \tag{2.141}$$

2.6.2   Fourth order Runge-Kutta method

By 1900, the German mathematicians Carl Runge and Wilhelm Kutta developped a method in numerical analysis called the Runge-Kutta (RK) methods [162], which is familiar to the implicit and explicit iterative methods and which include the well-known routine called Euler method. The Runge-Kutta method have several approximation. The first in order two called RK2 is the modified Euler method also known under the name Heun method. But the most widely known member of the Runge-Kutta family is generally referred to RK4 in 4th order approximations. The fourth order Runge-Kutta scheme is used also for the nonlinear partial differential equations [162, 163].

Let $h > 0$ be a sufficiently small stepsize defining a grid $t_{n+1} = t_n + h$ for $n = 0, 1, 2, ..., N_t$, then the following recursion

$$v_{n+1} = v_n + h f(v_n, t_n), \qquad (2.142)$$

generates approximations v_n for the solution $v(t_n)$ and $n = 0, 1, 2, ...$ with f the function. So, the RK4 Runge-Kutta methods usually denoted by

$$
\begin{aligned}
k_1 &= f(t_n, v_n), \\
k_2 &= f(t_n + \frac{h}{2}, v_n + h\frac{k_1}{2}), \\
k_3 &= f(t_n + \frac{h}{2}, v_n + h\frac{k_2}{2}), \\
k_4 &= f(t_n + h, v_n + h k_3), \\
t_{n+1} &= t_n + h \\
v_{n+1} &= v_n + \frac{h}{6}(k_1 + 2k_2 + 2k_3 + k_4).
\end{aligned}
\qquad (2.143)
$$

Here v_{n+1} is the RK4 approximation of $v(t_{n+1})$, and the next value v_{n+1} is determined by the present value v_n.

2.6.3 Finite Difference Approximations of Caputo Differentiation

In order to solve problems with initial conditions in several fields of science, Caputo's numerical approximation provides an answer through the manipulation of the operator by the well-known integral transform, also through the definition of the derivative of a convolution function and a power-law decay function.

Let consider the definition of Caputo given by (2.114) for the first derivation when $q = 1$, we have

$$
{}_a^C D_t^\alpha f(t) = \frac{1}{\Gamma(1-\alpha)} \int_a^t f^{(1)}(\tau) (t-\tau)^{-\alpha} d\tau. \qquad (2.144)
$$

Let assume the time step $\Delta t = T/l$ and the space step $\Delta x(b-a)/N$ in the interval $I = (a, b)$. On the setting of uniform grids x_i for $i = 0, 1, 2..., N$ and $t_n = n\Delta t$ for $n = 0, 1, 2, ..., l$. For $t = t_n$, $n \in \mathbb{N}$ and $0 < \alpha < 1$, we rewrite $\left[{}_0^C D_t^\alpha f(t) \right]_{t=t_n}$ as follow

$$
\begin{aligned}
\left[{}_0^C D_t^\alpha f(t) \right]_{t=t_n} &= \frac{1}{\Gamma(1-\alpha)} \int_{t_0}^{t_n} (t_n - \tau)^{-\alpha} f'(\tau) d\tau, \\
&= \frac{1}{\Gamma(1-\alpha)} \sum_{k=0}^{n-1} \int_{t_k}^{t_{k+1}} (t_n - \tau)^{-\alpha} f'(\tau) d\tau, \\
&\approx \frac{1}{\Gamma(1-\alpha)} \sum_{k=0}^{n-1} \int_{t_k}^{t_{k+1}} (t_n - \tau)^{-\alpha} \frac{f(t_{k+1}) - f(t_k)}{\Delta t} d\tau \\
&= \sum_{k=0}^{n-1} b_{n-k-1}(f(t_{k+1}) - f(t_k)),
\end{aligned}
\qquad (2.145)
$$

where

$$t_0 = 0, \quad b_k = \frac{\Delta t^{-\alpha}}{\Gamma(2-\alpha)} \left[(k+1)^{1-\alpha} - (k)^{1-\alpha} \right].$$

The L1 method below is often used by some researchers for the discretization of the time fractional differential equations, which can lead to unconditionally stable algorithms [160, 165–167].

2.7 Conclusion

In this chapter, we examined the analytical and numerical methods that have been used in our models to study the dynamics of the blood flow through the consideration of the propagation of heat exchanges, the rotation of the nanofluid. To this end, conservation laws were used to derive the various distribution equations, similar to the Navier-Stockes equations. The analytical methods used are Laplace transforms, Hankel transforms, fractional derivatives according to Caputo, and also according to Atangana-Baleanu. The numerical methods described are the finite difference method, the fourth-order Runge-Kutta method and Caputo's finite difference approximation. In the next chapter, we will apply these methods to our models, highlight the results and discuss.

Chapter 3

Results and Discussion

3.1 Introduction

In this chapter, we will be presenting the discussions and numerical observations related to the results of the models on the effect of the magnetic field and thermal radiation in a first step. Secondly, the effect of nanofluid rotations in a magnetized medium and under the influence of radiation and chemical reactions will be presented. The observed results will be compared with experimental studies proposed by other researchers for the cases where water is taken as the basic fluid, given its high percentage of its presence in blood. In this thesis, we use blood as a basic fluid thus and its interaction with the different chemical nanoparticles will be presented and argued in order to better understand their behaviour in this type of medium, the aim is to bring our contribution to master the treatments of carcinogenic, tumour and cardiovascular diseases, to name a few.

3.2 Effect of heat transfer, magnetic field under a fractionalized model

3.2.1 Analytical solution

To solve the mathematical model (2.68), we make use of the Laplace transform with respect to the time parameter and the Hankel transform with respect to the radial variable. The temporal

transformation then leads to the equations

$$S^a \overline{U}(r,s) = \frac{1}{R_e}\left[\frac{\partial^2 \overline{U}(r,s)}{\partial r^2} + \frac{1}{r}\frac{\partial \overline{U}(r,s)}{\partial r}\right] + \frac{b_0}{s} + \frac{b_1 s}{s^2 + \omega^2} + R\overline{V}(y,s) - (R + Ha^2)\overline{U}(r,s),$$

$$\overline{V}(r,s) = \frac{\overline{U}(r,s)}{GS^a + 1}$$

$$S^a \overline{T}(r,s) = \frac{\kappa}{\rho C_p}\left[\frac{\partial^2 \overline{T}(r,s)}{\partial r^2} + \frac{1}{r}\frac{\partial \overline{T}(r,s)}{\partial r}\right] - \frac{4\alpha^2}{\rho C_p}\overline{T}(r,s) + \frac{\hat{\mu}}{C_p}\left(\frac{\partial \overline{U}(r,s)}{\partial r}\right)^2$$

$$\qquad - \frac{\hat{\mu}}{C_p}\lim_{t\to 0}\left\{\int_0^t \left(\frac{\partial U(r,\tau)}{\partial r}\right)^2 d\tau\right\}, \tag{3.1}$$

with $\overline{U}(1,s) = 0$, $\overline{V}(1,s) = 0$, and $\overline{T}(1,s) = 0$. In the rest of study, it is considered that $\lim_{t\to 0}\left\{\int_0^t \left(\frac{\partial U(r,\tau)}{\partial r}\right)^2 d\tau\right\} \to 0$. Applying the Hankel transform [168, 169] of zero order to (3.1), and using the boundary conditions given in (2.69), we obtain

$$\frac{-r_n^2 \overline{U}_H(y_n,s)}{Re} = \left[\frac{GS^{2a} + [1 + G(R + \mathcal{H}^2)]S^a + \mathcal{H}^2}{GS^a + 1}\right]\overline{U}_H(r_n,s) - \left(\frac{b_0}{s} + \frac{b_1 s}{s^2 + \omega^2}\right)\frac{J_1(r_n)}{r_n}, \tag{3.2}$$

where $\overline{U}_H(r_n,s) = \int_0^1 r\overline{U}(r,s)J_0(rr_n)dy$ is the finite Hankel transform of function $\overline{U}(r,s)$ and $r_n(n = 1,2,....)$ are positive roots of the equation $J_0(\chi) = 0$, J_0 being the Bessel function of the first kind and order zero. The inverse Laplace transform for (3.2) of fluid can be written in the equivalent form

$$\overline{U}_H(r_n,s) = \frac{b_0 Re}{c_n}\left[(1 - Ga_{1n})\frac{s^{-1}}{s^a + a_{1n}} - (1 - Ga_{2n})\frac{s^{-1}}{s^a + a_{2n}}\right]\frac{J_1(r_n)}{r_n}$$

$$\qquad - \frac{b_1 Re}{c_n}\frac{s}{s^2 + \omega^2}\left[(1 - Ga_{1n})\frac{s^{-1}}{s^a + a_{1n}} - (1 - Ga_{2n})\frac{s^{-1}}{s^a + a_{2n}}\right]\frac{J_1(r_n)}{r_n}, \tag{3.3}$$

where

$$a_{1n} = \frac{b_n - c_n}{2ReG}, \quad a_{2n} = \frac{b_n + c_n}{2ReG}, \quad b_n = Re[1 + G(R + \mathcal{H}^2)] + Gr_n^2, \quad c_n = \sqrt{b_n^2 - 4R_e G(Re\mathcal{H}^2 + r_n^2)}. \tag{3.4}$$

Inserting (3.3) into the last equation given by (3.1) and applying the Hankel transform leads to

$$\overline{T}_H(r_n,s) = \frac{2\hat{\mu}Re\left(\frac{A_0}{s} + \frac{A_1 s}{s^2 + w^2}\right)}{C_p\left(\beta r_n^2 + s^\alpha + \frac{4\alpha^2}{C_p}\right)}\frac{\partial}{\partial r_n}\left[\left(\frac{1 - a_{1n}G}{s^a + a_{1n}} - \frac{1 - a_{2n}G}{s^a + a_{2n}}\right)\frac{J_1(r_n)}{r_n c_n}\right]. \tag{3.5}$$

To solve this last one, we used the Bessel expansion form given by

$$J_{n+1}(x) = \frac{nJ_n(x)}{x} - J_n'(x), \quad \text{and} \quad J_{n+1}(x) - J_{n-1}(x) = -2J_n'(x), \tag{3.6}$$

then we can assuming the approximation

$$\frac{\partial}{\partial r_n}\left(\frac{J_1(r_n)}{r_n c_n}\right) = -\frac{J_2}{r_n c_n} - \frac{c_n'}{c_n^2}(J_2 + J_1'),$$

$$\frac{\partial}{\partial r_n}\left(\frac{1 - a_{1n}G}{s^a + a_{1n}} - \frac{1 - a_{2n}G}{s^\alpha + a_{2n}}\right) = \left(\frac{-a_{1n}'G(s^a + a_{1n}) - a_{1n}'(1 - a_{1n}G)}{(s^a + a_{1n})^2} + \frac{a_{2n}'G(s^a + a_{2n}) + a_{2n}'(1 - a_{2n}G)}{(s^a + a_{2n})^2}\right), \tag{3.7}$$

56

which can be employed to expand (3.5) so that

$$\bar{T}_{H_1}(r_n, s) = \frac{2\hat{\mu}Re\left(\frac{A_0}{s} + \frac{A_1 s}{s^2 + w^2}\right)}{C_p\left(\beta r_n^2 + s^\alpha + \frac{4\alpha^2}{C_p}\right)}\left(\frac{1 - a_{1n}G}{s^a + a_{1n}} - \frac{1 - a_{2n}G}{s^a + a_{2n}}\right)\left[-\frac{J_2}{r_n c_n} - \frac{c_n'}{c_n^2}(J_2 + J_1')\right],$$

$$\bar{T}_{H_2}(r_n, s) = \frac{2\hat{\mu}Re\left(\frac{A_0}{s} + \frac{A_1 s}{s^2 + w^2}\right)}{C_p\left(\beta r_n^2 + s^\alpha + \frac{4\alpha^2}{C_p}\right)}\frac{J_1(r_n)}{r_n c_n}\frac{\partial}{\partial r_n}\left[\left(\frac{1 - a_{1n}G}{s^a + a_{1n}} - \frac{1 - a_{2n}G}{s^a + a_{2n}}\right)\right],$$

(3.8)

$$\bar{T}_H(r_n, s) = \bar{T}_{H_1}(r_n, s) + \bar{T}_{H_2}(r_n, s).$$

After developing and rearranging the terms we obtain

$$\bar{T}_{H_1}(r_n, s) = \frac{\gamma b_0 c_n'}{c_n^2}\frac{J_1}{r_n}\left[\frac{s^{-1}(1 - a_{2n}G)}{(s^a + l_{2n})(s^a + l_{1n})} - \frac{s^{-1}(1 - a_{1n}G)}{(s^a + k_{2n})(s^a + k_{1n})}\right]$$
$$+ \frac{s\gamma b_1 c_n'}{(s^2 + w^2)c_n^2}\frac{J_1}{r_n}\left[\frac{(1 - a_{2n}G)}{(s^a + l_{2n})(s^a + l_{1n})} - \frac{(1 - a_{1n}G)}{(s^a + k_{1n})(s^a + k_{2n}))}\right]$$
$$+ \frac{\gamma b_0}{c_n}\frac{J_2}{r_n}\left[\frac{(1 - a_{2n}G)s^{-1}}{(s^a + l_{2n})(s^a + l_{1n})} - \frac{(1 - a_{1n}G)s^{-1}}{(s^a + k_{2n})(s^a + k_{1n})}\right]$$
$$+ \frac{\gamma b_1 s}{c_n(s^2 + w^2)}\frac{J_2}{r_n}\left[\frac{(1 - a_{2n}G)}{(s^a + l_{2n})(s^a + l_{1n})} - \frac{(1 - a_{1n}G)}{(s^a + k_{2n})(s^a + k_{1n})}\right],$$

(3.9)

$$\bar{T}_{H_2}(r_n, s) = \frac{\gamma b_0 s^{-1}}{c_n}\frac{J_1}{r_n}\left[\frac{(-a_{1n}'G)}{(s^a + k_{2n})(s^a + k_{1n})} - \frac{a_{1n}'(1 - a_{1n}G)}{(s^a + a_{1n})(s^a + k_{2n})(s^a + k_{1n})}\right.$$
$$\left. + \frac{a_{2n}'G}{(s^a + l_{2n})(s^a + l_{1n})} + \frac{a_{2n}'(1 - a_{2n}G)}{(s^a + a_{2n})(s^a + l_{2n})(s^a + l_{1n})}\right]$$
$$+ \frac{\gamma b_1 s}{c_n(s^2 + w^2)}\frac{J_1}{r_n}\left[\frac{(-a_{1n}'G)}{(s^a + k_{2n})(s^a + k_{1n})} - \frac{a_{1n}'(1 - a_{1n}G)}{(s^a + a_{1n})(s^a + k_{2n})(s^a + k_{1n})}\right.$$
$$\left. + \frac{a_{2n}'G}{(s^a + l_{2n})(s^a + l_{1n})} + \frac{a_{2n}'(1 - a_{2n}G)}{(s^a + a_{2n})(s^a + l_{2n})(s^a + l_{1n})}\right],$$

where

$$a_{1n}' = \frac{(b_n' - c_n')}{2ReG}, \quad a_{2n}' = \frac{(b_n' + c_n')}{2ReG}, \quad b_n' = 2Gr_n, \quad b_{n1} = (\beta r_n^2 + p + a_{1n}), \quad b_{n2} = (\beta r_n^2 + p + a_{2n})$$

$$c_n' = \frac{2Gr_n}{c_n}\left(-Re + ReG(R + H_a^2) + Gr_n^2\right), \quad c_{n1} = \sqrt{(\beta r_n^2 + p + a_{1n})^2 - 4a_{1n}(p + \beta r_n^2)}$$

$$c_{n2} = \sqrt{(\beta r_n^2 + p + a_{2n})^2 - 4a_{2n}(p + \beta r_n^2)}, \quad k_{1n} = \frac{b_{n1} - c_{n1}}{2}, \quad k_{2n} = \frac{b_{n1} + c_{n1}}{2}$$

$$l_{1n} = \frac{b_{n2} - c_{n2}}{2}, \quad l_{2n} = \frac{b_{n2} + c_{n2}}{2}, \quad p = \frac{4\alpha^2}{C_p}, \quad \gamma = \frac{2\hat{\mu}Re}{C_p}.$$

(3.10)

In what follows, we make use of the special functions

$$L^{-1}\left\{\frac{1}{S^a + m}\right\} = F_a(-m, t) = \sum_{n=0}^{\infty}\frac{(-m)^n t^{(n+1)a-1}}{\Gamma(a(n+1))}, \qquad a > 0$$

(3.11)

$$L^{-1}\left\{\frac{S^\gamma}{S^a + m}\right\} = R_{a,\gamma} = \sum_{n=0}^{\infty}\frac{(-m)^n t^{(n+1)a-1-\gamma}}{\Gamma(a(n+1) - \gamma)}, \qquad R_e(a - \gamma) > 0,$$

where $F_a(.,.)$ is the Robotnov and Hartley's function, and $R_{a,\gamma}(.,.)$ is the Lorenzo and Hartley's function [173]. In particular case $a = 1$, (3.11) become

$$F_1(-m, t) = e^{-mt}, \qquad R_{1,-1}(-m, t) = \frac{1 - e^{-mt}}{m} \tag{3.12}$$

Based on the fact that $T(r, t) = T_1(r, t) + T_2(r, t)$, the inverse Hankel transform of (3.3) and (3.9) leads to the solutions

$$U(r, t) = 2 \sum_{n=1}^{\infty} \frac{J_0(rr_n)}{r_n J_1(r_n)} [F_{1n}(t) + F_{2n}(t)]$$

$$T_1(r, t) = 2 \sum_{n=1}^{\infty} \left(\frac{J_0(rr_n)}{r_n J_1(r_n)} [F_{3n}(t) + F_{4n}(t)] + \frac{J_0(rr_n) J_2(r_n)}{r_n J_1^2(r_n)} [F_{5n}(t) + F_{6n}(t)] \right) \tag{3.13}$$

$$T_2(r, t) = 2 \sum_{n=1}^{\infty} \frac{J_0(rr_n)}{r_n J_1(r_n)} [F_{7n}(t) + F_{8n}(t) + F_{9n}(t) + F_{10n}(t)], \qquad \text{for} \quad 0 < a < 1$$

and

$$U(r, t) = 2 \sum_{n=1}^{\infty} \frac{J_0(rr_n)}{r_n J_1(r_n)} [A_{1n}(t) + A_{2n}(t)]$$

$$T_1(r, t) = 2 \sum_{n=1}^{\infty} \left(\frac{J_0(rr_n)}{r_n J_1(r_n)} [A_{3n}(t) + A_{4n}(t)] + \frac{J_0(rr_n) J_2(r_n)}{r_n J_1^2(r_n)} [A_{5n}(t) + A_{6n}(t)] \right) \tag{3.14}$$

$$T_2(r, t) = 2 \sum_{n=1}^{\infty} \frac{J_0(rr_n)}{r_n J_1(r_n)} [A_{7n}(t) + A_{8n}(t) + A_{9n}(t) + A_{10n}(t)], \qquad \text{for} \quad a = 1$$

where F_{in} and A_{in} $(i = 1, ..., 10)$ are given in Appendices A and B, respectively.

3.2.2 Numerical results

We collect the information due to the fractional order parameter a and the other flow parameters, on temperature T, fluid velocity U and particle velocity V using numerical simulations and solutions (3.13) and (3.14). In that respect, we need positive solutions of the equation $J_0(x) = 0$. The corresponding results are recorded in Figs. 3.1-3.6, where the effect of a is studied in different situations related to changes in the Reynolds number (Re) and the Hartmann number $(\mathcal{H})$. For the rest of the calculations, other parameter values have been considered as: $A_0 = 10^{-7}, A_1 = 10^{-7}, t = 0.01, \omega = \pi/4, R = 0.2, \lambda = 0.5, \beta = 0.5$ and $G = 0.8$.

Figure 3.1: Profiles of blood temperature $T(r,t)$, axial velocity $U(r,t)$, and particle velocity $V(r,t)$ for small values of time t, with $S = 0.01$, $A_0 = 10^{-7}$, $A_1 = 10^{-7}$, $\omega = \pi/4$, $\beta = 0.5$, $\lambda = 0.5$, $G = 1.5$, $R = 0.2$, $Re = 3$ and $\mathcal{H} = 1$. Panels $(a_j)_{j=1,2,3}$ correspond to $t = 0.05$, panels $(b_j)_{j=1,2,3}$ give results for $t = 0.2$ and panels $(c_j)_{j=1,2,3}$ correspond to $t = 0.3$. In all panels, the fractional parameter takes the values $a = 0.3, 0.5, 0.7$ and 1.

In Figs. 3.1 and 3.2, we represent flow characteristics at small and high values of the time t, respectively. For the two cases, the temperature generally increases from the center of the vessel and drops near the wall. With the help of the fractional parameter, it is possible to control the increase of T, which is lower for $a = 1$. We should however stress that blood temperature which is higher for larger time. The same remark is made for the velocities, where the velocity of blood is higher than that of magnetic particles. This is different from the study proposed by Ali et al. [174], in which the fractional parameter was controlling only the velocities. In this work, the fractional parameter control both the velocities and the temperature.
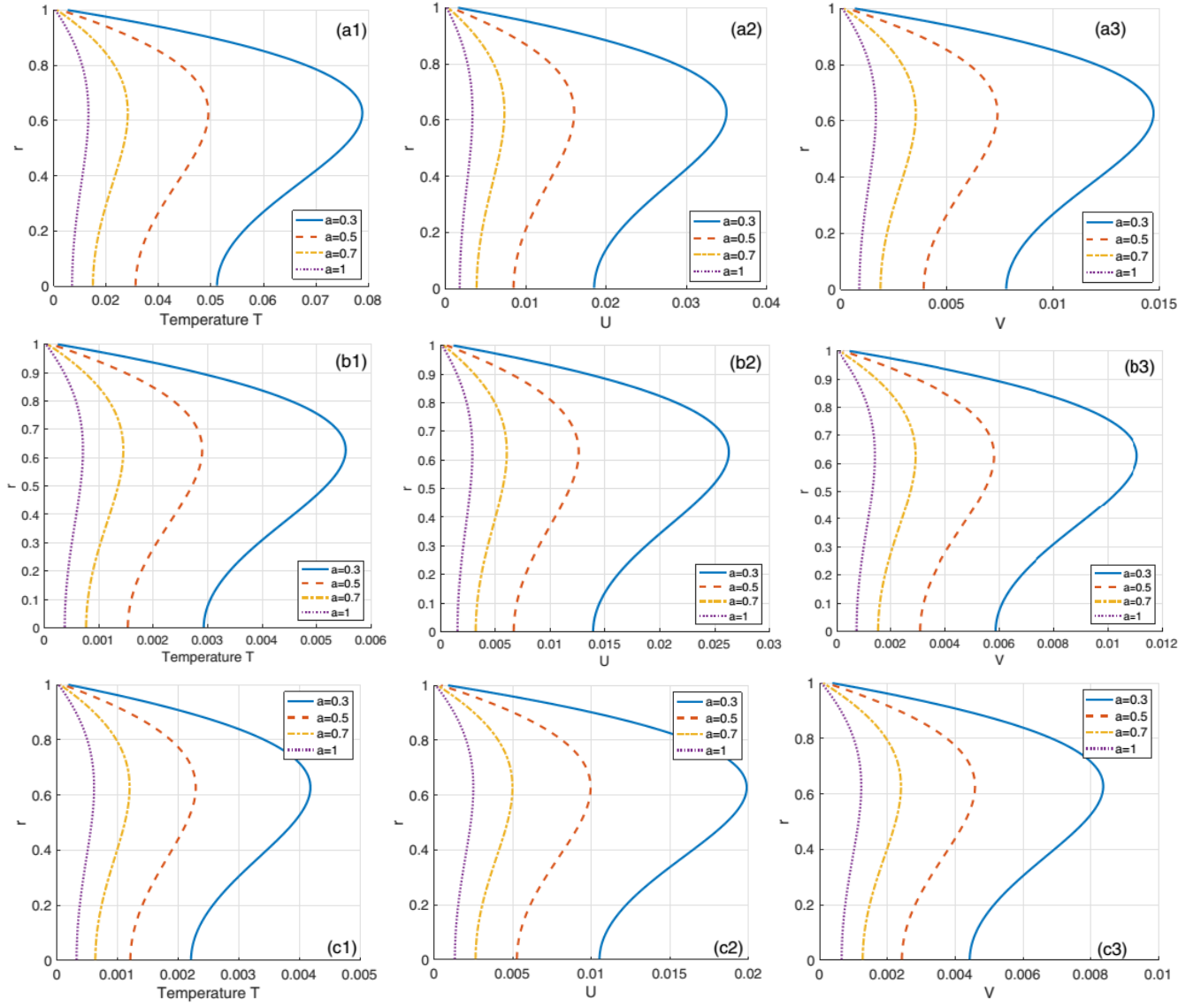
Figure 3.2: Profiles of blood temperature $T(r,t)$, axial velocity $U(r,t)$, and particle velocity $V(r,t)$ for large values of time t, with $S = 0.01$, $A_0 = 10^{-7}$, $A_1 = 10^{-7}$, $\omega = \pi/4$, $\beta = 0.5$, $\lambda = 0.5$, $G = 1.5$, $R = 0.2$, $Re = 3$ and $\mathcal{H} = 1$. Panels $(a_j)_{j=1,2,3}$ correspond to $t = 1$, panels $(b_j)_{j=1,2,3}$ give results for $t = 3$ and panels $(c_j)_{j=1,2,3}$ correspond to $t = 5$. In all panels, the fractional parameter takes the values $a = 0.3, 0.5, 0.7$ and 1.

Figure 3.3: Profiles of blood temperature $T(r,t)$, axial velocity $U(r,t)$, and particle velocity $V(r,t)$ for different values of Reynold number Re, at $t = 0.2$ (small value of time), with $S = 0.01$, $A_0 = 10^{-7}$, $A_1 = 10^{-7}$, $\omega = \pi/4$, $\beta = 0.5$, $\lambda = 0.5$, $G = 1.5$, $R = 0.2$ and $\mathcal{H} = 1$. Panels $(a_j)_{j=1,2,3}$ correspond to $Re = 3$, panels $(b_j)_{j=1,2,3}$ give results for $Re = 4$ and panels $(c_j)_{j=1,2,3}$ correspond to $Re = 5$. In all panels, the fractional parameter takes the values $a = 0.3, 0.5, 0.7$ and 1.

Fig. 3.3 gives the results for small values of time, i.e., $t = 0.2$, with differnt Reynolds number Re. For all values of the fractional parameter, temperature, blood velocity and particle velocity decrease as the fractional parameter increases. In the opposite case, the increase in velocity simply implies a decrease in blood viscosity. Also, the velocity in general is an increasing function of the fractional parameter as supported by the calculations. On the contrary, temperature decreases with a, although changing the value of Re does not really have a significant effect on the blood temperature inside the vessel. One also clearly notices that blood temperature is lower near the tissues and increases

progressively near the centerline. However, the temperature profile is such that there is a peak inside the vessel, which is significantly important in keeping the tissues safe.
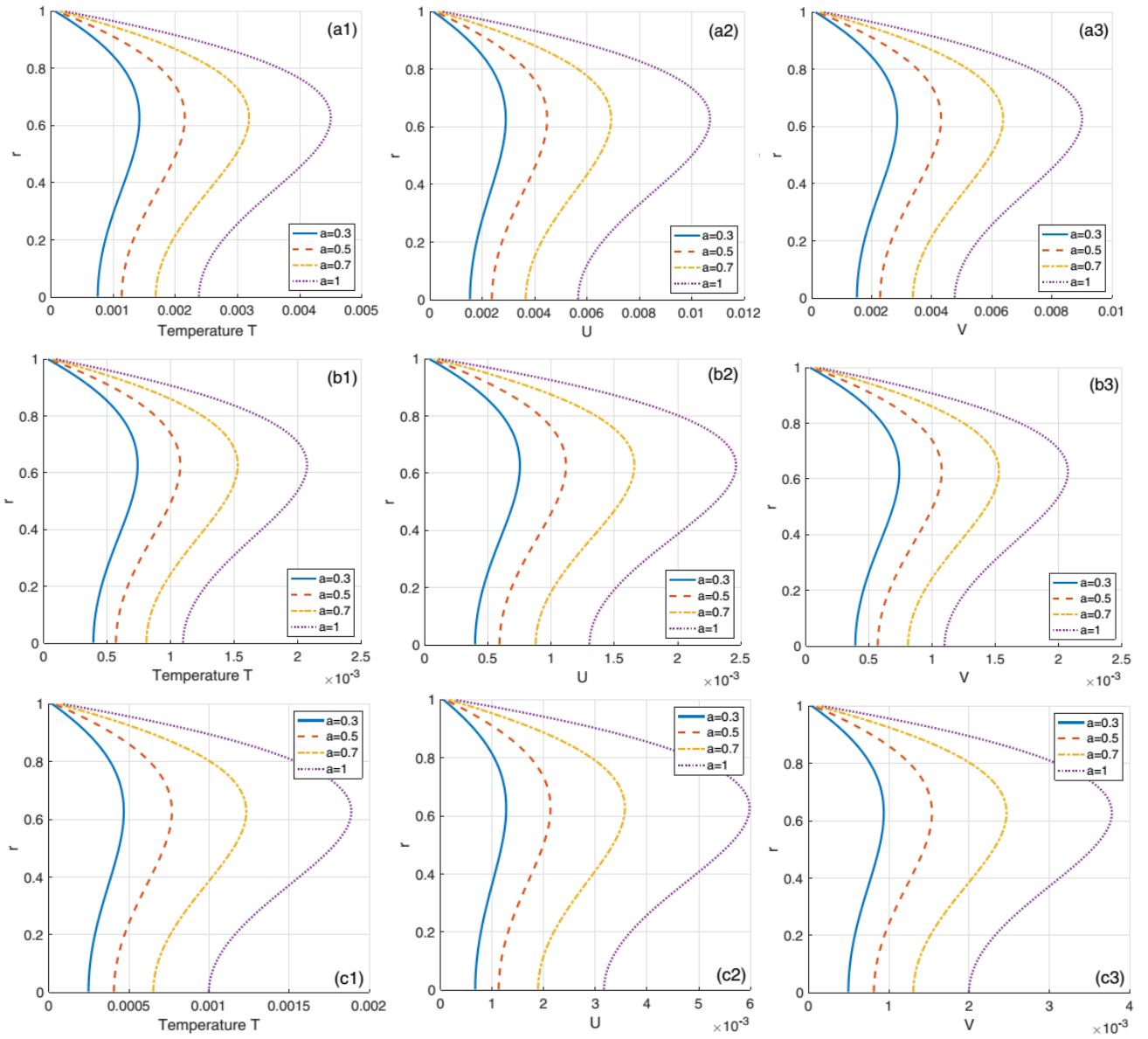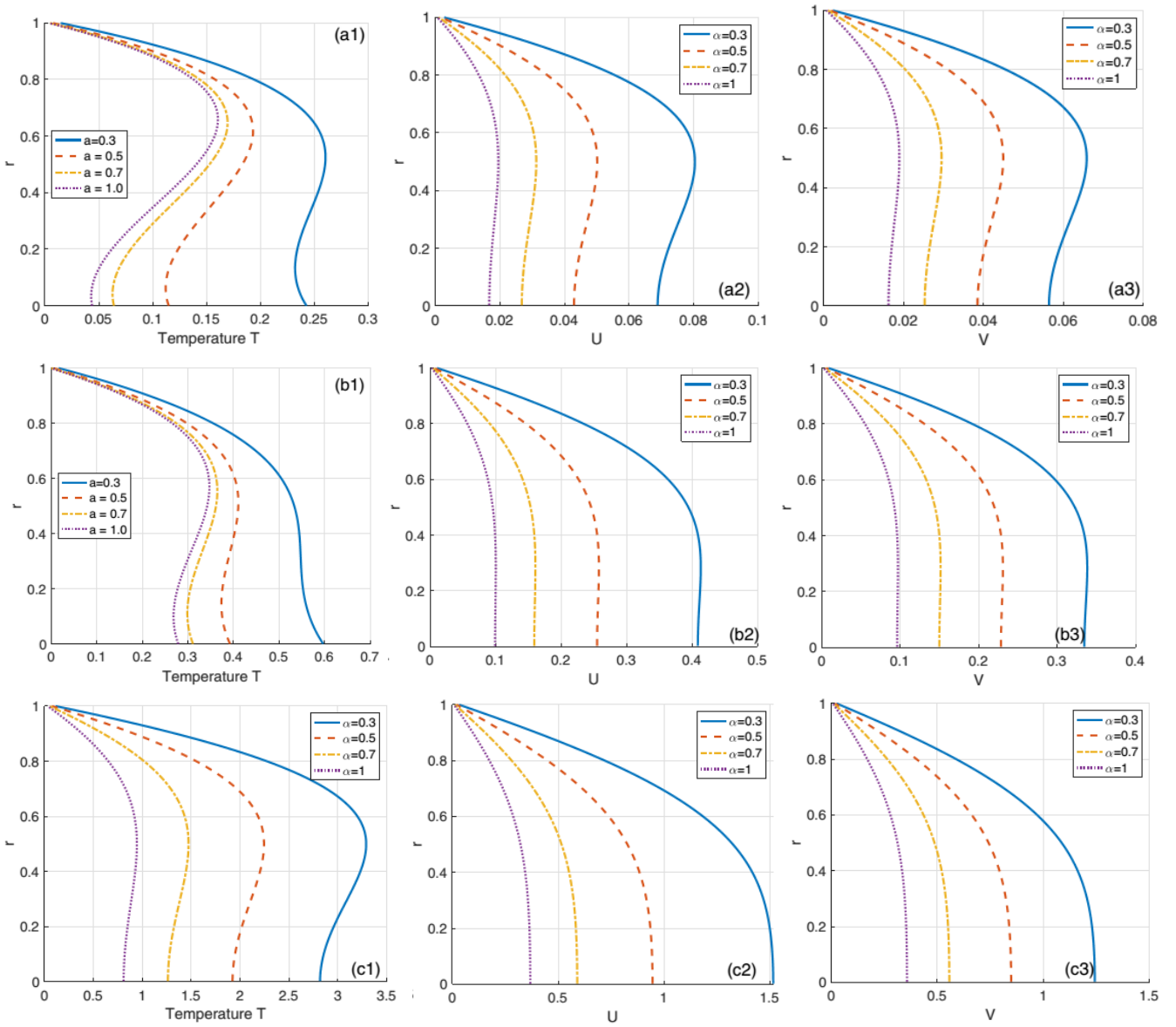

Figure 3.4: Profiles of blood temperature $T(r,t)$, axial velocity $U(r,t)$, and particle velocity $V(r,t)$ for different values of Reynold number Re, at $t = 3$ (large value of time), with $S = 0.01$, $A_0 = 10^{-7}$, $A_1 = 10^{-7}$, $\omega = \pi/4$, $\beta = 0.5$, $\lambda = 0.5$, $G = 1.5$, $R = 0.2$ and $\mathcal{H} = 1$. Panels $(a_j)_{j=1,2,3}$ correspond to $Re = 3$, panels $(b_j)_{j=1,2,3}$ give results for $Re = 4$ and panels $(c_j)_{j=1,2,3}$ correspond to $Re = 5$. In all panels, the fractional parameter takes the values $a = 0.3, 0.5, 0.7$ and 1.

For large values of time, i.e., $t = 3$ (Fig. 3.4), Re also takes the same values as in Fig. 3.3, but one notices small temperatures even though they still decrease with increasing of a. Blood and particle velocities also increase when Re changes, but they are very low compared with what was obtained in Fig. 3.4. This confirms the results obtained in [41], where particle were not included in the model. In addition, such behaviour has been described by Shah *et al.* [126], who also showed that the Reynolds number coupled with an increasing fractional parameter, can contribute to a significant increase in

blood velocity and cause acceleration of magnetic particles.

The influence of the magnetic field on the blood temperature, blood velocity and particlesvelocity is depicted in Figs. 3.5 and 3.6.
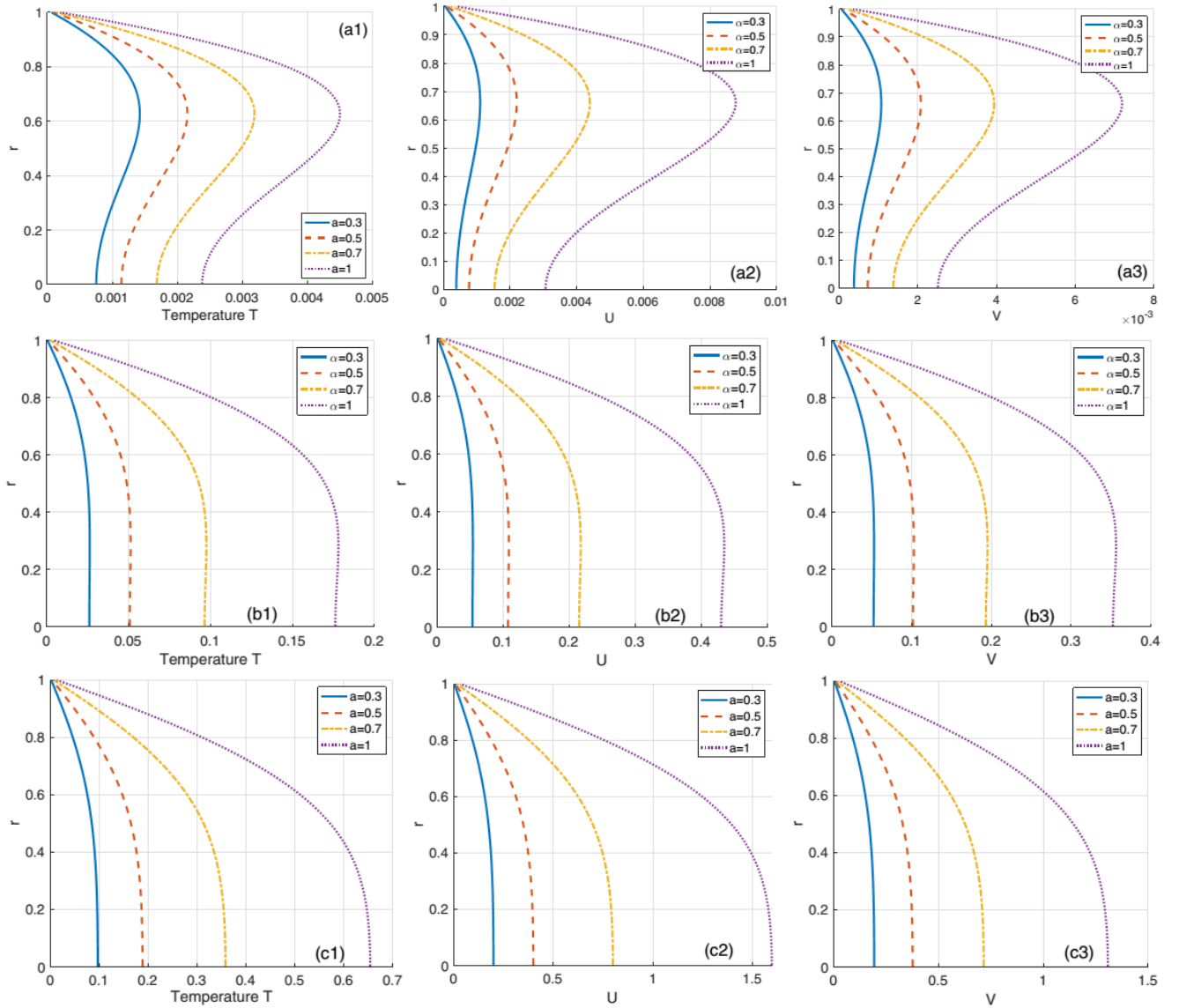

Figure 3.5: Profiles of blood temperature $T(r,t)$, axial velocity $U(r,t)$, and particle velocity $V(r,t)$ for different values of Hartmann number $\mathcal{H}$, at $t = 0.2$ (small value of time), with $S = 0.01$, $A_0 = 10^{-7}$, $A_1 = 10^{-7}$, $\omega = \pi/4$, $\beta = 0.5$, $\lambda = 0.5$, $G = 1.5$, $R = 0.2$ and $Re = 3$. Panels $(a_j)_{j=1,2,3}$ correspond to $\mathcal{H} = 1$, panels $(b_j)_{j=1,2,3}$ give results for $\mathcal{H} = 2$ and panels $(c_j)_{j=1,2,3}$ correspond to $\mathcal{H} = 3$. In all panels, the fractional parameter takes the values $a = 0.3, 0.5, 0.7$ and 1.

In Fig. 3.5, temperature and velocity profiles are recorded for a small value of time (t = 0.5) and columns from left to right correspond to $\mathcal{H} = 1, 2$ and 3 (Hartmann number). One notice that the velocities of the blood and the particles are reduced with increasing $\mathcal{H}$.
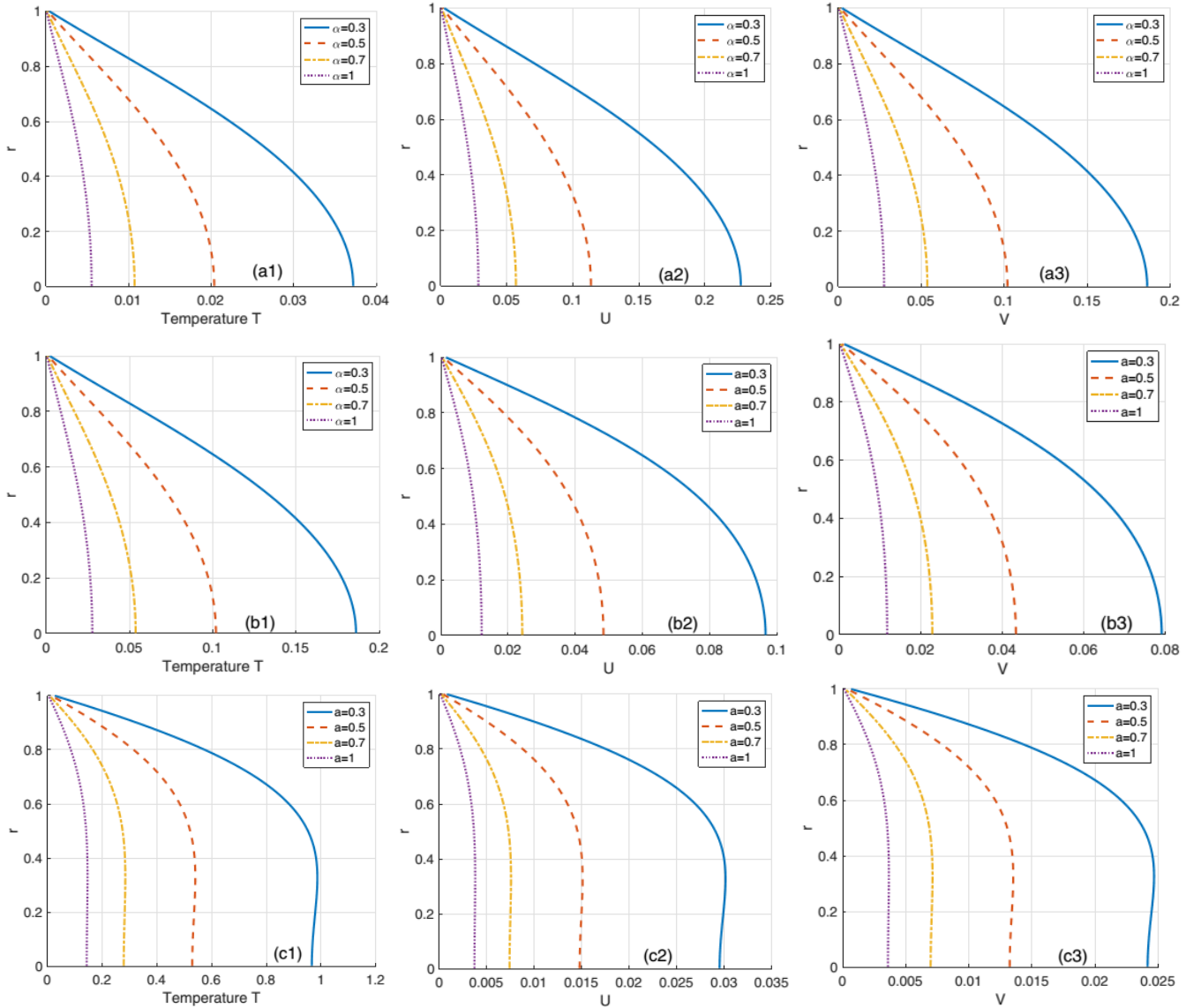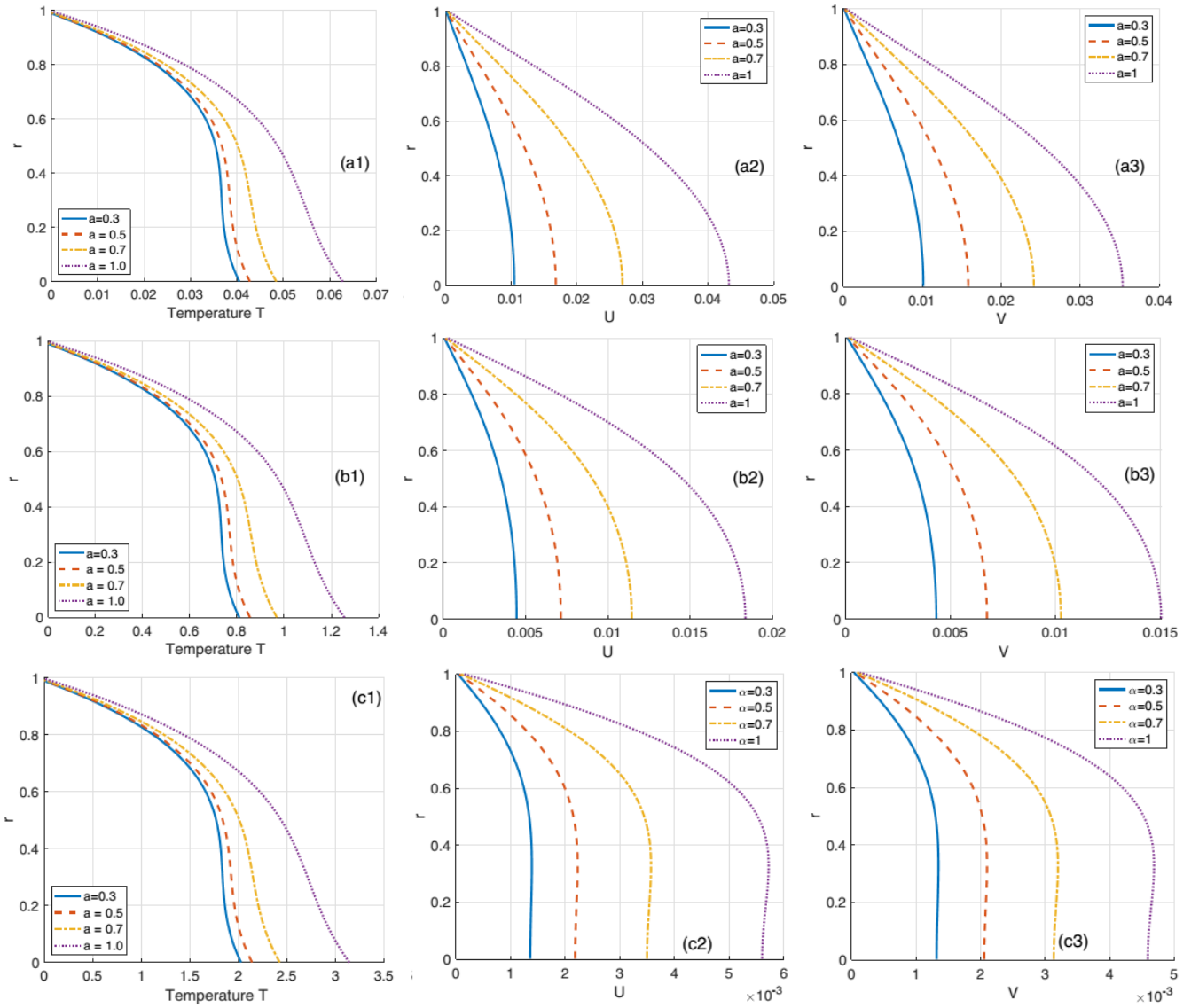
Figure 3.6: Profiles of blood temperature $T(r,t)$, axial velocity $U(r,t)$, and particle velocity $V(r,t)$ for different values of Hartmann number $\mathcal{H}$, at $t = 3$ (large value of time), with $S = 0.01$, $A_0 = 10^{-7}$, $A_1 = 10^{-7}$, $\omega = \pi/4$, $\beta = 0.5$, $\lambda = 0.5$, $G = 1.5$, $R = 0.2$ and $Re = 3$. Panels $(a_j)_{j=1,2,3}$ correspond to $\mathcal{H} = 1$, panels $(b_j)_{j=1,2,3}$ give results for $\mathcal{H} = 2$ and panels $(c_j)_{j=1,2,3}$ correspond to $\mathcal{H} = 3$. In all panels, the fractional parameter takes the values $a = 0.3, 0.5, 0.7$ and 1.

This becomes more predominant over long exposure time $t = 3$ as depicted in Fig. 3.6. In this last case, the temperature rather increases, which to our opinion has an impact not only on the blood viscosity, but also on the velocity of blood and the conveyed particles. Such a result is not surprising because, when a moving electrically conducting fluid is exposed to a magnetic field, there is electric induction in the fluid, and this is pronounced when magnetic particles are present.

For example, numerical and experimental works by Sharma *et al.* [124, 175, 176] revealed that Fe_3O_4 Magnetic particles can be efficiently captured when the applied magnetic field intensity is increased, with important applications in targeted drug delivery. Sheikholeslami and Shehzad [177]

showed that in such conditions, an increase in the nanoparticles may deeply affect the thermal conduction of blood, and the whole process may be favorable in slowing down the blood flow as a result of a Lorentz force that is created and retards the flow of blood. At that stage, the temperature of blood may be enhanced as observed by Akbar *et al.* [178], while the opposite trend is observed in the case of velocities of fluid and particles. In the meantime, the fractional parameter that varies also plays a role in controlling the flow characteristics. One can for example notice that temperature and both velocities are lower for the classical value of the fractional parameter, i.e., $a = 1$. The various values that can be attributed to make the model under our study flexible in the sense that it can be applied to a broad range of problems, each having specific applications either in technology or biomedicine.

3.3 Effects of chemical reaction and rotating nanofluid under a fractional magnetohydrodynamics model

3.3.1 Computational Scheme

Following the previous discussion on the mass and heat exchange of the medium, the magnetic particles being taken as a whole will then be observed independently to better understand their evolution in this medium and to highlight their impacts during interactions and propagations for different concentrations of the particles present. For this purpose, we will focus on the particles present in the blood and the synthesized carbon nanotube forms to observe their behavior on the different distributions taken into account. The study will be carried out numerically, by applying the L_1-algorithm method in (2.77). The time fractional-derivate ($0 < \alpha < 1$) is discretized through a finite difference approximation scheme [179] given by (2.145).

Applying the forward central difference method, one gets the discretized expressions

$$
\begin{aligned}
\left.\frac{\partial u}{\partial t}\right|_{t=t_k} &= \frac{u(r_i, t_k) - u(r_i, t_{k-1})}{\Delta t} + O(\Delta t), \\
\left.\frac{\partial u}{\partial r}\right|_{t=t_k} &= \frac{u(r_i, t_k) - u(r_{i-1}, t_k)}{\Delta r} + O(\Delta r), \\
\left.\frac{\partial^2 u}{\partial r^2}\right|_{t=t_k} &= \frac{u(r_{i+1}, t_k) - 2u(r_i, t_k) + u(r_{i-1}, t_k)}{\Delta r^2} + O(\Delta r^2),
\end{aligned}
\tag{3.15}
$$

in which Δr is a space step, and Δt is time step. With $t_k = (k-1)\Delta t$ and $r_i = (i-1)\Delta r$, $i = 1, 2, ..., M$.

Therefore, the problem to solve is reduced to the following discretized equations, obtained form

Eqs. (2.77):

$$
\begin{aligned}
u(r_i, t_k) =& \frac{1}{Y_1}\Bigg[e_0 Z_1 + \frac{E_4}{E_3}\Big(G_r \theta(r_i, t_k) + G_m \phi(r_i, t_k) \Big) + R v(r_i, t_k) \\
& + \frac{u(r_{i+1}, t_k)}{E_1 E_3 \Delta r^2} + \left(\frac{1}{E_1 E_3 \Delta r^2} - \frac{S}{\Delta r} \right) u(r_{i-1}, t_k) \Bigg], \\
v(r_i, t_k) =& \frac{1}{Y_1}\Bigg[e_0 Z_2 - R u(r_i, t_k) + \frac{v(r_{i+1}, t_k)}{E_1 E_3 \Delta r^2} + \left(\frac{1}{E_1 E_3 \Delta r^2} - \frac{S}{\Delta r} \right) v(r_{i-1}, t_k) \Bigg], \\
\theta(r_i, t_k) =& \frac{1}{Y_2}\Bigg[e_0 Z_3 + \frac{E_2}{P_r E_5 \Delta r^2} \theta(r_{i+1}, t_k) + \left(\frac{E_2}{P_r E_5 \Delta r^2} - \frac{S}{\Delta r} \right) \theta(r_{i-1}, t_k) \Bigg], \\
\phi(r_i, t_k) =& \frac{1}{Y_3}\Bigg[e_0 Z_4 + \left(\frac{1}{L_e \Delta r^2} + \frac{N_t}{L_e N_b \Delta r^2} \right) \phi(r_{i+1}, t_k) + \left(\frac{1}{L_e \Delta r^2} + \frac{N_t}{L_e N_b \Delta r^2} - \frac{S}{\Delta r} \right) \phi(r_{i-1}, t_k) \Bigg],
\end{aligned}
$$
$$(3.16)$$

where

$$
Z_1 = \lambda_{k-1} u(r_i, t_0) + \sum_{A=1}^{k-1} (\lambda_{A-1} - \lambda_A) u(r_i, t_{k-A}), \quad Z_2 = \lambda_{k-1} v(r_i, t_0) + \sum_{A=1}^{k-1} (\lambda_{A-1} - \lambda_A) v(r_i, t_{k-A}),
$$

$$
Z_3 = \lambda_{k-1} \theta(r_i, t_0) + \sum_{A=1}^{k-1} (\lambda_{A-1} - \lambda_A) \theta(r_i, t_{k-A}), \quad Z_4 = \lambda_{k-1} \phi(r_i, t_0) + \sum_{A=1}^{k-1} (\lambda_{A-1} - \lambda_A) \phi(r_i, t_{k-A}),
$$

$$
Y_1 = \frac{\Delta t^{-\alpha}}{\Gamma(2-\alpha)} + \frac{2}{E_1 E_3 \Delta r^2} + \frac{E_6}{E_3} M^2 - \frac{S}{\Delta r} + \frac{K_p}{E_1 E_3},
$$

$$
Y_2 = \frac{\Delta t^{-\alpha}}{\Gamma(2-\alpha)} + \frac{2 E_2}{P_r E_5 \Delta r^2} + \frac{Q}{P_r E_5} - \frac{S}{\Delta r},
$$

$$
Y_3 = \frac{\Delta t^{-\alpha}}{\Gamma(2-\alpha)} + \frac{2}{L_e \Delta r^2} + \frac{N_t}{L_e N_b \Delta r^2} - \frac{S}{\Delta r} + L_e \lambda^* (1 + \gamma \theta(r_i, t_k))^m \exp\left(-\frac{EE}{1 + \gamma \theta(r_i, t_k)}\right),
$$

$$
e_0 = \frac{\Delta t^{-\alpha}}{\Gamma(2-\alpha)}, \quad \lambda_A = (A+1)^{1-\alpha} - (A)^{1-\alpha}.
$$

3.3.2 Numerical results

The numerical solutions for the velocity, temperature and concentration are obtained by means of the above developed finite difference method combined with an L_1-algorithm. The effects of the nanoparticle volume fraction ψ, fractional derivative parameters α, magnetic parameter M together with nanoparticle shape factor $m = \frac{3}{\eta}$, with η being the sphericity of nanoparticles on flow and heat transfer are analyzed. The numerical results are addressed for $\alpha = 0.5, M = 55, Gr = 250, Gm = 150, F = 1, Pr = 300, R = 500, m = 1, Kp = 500, \lambda^* = 2.5, Le = 30, \gamma = 1.5, Nt = 0.3, Nb = 0.3, EE = 1, Q = 3000, S = -20$. In figure 3.7, the variation of nanoparticles for the value of $\psi = 0.05$ shows us that the $SWCNTs$ particles accelerate the movement of the nanofluid the most compared to the others: Cu, TiO_2 and Al_2O_3, respectively. Moreover, the Cu particles have a higher velocity than the Al_2O_3 particles in the blood nanofluid, represented here by the first figure on the left. This behaviour has also been observed in Ref. [3].
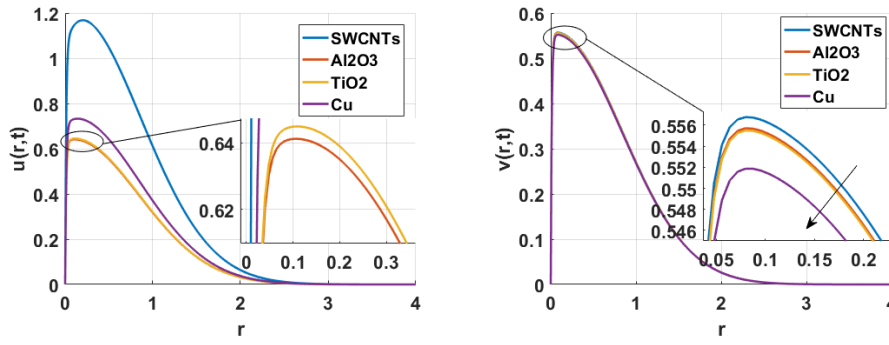
Figure 3.7: Velocities of differents nanoparticles for $\psi = 0.05$.

The right panel of figure 3.7 explains the motion of the nanoparticles in rotation, we observe a decrease in the velocities of Cu which has the lowest velocity followed by TiO_2, Al_2O_3 and $SWCNTs$ respectively in an increasing manner.
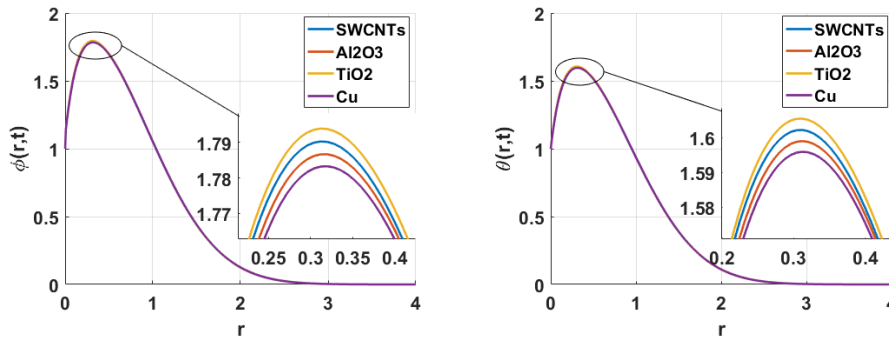
Figure 3.8: Concentration and Temperature of differents nanoparticles for $\psi = 0.05$.

Figure 3.8 shows the evolution of the concentration and the temperature in the medium. We noticed that TiO_2 has the highest temperature and concentration, followed, respectively, by $SWCNTs$, Al_2O_3 and Cu. This has been extensively studied by Hady at $al.$ [188] who obtained results different form those presented in this work. This is probably due to the fact that TiO_2 nanoparticles are proved to have better cooling performance for this problem than the other two types of nanoparticles Cu and Al_2O_3.
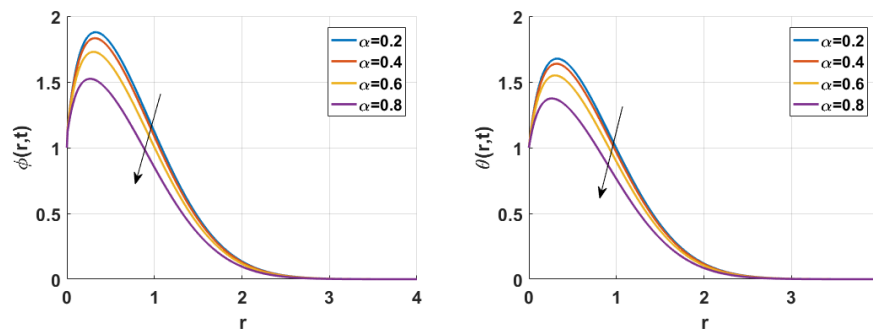
Figure 3.9: Effect of fractional parameter for the concentration and temperature respectively.
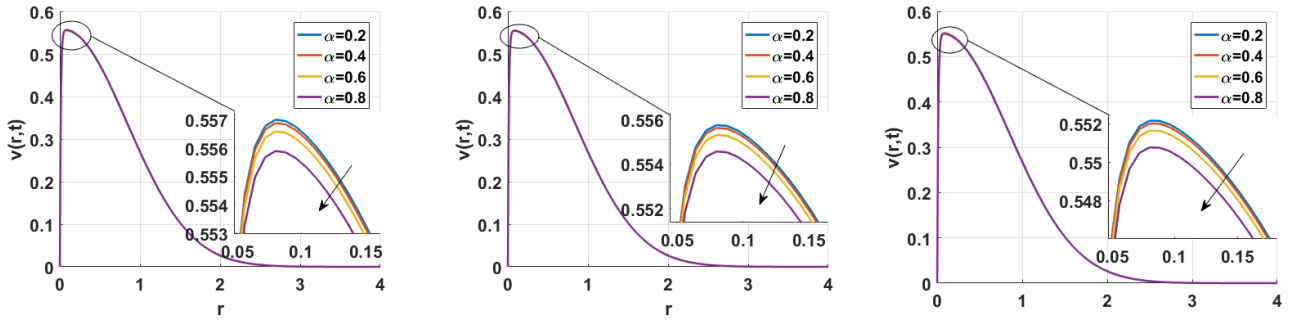
Figure 3.10: Effect of fractional parameter on velocity of nanoparticles: SWCNTs, TiO_2, Cu respectively.
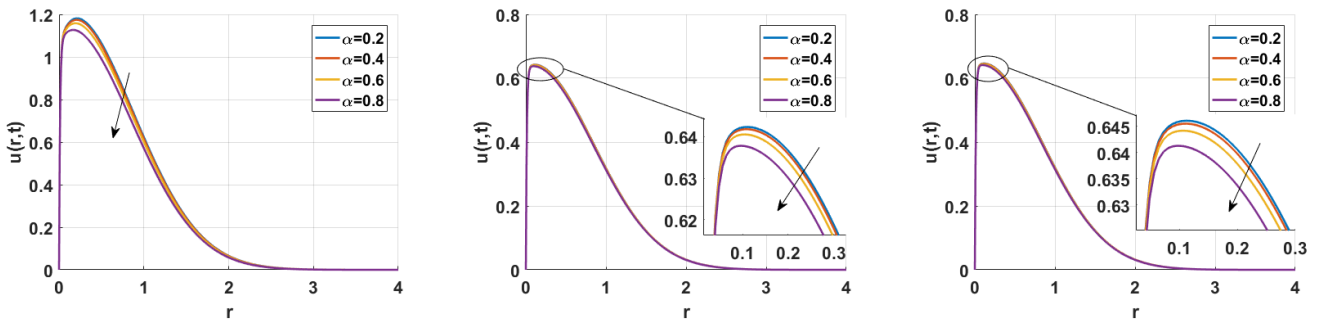
Figure 3.11: Effect of fractional parameter on velocity of nanofluid for: SWCNTs, Al_2O_3, TiO_2 respectively.

In Figures 3.9, 3.10 and 3.11, the impact of the fractional-order parameter is studied. We observe that the increase of α causes a decrease in the concentration, temperature, particle velocity and even fluid velocity. This parameter reacts more significantly in the case of SWCNTs compared to the various other nanoparticles which is illustrated in figure 3.11. The fractional-order parameter plays a very important role in the calibration of velocity, concentration and temperature distributions [41, 139, 180, 181]. It allows an initialization of the system according to the study and treatment carried out, generally observed during surgical interventions, on the optimisation or stability of energy transport in many dynamic systems.
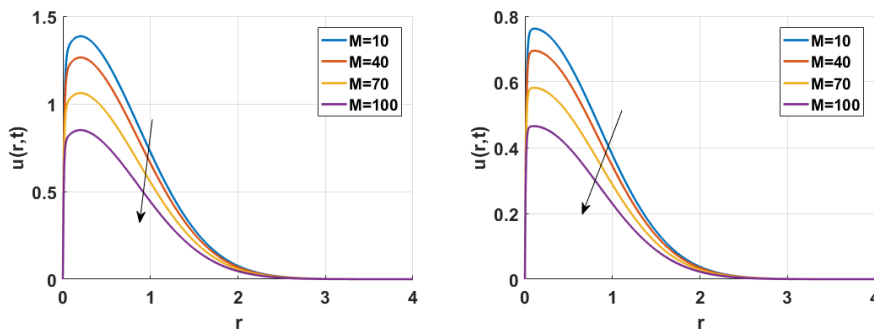
Figure 3.12: Effect of magnetic parameter on velocities for: SWCNTs and Al_2O_3.

In Figure 3.12, the increase of the magnetic field also causes the decrease of different velocities, thus making the medium more viscous which produces forces of resistance making the velocity to slow down [182]. The very low values of the magnetic field in the two nanoparticle cases considered in Figure 3.12, increasingly boost the velocity distributions initially obtained in Figure 3.7.
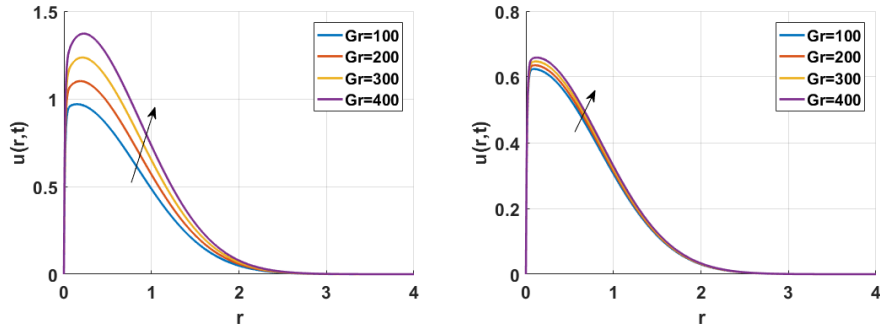
Figure 3.13: Effect of thermal Grashof number for: SWCNTs and Al_2O_3.
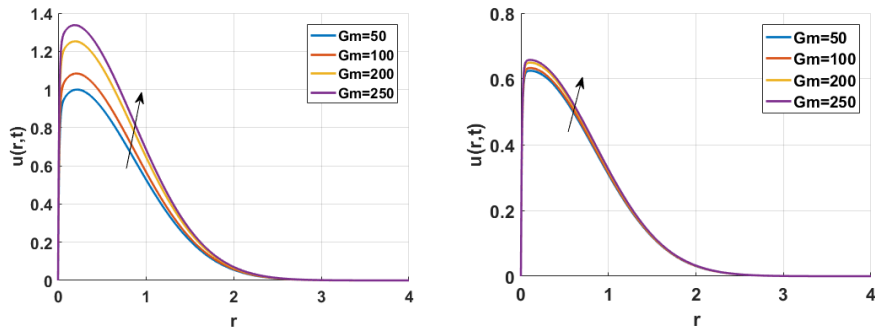
Figure 3.14: Effect of mass Grashof number for: SWCNTs and Al_2O_3.

The Grashof parameters in Figures 3.13 and 3.14, contribute to the increase of the velocity of nanofluid when they also increase.
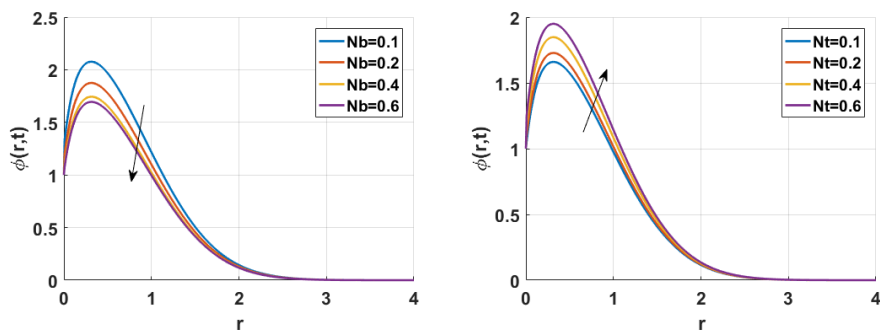
Figure 3.15: Effect of Brownian motion and Thermophoresis parameter.

The concentration of the medium grows with increasing values of the thermophoresis parameter shown by Figure 3.15. This parameter is greater than the noise parameter, which causes the decrease of concentration. The thermophoretic force cause the concentration layer to move from the lower

region to the higher one. Similarly, the faster random motion of particles in nanofluids elevates the Brownian forces to boost the concentration layer.
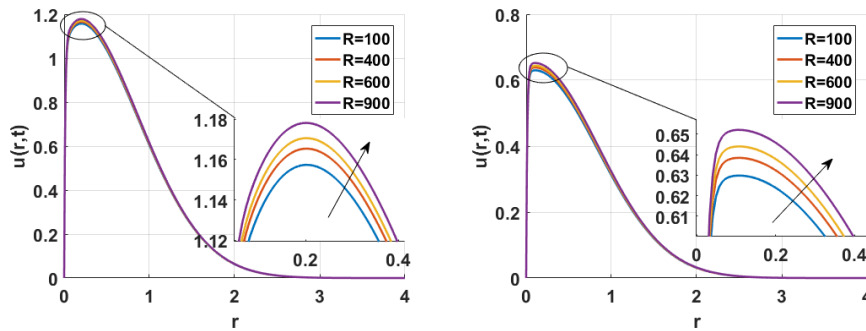
Figure 3.16: Effect of rotating parameter on nanofluid velocity for: SWCNTs and Al_2O_3.
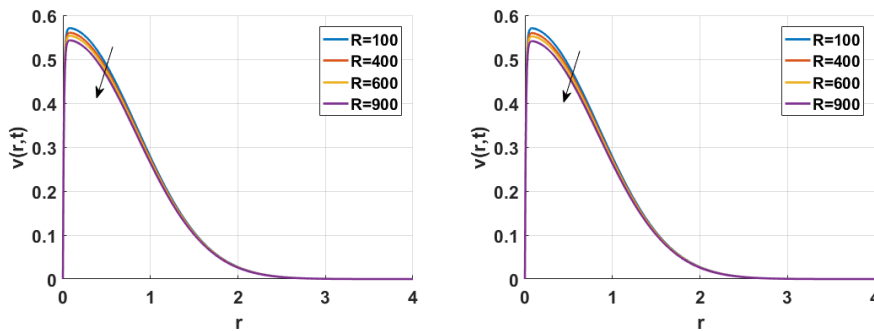
Figure 3.17: Effect of rotating parameter on nanoparticles velocity for: SWCNTs and Al_2O_3.

For the rotation parameter, Figures 3.16 and 3.17, show that the more the rotational movement of the nanoparticles accelerates, the more the velocity of the nanofluid increases and the nanoparticles decrease. So the rotational motion allows the particles to calibrate their velocities and move either slowly or quickly [141, 186].
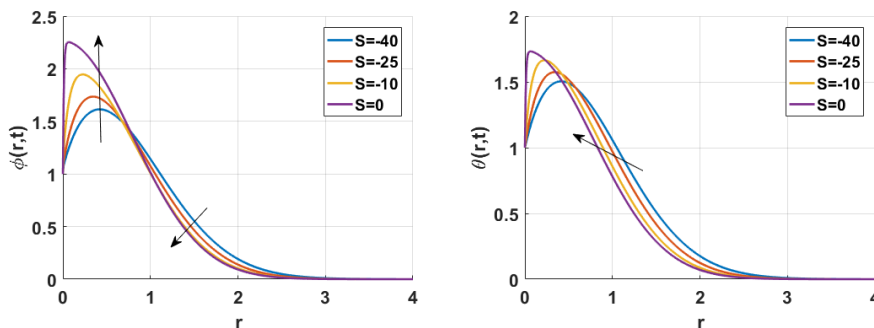
Figure 3.18: Effect of suction parameter on the concentration and temperature case of SWCNTs.
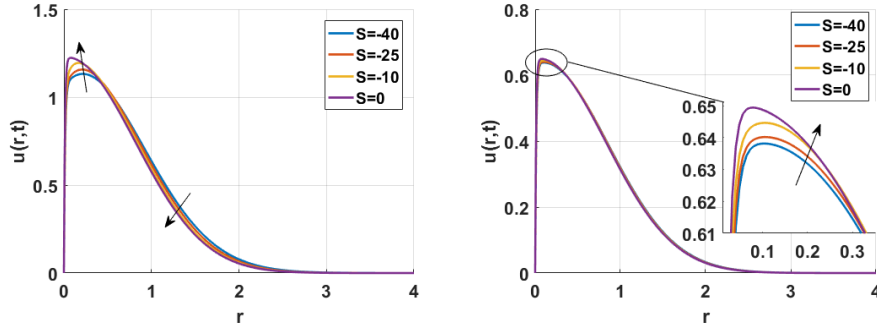
Figure 3.19: Effect of suction parameter on the nanofluid velocity for: SWCNTs and Al_2O_3.

Figures 3.18 and 3.19, give the evolution of the parameter of the velocity of the global transport. For increasing values of this parameter, the concentration has two domains. The first one increases with the amplitude of the concentrations. For the second one, more the parameter increases, more the concentration decreases. This marks an inflection zone between the central lines and the walls of the tube. Thus, as the suction parameter increases, the temperature increases, creating a bifurcation in the spatial evolution of the concentration for the different particles and the blood-nanofluid velocity distribution, as noticed for $SWCNTs$, while for Al_2O_3, the increase of the suction parameter increases with the ensembled velocity and does not produce any bifurcation.
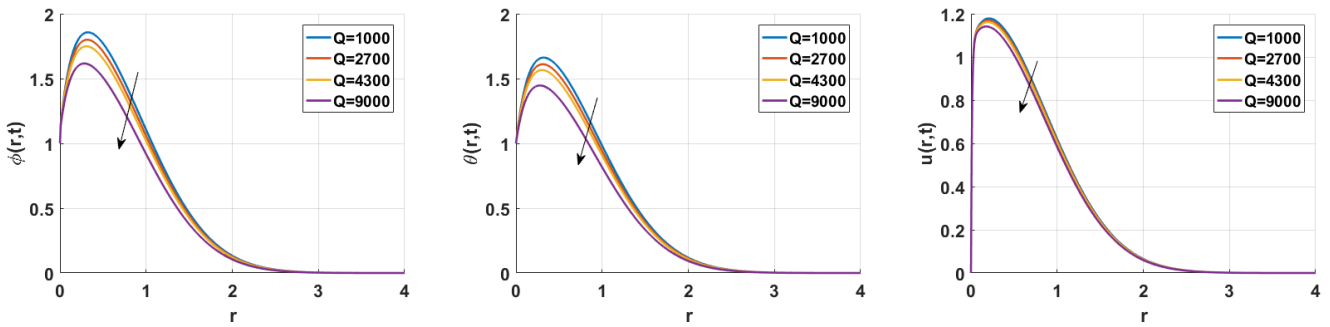
Figure 3.20: Effect of heat source parameter case of SWCNTs.

While for the temperature the evolution of this number increases the amplitude. The increase of the heat source variable in Figure 3.20, contributes to the decrease of the system. The same remarks are valuable for the case of $SWCNTs$, whose concentration, temperature and velocity distributions are decreasing. This also applies to the other nanoparticles, Al_2O_3, T_iO_2, Cu, which also decrease with the heat source parameter. This is in line with the study done by Choi and Eastman, and Tabi [4, 139] where nanoparticles were not taken into account.
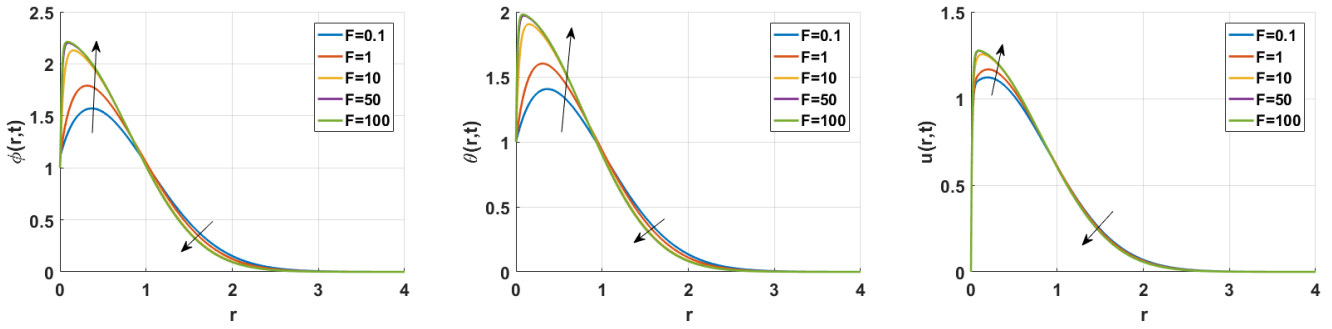
Figure 3.21: Effect of the radiation parameter case of SWCNTs.
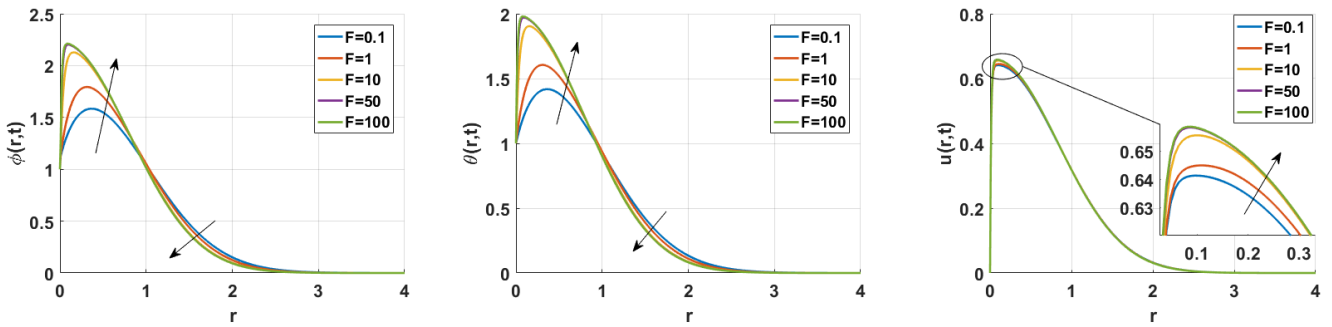
Figure 3.22: Effect of the radiation parameter case of TiO_2.

The radiation parameter F is investigated in Figures 3.21 and 3.22, respectively for the cases of SWCNTs and T_iO_2. Bifurcations are created in all distributions of the system where the values are increasing in the central lines and decreasing near the vessel walls for increasing values of the radiative parameter as shown in Figures 3.21 and 3.22. An increase in F leads to an enhancement in the velocity, temperature and concentration distributions across the boundary layer. The effect of thermal radiation is to enhance heat transfer, this is because thermal boundary layer thickness increases with an increase in the thermal radiation.
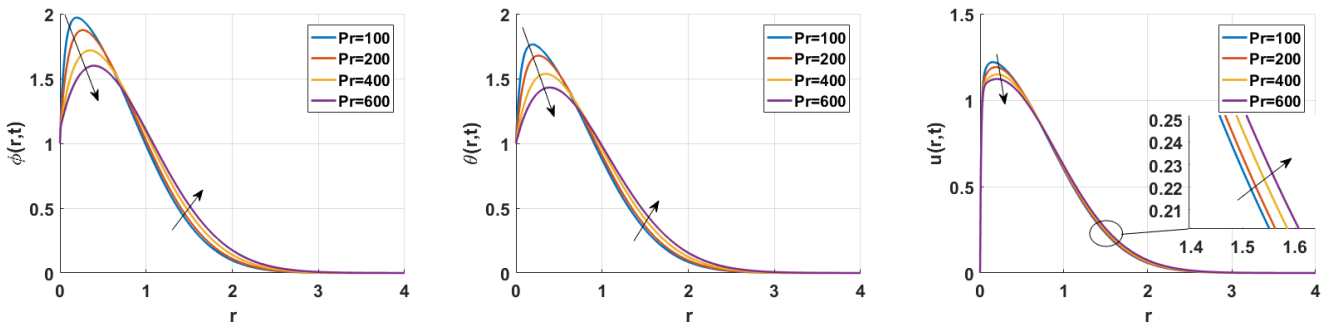
Figure 3.23: Effect of Prandt number.

The Prandtl number, as shown in Figure 3.23, also gives rise to an inflection zone in the system. The more this number increases, the more the amplitude of the system decreases and the first zone

decreases up to a certain distance. Then, we observe a growth of the system.

These parameters in Figures 3.20, 3.21, 3.22 and 3.23, allow us to better control the problems related to thermoregulation during hyperthermia in the presence of a heat source.
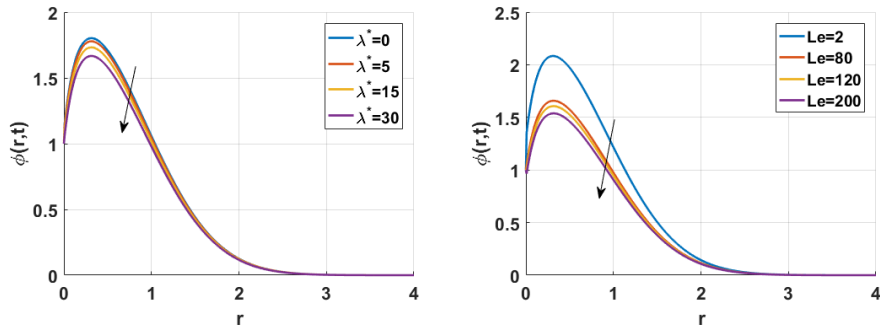
Figure 3.24: Effect of chemical reaction rate and Lewis number.

Figure 3.24 displays the chemical reaction rate, when it increases, the concentration in the medium also decreases, and for the Lewis number the more it increases, the less are the concentration, which makes the medium less viscous.
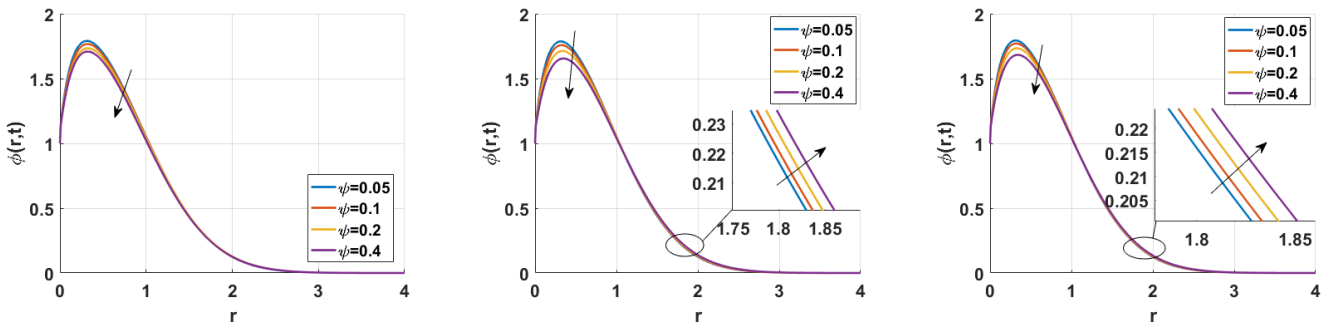
Figure 3.25: Concentration of SWCNTs, Al_2O_3, TiO_2 for $\psi \in [0.05, 0.4]$.
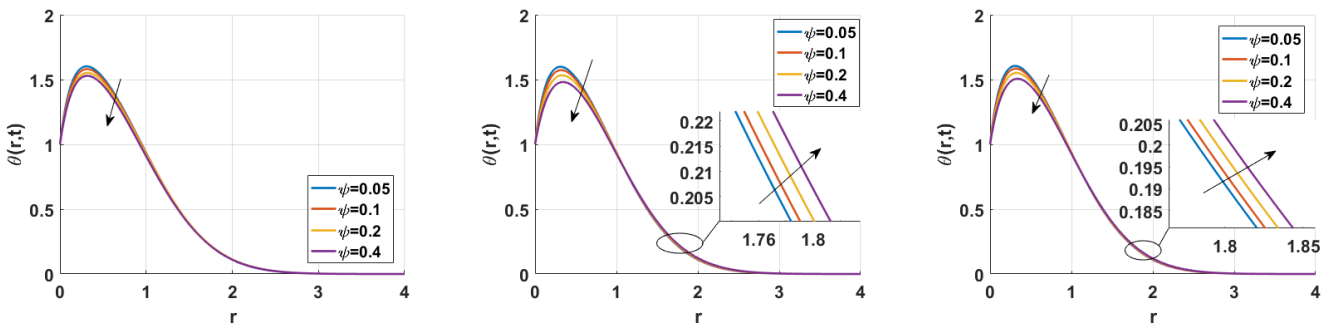
Figure 3.26: Temperature of SWCNTs, Al_2O_3, TiO_2 for $\psi \in [0.05, 0.4]$.

We noticed a decrease in both the concentration and the temperature for the increasing values of ψ, and for Figures 3.25, 3.26 the solid volume fraction evolves in an increasing manner and higher than

the value 0.1, to observe its evolution for different structures. It is observed, for the concentration and the temperature, a birth of an inflection zone for which of an initial time until a certain time, we have a decrease of the parameters of distributions. After this time, a growth of the system is observed, then for small values of ψ, we observe a certain order of the system and for large values of ψ a certain disorder is observed. This is illustrated by Figures 3.27 and 3.28, which led us to study the evolution of nanoparticles for larges values of ψ.
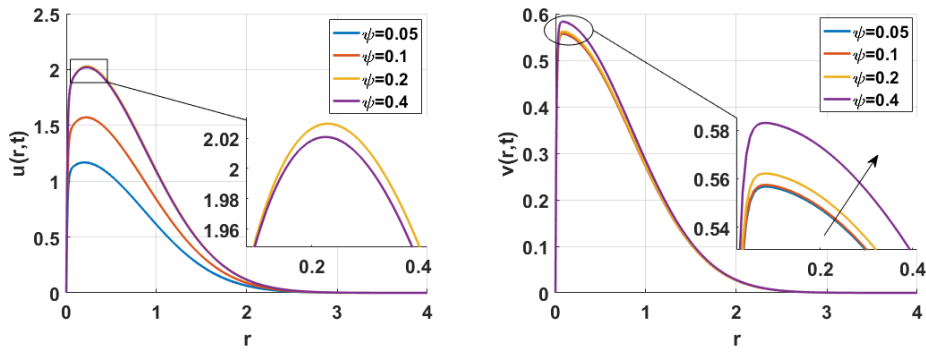
Figure 3.27: Velocity of SWCNTs for $\psi \in [0.05, 0.4]$.
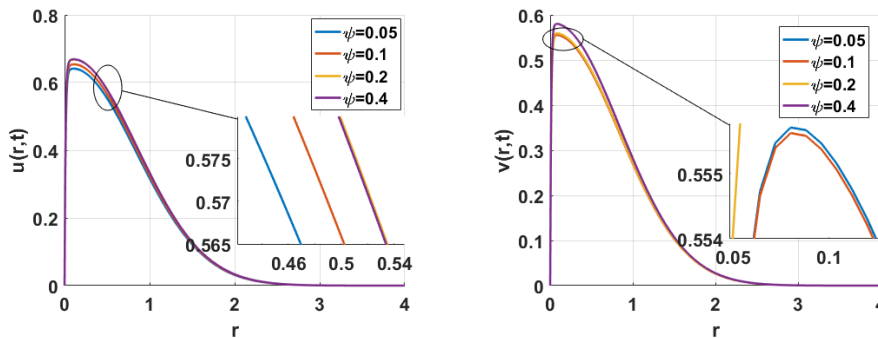
Figure 3.28: Velocity of Al_2O_3 for $\psi \in [0.05, 0.4]$.

We note the drop in concentration and temperature of TiO_2 up to the inflection point, while for the velocities it turns out that the $SWCNTs$ particle has to be able to move faster in the medium and to accelerate the dynamics of the nanofluid showing by Figure 3.29. As far as Cu is concerned, it moves slowly but with this ability to speed up the velocity of the nanofluid compare to Al_2O_3 and TiO_2 for a large ψ.
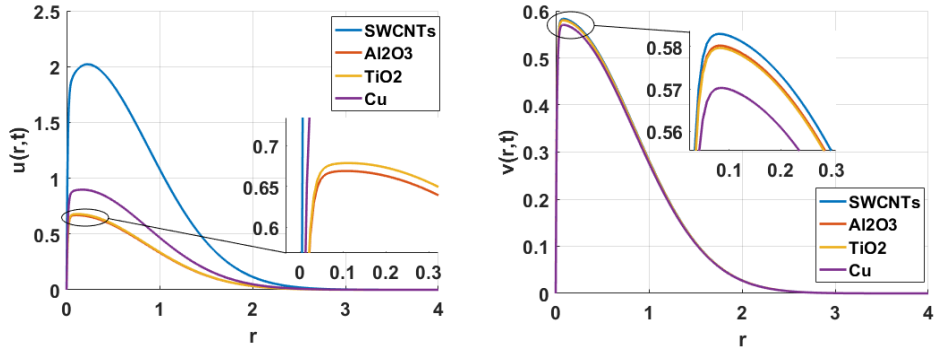
Figure 3.29: Velocities of differents nanoparticles for $\psi = 0.4$.
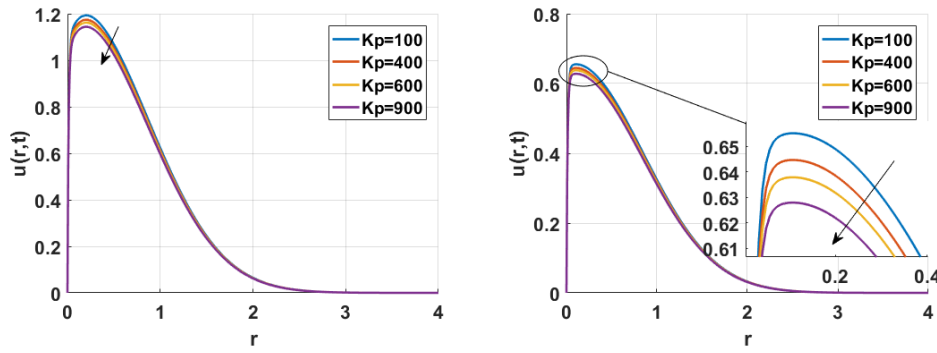
Figure 3.30: Effect of porosity parameter for SWCNTs and Al_2O_3.
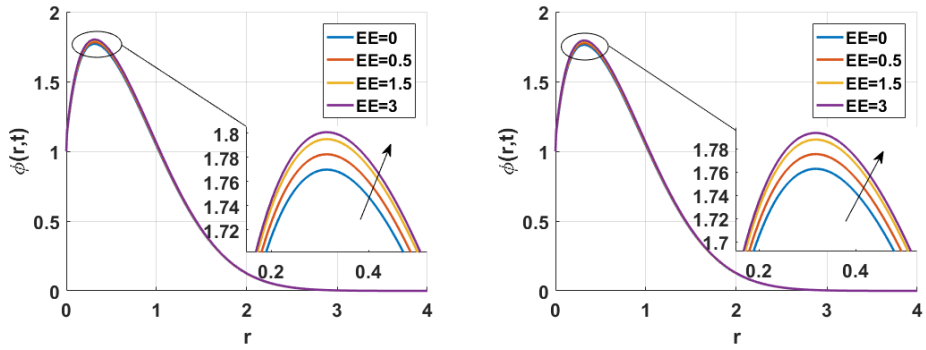
Figure 3.31: Effect of activation energy for SWCNTs and Cu.

Figure 3.30, gives the evolution of the velocity of the fluid for the increasing porosity parameter, it allows the decrease of the velocity and thus makes the medium more viscous. And so, we observe in Figure 3.31 an increase in the activation energy allowing a growth of the concentration characterizing the presence of several nanoparticles.
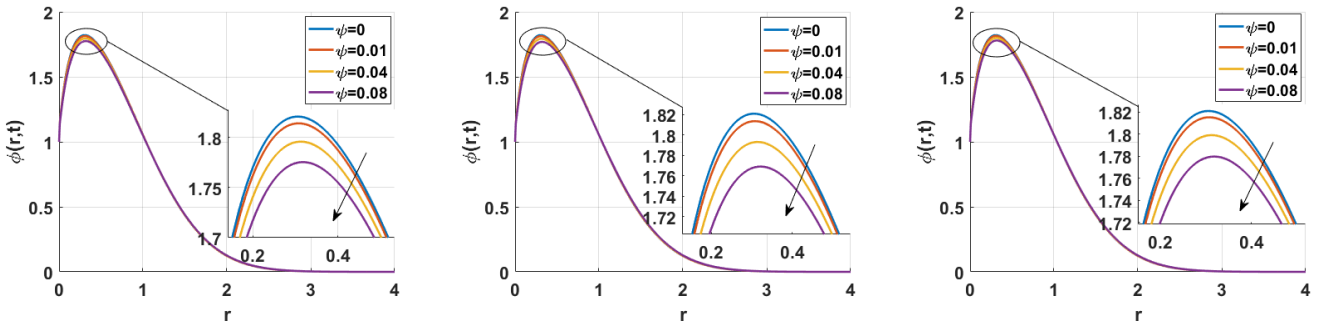
Figure 3.32: Concentration of SWCNTs, Al_2O_3, TiO_2 for $\psi < 0.1$.
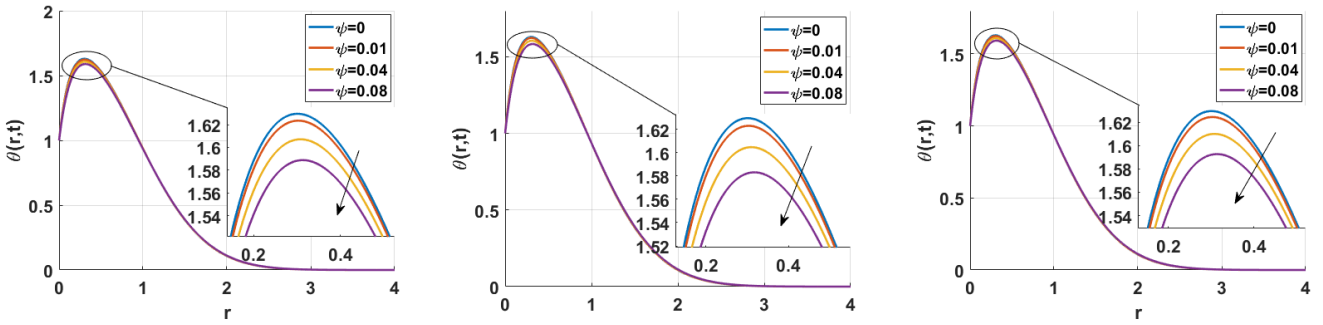
Figure 3.33: Temperature of SWCNTs, Al_2O_3, TiO_2 for $\psi < 0.1$.

So for small value of L_e the concentration tends to be very high and we have high mass diffusivity. Figures 3.32 and 3.33 show the concentration and temperature respectively of the solid volume fraction of nanoparticles for the values $\psi < 0.1$.
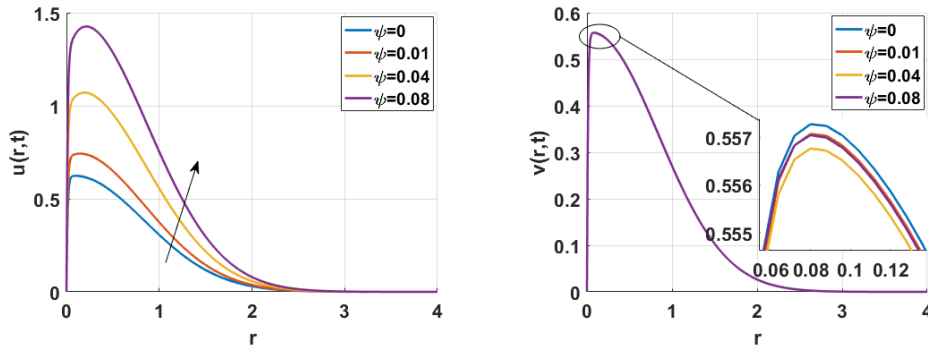
Figure 3.34: Velocity of SWCNTs for $\psi < 0.1$.
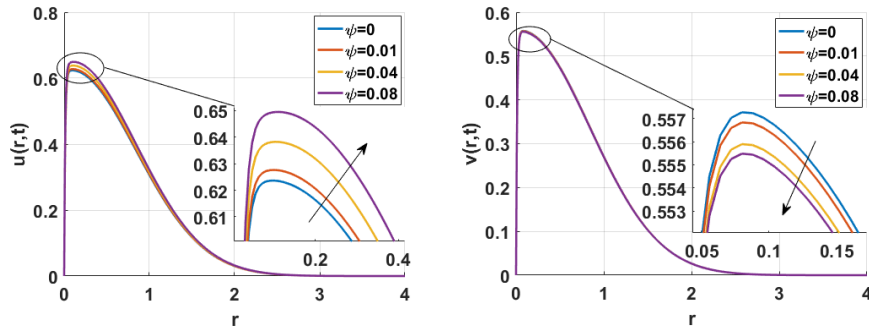
Figure 3.35: Velocity of Al_2O_3 for $\psi < 0.1$.

Then, for the case of $SWCNTs$ and Al_2O_3, the velocity are represented in Figures 3.34 and 3.35, where the overall velocity of the nanofluid increases with the increase of the solid volume fraction parameter. On the other hand, the velocity of the nanoparticles decreases for the case of Al_2O_3. In another development, for the case of $SWCNTs$, we observe a random decrease of the nanoparticles velocity with the increase of ψ. This is similar to the study of Zahir *et al.* [146].
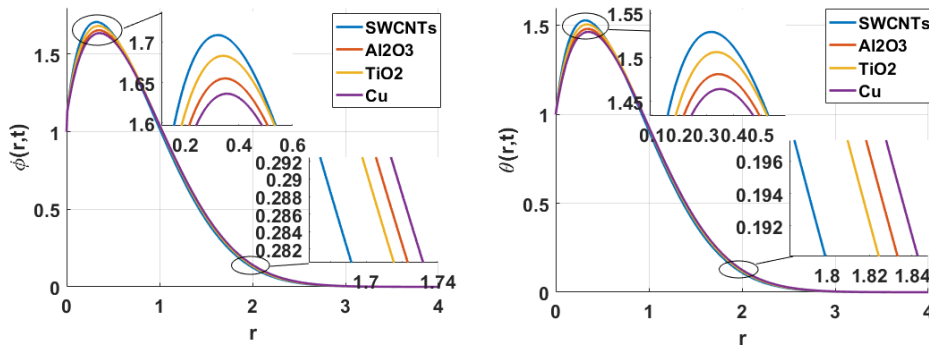
Figure 3.36: Concentration and Temperature of differents nanoparticles for $\psi = 0.4$.

In figure 3.36, the evolution of concentration and temperature have been expressed. We realized that for a big value of ψ the nanoparticle TiO_2 reduced considerably compared to the small value of ψ, then in this case, when the viscocity of nanofluid increases the concentration and the temperature of the medium tend to decrease.
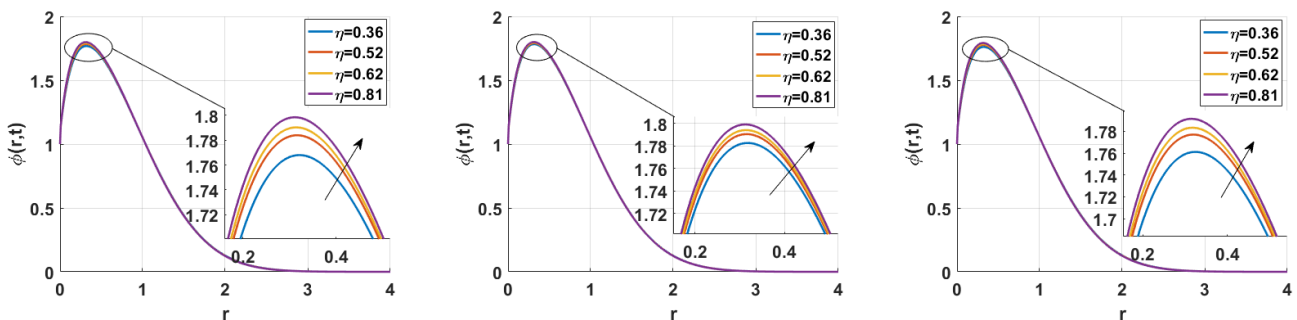
Figure 3.37: Effect of different Sphericity parameter for SWCNTs, TiO_2 and Cu.
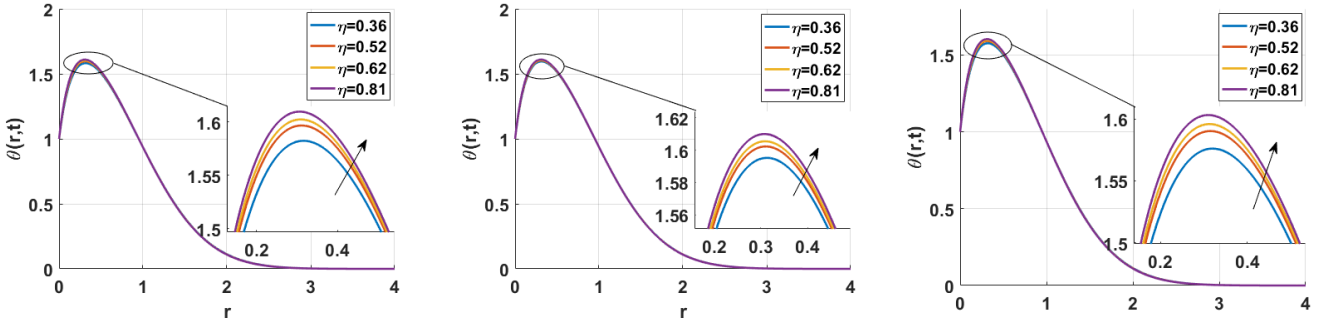
Figure 3.38: Effect of different Sphericity parameter for SWCNTs, TiO_2 and Cu.
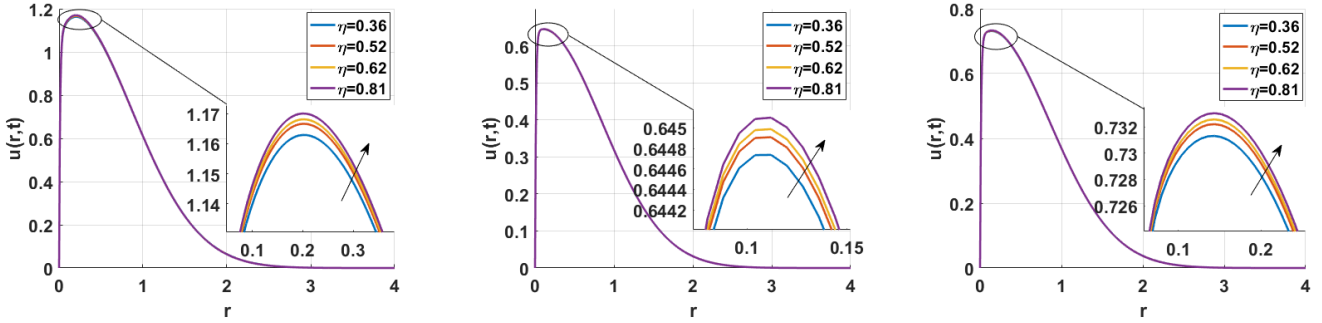
Figure 3.39: Effect of different Sphericity parameter for SWCNTs, TiO_2 and Cu.

Figures 3.37, 3.38, and 3.39 show the behaviour of the sphericity parameter of nanoparticle shapes in the case of $SWCNTs$, TiO_2, Cu, the more this parameter increases, the more the concentration, the temperature and the velocity of the nanofluid evolve. Thus, adding to this type of study, which was carried out by Timofeeva *et al.* [144] who were interested in the effects of particle shape on the thermophysical properties of alumina nanofluids considered as base fluid.

3.4 Effects on temperature field in superdiffusion medium under a fractional model

3.4.1 Numerical technique

After taking into account the influence of nanoparticles in the vessel by observing the reaction of the different distributions of the system, we now consider the highly diffusive medium by taking the cases without and with doping to highlight the behavior of nanoparticles in this type of medium. This will allow to better understand the behavior of nanoparticles when they are in a superdiffusive medium and to make predictions on how the medium could be doped. This study is conducted numerically using the L_1-algorithm method in (2.86), the time fractional derivate $(0 < \alpha < 1)$ is discretized based on a finite difference approximation formulation shows in (2.145).

78

Applying the forward, central difference given below:

$$
\begin{aligned}
\left.\frac{\partial u}{\partial t}\right|_{t=t_k} &= \frac{u(y_i, t_k) - u(y_i, t_{k-1})}{\Delta t} + O(\Delta t), \\
\left.\frac{\partial u}{\partial y}\right|_{t=t_k} &= \frac{u(y_{i+1}, t_k) - u(y_{i-1}, t_k)}{2\Delta y} + O(\Delta y), \\
\left.\frac{\partial^2 u}{\partial y^2}\right|_{t=t_k} &= \frac{u(y_{i+1}, t_k) - 2u(y_i, t_k) + u(y_{i-1}, t_k)}{\Delta y^2} + O(\Delta y^2), \\
\left.\frac{\partial^4 u}{\partial y^4}\right|_{t=t_k} &= \frac{u(y_{i-2}, t_k) - 4u(y_{i-1}, t_k) + 6u(y_i, t_k) - 4u(y_{i+1}, t_k) + u(y_{i+2}, t_k)}{\Delta y^4} + O(\Delta y^4),
\end{aligned}
\tag{3.17}
$$

where, Δy is a space step, Δt is time step. With $t_k = (k-1)\Delta t$ and $y_i = (i-1)\Delta y$, $i = 1, 2, ..., M$.

Then, taking (2.145) in (2.86) and considering the finite differences above, we get the following numerical result:

$$
\begin{aligned}
u_i^k =& \frac{1}{Y_1}\left[e_0 Z_1 + \lambda^{-\alpha}\left(\frac{1}{E_3}(A_0 + A_1\cos(\omega t)) - Pv_i^k\left(\frac{u_{i+1}^k - u_{i-1}^k}{2\Delta y}\right) + \frac{1}{E_1 E_3 R_e}\left(\frac{u_{i+1}^k + u_{i-1}^k}{\Delta y^2}\right)\right.\right. \\
& \left.\left. - \frac{R}{E_3}\left(\frac{u_{i-2}^k - 4u_{i-1}^k - 4u_{i+1}^k + u_{i+2}^k}{\Delta y^4}\right) + \frac{E_4}{E_3}Gr T_i^k\right)\right], \\
T_i^k =& \frac{1}{Y_2}\left[e_0 Z_2 + \lambda^{-\alpha}\left(\frac{E_2}{E_5 P_e}\left(\frac{T_{i+1}^k + T_{i-1}^k}{\Delta y^2}\right) - \frac{E_2}{E_5 P_{e1}}\left(\frac{T_{i-2}^k - 4T_{i-1}^k - 4T_{i+1}^k + T_{i+2}^k}{\Delta y^4}\right)\right.\right. \\
& \left.\left. - Pv_i^k\left(\frac{T_{i+1}^k - T_{i-1}^k}{2\Delta y}\right) + \frac{Da}{E_1 E_5 Q}\left(\frac{u_{i+1}^k - u_{i-1}^k}{2\Delta y}\right)^2 + \frac{E_6 M^2}{E_5 Q}\left(u_i^k\right)^2\right)\right],
\end{aligned}
\tag{3.18}
$$

with

$$
Z_1 = \lambda_{k-1}u(y_i, t_0) + \sum_{A=1}^{k-1}(\lambda_{A-1} - \lambda_A)u(y_i, t_{k-A}), \qquad Z_2 = \lambda_{k-1}T(y_i, t_0) + \sum_{A=1}^{k-1}(\lambda_{A-1} - \lambda_A)T(y_i, t_{k-A}),
$$

$$
Y_1 = \frac{\Delta t^{-\alpha}}{\Gamma(2-\alpha)} + \frac{2\lambda^{-\alpha}}{E_1 E_3 R_e \Delta y^2} + \frac{6R\lambda^{-\alpha}}{E_3 \Delta y^4}, \qquad Y_2 = \frac{\Delta t^{-\alpha}}{\Gamma(2-\alpha)} + \frac{2E_2\lambda^{-\alpha}}{E_5 P_e \Delta y^2} + \frac{6E_2\lambda^{-\alpha}}{E_5 P_{e1}\Delta y^4},
$$

$$
e_0 = \frac{\Delta t^{-\alpha}}{\Gamma(2-\alpha)}, \quad \lambda_A = (A+1)^{1-\alpha} - (A)^{1-\alpha}.
$$

3.4.2 Numerical results

The different information on the flows will be obtained by numerical simulations, using the solution given by relation (3.18) above, itself obtained by the L_1-algorithm method which will allow us to have a numerical scheme of speed and temperature distribution under the influence of the fractional parameter. The numerical results are presented in figures (3.40) to (3.55), where the temperature and velocity distributions of the fluid under the influence of the fractional parameter are represented graphically. The effects of the latter are discussed in various cases where they are taken for the large and small values respectively of the magnetic parameter (M), the Grashof number (Gr), the porosity parameter (Da), the parameter translating the sources of metabolic heat (Q), the radiation parameter (P), the Peclet number (Pe), the Reynold number (Re), and the rotation parameter of the

particles in the ambient environment, all of which are variables. On the other hand, figures (3.56) and (3.57) show the variations in the amplitude of the wave by varying the parameter (A_0) which is the amplitude given by the pressure gradient. The result represented here brings a certain interest in the studies carried out by Misra *et al.* [150] who did not insist on a very diffusive heat exchange medium within fractional effect. In the set of numerical results presented below, the rest of the parameter values have been set as follows: $q = 4$, $M = 300$, $Gr = 2.5 * 10^3$, $Da = 50$, $Q = 1$, $P = 400$, $P_1 = 100$, $Pe = 1$, $Pe1 = 10^6$, $Re = 0.5$, $R = 10^{-6}$, $A_0 = 2.5 * 10^3$, $A_1 = 13$, and $\omega = \pi/4$.
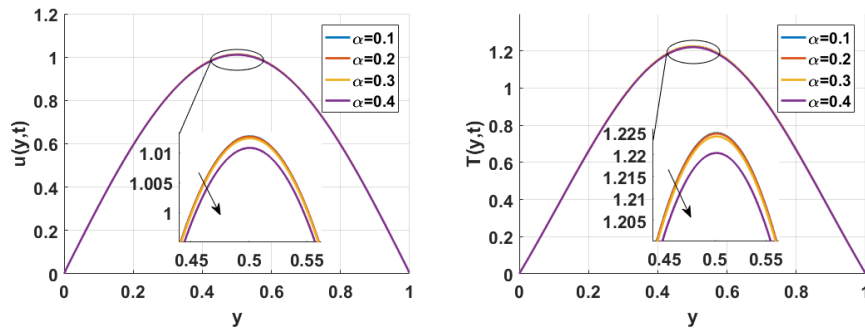
Figure 3.40: Effects of small values of fractional parameter on the velocity and temperature respectively.
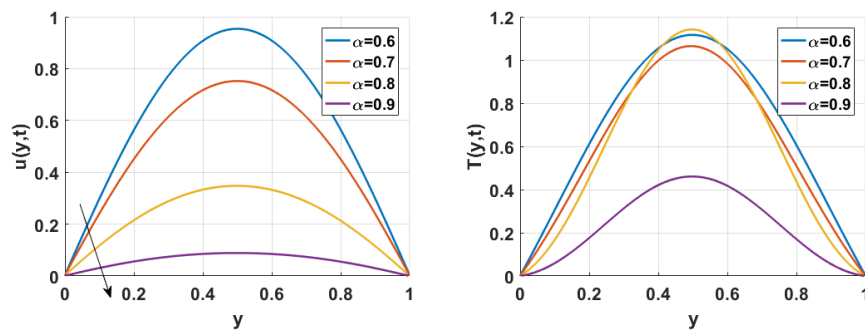
Figure 3.41: Effect of high values of fractional parameter on the velocity and temperature respectively.
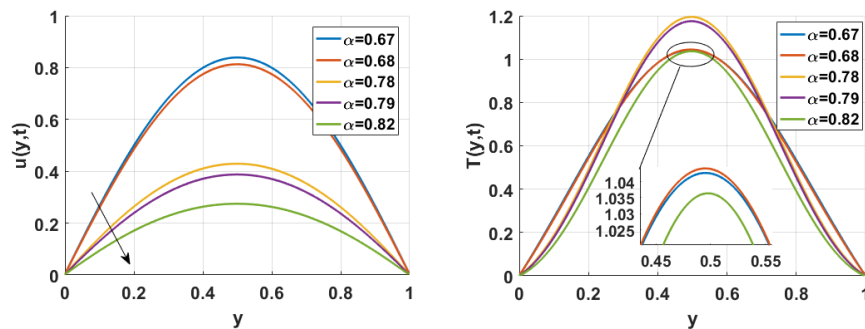
Figure 3.42: Effect of fractional parameter between 0.67 and 0.82 on the velocity and temperature respectively.

In our system the fractional derivative parameter lowers the distributions of heat and velocity represented by figure (3.40) and (3.41), up to a critical value of $\alpha = 0.68$ illustrated in figure (3.42), where we observe the birth of three zones at the extremities of the plates.
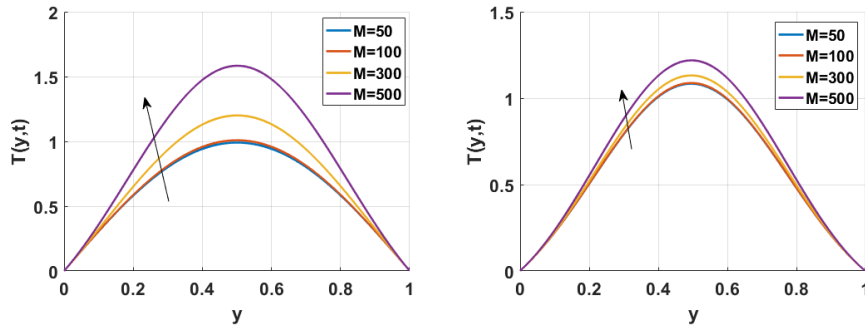
Figure 3.43: Effect of the magnetic parameter on the temperature respectively for the case of $\alpha = 0.5$ and $\alpha = 0.73$.

The effects of the magnetic field were observed for the mean value of the fractional parameter $\alpha = 0.5$, before that of the critical zone figure (3.43). We note that, for small values of α, the magnetic parameter increases considerably with the growth of the field, while for large values of α precisely in the zone of disturbance the temperature evolves very slightly with the increase of the magnetic field.
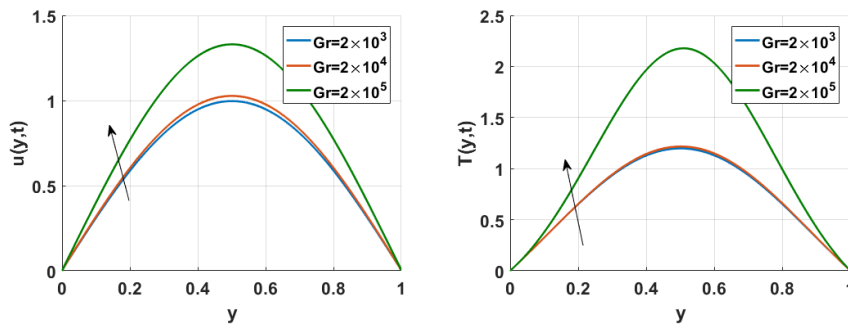
Figure 3.44: Effect of the thermal Grashof number for $\alpha = 0.5$.

The same phenomenon is also observed for the Grashof parameter in figure (3.44) for the mean value of α, where velocity and temperature increase strongly with the growth of Gr. For the value $\alpha = 0.73$ in figure (3.45) the temperature changes its behavior and decreases with the evolution of Grashof, while the velocity decreases in amplitude but continues to increase with the increase of Gr.
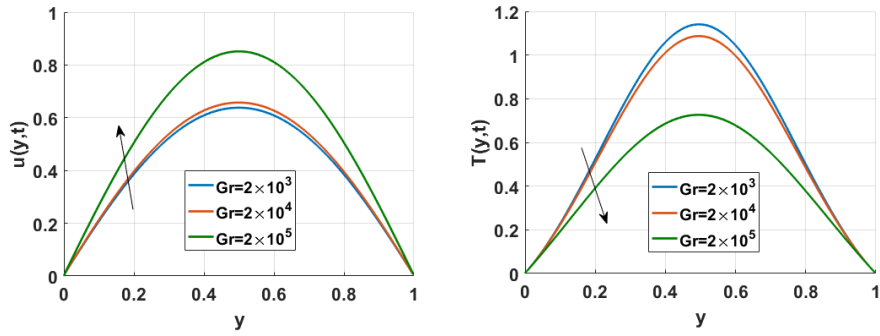
Figure 3.45: Effect of thermal Grashof number for $\alpha = 0.73$.

This implies that in figure (3.44), the forces of gravity have dominated the viscocity of the medium. The less viscous the medium is, the more the flow is accelerated and the temperature of the medium increases. On the other hand, in the case of figure (3.45), the gravity forces are dominated by the viscocity of the medium. Therefore, the more viscous the medium, the less the flow of the fluid. This makes the temperature distribution less turbulent.
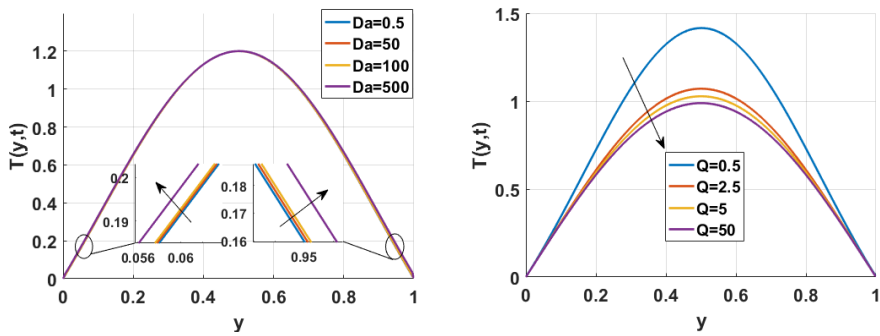
Figure 3.46: Effect of porosity and heat source parameter for $\alpha = 0.5$.
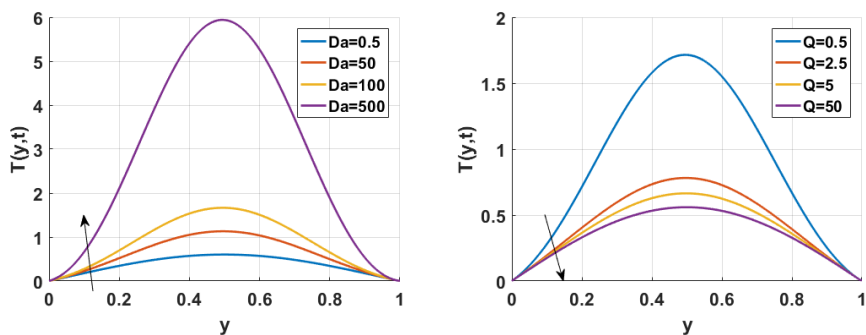
Figure 3.47: Effect of porosity and heat source parameter for $\alpha = 0.73$.

The effect of porosity here is illustrated in figure (3.46) and (3.47), for the value of $\alpha = 0.5$ the temperature of the system increases with increasing porosity, which is very slight. For the value $\alpha = 0.73$, we noticed a strong increase in temperature. In figure (3.46) and (3.47), the effect of

metabolic heat on the system is observed, for the value $\alpha = 0.5$ the temperature decreases slightly with a small initial amplitude. While for the value $\alpha = 0.73$, the amplitude spike is more pronounced and we always observe this rapid decrease in temperature for increasing values of Q.
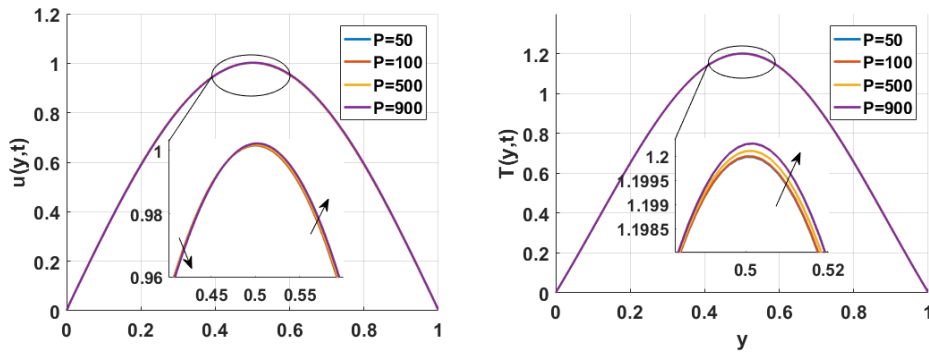
Figure 3.48: Effect of radiation parameter for $\alpha = 0.5$.
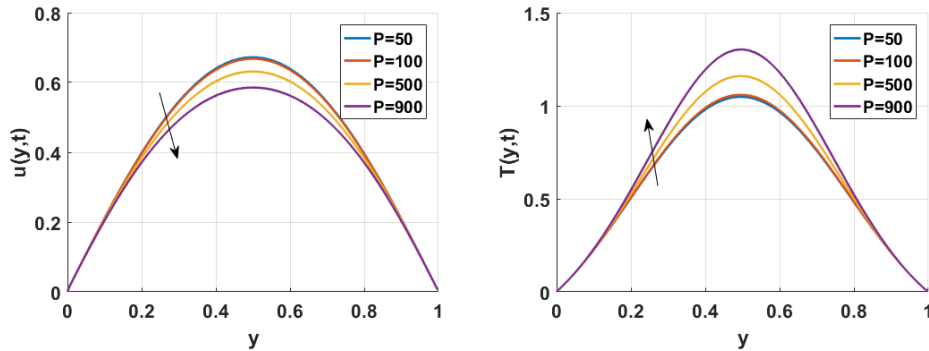
Figure 3.49: Effect of radiation parameter for $\alpha = 0.73$.

For the radiation parameter, we observe in figure (3.48) the evolution of the temperature and the velocity of the medium for the value $\alpha = 0.5$. The more the radiation parameter is increasing, the temperature of the system increases slightly. While for the velocity, we noticed the existence of two zones, the first one being close to the initial plate showing a slight decrease of the velocity up to a certain distance, suggesting a stagnation region of the particles in the medium. After this region, we observed a slight increase in velocity towards the second plate. However, for the value $\alpha = 0.73$, the temperature and velocity variations are more pronounced with a general decrease in temperature and velocity. The disappearance of the stagnation region is observed and the velocity distribution decreases with the increase of the radiation parameter P.
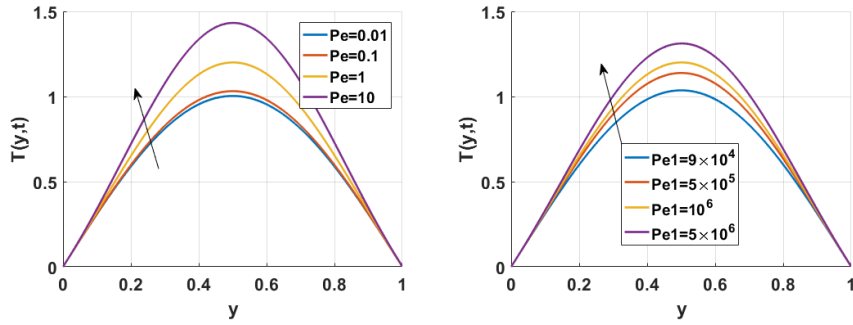
Figure 3.50: Effect of Peclet number for $\alpha = 0.5$.
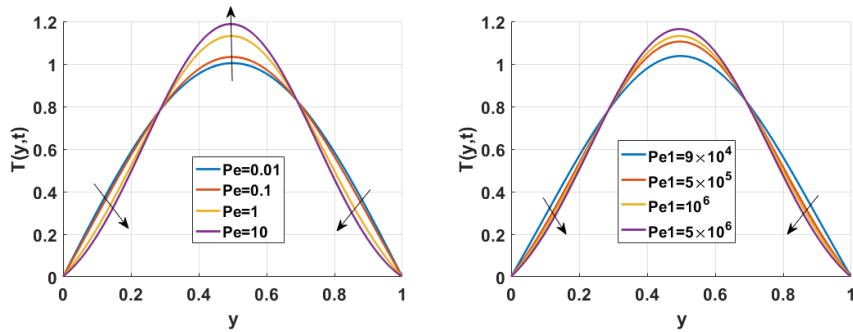
Figure 3.51: Effect of Peclet number for $\alpha = 0.73$.

Figures (3.50) and (3.51) show the evolution of P_e and P_{e1} respectively for $\alpha = 0.5$ and $\alpha = 0.73$. We note that, for the value $\alpha = 0.5$, the increase of the Peclet number and of the modified one increases the temperature of the medium which is the same behaviour observed by Ali *et al.* [183]. The temperature variations are more pronounced for the Peclet parameter and less for the modified one. Thus for the value $\alpha = 0.73$, we observed three regions in the evolution of the temperature, at the end of the plates the temperature decreases while at the center of the tube it increases with the increase of the Peclets. This implies that for a problem of stenosis to boost the temperature in the center of the vessel and consequently create the particles, the large values of Peclet are recommended. In addition, small values of Peclets are necessary to increase turbulence on the walls.
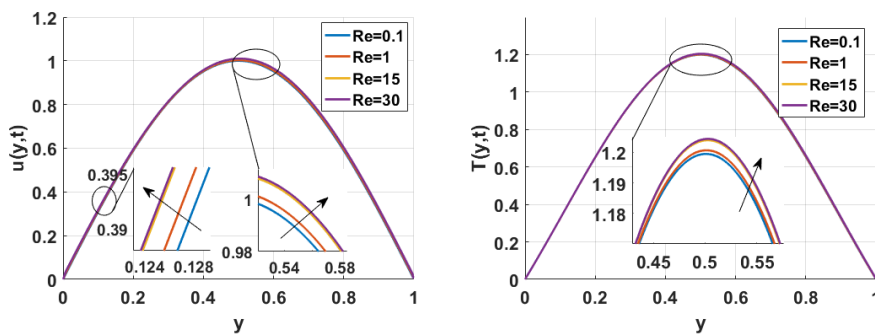
Figure 3.52: Effect of Reynold number for $\alpha = 0.5$.
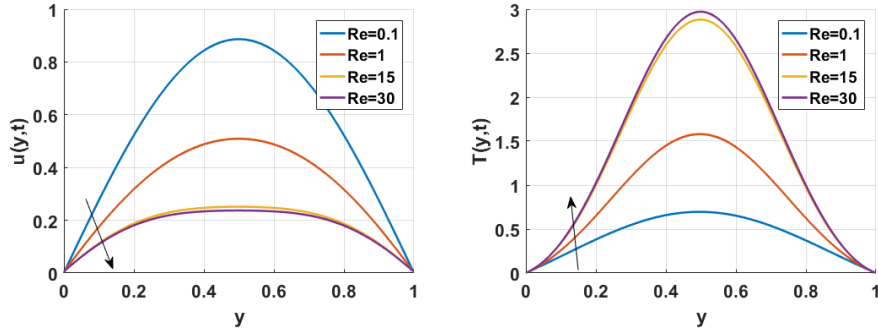
Figure 3.53: Effect of Reynold number for $\alpha = 0.73$.

Figures (3.52) and (3.53) express the effect of Reynold's number in the system. For the value of $\alpha = 0.5$, the Reynold's number increases with a slight increase of the temperature and the velocity increases but in a very slight way. Therefore, for the value of $\alpha = 0.73$, the temperature of the medium varies very significantly up to a certain limit. And for this limit, the velocity of the fluid becomes very low and uniform. In this case, the increase of R_e causes a decrease in the velocity distribution which is the opposite behaviour to that of $\alpha = 0.5$. These results are in the same line with those of Shang *et al.* [184].
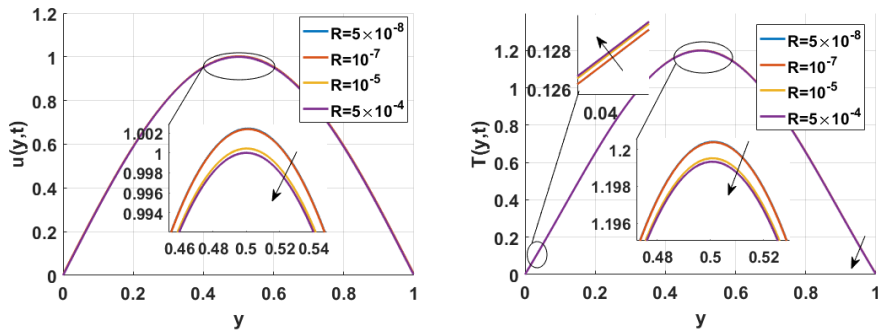
Figure 3.54: Effect of rotating parameter for $\alpha = 0.5$.
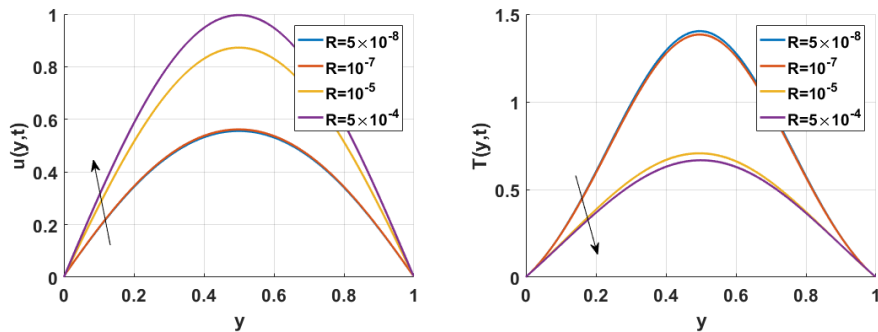
Figure 3.55: Effect of rotating parameter for $\alpha = 0.73$.

The increase of the rotating parameter R is observed in the figures (3.54) and (3.55). For the value of $\alpha = 0.5$, the variation of temperature and velocity is very small. For temperature, an increase in

temperature is observed at the first plate and an increase in the rest of the regions. There is therefore a reduction in velocity for this parameter. Finally, for the value of $\alpha = 0.73$ the variations are very strong, with an increase in speed and a decrease in temperature. This behavior is very different from that of the value $\alpha = 0.5$.
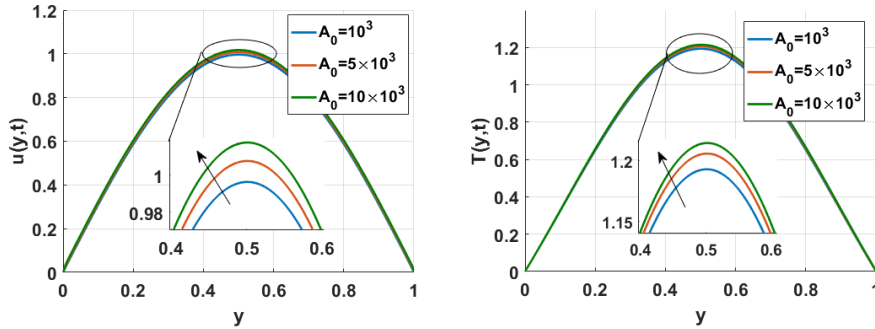
Figure 3.56: Effect of the amplitude parameter of the pressure gradient for $\alpha = 0.5$.
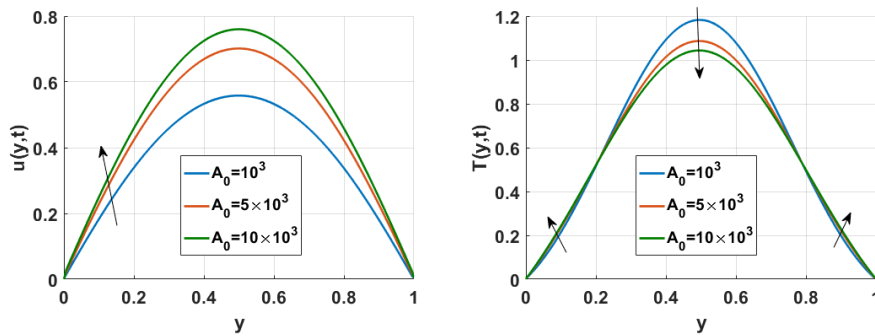
Figure 3.57: Effect of the amplitude parameter of the pressure gradient for $\alpha = 0.73$.

Figures (3.56) and (3.57) illustrate the influence of the pressure gradient amplitude parameter. For $\alpha = 0.5$, the increase in amplitude leads to a slight increase in the system amplitudes in a very slight way. While for $\alpha = 0.73$, the velocity of the medium always increases considerably. On the other hand for the temperature, three zones are created including that near the plates with a tendency to increase very slightly. But in the center of the tube, a decrease in amplitude and temperature is observed.

In the following, we observe the behaviour of different nanoparticles (SWCNTs, MWCNTs, Fe_2O_3, TiO_2, CuO) on the propagation of velocity waves and temperature distribution, by varying the fractional parameters, the volume fraction and the rotation parameter. We will make a comparative study between the cases where nanoparticles are neglected and the case where they are fully taken into account with immediate effect.
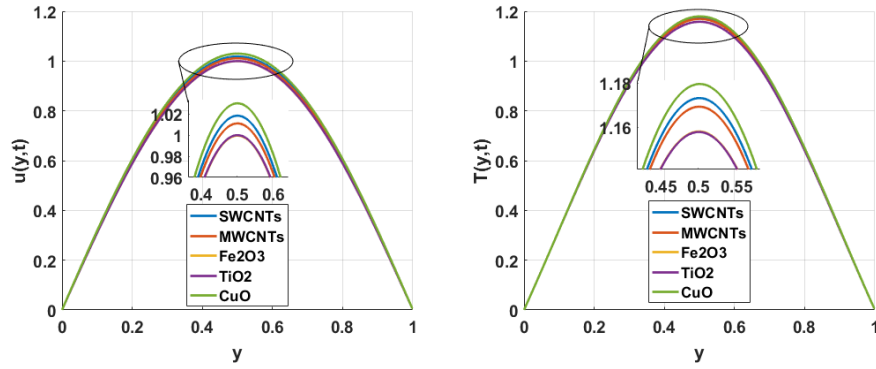
Figure 3.58: Velocity and Temperature of differents nanoparticles for $\alpha = 0.5$, $\psi = 0.05$ when $R = 10^{-5}$.

Figure (3.58) shows the effect of the variations of the fractional parameter ($\alpha = 0.5$), the volume fraction ($\psi = 0.05$) and the rotation parameter ($R = 10^{-5}$). For these particular values we observe a very small variation for different nanoparticles (SWCNTs, MWCNTs, Fe_2O_3, TiO_2, CuO) both for the velocity propagation and the temperature distribution. These phenomena have already been observed in [185, 186].
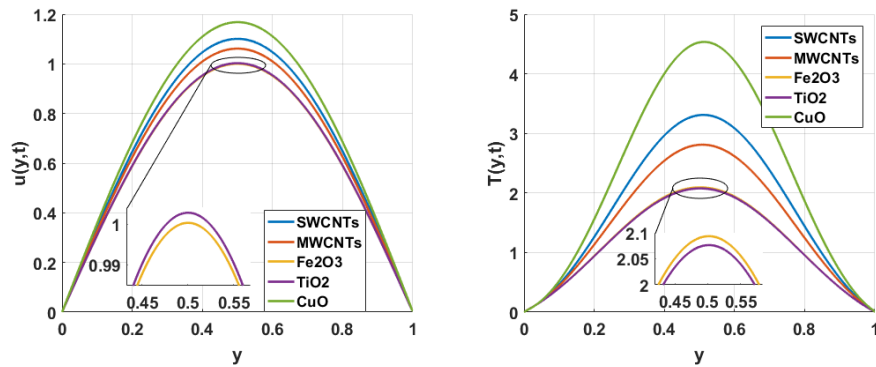
Figure 3.59: Velocity and Temperature of differents nanoparticles for $\alpha = 0.5$, $\psi = 0.4$ when $R = 10^{-5}$.

Moreover, when we keep the values of the fractional parameter and the rotation parameter and increase the fraction volume to $\psi = 0.4$, the variations are very significant as observed in figure (3.59). This clearly confirms the results of [4, 23, 185, 188] with a regain of amplitude for the temperature distribution, and a more explicit variation of the velocity waves.

We continue the same work, by taking a larger value of the fractional parameter ($\alpha = 0.73$).
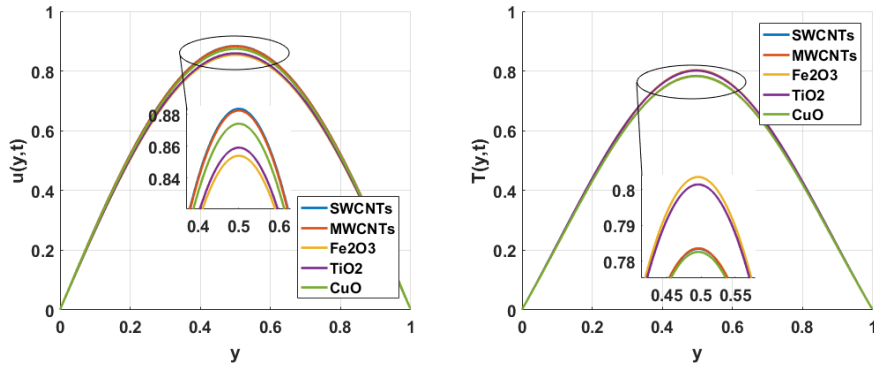
Figure 3.60: Velocity and Temperature of differents nanoparticles for $\alpha = 0.73$, $\psi = 0.05$ when $R = 10^{-5}$.
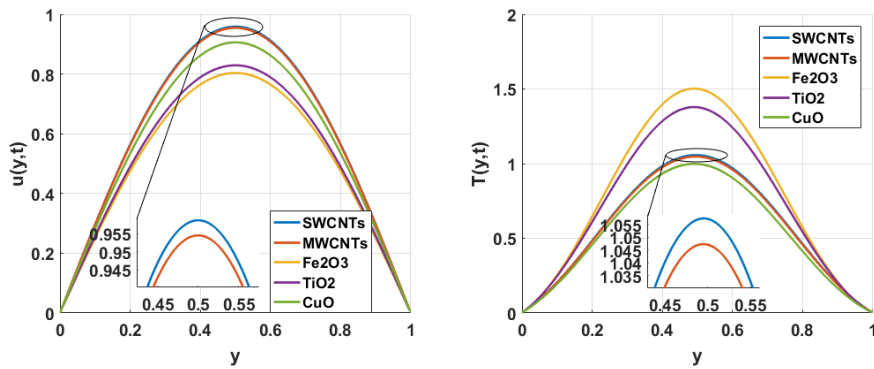
Figure 3.61: Velocity and Temperature of differents nanoparticles for $\alpha = 0.73$, $\psi = 0.4$ when $R = 10^{-5}$.

It also appears that for $\psi = 0.05$, the propagation of the velocity and the temperature distribution vary very weakly with a fall in term of amplitude of propagation. But on the other hand for $\psi = 0.4$, the variations remain significant with a conservation of the amplitude for the velocities of the nanoparticles and a slight increase of the latter for the temperature distribution. It emerges from this study that the nanoparticles investigated behave like energy activators capable of accelerating or retarding the propagation speed of the fluid and the temperature distribution when "ψ" is taken in a precise manner and α depending on the case. This is confirmed by the work of Ndjawa Yomi *et al.* [185], who studied the fractional blood flow in a rotating nanofluid with nanoparticles of different shapes under the influence of activation energy and thermal radiation. In addition, our results are correlated with those of Timofeeva *et al.* [144], who investigated different shapes of particles and their thermophysical properties. From a biological point of view, it follows that cardiovascular diseases, different forms of cancer such as blood cancer in particular can be targeted and localised more precisely, and thus attacked more effectively by means of nanoparticles through a boost of energy or a loss depending on the case [189]. This reflects the fact that nanoparticles play a very important role in new generation technology for the treatment of particular diseases such as cancer.

After performing the variations of figures (3.58), (3.59), (3.60) and (3.61), for the case of the large rotation parameter, the rest of the figures will be considered for this parameter when it is small.
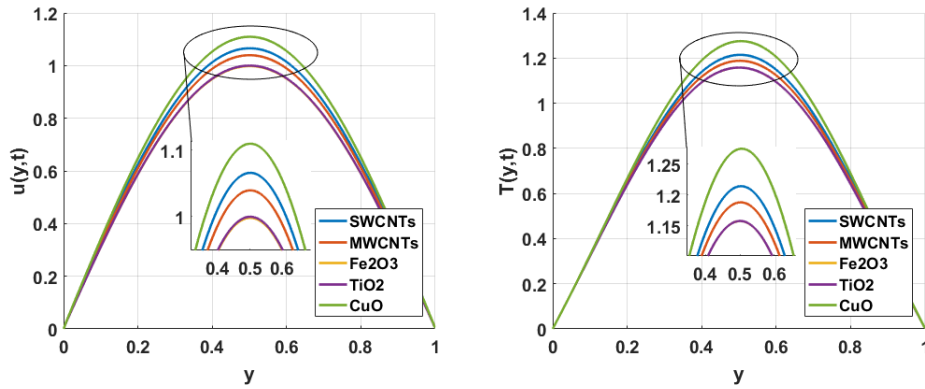
Figure 3.62: Velocity and Temperature of differents nanoparticles for $\alpha = 0.5$, $\psi = 0.05$ when $R = 10^{-6}$.
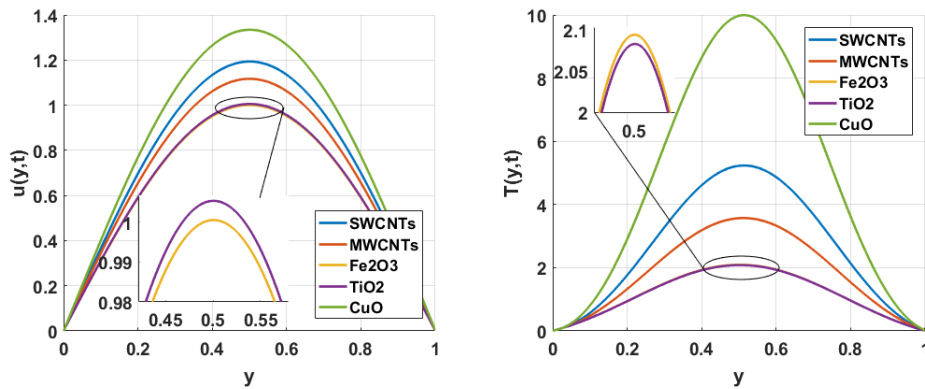
Figure 3.63: Velocity and Temperature of differents nanoparticles for $\alpha = 0.5$, $\psi = 0.4$ when $R = 10^{-6}$.

Figures (3.62) and (3.63) show the variation of the ψ parameter once more, but with ($R = 10^{-6}$) and ($\alpha = 0.5$). This result is similar to the one observed in the work of Hady et $al.$ [188], Misra et $al.$ [150]. Contrary to the previous study, we have a cohesion on the evolution of the velocity wave and the temperature distribution for the value $\psi = 0.05$. This is because we have a very important growth of "CuO" but a clear superposition of Fe_2O_3 and TiO_2, which translates an identity in their behaviour. However, they have different physicochemical properties.

In figure (3.63), for $\psi = 0.4$, we observe a slight decolourisation between the two latter nanoparticles, this may imply on the biological level a perfect cohesion and synchronisation of the red blood cells and an agent which can be considered here as a doping agent. It may or may not lower the blood clotting rate. It may or not make them more efficient, and so on.
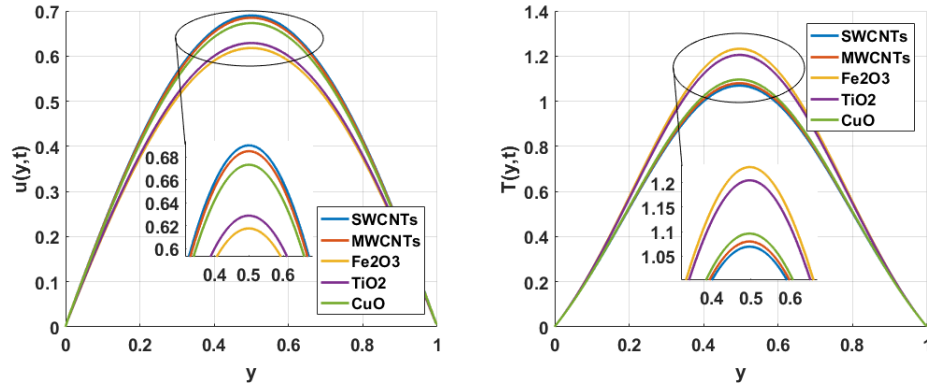
Figure 3.64: Velocity and Temperature of differents nanoparticles for $\alpha = 0.73$, $\psi = 0.05$ when $R = 10^{-6}$.

Figure (3.64) shows the behaviour of the nanoparticles for the reduced rotational motion. It appears a decrease of the velocity waves and an increase of the temperature distribution, with a clear distinction of different nanoparticles.
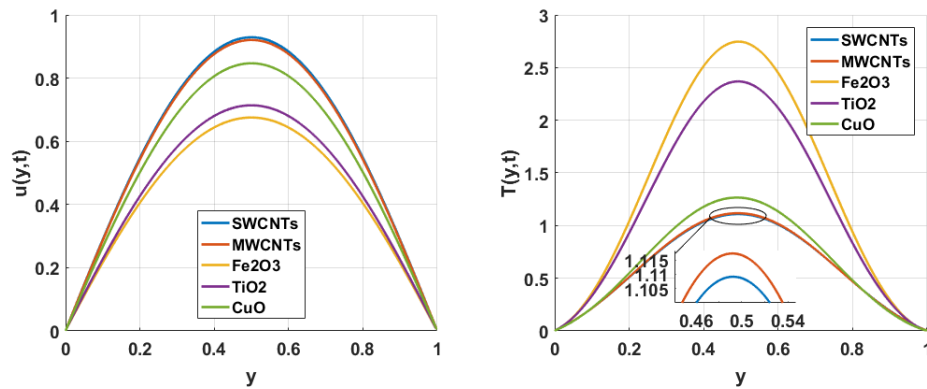
Figure 3.65: Velocity and Temperature of differents nanoparticles for $\alpha = 0.73$, $\psi = 0.4$ when $R = 10^{-6}$.

In figure (3.65), the fraction volume being high, we observe a very preponderant increase of the temperature, causing an increase of the velocity. It should be noted that the higher the temperature of a nanoparticle, the less it will move in the medium. Biologically, the high presence of iron oxide provides information on secondary iron overload and other forms of animal diseases such as hereditary haemochromatosis, cancers, inflammatory disorders (chronic viral hepatitis, alcoholic hepatitis, etc.).
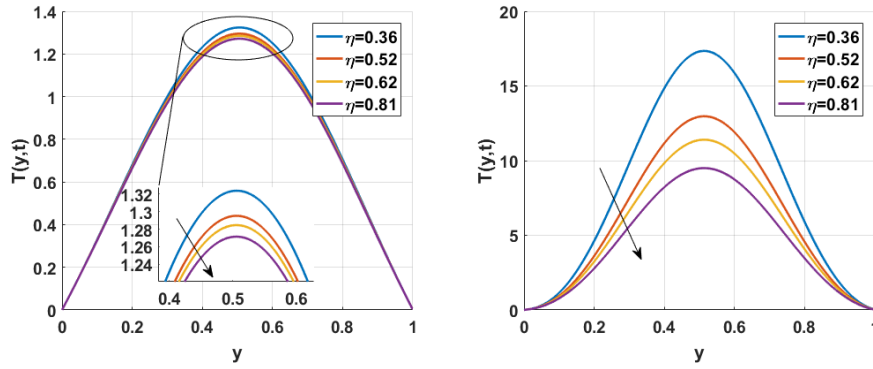
Figure 3.66: Effect of different Sphericity parameter for CuO respectively the case of $\psi = 0.05$ and $\psi = 0.4$ when $\alpha = 0.5$ and $R = 10^{-6}$.
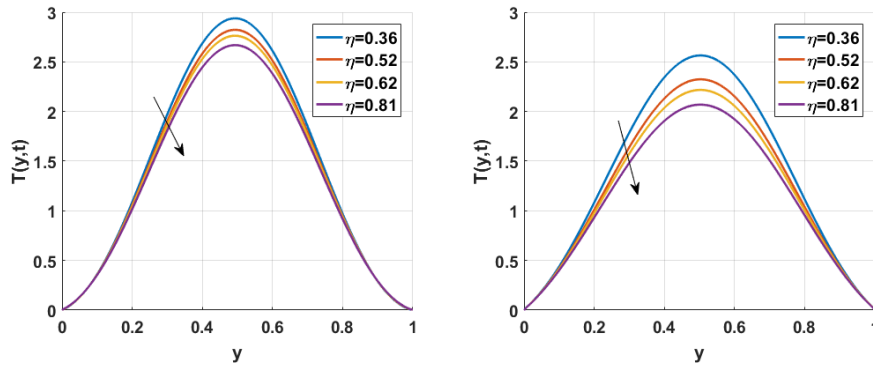
Figure 3.67: Effect of different Sphericity parameter for Fe_2O_3 respectively the case of $\alpha = 0.73$ and $\alpha = 0.5$ when $\psi = 0.4$ and $R = 10^{-6}$.

With a view to reducing these iron oxide and copper oxide overloads, figures (3.66) and (3.67) show the variation in the sphericity of the nanoparticles. Here, we see that the larger the sphericity, the more the temperature and velocity distributions are reduced.

3.5   Conclusion

At the end of this chapter, the analytical and numerical studies of our different blood flow models under the influence of magnetic field, heat transfer, thermal radiation, chemical reactions, nanofluid rotations and fractional order derivatives were presented. The results obtained are a convergence of ideas resolved by the analytical and numerical methods proposed. It follows that parameters such as sphericity, volume fraction, magnetic field, Reynold's number play a key role in the understanding of the blood dynamics. The contribution of fractional order derivatives has allowed a clear observation of the critical zones encountered in the flow, leading to a better control of the velocity, temperature and concentration of the medium studied in time. The results also allow a good perception of the

interactions and the evolution of the system between the nanoparticles present in the medium and the different distributions studied.

General Conclusion

At the end of our thesis, the fractional dynamics of blood flow in the presence of magnetic field, thermal radiation, chemical reactions through a rotating nanofluid frame with different shapes nanoparticles have been investigated. In the first chapter, we focused on the generalities of nanoscience and nanotechnology in blood flow. The description of the different structures and materials encountered was presented, as well as their thermo-physical characteristics and their roles in the different diseases encountered in the vessels. In the second chapter, we first presented the conservation law which allowed us to derive the equations of motion and energy of the fluid for the case of an incompressible fluid in a continuous medium. By applying considerations on the general forms of isotropy more precisely in the case of Newtonian fluid, we end up with the Navier-Stockes equations considered as a good approximation for the treatment of viscous media, 3-dimensional micro-fluid dynamics.

Subsequently, we presented the different fractional models used with the presence of external magnetic field, thermal radiation, and nanoparticles. And finally, the presentation of the analytical and numerical methods considered. As main we have the Laplace and Hankel transforms, the Caputo approximation by finite differences (L_1 algorithm method) which will be introduced in the velocity, temperature and concentration distributions of our models. Chapter 3 presents the main results and contribution of this thesis through the application of the analytical methods of Laplace and Hankel, the fractional order derivatives according to Caputo and also through the application of numerical methods such as finite differences, the Runge-Kutta method of order 4 (RK4), and the L_1 algorithm method. It follows from this theoretical study that the motion of magnetic particles and blood flow in the presence of temperature and Caputo's fractional derivative. Considering the blood vessel as a cylindrical elastic tube, analytical solutions for the nonlinear fractional equations have been obtained through the Laplace transform, with respect to the time variable, and finite Hankel transform. Numerical calculations have been conducted, where information have been recorded for the blood temperature and both the blood and magnetic particle velocities. In general, for short intervals of time the blood flows faster than the particles, while the inverse is observed for large values of time, with magnetic particles being accelerated. The temperature increases from the center of the vessel and drops near the wall and all flow characteristics remain very sensitive to the change

in the fractional-order parameter. The same results are obtained when the Reynolds number changes, since the temperature, the blood velocity and particle velocity decrease with increasing the fractional parameter. One also notices that the velocities of blood and particles are reduced with increasing $\mathcal{H}$, while the temperature remains an increasing function for both short and long time periods.

When the shapes of the different magnetized particles are taken into account along with the rotations of the nanofluid under the effects of thermal radiation, thermal reaction and the external magnetic field through a magnetohydrodynamic blood flow. The solution of the equations governed by this problem will be observed numerically. We used the numerical L_1-algorithm method of Caputo fractional-order derivative operator. The results were plotted by using a Matlab code with different parameters, such as magnetic (M), solid volume fraction (ψ), sphericity (η), etc., to observe their influence in the velocity, temperature, and concentration. We concluded that mass transfer of blood, alumina, tin, copper and SWCNTs onto a flat plate in the presence of a chemical reaction produces a bifurcated system for high values of sphericity ψ for different forms of nanoparticles between the central line and the vessel walls with oscillating flow. The presence of Cu-blood and SWCNT-blood plays a dominant role in the flow field. Thermal radiation can influence the effective viscosity of the fluid, which indirectly affects the velocity profile and increases the temperature at the vessel centerline, which is very important during hyperthermia. This study improves on the one proposed by Asifa *et al.* [187], where the model was a compressible form of heat transfer with a nanofluid hybrid flowing over a rotating disk, and gives an idea of the influence of the shape of the nanoparticles in the fractional blood flow model. It emerges from this study that the nanoparticles we are studying here behave as energy activators capable of accelerating or retarding the propagation speed of the fluid and the temperature distribution when "ψ" is taken in a precise manner and α depending on the case. This complements and confirms the experimental study conducted by Timofeeva *et al.* [144], who investigated the different shapes of the particles and their thermophysical properties. From a biological point of view, it follows that cardiovascular diseases, different forms of cancer such as blood cancer can be targeted and localised more precisely, and thus attacked more effectively by means of nanoparticles through a boost in energy or a loss depending on the case [189]. This reflects the fact that nanoparticles play a very important role in new generation technology for the treatment of particular diseases such as cancer. On the other hand, for a case of fractional parameter variation in superdiffusive medium, we have observed for the case of small values, a slight variation of the distributions. While for large values of the fractional parameter we observed a large influence which makes the system non-predictive for a precise interval and a decrease in the flow velocity. The addition of fraction volume parameter which is the percentage of presence of nanoparticles and their forms must be taken with caution, given the biological anomalies encountered. This allows a good regulation of temperature and velocity distribution in the blood vessels. The shape and the nanoparticle parameter thus play a very essential role for the temperature decrease in a fractional model. This study could

shed light on the behavior of particles in the center and walls of the tube allowing the understanding of blood diseases and also the transport of different organic cells in important and significant temperature gradients, allowing a better dynamics.

★ Open problems and future directions

Despite the results obtained in this thesis, other points of interest may be solved in the future:

♦ A fractional nanofluid in rotating blood flow in an oscillating elastic tube with thermal radiation, magnetic field effects were realized with a periodic pressure gradient and the fractional model includes the activation energy and shapes of nanoparticles. Some important phenomena are observed such as heat propagation, particles concentration, motion and behavior of nanoparticles were examined in the tube. Then the localization of the chaotic zones will be studied in our future works.

♦ Velocity, temperature and concentration play an important role in the internal dynamics of the blood flow. The nanofluid flow is in contact with a thermal bath in the cell. Therefore, the concentration of nanoparticles must be examined very carefully. Thus, it is necessary to explore the role of different parameters with noise models in the formation of localized structures, where the interaction of nanoparticles will be considered in the medium.

♦ Introduce machine learning models to better predict and optimize our different forms of magneto-hydrodynamic models to make them more realistic in understanding the Physico-chemical phenomena in the vessels.

Bibliography

[1] R. Feynman. "Nanotechnology." *Caltech Eng. Sci.* **23**, 22–36 (1960).

[2] S. Bayda, M. Adeel, T. Tuccinardi, M. Cordani, F. Rizzolio. "The History of Nanoscience and Nanotechnology: From Chemical-Physical Applications to Nanomedicine." *Molecules.* **25**, 112 (2020).

[3] K. S. R. Vani and D. Rao. "Effect of thermal radiation on unsteady convective heat transfer flow of a rotating nano-fluid past a vertical plate." *Adv. Appl. Sci. Res.* **7**, 83–94 (2016).

[4] S. U. S. Choi and J. A. Eastman. "Enhancing thermal conductivity of fluids with nanoparticles." (*Argonne National Laboratory, Illinois,* 1995).

[5] G. Aaiza, I. Khan, and S. Shafie. "Energy transfer in mixed convection MHD flow of nanofluid containing different shapes of nanoparticles in a channel filled with saturated porous medium." *Nanoscale Res. Lett.* **10**, 490–504 (2015).

[6] M. Lomascolo, G. Colangelo, M. Milanese, and A. De Risi. "Review of heat transfer in nanofluids: Conductive, convective and radiative experimental results." *Renew. Sust. Energ. Rev.* **43**, 1182–1198 (2015).

[7] S. Inoue, and M. Kabaya. "Biological activities caused by far-infrared radiation." *Int. J. Biometeorol.* **33**, 145–150 (1989).

[8] Y. Kobu. "Effects of infrared radiation on intraosseous blood flow and oxygen tension in the rat tibia." *Kobe J. Med. Sci.* **45**, 27–39 (1999).

[9] S. Majee and G. C. Shit. "Numerical investigation of MHD flow of blood and heat transfer in a stenosed arterial segment." *J. Magn. Magn. Mater.* **424**, 137–147 (2017).

[10] T. Chinyoka, O.D. Makinde. "Computational dynamics of arterial blood flow in the presence of magnetic field and thermal radiation therapy." *Adv. Math. Phys.* **43**, 2014:915640. ID, (2014).

[11] C. B. Tabi, T. G. Motsumi, C. D. K. Bansi and A. Mohamadou. "Nonlinear excitations of blood flow in large vessels under thermal radiations and uniform magnetic field." *Commun. Nonlinear Sci. Numer. Simul.* **49**, 1–8 (2017).

[12] A. Kolin. "An electromagnetic flowmeter. Principle of the method and its application to bloodflow measurements." *Proc. Soc. Exp. Biol. Med.* **35**, 53 (1936).

[13] E.M. Korchevskii and L. S. Marochnik. "Magnetohydrodynamic version of movement of blood." *Biophysics.* **10**, 411–414 (1965).

[14] G.C. Schit, M. Roy. "Pulsatile flow and heat transfer of a magneto-micropolar fluid through a stenosed artery under the influence of body acceleration." *J. Mech. Med. Biol.* **11**, 643–661 (2011).

[15] A. Ogulu and A. R. Bestman. "Deep heat muscle treatment a mathematical model–I." *Acta Physica Hungarica.* **73**, 3–16 (1993).

[16] D.S. Sankar, K. Hemalatha. "Pulsatile flow of Hersche-Bulkley fluid through stenosed arteries–A mathematical model." *Int. J. Non-Linear Mech.* **41**, 979–990 (2006).

[17] P.K. Mandal. "An unsteady analysis of non-Newtonian blood flow through tapered arteries with a stenosis." *Int. J. Non-Linear Mech.* **40** 151–164 (2005).

[18] K. Vajravelu, K. Ramesh, S. Sreenadh, P.V. Arunachalam. "Pulsatile flow between permeable beds." *Int. J. Non-Linear Mech.* **38**, 999–1005 (2003).

[19] M.K. Sharma, P.R. Sharma, V. Nasha. "Pulsatile MHD arterial blood flow in the presence of double stenoses." *J. Appl. Fluid Mech.* **6**, 331–338 (2013).

[20] A. Mondal, G.C. Shit. "Transport of magneto-nanoparticles during electro-osmotic flow in a micro-tube in the presence of magnetic field for drug delivery application." *J. Magn. Magn. Mater.* **442**, 319–328 (2017).

[21] Y. Haik, J.C. Chen, V.M. Pai. "Development of bio-magnetic fluid dynamics." *In Proceedings of the IX International Symposium on Transport Properties in Thermal Fluids Engineering, Singapore, Pacific Center of Thermal Fluid Engineering, Hawaii, USA,* 121–126 (1996).

[22] Y. He, M. Shirazaki, H. Liu, R. Himeno, and Z. Sun. "A numerical coupling model to analyze the blood flow, temperature, and oxygen transport in human breast tumor under laser irradiation." *Comput. Biol. Med.* **36**, 1336–1350 (2006).

[23] C. B. Tabi, T. G. Motsumi, C. D. Bansi Kamdem, and A. Mohamadou. "Nonlinear excitations of blood flow in large vessels under thermal radiations and uniform magnetic field." *Commun. Nonlinear Sci. Numer. Simul.* **49**, 1–8 (2017).

[24] A. Szasz, and others. "Hyperthermia, a modality in the wings." *J. Cancer Res. Ther.* **3**, 56 (2007).

[25] HI Roste. "Magnetofluid dynamics for engineers and applied physicists: McGraw-Hill." *New York,* 1–350, (1973).

[26] M. K. Sharma, P. R. Sharma and V. Nasha. "Pulsatile MHD arterial blood flow in the presence of double stenoses." *J. Appl. Fluid Mech.* **6**, 331–338 (2013).

[27] Kh. S. Mekheimer, and El M. A. Kot. "Suspension model for blood flow through catheterized curved artery with time-variant overlapping stenosis." *Int. J. Eng. Sci. Technol.* **18**, 452–462 (2015).

[28] O. I. Craciunescu, and S. T. Clegg. "Pulsatile blood flow effects on temperature distribution and heat transfer in rigid vessels." *J. Biomech. Eng.* **123**, 500–505 (2001).

[29] Tzyy-Leng Horng, and Win-Li Lin, Chihng-Tsung Liauh, and Tzu-Ching Shih. "Effects of pulsatile blood flow in large vessels on thermal dose distribution during thermal therapy." *Med. Phys.* **34**, 1312–1320 (2007).

[30] T. Higashi, A. Yamagishi, T. Takeuchi, N. Kawaguchi, S. Sagawa, S. Onishi, and others. "Orientation of erythrocytes in a strong static magnetic field." *Blood.* **82**, 1328–1334 (1993).

[31] A. Yamagishi. "Biological systems in high magnetic field." *J. Magn. Magn. Mater.* **90**, 43–46 (1990).

[32] A. R. Khaled, K. Vafai. "The role of porous media in modeling flow and heat transfer in biological tissues." *Int. J. Heat Mass Transf.* **46**, 4989–5003 (2003).

[33] R. Kandasamy, R. Mohamad, M. Ismoen. "Impact of chemical reaction on Cu, Al2O3 and SWCNTs?nanofluid flow under slip conditions." *Int. J. Eng. Sci. Technol.* **19**, 700–709 (2016).

[34] S. Pramanik. "Casson fluid flow and heat transfer past an exponentially porous stretching surface in presence of thermal radiation." *Ain Shams Eng. J.* **5**, 205–212 (2014).

[35] H. R. Kataria, H. R. Patel. "Radiation and chemical reaction effects on MHD Casson fluid flow past an oscillating vertical plate embedded in porous medium." *Alex. Eng. J.* **55**, 583–595 (2016).

[36] M. Qayyum, and H. Khan. "Behavioral study of unsteady squeezing flow through porous medium." *J. Porous Media* **19**, (2016).

[37] A. Khalid, I. Khan, A. Khan, and S. Shafie. "Unsteady MHD free convection flow of Casson fluid past over an oscillating vertical plate embedded in a porous medium." *Eng. Sci. Tech. Int. J.* **18**, 309–317 (2015).

[38] B. S. T. Alkahtani, and A. Atangana. "Analysis of non-homogeneous heat model with new trend of derivative with fractional order." *Chaos Solit. Fractals* **89**, 566–571 (2016).

[39] D. Baleanu, and A. Fernandez. "On some new properties of fractional derivatives with Mittag-Leffler kernel." *Commun. Nonlinear Sci. Numer. Simul.* **59**, 444–462 (2018).

[40] A. Khan, K. Ali Abro, A. Tassaddiq, and I. Khan. "Atangana-Baleanu and Caputo Fabrizio analysis of fractional derivatives for heat and mass transfer of second grade fluids over a vertical plate: a comparative study." *Entropy* **19**, 1–12 (2017).

[41] C. D. Bansi Kamdem, C. B. Tabi, T. G. Motsumi, A. Mohamadou. "Fractional blood flow in oscillatory arteries with thermal radiation and magnetic field effects." *J. Magn. Magn. Mater.* **456**, 38–45 (2018).

[42] J. Zhao, L. Zheng, X. Zhang, and F. Liu. "Unsteady boundary layer natural convection heat transfer of Maxwell viscous fluid over a vertical plate." *Int. J. Heat Mass Transf.* **97**, 760–766 (2016).

[43] J. Zhao, L. Zheng, X. Zhang, and F. Liu. "Convection heat and mass transfer of fractional MHD Maxwell fluid in a porous medium with Soret and Dufour effects." *Int. J. Heat Mass Transf.* **103**, 203–210 (2016).

[44] A. Gnach, T. Lipinski, A. Bednarkiewicz, J. Rybka, and J.A. Capobianco. "Upconverting nanoparticles: assessing the toxicity." *Chem. Soc. Rev.* **44**, 1561–1584 (2015).

[45] J. Jeevanandam, A. Barhoum, Y.S. Chan, A. Dufresne, M.K. Danquah. "Review on nanoparticles and nanostructured materials: history, sources, toxicity and regulations." *Beilstein J. Nanotechnol.* **9**, 1050–1074 (2018).

[46] https://www.bioworld.com/articles/515680-catalog-of-protein-isoforms-in-blood-cells-can-predict-organ-rejection, (2022).

[47] H.W. Kroto, J.R. Heath, S.C. O'Brien, R.F. Curl, and R.E. Smalley. "C_{60}: Buckminster-fullerene." *Nature.* **318**, 162–163 (1985).

[48] https://www.turbosquid.com/3d-models/nanotechnology-atom-carbon-graphene-3d-model/806317, (2022).

[49] S. Iijima. "Helical microtubules of graphitic carbon." *Nature.* **354**, 56–58 (1991).

[50] P.M. Ajayan and S. Iijima. "Smallest carbon nanotube." *Nature.* **358**, 23–23 (1992).

[51] S. Aman, I. Khan, Z. Ismail, M. Z. Salleh, A.S. Alshomrani, M.S. Alghamdi. "Magnetic field effect on Poiseuille flow and heat transfer of carbon nanotubes along a vertical channel filled with Casson fluid." *AIP Adv.* **7**, 015036 (2017).

[52] J.W. Mintmire, B.I. Dunlap, C.T. White. "Are fullerene tubules metallic? " *Phys. Rev. Lett.* **68**, 631 (1992).

[53] S.J. Tans, M.H. Devoret, H. Dai, A. Thess, R.E. Smalley, L.J. Geerligs, and C. Dekker. "Individual single-wall carbon nanotubes as quantum wires." *Nature.* **386**, 474–477 (1997).

[54] J. Goldberger, R. He, Y. Zhang, S. Lee, H. Yan, H.J. Choi, and P. Yang. "Single-crystal gallium nitride nanotubes." *Nature.* **422**, 599–602 (2003).

[55] https://www.vectorstock.com/royalty-free-vector/symbol-and-electron-diagram-for-gallium-vector-6373908, (2022).

[56] https://en.wikipedia.org/wiki/Gallium_nitride_nanotube, (2022).

[57] https://www.istockphoto.com/search/2/image?phrase=silicon+atom, (2022).

[58] H. Li, H. Li, W. Dai, M. Qiao. "Preparation of the Ni-B amorphous alloys with variable boron content and its correlation to the hydrogenation activity." *Appl. Catal. A: Gen.* **238**, 119–130 (2003).

[59] C. Mu, Q. Zhao, D. Xu, Q. Zhuang, and Y. Shao. "Silicon Nanotube Array/Gold Electrode for Direct Electrochemistry of Cytochrome c." *J. Phys. Chem. B.* **111**, 1491–1495 (2007).

[60] J. Sha, J. Niu, X. Ma, J. Xu, X. Zhang, Q. Yang, and D. Yang. "Silicon nanotubes." *Adv. Mater.* **14**, 1219–1221 (2002).

[61] X. Huang, R. Gonzalez-Rodriguez, R. Rich, Z. Gryczynski, and J. L. Coffer. "Fabrication and size dependent properties of porous silicon nanotube arrays." *Chem. Commun.* **49**, 5760–5762 (2013).

[62] Ishai, Moshit Ben and Patolsky, Fernando. "Shape-and dimension-controlled single-crystalline silicon and SiGe nanotubes: toward nanofluidic FET devices." *J. Am. Chem. Soc.* **131**, 3679–3689 (2009).

[63] L. Liang, J. Wang, W. Lin, B.G. Sumpter, V. Meunier, and M. Pan. "Electronic bandgap and edge reconstruction in phosphorene materials." *Nano Lett.* **14**, 6400–6406 (2014).

[64] K. S. Novoselov, A. K. Geim, S. V. Morozov, De-eng Jiang, Y. Zhang, S. V. Dubonos, I. V. Grigorieva, and A. A. Firsov. "Electric field effect in atomically thin carbon films." *Science.* **306**, 666–669 (2004).

[65] Z. Li, L. Chen, S. Meng, L. Guo, J. Huang, Y. Liu, W. Wang, and X. Chen. "Field and temperature dependence of intrinsic diamagnetism in graphene: Theory and experiment." *Phys. Rev. B Condens. Matter.* **91**, 094429 (2015).

[66] R.R. Nair, P. Blake, A.N. Grigorenko, K.S. Novoselov, T.J. Booth, T. Stauber, N.M.R. Peres, A.K Geim. "Universal dynamic conductivity and quantized visible opacity of suspended graphene." *arXiv preprint arXiv*:0803.3718, (2008).

[67] C. Lee, W. Xiaoding, W. Jeffrey. "Measurement of the elastic properties and intrinsic strength of monolayer graphene." Science **321**, 385–388 (2008).

[68] K. Cao, S. Feng, Y. Han, L. Gao, T. Hue Ly, and Z. Xu, and Y. Lu. "Elastic straining of free-standing monolayer graphene." *Nat. Commun.* **11**, 1–7 (2020).

[69] J. Lloyd-Hughes, and Tae-In Jeon. "A review of the terahertz conductivity of bulk and nano-materials." *J. Infrared Millim and Terahertz Waves* **33**, 871 (2012).

[70] A. Tahiri. "Contribution à l'étude des transferts thermo convectifs d'un fluide non-Newtonien en écoulement dans un conduit." *PhD Thesis, University of M'HAMED BOUGARA-BOUMERDES,* (2018).

[71] G. Bachir. "Contribution à l'étude de la convection naturelle dans les nanofluides en configuration de Rayleigh-Bénard." University of Toulouse, (2010).

[72] S.U.S Choi, Z. Zhang, W. Yu, F.E Lockwood,and E.A Grulke. "Anomalous thermal conductivity enhancement in nanotube suspensions." *Appl. Phys. Lett.* **79**, 2252–2254 (2001).

[73] J. A. Eastman, S.U.S Choi, S. Li, W. Yu, and L.J Thompson. "Anomalously increased effective thermal conductivities of ethylene glycol-based nanofluids containing copper nanoparticles." *Appl. Phys. Lett.* **78**, 718–720 (2001).

[74] P. Keblinski, J.A. Eastman, D.G. Cahill. "Nanofluids for thermal transport." *Mater. today.* **8**, 36–44 (2005).

[75] Y. Yang, Z.G. Zhang, E.A. Grulke, W.B. Anderson, and G. Wu. "Heat transfer properties of nanoparticle-in-fluid dispersions (nanofluids) in laminar flow." *Int. J. Heat Mass Transf.* **48**, 1107–1116 (2005).

[76] H. Masuda, A. Ebata, K. Teramae. "Alteration of thermal conductivity and viscosity of liquid by dispersing ultra-fine particles. Dispersion of Al2O3, SiO2 and TiO2 ultra-fine particles." (1993).

[77] J. A. Eastman, U.S. Choi, S. Li, L.J. Thompson, S. Lee. "Enhanced thermal conductivity through the development of nanofluids." *MRS Online Proceedings Library (OPL).* **457**, (1996).

[78] S. Lee, S.U.S. Choi, S. Li, J.A. Eastman. "Measuring thermal conductivity of fluids containing oxide nanoparticles." *J. Heat Transfer.* **121**, 280–289 (1999).

[79] C. H. Li, G.P. Peterson. "Experimental investigation of temperature and volume fraction variations on the effective thermal conductivity of nanoparticle suspensions (nanofluids)." *Int. J. Appl. Phys.* **99**, 084314 (2006).

[80] B. C. Pak, Y.I. Cho. "Hydrodynamic and heat transfer study of dispersed fluids with submicron metallic oxide particles." *Exp. Heat Transf.* **11**, 151–170 (1998).

[81] S. M. S. Murshed, K. C. Leong, C. Yang. "Investigations of thermal conductivity and viscosity of nanofluids." *Int. J. Therm. Sci.* **47**, 560–568 (2008).

[82] N. Bouguerra. "Caractérisation des propriétés thermiques et rhéologiques des nanofluides eau-alumine : compréhension des mécanismes thermophysiques, régimes de dispersion et étude du phénomène d'hystérésis." *University of Sherbrooke.* (2018).

[83] Y. Xuan, Q. Li. "Heat transfer enhancement of nanofluids." Int. *J. Heat Fluid Flow.* **21**, 58–64 (2000).

[84] H. E. Patel, S. K. Das, T. Sundararajan, A. Sreekumaran Nair, B. George. "Pradeep, T1: CAS: 528: DC% 2BD3sXnvVGntL0% 3D: Thermal conductivities of naked and monolayer protected metal nanoparticle based nanofluids: Manifestation of anomalous enhancement and chemical effects. vol. 83." *Appl. Phys. Lett.* **83**, 2931–2933 (2003).

[85] D. H. Kumar, H. E. Patel, V. R. R. Kumar, T. Sundararajan, T. Pradeep, S.K. Das. "Model for heat conduction in nanofluids." *Phys. Rev. Lett.* **93**, 144301 (2004).

[86] T. H. K. Barron, G. K. White. "The International Cryogenics Monograph Series", *Heat Capacity and Thermal Expansion at Low Temperatures-Springer US.* (1999).

[87] Y. Xuan and W. Roetzel. "Conceptions for heat transfer correlation of nanofluids." *Int. J. Heat Mass Transf.* **43**, 3701–3707 (2000).

[88] A. Einstein. "Investigations on the Theory of the Brownian Movement." *Dover Publications, New York,* (1956).

[89] D. A. Drew and S. L. Passman. "Classical Theory of Solutions." *Springer*, 59–61 (1999).

[90] H. C. Brinkman. "The viscosity of concentrated suspensions and solutions." *Chem. Phys.* **20**, 571–571 (1952).

[91] S. S. Botha. "Synthesis and Characterization of Nanofluids for Cooling Applications." *PhD Thesis, University of the Western Cape*, (2007).

[92] J. Maxwell, Oxford University Press, London, UK, **2**, 615–833 (1891).

[93] R. L. Hamilton and O.K. Crosser. "Thermal conductivity of heterogeneous two-component systems." *Ind. Eng. Chem. Fundam.* **1**, 187–191 (1962).

[94] W. Yu and S.U.S. Choi. "The role of interfacial layers in the enhanced thermal conductivity of nanofluids: a renovated Maxwell model." *J. Nanoparticle Res.* **5**, 167–171 (2003).

[95] O. Madelung, A. B. Lidiard, J. M. Stevels, E. Darmois. "Electrical Conductivity II_Elektrische Leitungsphänomene II." *Handbuch der Physik_ Encyclopedia of Physics 4_ 20, Springer-Verlag Ber*, (1957).

[96] https://www.britannica.com/science/white-blood-cell, 2022.

[97] https://commons.wikimedia.org/w/index.php?search=artery&title=Special:MediaSearch &go=Go&type=image, 2022.

[98] C. D. K. Bansi. "Nonlinear Dynamics of incompressible fluid in elastic tube with heat transfer, thermal radiation and magnetic field effect." *University of Yaounde 1, PhD Thesis,* (2019).

[99] http://saypeople.com/2014/07/08/task-force-recommends-against-screening-for-carotid-artery-stenosis-in-general-adult-population/#.Ys3v0HbMLIU, 2022.

[100] https://ressourcessante.salutbonjour.ca/condition/getcondition/anevrisme, (2022).

[101] https://commons.wikimedia.org/wiki/File:Abdominal_Aortic_Aneurysm_Location.png, 2022.

[102] https://commons.wikimedia.org/wiki/File:Blausen_0089_BloodClot_Motion.png, 2022.

[103] https://sante.journaldesfemmes.fr/fiches-maladies/2702809-thrombose-definition-symptomes-veineuse-arterielle-traitement-vaccin-covid/, (2022).

[104] F. Peng, M. I. Setyawati, J. K. Tee, X. Ding, J. Wang, M. E. Nga, H. K. Ho, and D. T. Leong. "Nanoparticles promote in vivo breast cancer cell intravasation and extravasation by inducing endothelial leakiness." *Nat. Nanotechnol.* **14**, 279–286 (2019).

[105] S.S. Laha, N.D. Thorat, G. Singh, C.I. Sathish, J. Yi, A. Dixit and A. Vinu. "Earth Doped Iron Oxide Nanostructure for cancer theranostics: Magnetic hyperthermia and magnetic resonnance imaging." *Small.* **18**, 2104855 (2022).

[106] F. Babinger, L H. Heydenreich. "Vier Bauvorschläge Lionardo da Vinci's an Sultan Bajezid II.(1502/3)." *Vandenhoeck & Ruprecht,* (1952).

[107] I. Newton, N. W. Chittenden. "Newton's Principia: the mathematical principles of natural philosophy." *Geo. P. Putnam,* (1850).

[108] Cx K. Batchelor and George Keith Batchelor. "An introduction to fluid dynamics." *Cambridge university press*, (2000).

[109] R. L. Panton. "Incompressible flow." John Wiley & Sons, (2013).

[110] D. F. Elger, B. A. LeBret, C. T. Crowe, J. A. Roberson. "Engineering fluid mechanics." *John Wiley & Sons*, (2020).

[111] D. F. Young, B. R. Munson, T. H. Okiishi, and W. W. Huebsch, A brief introduction to fluid mechanics, *John Wiley & Sons*, (2010).

[112] J. Boussinesq. "Théorie analytique de la chaleur: mise en harmonie avec la thermodynamique et avec la théorie mécanique de la lumière." *Gauthier-Villars*, **2**, (1903).

[113] A. Oberbeck, *Ann. Phys.* **243**, 271–292 (1879).

[114] H. A. Lorentz. "La Théorie electromagnétique de Maxwell et son application aux corps mouvants." *Dutch Archives of Exact and Natural Sciences.* **25**, 363–552, (1892).

[115] Yehuda Elkana. "*The Discovery of the Conservation of Energy.*" *Harvard University Press*, (1974).

[116] httpsjournals.aps.orgpreabstract10.1103PhysRevE.84.011905, (2022).

[117] httpsphysics.stackexchange.comquestions134542how-do-we-conclude-that-polarized-dielectric-in-electric-field-reduces-overall-f, (2022).

[118] H. P. Greenspan. "The theory of rotating fluids." *Massachusetts Inst of Tech Cambridge Dept of Mathematics*, (1968).

[119] J. A. Rayne and B. S. Chandrasekhar. "Elastic constants of iron from 4.2 to 300 K." *Phys. Rev.* **122**, 1714 (1961).

[120] W. V. R. Malkus. "Equatorial planetary waves." *Tellus*, **20**, 545–547 (1968).

[121] R. P. Davies-Jones and P. A. Gilman. "Convection in a rotating annulus uniformly heated from below." *J. Fluid Mech.* **46**, 65–81 (1971).

[122] K. Zhang, X. Liao, "Theory and Modeling of Rotating Fluids: Convection." *Inertial Waves and Precession (Cambridge Monographs on Mechanics). Cambridge University Press,* (2017).

[123] S. Srinivas, M. Kothandapani. "The influence of heat and mass transfer on MHD peristaltic flow through a porous space with compliant walls." *Appl. Math. Comput.* **213**, 197–208 (2009).

[124] S. Sharma, U. Singh, V.K. Katiyar. "Magnetic field effect on flow parameters of blood along with magnetic particles in a cylindrical tube." *J. Magn. Magn. Mater.* **377**, 395–401 (2015).

[125] F. Ali, A. Imtiaz, I. Khan, N.A. Sheikh. "Flow of magnetic particles in blood with isothermal heating: A fractional model for two-phase flow." *J. Magn. Magn. Mater.* **456**, 413–422 (2018).

[126] N. Ali Shah, D. Vieru, and C. Fetecau. "Effects of the fractional order and magnetic field on the blood flow in cylindrical domains." *J. Magn. Magn. Mater.* **409**, 10–19 (2016).

[127] E. E. Tzirtzilakis. "A mathematical model for blood flow in magnetic field." *Phys. Fluids* **17**, 077103 (2005).

[128] A. C. Cogley, W. G. Vincent, S. E. Gilles. "Differential approximation for radiative transfer in a nongrey gas near equilibrium." *AIAA J.* **6**, 551–553 (1968).

[129] C. B. Tabi. "Dynamical analysis of the FitzHugh?Nagumo oscillations through a modified Van der Pol equation with fractional-order derivative term." *Int. J. Non-Linear Mech.* **105**, 173–178 (2018).

[130] E. F. Doungmo Goufo, and C. B. Tabi. "On the chaotic pole of attraction for Hindmarsh-Rose neuron dynamics with external current input." *Chaos* **29**, 023104 (2019).

[131] D. Baleanu, and O. M. P. Agrawal. "Fractional Hamilton formalism within Caputo's derivative." *Czechoslov. J. Phys.* **354**, 1087–1092 (2006).

[132] Z. Odibat. "Approximations of fractional integrals and Caputo fractional derivatives." *Appl. Math. Comput.* **178**, 527–533 (2006).

[133] M. Caputo, and M. Fabrizio. "A new definition of fractional derivative without singular kernel." *Prog. Fract. Differ. Appl.* **1**, 73–85 (2015).

[134] E. F. D. Goufo, S. Kumar, and S. B. Mugisha. "Similarities in a fifth-order evolution equation with and with no singular kernel." *Chaos Solit. Fractals* **130**, 109467 (2020).

[135] A. Atangana, and E. F. D. Goufo. "Conservatory of Kaup-Kupershmidt equation to the concept of fractional derivative with and without singular kernel." *Acta Math. Appl. Sin., English Series.* **34**, 351–361 (2018).

[136] A. Atangana, and I. Koca. "Chaos in a simple nonlinear system with Atangana-Baleanu derivatives with fractional order." *Chaos. Solit. Fractals* **89**, 447–454 (2016).

[137] E. F. Doungmo Goufo. "Strange attractor existence for non-local operators applied to four-dimensional chaotic systems with two equilibrium points." *Chaos* **29**, 023117 (2019).

[138] E. F. Doungmo Goufo. "Chaotic processes using the two-parameter derivative with non-singular and non-local kernel: Basic theory and applications." *Chaos* **26**, 084305 (2016).

[139] C.B Tabi, P.A. Ndjawa, T.G. Motsumi, C.D. Bansi Kamdem, and T.C. Kofané. "Magnetic field effect on a fractionalized blood flow model in the presence of magnetic particles and thermal radiations." *Chaos Solit. Fractals,* **131**, 109540 (2020).

[140] A. N. Brooks and T. J. R. Hughes. "Streamline upwind/Petrov-Galerkin formulations for convection dominated flows with particular emphasis on the incompressible Navier-Stokes equations." *Comput. Methods Appl. Mech. Eng.* **32**, 199–259 (1996).

[141] B. Ali, and Y. Nie, S. Hussain, and A. Manan, and M.T. Sadiq. "Unsteady magneto-hydrodynamic transport of rotating Maxwell nanofluid flow on a stretching sheet with Cattaneo?Christov double diffusion and activation energy." *Therm. Sci. Eng. Prog.* **20**, 100720 (2020).

[142] F. Ali, S. Murtaza, N. A. Sheikh, and I. Khan. "Heat transfer analysis of generalized Jeffery nanofluid in a rotating frame: Atangana?Balaenu and Caputo?Fabrizio fractional models." *Chaos Solit. Fractals,* **129**, 1–15 (2019).

[143] A. Atangana, and D. Baleanu. "New fractional derivatives with nonlocal and non-singular kernel: theory and application to heat transfer model." *arXiv preprint arXiv*:1602.03408, (2016).

[144] E. V. Timofeeva, J. L. Routbort, and D. Singh. "Particle shape effects on thermophysical properties of alumina nanofluids." *Int. J. Appl. Phys.* **106**, 014304 (2009).

[145] Ilyas Khan. "New idea of Atangana and Baleanu fractional derivatives to human blood flow in nanofluids." *Chaos.* **29**, 013121 (2019).

[146] Zahir Shah, Ebenezer Bonyah, Saeed Islam, and Taza Gul. "Impact of thermal radiation on electrical MHD rotating flow of carbon nanotubes over a stretching sheet." *AIP Adv.* **9**, 015115 (2019).

[147] A.I. Aliyu, M. Inc, A. Yusuf, and D. Baleanu. "A fractional model of vertical transmission and cure of vector-borne diseases pertaining to the Atangana?Baleanu fractional derivatives." *Chaos Solit. Fractals* **116**, 268–277 (2018).

[148] M. Caputo. "Linear Models of Dissipation whose Q is almost Frequency Independent–II." *Geophys. J. Int.* **13.5**, 529–539 (1967).

[149] A. A. A. Kilbas, H. M. Srivastava, and J. J. Trujillo. "Theory and Applications of Fractional Differential Equations." *Elsevier Science Limited.* **204**, (2006).

[150] J. C. Misra, S. D. Adhikary, B. Mallick, A. Sinha. "Pulsatile flow and heat transfer of blood in an overlapping vibrating atherosclerotic artery: A numerical study." *J. Mech. Med. Biol.* **18**, 185001 (2018).

[151] M. Caputo. "Elasticita e dissipazione." *Zanichelli,* (1969).

[152] G. N. Watson. "A Treatise on the Theory of Bessel Functions." *2nd Edition, Cambridge University Press, London,* (1931).

[153] E. D. Rainville. "Special Functions." *MacMillan, New York,* (1960).

[154] A. M. Cohen, "Numerical methods for Laplace transform inversion." *Numerical Methods and Algorithms, Springer,* (2007).

[155] N. H. Asmar. "Partial differential equations with Fourier series and boundary value problems." (2016).

[156] R. L. Magin. "Fractional calculus in bioengineering." *Begell House Redding*, **2** (2006).

[157] I. Podlubny. "Fractional differential equations: an introduction to fractional derivatives, fractional differential equations, to methods of their solution and some of their applications." (1998).

[158] T. Yokoyama. "The Hankel transform." (2018).

[159] R. N. Bracewell, "The Fourier Transform And Its Applications." *McGraw Hill,* (2000).

[160] Q. Yang. "Novel analytical and numerical methods for solving fractional dynamical systems." *Qeensland University of Technology, PhD Thesis,* (2010).

[161] L. N. Trefethen, "Finite Difference & Spectral Methods for ODE & PDE." *SIAM,* (1996).

[162] E. Hairer, M. Roche, C. Lubich, "The Numerical Solution of Differential-Algebraic Systems by Runge-Kutta Methods." *Lecture Notes in Mathematics 1409, Springer*, (1989).

[163] D. Belobo Belobo, "Dynamics of Matter-Wave Condensates: Effects of Quantum Fluctuations and Three-Body Interatomic Interactions." *University of Yaounde 1, PhD Thesis* (2015).

[164] G. H. Gao, Z. Z. Sun. "A compact finite difference scheme for the fractional sub-diffusion equations." *J. Comput. Phys.* **230**, 586–595 (2011).

[165] Y. Jiang, J. Ma. "High-order finite element methods for time-fractional partial differential equations." *J. Comput. Appl. Math.* **235**, 3285–3290 (2011).

[166] T. Langlands, B. I. Henry. "The accuracy and stability of an implicit solution method for the fractional diffusion equation." *J. Comput. Phys.* **205**, 719–736 (2005).

[167] C. Li, F. Zeng. "Numerical methods for fractional calculus." *CRC Press,* **24**, (2015).

[168] W. N. Everitt, and H. Kalf. "The Bessel differential equation and the Hankel transform." *J. Comput. Appl. Math.* **208**, 3–19 (2007).

[169] Xian-Jin Li. "On the Hankel transformation of order zero." *J. Math. Anal. Appl.* **335**, 935–940 (2007).

[170] H.Singh, D. Kumar, D. Baleanu. "Methods of mathematical modelling (Fractional differential equations)." *CRC Press*, (2020).

[171] K. M. Owolabi, A. Atangana. "Numerical methods for fractional differentiation." **54**, (2019).

[172] R. Piessens, "*The transforms and applications handbook.*" **2**, (2000).

[173] B. Rubinsky. "Microscale heat transfer in biological systems at low temperatures." *Exp. Heat Transf.* **10**, 1–29 (1997).

[174] F. Ali, N. A. Sheikh, I. Khan, M. Saqib. "Magnetic field effect on blood flow of Casson fluid in axisymmetric cylindrical tube: A fractional model." *J. Magn. Magn. Mater.* **423**, 327–336 (2017).

[175] S. Sharma, A. Gaur, U. Singh and V. K. Katiyar. "Capture efficiency of magnetic nanoparticles in a tube under magnetic field." *Procedia Materials Science* **10**, 64–69 (2015).

[176] S. Sharma, R. Kumar and A. Gaur. "A model for magnetic nanoparticles transport in a channel for targeted drug delivery." *Procedia Materials Science* **10**, 44–49 (2015).

[177] M. Sheikholeslami and S. A. Shehzad. "Magnetohydrodynamic nanofluid convection in a porous enclosure considering heat flux boundary condition." *Int. J. Heat Mass Transf.* **106**, 1261–1269 (2017).

[178] N. Sher Akbar and A. W. Butt. "Bio mathematical venture for the metallic nanoparticles due to ciliary motion." *Comput. Methods. Programs. Biomed.* **134**, 43–51 (2016).

[179] F. Liu, P. Zhuang, V. Anh, I. Turner and K. Burrage. "Stability and convergence of the difference methods for the space?time fractional advection?diffusion equation." *Appl. Math. Comput.* **191**, 12–20 (2007).

[180] A. Farhad, A.S Nadeem, I. Khan, M. Saqid. "Magnetic field effect on blood flow of Casson fluid in axisymmetric cylindrical tube: A fractional model." *J. Magn. Magn. Mater.* **423**, 327–336 (2017).

[181] S. Ijaz, Z. Iqbal, E.N. Maraj and S. Nadeem. "Investigation of Cu-CuO/blood mediated transportation in stenosed artery with unique features for theoretical outcomes of hemodynamics." *J. Mol. Liq.* **254**, 421–432 (2018).

[182] A.S. Nehad, V. Dumitru, and F. Constantin. "Effects of the fractional order and magnetic field on the blood flow in cylindrical domains." *J. Magn. Magn. Mater.* **409**, 10–19 (2016).

[183] F. Ali, I. Khan, N. A. Sheikh, M. Gohar, I. Tlili, and others. "Study of hybrid nanofluid containing graphene oxide and molybdenum disulfide nanoparticles with engine oil base fluid: A non-singular fractional approach." *Sci. Rep.* **8**, 1-13 (2018).

[184] D. Y. Shang, L.C. Zhong. "Hydrodynamics: Heat Transfer of Laminar Mixed Convection of Liquid." *Springer*, 67-75 (2016).

[185] P. A. Ndjawa Yomi, C. D. Bansi Kamdem, T. Nkoa Nkomom, C. B. Tabi, A. Mohamadou and T. C. Kofane. "Fractional blood flow in rotating nanofluid with different shapes nanoparticles in the influence of activation energy and thermal radiation." *Chaos* **31**, 093109 (2021).

[186] R. Sharma, S.M. Hussain, H. Joshi, and G.S. Seth. "Analysis of radiative magneto-nanofluid over an accelerated plate in a rotating medium with Hall effects." *Trans. Tech. Publ.* **11**, 129–145 (2017).

[187] A. Tassaddiq, S. Khan, M. Bilal, T. Gul, S. Mukhtar, Z. Shah, and E. Bonyah. "Heat and mass transfer together with hybrid nanofluid flow over a rotating disk." *AIP Adv.* **10**, 055317 (2020).

[188] F. M. Hady, and F. S. Ibrahim, S. M. Abdel-Gaied, and M. R. Eid. "Radiation effect on viscous flow of a nanofluid and heat transfer over a nonlinearly stretching sheet." *Nanoscale Res. Lett.* **7**, 1–13 (2012).

[189] V. Z. Zulfa, U. Farahdina, M. Firdhaus, I. Aziz, Nasori, Darsono and A. Rubiyanto. "Magnetic field distribution of silver blood cancer with finite difference time domain (FDTD) simulation." *AIP Conf. Proc.* **2360**, 050028 (2021).

Appendices

APPENDIX A:

$$F_{1n}(t) = \frac{b_0 R_e}{c_n}[(1 - Ga_{1n})R_{a,-1}(-a_{1n}, t) - (1 - Ga_{2n})R_{a,-1}(-a_{2n}, t)],$$

$$F_{2n}(t) = \frac{b_1 R_e \cos(\omega t)}{c_n}[(1 - Ga_{1n})F_a(-a_{1n}, t) - (1 - Ga_{2n})F_a(-a_{2n}, t)],$$

$$F_{3n}(t) = \frac{\gamma b_0 c'_n}{c_n^2}[R_{\alpha,-1}(-l_{2n}, t)F_\alpha(-l_{1n}, t)(1 - a_{2n}G) - R_{\alpha,-1}(-k_{2n}, t)F_\alpha(-k_{1n}, t)(1 - a_{1n}G)]$$

$$F_{4n}(t) = \frac{\gamma b_1 c'_n \cos(\omega t)}{c_n^2}[F_\alpha(-l_{2n}, t)F_\alpha(-l_{1n}, t)(1 - a_{2n}G) - F_\alpha(-k_{1n}, t)F_\alpha(-k_{2n}, t)(1 - a_{1n}G)]$$

$$F_{5n}(t) = \frac{\gamma b_0}{c_n}[R_{\alpha,-1}(-l_{2n}, t)F_\alpha(-l_{1n}, t)(1 - a_{2n}G) - R_{\alpha,-1}(-k_{2n}, t)F_\alpha(-k_{1n}, t)(1 - a_{1n}G)]$$

$$F_{6n}(t) = \frac{\gamma b_1 \cos(\omega t)}{c_n}[F_\alpha(-l_{2n}, t)F_\alpha(-l_{1n}, t)(1 - a_{2n}G) - F_\alpha(-k_{2n}, t)F_\alpha(-k_{1n}, t)(1 - a_{1n}G)]$$

$$F_{7n}(t) = \frac{\gamma b_0 G}{c_n}[a'_{2n}R_{\alpha,-1}(-l_{2n}, t)F_\alpha(-l_{1n}, t) - a'_{1n}R_{\alpha,-1}(-k_{2n}, t)F_\alpha(-k_{1n}, t)]$$

$$F_{8n}(t) = \frac{\gamma b_0}{c_n}[a'_{2n}(1 - a_{2n}G)F_\alpha(-a_{2n}, t)(R_{\alpha,-1}(-l_{2n}, t)F_\alpha(-l_{1n}, t))$$
$$- a'_{1n}(1 - a_{1n}G)F_\alpha(-a_{1n}, t)(R_{\alpha,-1}(-k_{2n}, t)F_\alpha(-k_{1n}, t))]$$

$$F_{9n}(t) = \frac{\gamma b_1 G \cos(\omega t)}{c_n}[a'_{2n}F_\alpha(-l_{2n}, t)F_\alpha(-l_{1n}, t) - a'_{1n}F_\alpha(-k_{2n}, t)F_\alpha(-k_{1n}, t)]$$

$$F_{10n}(t) = \frac{\gamma b_1 \cos(\omega t)}{c_n}[a'_{2n}(1 - a_{2n}G)F_\alpha(-a_{2n}, t)(F_\alpha(-l_{2n}, t)F_\alpha(-l_{1n}, t))$$
$$- a'_{1n}(1 - a_{1n}G)F_\alpha(-a_{1n}, t)(F_\alpha(-k_{2n}, t)F_\alpha(-k_{1n}, t))]$$

APPENDIX B:

$$A_{1n}(t) = \frac{b_0 R_e}{c_n}\left[\frac{c_n}{r_n^2 - R_e H_A^2} - \frac{(1 - Ga_{1n})e^{-a_{1n}t}}{a_{1n}} + \frac{(1 - Ga_{2n})e^{-a_{2n}t}}{a_{2n}}\right]$$

$$A_{2n}(t) = \frac{b_1 R_e}{c_n}\left[\frac{(1 - Ga_{1n})}{a_{1n}^2 + \omega^2}(a_{1n}\cos(\omega t) + \omega\sin(\omega t) - a_{1n}e^{-a_{1n}t})\right.$$
$$\left. + \frac{(1 - Ga_{2n})}{a_{2n}^2 + \omega^2}(a_{2n}\cos(\omega t) + \omega\sin(\omega t) - a_{2n}e^{-a_{2n}t})\right]$$

$$A_{3n}(t) = \frac{\gamma b_0 c_n'}{c_n^2}\left[(1 - a_{2n}G)\left(\frac{1 - e^{-l_{1n}t}}{l_{2n}l_1 n} + \frac{e^{-l_{1n}t} - e^{-l_{2n}t}}{l_{2n}(l_{1n} - l_{2n})}\right)\right.$$
$$\left. - (1 - a_{1n}G)\left(\frac{1 - e^{-k_{1n}t}}{k_{2n}k_1 n} + \frac{e^{-k_{1n}t} - e^{-k_{2n}t}}{k_{2n}(k_{1n} - k_{2n})}\right)\right]$$

$$A_{4n}(t) = \frac{\gamma b_1 c_n'\cos\omega t}{c_n^2}\left[\frac{(1 - a_{2n}G)(e^{-l_{2n}t} - e^{-l_{1n}t})}{(l_{1n} - l_{2n})} - \frac{(1 - a_{1n}G)(e^{-k_{2n}t} - e^{-k_{1n}t})}{(k_{1n} - k_{2n})}\right]$$

$$A_{5n}(t) = \frac{\gamma b_0}{c_n}\left[(1 - a_{2n}G)\left(\frac{1 - e^{-l_{1n}t}}{l_{2n}l_1 n} + \frac{e^{-l_{1n}t} - e^{-l_{2n}t}}{l_{2n}(l_{1n} - l_{2n})}\right)\right.$$
$$\left. - (1 - a_{1n}G)\left(\frac{1 - e^{-k_{1n}t}}{k_{2n}k_1 n} + \frac{e^{-k_{1n}t} - e^{-k_{2n}t}}{k_{2n}(k_{1n} - k_{2n})}\right)\right]$$

$$A_{6n}(t) = \frac{\gamma b_1\cos\omega t}{c_n}\left[\frac{(1 - a_{2n}G)(e^{-l_{2n}t} - e^{-l_{1n}t})}{(l_{1n} - l_{2n})} - \frac{(1 - a_{1n}G)(e^{-k_{2n}t} - e^{-k_{1n}t})}{(k_{1n} - k_{2n})}\right]$$

$$A_{7n}(t) = \frac{\gamma b_0 G}{c_n}\left[a_{2n}'\left(\frac{1 - e^{-l_{1n}t}}{l_{2n}l_{1n}} + \frac{e^{-l_{1n}t} - e^{-l_{2n}t}}{l_{2n}(l_{1n} - l_{2n})}\right) - a_{1n}'\left(\frac{1 - e^{-k_{1n}t}}{k_{2n}k_{1n}} + \frac{e^{-k_{1n}t} - e^{-k_{2n}t}}{k_{2n}(k_{1n} - k_{2n})}\right)\right]$$

$$A_{8n}(t) = \frac{\gamma b_0}{c_n}\left[a_{2n}'(1 - a_{2n}G)\left(\frac{1}{l_{2n}l_{1n}}\left(\frac{1 - e^{-a_{2n}t}}{a_{2n}l_{1n}} + \frac{e^{-a_{2n}t} - e^{-l_{1n}t}}{l_{1n}(a_{2n} - l_{1n})}\right)\right.\right.$$
$$\left.\left. + \frac{1}{l_{2n}(l_{1n} - l_{2n})}\left(\frac{e^{-a_{2n}t} - e^{-l_{1n}t}}{l_{1n} - a_{2n}}\right) - \frac{1}{l_{2n}(l_{1n} - l_{2n})}\left(\frac{e^{-a_{2n}t} - e^{-l_{2n}t}}{l_{2n} - a_{2n}}\right)\right)\right.$$
$$\left. - a_{1n}'(1 - a_{1n}G)\left(\frac{1}{k_{2n}k_{1n}}\left(\frac{1 - e^{-a_{1n}t}}{a_{1n}k_{1n}} + \frac{e^{-a_{1n}t} - e^{-k_{1n}t}}{k_{1n}(a_{1n} - k_{1n})}\right)\right.\right.$$
$$\left.\left. + \frac{1}{k_{2n}(k_{1n} - k_{2n})}\left(\frac{e^{-a_{1n}t} - e^{-k_{1n}t}}{k_{1n} - a_{1n}}\right) - \frac{1}{k_{2n}(k_{1n} - k_{2n})}\left(\frac{e^{-a_{1n}t} - e^{-k_{2n}t}}{k_{2n} - a_{1n}}\right)\right)\right]$$

$$A_{9n}(t) = \frac{\gamma b_1 G\cos\omega t}{c_n}\left[a_{2n}'\frac{e^{-l_{2n}t} - e^{-l_{1n}t}}{(l_{1n} - l_{2n})} - a_{1n}'\frac{e^{-k_{2n}t} - e^{-k_{1n}t}}{(k_{1n} - k_{2n})}\right]$$

$$A_{10n}(t) = \frac{\gamma b_1\cos\omega t}{c_n}\left[\frac{a_{2n}'(1 - a_{2n}G)}{l_{1n} - l_{2n}}\left(\frac{e^{-a_{2n}t} - e^{-l_{2n}t}}{l_{2n} - a_{2n}} - \frac{e^{-a_{2n}t} - e^{-l_{1n}t}}{l_{1n} - a_{2n}}\right)\right.$$
$$\left. - \frac{a_{1n}'(1 - a_{1n}G)}{k_{1n} - k_{2n}}\left(\frac{e^{-a_{1n}t} - e^{-k_{2n}t}}{k_{2n} - a_{1n}} - \frac{e^{-a_{1n}t} - e^{-k_{1n}t}}{k_{1n} - a_{1n}}\right)\right]$$

list of publications

1. C.D. Bansi Kamdem, **P. A. Ndjawa Yomi**, C. B. Tabi, A. Mohamadou, "*Modulated blood waves in the coupled complex Ginzburg-Landau equations of Jeffrey fluids in arteries*" Eur. Phys. J. Plus, **138** : 176, (2023).

2. **P. A. Ndjawa Yomi**, C. D. Bansi Kamdem, T. Nkoa Nkomom, C. B. Tabi, A. Mohamadou and T. C. Kofane, **Erratum:** "*Fractional Blood Flow in Rotating Nanofluid with Different Shapes Nanoparticles in the Influence of Activation Energy and Thermal Radiation*" Chaos **32** 089902 (2022).

3. **P. A. Ndjawa Yomi**, C. D. Bansi Kamdem, T. Nkoa Nkomom, C. B. Tabi, A. Mohamadou and T. C. Kofane, "*Fractional Blood Flow in Rotating Nanofluid with Different Shapes Nanoparticles in the Influence of Activation Energy and Thermal Radiation*" Chaos **31** 093109 (2021).

4. C. B. Tabi, **P. A. Ndjawa Yomi**, T. G. Motsumi, C. D. K. Bansi and T. C. Kofane, "*Magnetic field effect on a fractionalized blood flow model in the presence of magnetic particles and thermal radiations*" Chaos, Solitons & Fractals **131** 109540 (2019).

Magnetic field effect on a fractionalized blood flow model in the presence of magnetic particles and thermal radiations

C.B. Tabi [a,*], P.A.Y. Ndjawa [b], T.G. Motsumi [c], C.D.K. Bansi [b], T.C. Kofané [a,d]

[a] *Department of Physics and Astronomy, Botswana International University of Science and Technology, Private Mail Bag 16 Palapye, Botswana*
[b] *Laboratoire de Biophysique, Département de Physique, Faculté des Sciences, Université de Yaoundé I, Yaoundé B.P. 812, Cameroun*
[c] *Department of Mathematics, University of Botswana, Private Mail Bag 22 Gaborone, Botswana*
[d] *Laboratoire de Mécanique, Département de Physique, Faculté des Sciences, Université de Yaoundé I Yaoundé B.P. 812, Cameroun*

ARTICLE INFO

ABSTRACT

The presence of magnetic particles is considered in a magneto-hydrodynamic blood flow through a circular cylinder. The fluid inside the tube is acted by an oscillating pressure gradient and an external constant magnetic field. The blood temperature is assumed to change with the blood and particle velocities, and the whole study is based on a mathematical model that includes Caputo fractional-order derivatives. Solutions for the particle and blood velocities, and blood temperature distribution, are obtained via the combination of the Laplace and Hankel transformation methods. Effects of the fractional-order parameter and magnetic field are addressed using numerical simulations. Results show that the applied magnetic field reduces the velocities of the fluid and particles, which remarkably affects the blood temperature. This is obvious for short and long time intervals. However, under long time intervals, particles seem to be accelerated, but their velocity is suitably controlled by the fractional-order parameter which also monitors the increase in blood temperature.

1. Introduction

Biomagnetic fluid dynamics (BFD) is a new branch of science which is devoted to the study of fluids that flow under the influence of an external magnetic field. Recent advances in bioengineering and medical sciences have brought forth the importance of Biomagnetic fluids, with specific applications in targeted drug delivery [1], conception and development of magnetic devices for cell separation [2], attenuation of bleeding during surgeries and treatment of cancer tumors through magnetic hyperthermia [3]. Indeed, blood is a biomagnetic fluid, due to the strong presence of the erythrocytes playing the role of magnetic particles and the plasma as liquid carrier. Erythrocytes, or red blood cells (RBCs), are in fact negative charge carriers and this creates a magnetic field on the vessel wall, capable of influencing the pulsatile character of the blood flowing inside the vessel [4,5]. Moreover, the magnetization of blood can be augmented by adding artificially created nanoparticles to the flow as usually done in targeted drug delivery. More precisely, this implies that biofluids can behave like ferromagnetic fluids, reason why most of the magnetic particles that are fre-

quently used in bio-medicine are manganese ferrite ($CoFe_2O_4$), iron oxides (Fe_2O_3 or Fe_3O_4), cobalt ferrite ($CoFe_2O_4$) [6], just to cite a few. One of the first models to address such aspect of BFD was proposed by Haik et al. [7], where they made a comparative study between mathematical models for BFD and ferrohydrodynamics (FHD). However, they did not consider the induced magnetic field, but rather assumed that the flow was under the effect of an applied magnetic field. This otherwise implies that biofluids should be considered electrically poor conductors, contrarily to what is reported in Refs. [8,9] and which supports that blood exhibits significantly high electrical conductivity, especially when additional magnetic particles are injected in blood to carry drugs. This may justify the use of the principles of magnetohydrodynamics (MHD) [10,11], which rely on the generation of Lorentz forces, in elaborating suitable mathematical models. Sharma et al. [12] studied for example the effect of external uniform magnetic field on flow parameters of both blood and magnetic particles based on a mathematical model using the MHD approach. Magnetic Drug Targeting (MDT) technique was used by Bose and Banerjee [13], where FHD and MHD principles were coupled to track the magnetic particles under the effect of a magnetic field. Mondal and Shit [6] studied the motion of magnetic nano-particles in a biofluid, in the presence of externally applied magnetic field, with strong applications to drug delivery for some therapeutic procedures in the treatment of tumor

* Corresponding author.
  E-mail addresses: conrad@aims.ac.za, tabic@biust.ac.bw (C.B. Tabi), teko@aims.ac.za (T.G. Motsumi).

cells, infections and removing blood clots. Kefayati [14] studied the effect of a magnetic field on non-Newtonian blood flow between two-square concentric duct annuli, and further extended the study to non-Newtonian blood flow in a cavity driven by the motion of two facing lids [15]. In both cases, the results showed that the increment of Reynolds number augments the magnetic field effect on the flow of blood.

In most of the above contributions, biofluid-related problems were solved using classical models, i.e., with integer derivatives. Most of physical problems nowadays have found suitable formulation using the idea of fractional derivative, with applications in dynamical systems [16,17], neural systems [18,19], biophysics [20], mathematical biology [21], viscoelasticity [22,23] and fluid dynamics [24,25]. In that respect, Nehad et al. [26] and Ali et al. [27] studied blood flow with magnetic particles and magnetic field effect using the Caputo fractional derivatives concept in the fractal theory, starting from the classical model [28–32]. Generalized second grade fluids with Caputo-Fabrizio derivative were studied by Sheikh et al. [33], using the MHD formulation. Heat and mass transfer of differential-type fluids, with fractional Caputo derivatives were analyzed by Imran et al. [34]. Bansi et al. [5,35] proposed a fractionalized model to study the effect of heat transfer and magnetic field on the blood flowing inside oscillatory arteries and periodic pressure gradient. More recently, the effect of magnetic fields on blood flow was studied by Ali et al. [36] using the Caputo-Fabrizio derivative, with blood considered as a Casson fluid, with magnetic particles, flowing in the cylindrical domain.

The main objective of the present work is to study a mathematical model of blood flow in presence of magnetic particles and blood temperature, using Caputo fractional derivatives[37,38]. External magnetic effects are considered and the blood in the vessel is assumed to be acted by a periodic pressure gradient. The mathematical model, which includes Caputo fractional derivatives, is generalized from the model containing integer derivatives, and solutions for the blood velocity, particle velocity and blood temperature are obtained by conjointly making use of the finite Hankel and Laplace transforms. Since Laplace transformed expressions of velocities and temperature are functions of a modified Bessel function, the inverse Laplace transform is difficult to find traditionally. This is therefore done numerically, where we address the effect of some flow parameters such as the Reynolds and Hartmann numbers on the joint dynamics of blood and particles, along with the change in blood temperature, when the fractional-order parameter is varied.

2. Model equation and general analytical solution

2.1. Mathematical modeling of the problem

In the present model, blood, which is considered as a non-Newtonian fluid, is assumed to flow in a cylindrical vessel of radius R_0, together with magnetic particles (see Fig. 1). This makes a two-phase mixture, with the solid phase consisting of magnetic particles and the liquid phase being the blood. We consider the magnetic particles to be uniformly distributed in the blood, while the ensemble flows in the axial direction x of the vessel. The magnetic field acts perpendicular to the vessel and the induced magnetic field is neglected because of the smallness of the magnetic Reynold's number [39]. The particles, the tube and the blood inside are supposed to be at rest at $t = 0$. Particles are subjected to an electromotive force resulting from the interaction of current with the magnetic field. Its expression can be found in Refs. [6,12,36] in the form

$$\overrightarrow{f_{em}} = -\sigma B_0^2 U(r, t) \, \overrightarrow{i},$$ (1)
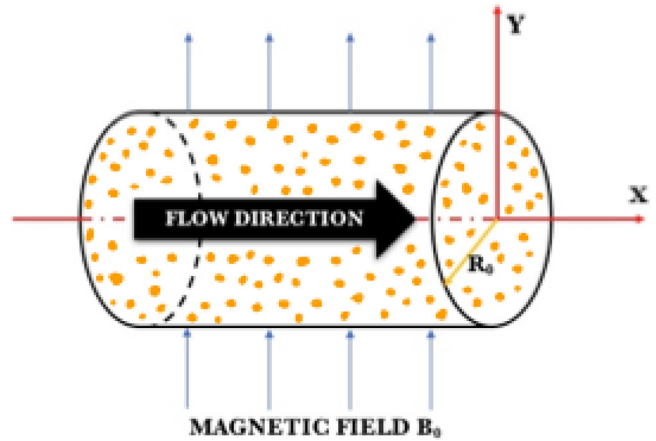
Fig. 1. Schematic representation of the model geometry with orange spots being the magnetic particles.

with $\overrightarrow{i}$ being the unit vector in the x−direction and $U(r, t)$, the axial velocity of the blood. B_0 is a uniform magnetic field and σ the electrical conductivity. The equation describing the motion of magnetic particles is governed by the Newton's second law and is given in the form [6,12,36]

$$m\frac{\partial v}{\partial t} = K(U - V),$$ (2)

where K is the Stokes constant, m is the average mass of the magnetic particles and V is the velocity of the particles.

The unsteady pulsatile flow of blood in an axisymmetric cylindrical blood vessel of radius R_0, considered to be affected by a uniform transverse magnetic field B_0, is governed by the following momentum equation in polar coordinates [5,35]

$$\rho\frac{\partial U}{\partial t} = -\frac{\partial P}{\partial x} + \frac{1}{r}\frac{\partial}{\partial r}\left(r\mu\frac{\partial U}{\partial r}\right) + KN(V - U) - \sigma B_0^2 U,$$ (3)

where P is the blood pressure. μ, σ and ρ are the dynamic coefficient of viscosity, the electrical conductivity and the density of blood, respectively. N is the number of magnetic particles per unit volume. The first three terms on the right-hand side of Eq. (3) represent the pressure gradient, the viscosity and the force generated by the relative motion between the fluid and the particle. The last term stands for the Lorentz force brought by the magnetic field. The oscillating pressure gradient $\frac{\partial P}{\partial x}$ is given by

$$-\frac{\partial P}{\partial x} = b_0 + b_1 \cos(\omega t), \quad t > 0$$ (4)

where b_0 and b_1 are the amplitude of the systolic and diastolic pressure gradient, respectively [12,35,40], with ω being the frequency. Eq. (3) can also be rewritten, by introducing the kinematic viscosity $\hat{\mu} = \mu/\rho$, as

$$\frac{\partial U}{\partial t} = \frac{1}{\rho}(b_0 + b_1 \cos(\omega t)) + \frac{1}{r}\frac{\partial}{\partial r}\left(r\hat{\mu}\frac{\partial U}{\partial r}\right) + \frac{KN}{\rho}(V - U) - \frac{\sigma B_0^2 U}{\rho}.$$ (5)

The energy equation, related to thermal radiation is given by [4,5]

$$\rho C_p \frac{\partial T}{\partial t} = \kappa \frac{1}{r}\frac{\partial}{\partial r}\left(r\frac{\partial T}{\partial r}\right) - \frac{\partial q_r}{\partial r} + \mu\left(\frac{\partial U}{\partial r}\right)^2, \quad t > 0, \quad r \in [0, R_0],$$ (6)

where the term $\hat{\mu}\left(\frac{\partial U}{\partial r}\right)^2$ in (6) represents the viscous dissipation due to the assumption of the unidirectional flow. C_p and κ represent the specific heat at constant pressure and thermal conductivity. The radiative flux q_r is written assuming that blood is an

optically thin fluid with a relatively low density and heat absorption coefficient. q_r can then be simplified as proposed by Cogley et al. [41] in the form

$$\frac{\partial q_r}{\partial r} = 4\alpha^2 (T - T_\infty),$$

$$\frac{\partial U}{\partial x} = 0, \quad T = T_\infty \quad \text{on} \quad r = 0 \qquad (7)$$

$$U = 0, \quad T = T_w \quad \text{on} \quad r = R_0,$$

where $\alpha^2 = \int_0^\infty \phi \chi \frac{\partial B}{\partial T}$ is the linear Planck mean absorption coefficient, with B and ϕ being respectively the Planck's constant and radiation absorption coefficient, and χ being the frequency. The above formulated models equations correspond to the initial and boundary conditions

$$\begin{aligned} U(r, 0) &= 0, \quad V(r, 0) = 0, \quad T(r, 0) = T_\infty, \quad r \in [0, R_0]; \\ U(R_0, t) &= 0, \quad V(R_0, t) = 0, \quad T(R_0, t) = T_w, \quad t > 0. \end{aligned} \qquad (8)$$

The set of model Eqs. (2), (3) and (6) can be generalized to their time-fractional versions by multiplying each of them by $\lambda = \sqrt{\frac{R_0 \rho}{b_0}}$. This leads to the fractional-order equations

$$\begin{aligned} \lambda^a D_t^a U &= \frac{\lambda}{\rho} [b_0 + b_1 \cos(\omega t)] + \lambda \hat{\mu} \left(\frac{\partial^2 U}{\partial r^2} + \frac{1}{r} \frac{\partial U}{\partial r} \right) \\ &\quad - \frac{\lambda K N}{\rho} (V - U) - \frac{\lambda \sigma B_0^2}{\rho} U, \end{aligned} \qquad (9a)$$

$$\lambda^a D_t^a V = \frac{\lambda K}{m} (U - V), \qquad (9b)$$

$$-\lambda^a D_t^a T = -\frac{\kappa}{\rho C_p} \left(\frac{\partial^2 T}{\partial r^2} - \frac{1}{r} \frac{\partial T}{\partial r} \right) + \frac{4\alpha^2}{\rho C_p} (T - T_\infty) + \frac{\mu}{\rho C_p} \left(\frac{\partial U}{\partial r} \right)^2, \qquad (9c)$$

where

$$D_t^a f(r, t) = \frac{1}{\Gamma(1 - a)} \int_0^t \frac{1}{(t - \tau)^a} \frac{\partial f(r, \tau)}{\partial \tau} d\tau \qquad (10)$$

is the Caputo fractional derivative of order a [18,19,37,38]. In the meantime, recent works have developed new directions in fractional derivative operators and using Mittag-Leffler functions. For example, a new definition of fractional derivative, with a smooth kernel which considers two different representations for the temporal and spatial variable, was proposed in Ref. [42]. Operators including the Atangana-Beleanu (AB) derivative and the Caputo-Fabrizio derivative, respectively related to the Mittag-Leffler law and the exponential law were applied to the non-linear Kaup-Kupershmidt equation [43]. Making use of the traditional Caputo derivative and Caputo-Fabrizio derivative with fractional order and no singular kernel, the nonlinear Kaup-Kupershmidt was extended to the span of fractional calculus by Atangana and Doungmo [44]. Moreover, further relationship and new results of Atangana-Baleanu derivative, with some integral transform operators, were obtained from a simple nonlinear system [45]. Another important feature of the non-local and non-singular kernel operator was pointed out and applied to chaotic models whose the bifurcation, period doubling dynamics and chaotic behaviors were discussed [46,47]. Additionally, the AB fractional derivative with non-singular kernel and non-local kernel was applied to chaotic processes with two-parameter derivative, including non-singular and non-local kernel based on the one-parameter Mittag-Leffler function [46,47]. To further proceed, the following dimensionless variables can be introduced

$$r^* = \frac{r}{R_0}, \quad t^* = \frac{t}{\lambda}, \quad U^* = \frac{U}{U_0}, \quad V^* = \frac{V}{U_0}, \quad b_0^* = \frac{\lambda b_0}{\rho U_0}, \quad b_1^* = \frac{\lambda b_1}{\rho U_0},$$

$$\omega^* = \lambda \omega, \quad T^* = \frac{T - T_\infty}{T_w - T_\infty}. \qquad (11)$$

Considering all the above and dropping the (*) notation, we get the following fractionalized set of equations

$$D_t^a U = [b_0 + b_1 \cos(\omega t)] + \frac{1}{Re} \left(\frac{\partial^2 U}{\partial r^2} + \frac{1}{r} \frac{\partial u}{\partial r} \right) - R(V - U) - \mathcal{H}^2 U, \qquad (12a)$$

$$G D_t^a V = U - V, \qquad (12b)$$

$$-D_t^a T + \frac{\kappa}{\rho C_p} \left(\frac{\partial^2 T}{\partial r^2} + \frac{1}{r} \frac{\partial T}{\partial r} \right) - \frac{4\alpha^2}{\rho C_p} T = -\frac{\hat{\mu}}{C_p} \left(\frac{\partial U}{\partial r} \right)^2, \qquad (12c)$$

where $Re = \frac{R_0^2}{\lambda \hat{\mu}}$ is a Reynold number, $R = \frac{KN\lambda}{\rho}$ is a particle concentration parameter, $\mathcal{H} = B_0 R_0 \sqrt{\frac{\sigma}{\mu}}$ is a magnetic parameter or Hartmann number, $G = \frac{m}{K\lambda}$ is the particle mass parameter. The initial and boundary conditions then become

$$\begin{aligned} U(r, 0) &= 0, \quad V(r, 0) = 0, \quad T(r, 0) = 0, \quad r \in [0, 1], \\ U(1, t) &= 0, \quad V(1, t) = 0, \quad T(1, t) = 0, \quad t > 0. \end{aligned} \qquad (13)$$

3. Solution of the mathematical model

To solve the mathematical model (12), we make use of the Laplace transform with respect to time and the Hankel transform with respect to the radial variable. The temporal transformation then leads to the equations

$$\begin{aligned} s^a \overline{U}(r, s) &= \frac{1}{Re} \left[\frac{\partial^2 \overline{U}(r, s)}{\partial r^2} + \frac{1}{r} \frac{\partial \overline{U}(r, s)}{\partial r} \right] + \frac{b_0}{s} + \frac{b_1 s}{s^2 + \omega^2} + R \overline{V}(y, s) \\ &\quad - (R + \mathcal{H}^2) \overline{U}(r, s), \end{aligned} \qquad (14a)$$

$$\overline{V}(r, s) = \frac{\overline{U}(r, s)}{G s^a + 1} \qquad (14b)$$

$$\begin{aligned} s^a \overline{T}(r, s) &= \frac{\kappa}{\rho C_p} \left[\frac{\partial^2 \overline{T}(r, s)}{\partial r^2} + \frac{1}{r} \frac{\partial \overline{T}(r, s)}{\partial r} \right] - \frac{4\alpha^2}{\rho C_p} \overline{T}(r, s) \\ &\quad + \frac{\hat{\mu}}{C_p} \left(\frac{\partial \overline{U}(r, s)}{\partial r} \right)^2 - \frac{\hat{\mu}}{C_p} \lim_{t \to 0} \left\{ \int_0^t \left(\frac{\partial U(r, \tau)}{\partial r} \right)^2 d\tau \right\}, \end{aligned} \qquad (14c)$$

with $\overline{U}(1, s) = 0$, $\overline{V}(1, s) = 0$, and $\overline{T}(1, s) = 0$. In the rest of study, it is considered that $\lim_{t \to 0} \left\{ \int_0^t \left(\frac{\partial U(r, \tau)}{\partial r} \right)^2 d\tau \right\} \to 0$. Applying the Hankel transform [48,49] of zero order to Eqs. (14a) and (14c), and using the boundary conditions given in (13), we obtain

$$\begin{aligned} -\frac{r_n^2 \overline{U}_H(y_n, s)}{Re} &= \left[\frac{G s^{2a} + [1 + G(R + \mathcal{H}^2)] s^a + \mathcal{H}^2}{G s^a + 1} \right] \overline{U}_H(r_n, s) \\ &\quad - \left(\frac{b_0}{s} + \frac{b_1 s}{s^2 + \omega^2} \right) \frac{J_1(r_n)}{r_n}, \end{aligned} \qquad (15)$$

where $\overline{U}_H(r_n, s) = \int_0^1 r \overline{U}(r, s) J_0(rr_n) dy$ is the finite Hankel transform of function $\overline{U}(r, s)$ and r_n $(n = 1, 2, \ldots.)$ are positive roots of the equation $J_0(\chi) = 0$, J_0 being the Bessel function of the first kind of order zero. The inverse Laplace transform for Eq. (15) of fluid can be written in the equivalent form

$$\begin{aligned} \overline{U}_H(r_n, s) &= \frac{b_0 Re}{c_n} \left[(1 - G a_{1n}) \frac{s^{-1}}{s^a + a_{1n}} - (1 - G a_{2n}) \frac{s^{-1}}{s^a + a_{2n}} \right] \frac{J_1(r_n)}{r_n} \\ &\quad - \frac{b_1 Re}{c_n} \frac{s}{s^2 + \omega^2} \left[(1 - G a_{1n}) \frac{s^{-1}}{s^a + a_{1n}} \right. \\ &\quad \left. - (1 - G a_{2n}) \frac{s^{-1}}{s^a + a_{2n}} \right] \frac{J_1(r_n)}{r_n}, \end{aligned} \qquad (16)$$

Fig. 2. Profiles of blood temperature $T(r, t)$, axial velocity $u(r, t)$, and particle velocity $v(r, t)$ for small values of time t, with $S = 0.01$, $A_0 = 10^{-7}$, $A_1 = 10^{-7}$, $\omega = \pi/4$, $\beta = 0.5$, $\lambda = 0.5$, $G = 1.5$, $R = 0.2$, $Re = 3$ and $\mathcal{H} = 1$. Panels $(aj)_{j=1,2,3}$ correspond to $t = 0.05$, panels $(bj)_{j=1,2,3}$ give results for $t = 0.2$ and panels $(cj)_{j=1,2,3}$ correspond to $t = 0.3$. In all the panels, the fractional parameter takes the values $a = 0.3$, 0.5, 0.7 and 1.

where

$$a_{1n} = \frac{b_n - c_n}{2ReG}, \quad a_{2n} = \frac{b_n + c_n}{2ReG}, \quad b_n = Re[1 + G(R + \mathcal{H}^2)] + Gr_n^2$$

$$c_n = \sqrt{b_n^2 - 4ReG(Re\mathcal{H}^2 + r_n^2)}. \tag{17}$$

Inserting Eq. (16) into Eq. (14c) and applying the Hankel transform leads to

$$\bar{T}_H(r_n, s) = \frac{2\hat{\mu}Re\left(\frac{A_0}{s} + \frac{A_1 s}{s^2 + w^2}\right)}{C_p\left(\beta r_n^2 + s^a + \frac{4\alpha^2}{C_p}\right)} \frac{\partial}{\partial r_n}\left[\left(\frac{1 - a_{1n}G}{s^a + a_{1n}} - \frac{1 - a_{2n}G}{s^a + a_{2n}}\right)\frac{J_1(r_n)}{r_n c_n}\right]. \tag{18}$$

The Bessel expansion form, given by

$$J_{n+1}(x) = \frac{nJ_n(x)}{x} - J_n'(x) \quad \text{and} \quad J_{n+1}(x) - J_{n-1}(x) = -2J_n'(x), \tag{19}$$

and the approximation

$$\frac{\partial}{\partial r_n}\left(\frac{J_1(r_n)}{r_n c_n}\right) = -\frac{J_2(r_n)}{r_n c_n} - \frac{c_n'}{c_n^2}(J_2(r_n) + J_1'(r_n)),$$

$$\frac{\partial}{\partial r_n}\left(\frac{1 - a_{1n}G}{s^a + a_{1n}} - \frac{1 - a_{2n}G}{s^a + a_{2n}}\right) = \frac{-a_{1n}'G(s^a + a_{1n}) - a_{1n}'(1 - a_{1n}G)}{(s^a + a_{1n})^2}$$
$$+ \frac{a_{2n}'G(s^a + a_{2n}) + a_{2n}'(1 - a_{2n}, G)}{(s^a + a_{2n})^2} \tag{20}$$

can be employed to expand Eq. (18) so that

$$\bar{T}_{H_1}(r_n, s) = \frac{\gamma b_0 c_n'}{c_n^2}\frac{J_1(r_n)}{r_n}\left[\frac{s^{-1}(1 - a_{2n}G)}{(s^a + l_{2n})(s^a + l_{1n})} - \frac{s^{-1}(1 - a_{1n}G)}{(s^a + k_{2n})(s^a + k_{1n})}\right]$$
$$+ \frac{s\gamma b_1 c_n'}{(s^2 + w^2)c_n^2}\frac{J_1(r_n)}{r_n}\left[\frac{(1 - a_{2n}G)}{(s^a + l_{2n})(s^a + l_{1n})}\right.$$
$$\left. - \frac{(1 - a_{1n}G)}{(s^a + k_{1n})(s^a + k_{2n})}\right] + \frac{\gamma b_0}{c_n}\frac{J_2}{r_n}\left[\frac{(1 - a_{2n}G)s^{-1}}{(s^a + l_{2n})(s^a + l_{1n})}\right.$$
$$\left. - \frac{(1 - a_{1n}G)s^{-1}}{(s^a + k_{2n})(s^a + k_{1n})}\right] + \frac{\gamma b_1 s}{c_n(s^2 + w^2)}$$
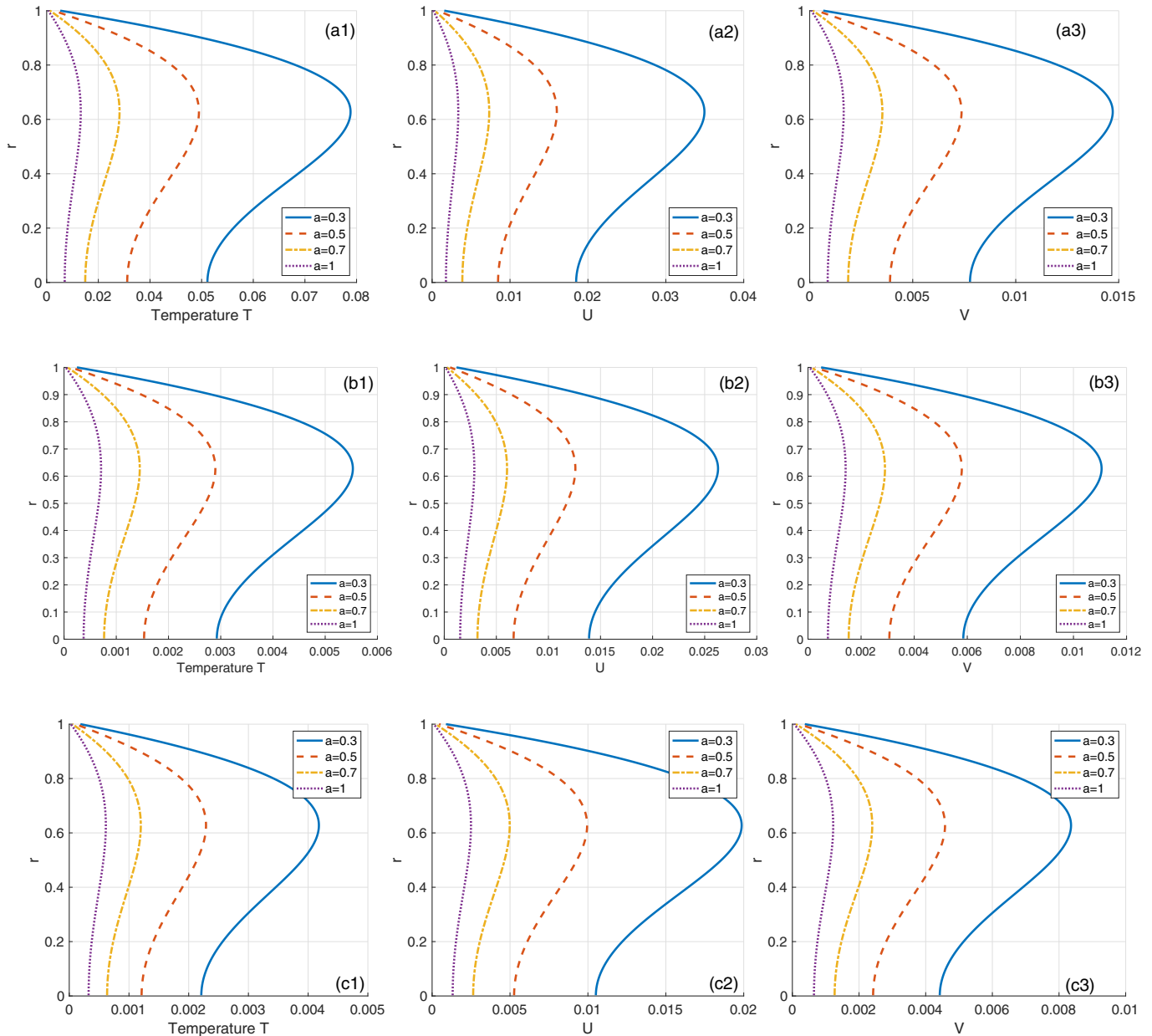
Fig. 3. Profiles of blood temperature $T(r, t)$, axial velocity $u(r, t)$, and particle velocity $v(r, t)$ for large values of time t, with $S = 0.01$, $A_0 = 10^{-7}$, $A_1 = 10^{-7}$, $\omega = \pi/4$, $\beta = 0.5$, $\lambda = 0.5$, $G = 1.5$, $R = 0.2$, $Re = 3$ and $\mathcal{H} = 1$. Panels (aj)$_{j=1,2,3}$ correspond to $t = 1$, panels (bj)$_{j=1,2,3}$ give results for $t = 3$ and panels (cj)$_{j=1,2,3}$ correspond to $t = 5$. In all the panels, the fractional parameter takes the values $a = 0.3$, 0.5, 0.7 and 1.

$$\times \frac{J_2}{r_n} \left[\frac{(1 - a_{2n}G)}{(s^a + l_{2n})(s^a + l_{1n})} - \frac{(1 - a_{1n}G)}{(s^a + k_{2n})(s^a + k_{1n})} \right], \quad (21a)$$

$$\bar{T}_{H_2}(r_n, s) = \frac{\gamma b_0 s^{-1}}{c_n} \frac{J_1(r_n)}{r_n} \left[\begin{array}{c} \frac{(-a'_{1n}G)}{(s^a + k_{2n})(s^a + k_{1n})} - \frac{a'_{1n}(1 - a_{1n}G)}{(s^a + a_{1n})(s^a + k_{2n})(s^a + k_{1n})} \\ + \frac{a'_{2n}G}{(s^a + l_{2n})(s^a + l_{1n})} + \frac{a'_{2n}(1 - a_{2n}G)}{(s^a + a_{2n})(s^a + l_{2n})(s^a + l_{1n})} \end{array} \right]$$

$$+ \frac{\gamma b_1}{c_n(s^2 + w^2)} \frac{s J_1(r_n)}{r_n} \left[\begin{array}{c} \frac{(-a'_{1n}G)}{(s^a + k_{2n})(s^a + k_{1n})} - \frac{a'_{1n}(1 - a_{1n}G)}{(s^a + a_{1n})(s^a + k_{2n})(s^a + k_{1n})} \\ + \frac{a'_{2n}G}{(s^a + l_{2n})(s^a + l_{1n})} + \frac{a'_{2n}(1 - a_{2n}G)}{(s^a + a_{2n})(s^a + l_{2n})(s^a + l_{1n})} \end{array} \right], \quad (21b)$$

where

$$a'_{1n} = \frac{(b'_n - c'_n)}{2ReG}, \quad a'_{2n} = \frac{(b'_n + c'_n)}{2ReG}, \quad b'_n = 2 Gr_n, \quad b_{n1} = (\beta r_n^2 + p + a_{1n}),$$

$$b_{n2} = (\beta r_n^2 + p + a_{2n}),$$

$$c'_n = \frac{2 Gr_n}{c_n} \left(-Re + ReG(R + \mathcal{H}^2) + Gr_n^2 \right),$$

$$c_{n1} = \sqrt{(\beta r_n^2 + p + a_{1n})^2 - 4a_{1n}(p + \beta r_n^2)},$$

$$c_{n2} = \sqrt{(\beta r_n^2 + p + a_{2n})^2 - 4a_{2n}(p + \beta r_n^2)}, \quad k_{1n} = \frac{b_{n1} - c_{n1}}{2}, \quad k_{2n} = \frac{b_{n1} + c_{n1}}{2},$$

$$l_{1n} = \frac{b_{n2} - c_{n2}}{2}, \quad l_{2n} = \frac{b_{n2} + c_{n2}}{2}, \quad p = \frac{4\alpha^2}{C_p}, \quad \gamma = \frac{2\hat{\mu}Re}{C_p}. \quad (22)$$

In what follows, we make use of the special functions

$$L^{-1}\left\{ \frac{1}{S^a + m} \right\} = F_a(-m, t) = \sum_{n=0}^{\infty} \frac{(-m)^n t^{(n+1)a-1}}{\Gamma(a(n+1))}, \quad a > 0$$

$$L^{-1}\left\{ \frac{S^\gamma}{S^a + m} \right\} = R_{a,\gamma} = \sum_{n=0}^{\infty} \frac{(-m)^n t^{(n+1)a-1-\gamma}}{\Gamma(a(n+1) - \gamma)}, \quad Re(a - \gamma) > 0, \quad (23)$$
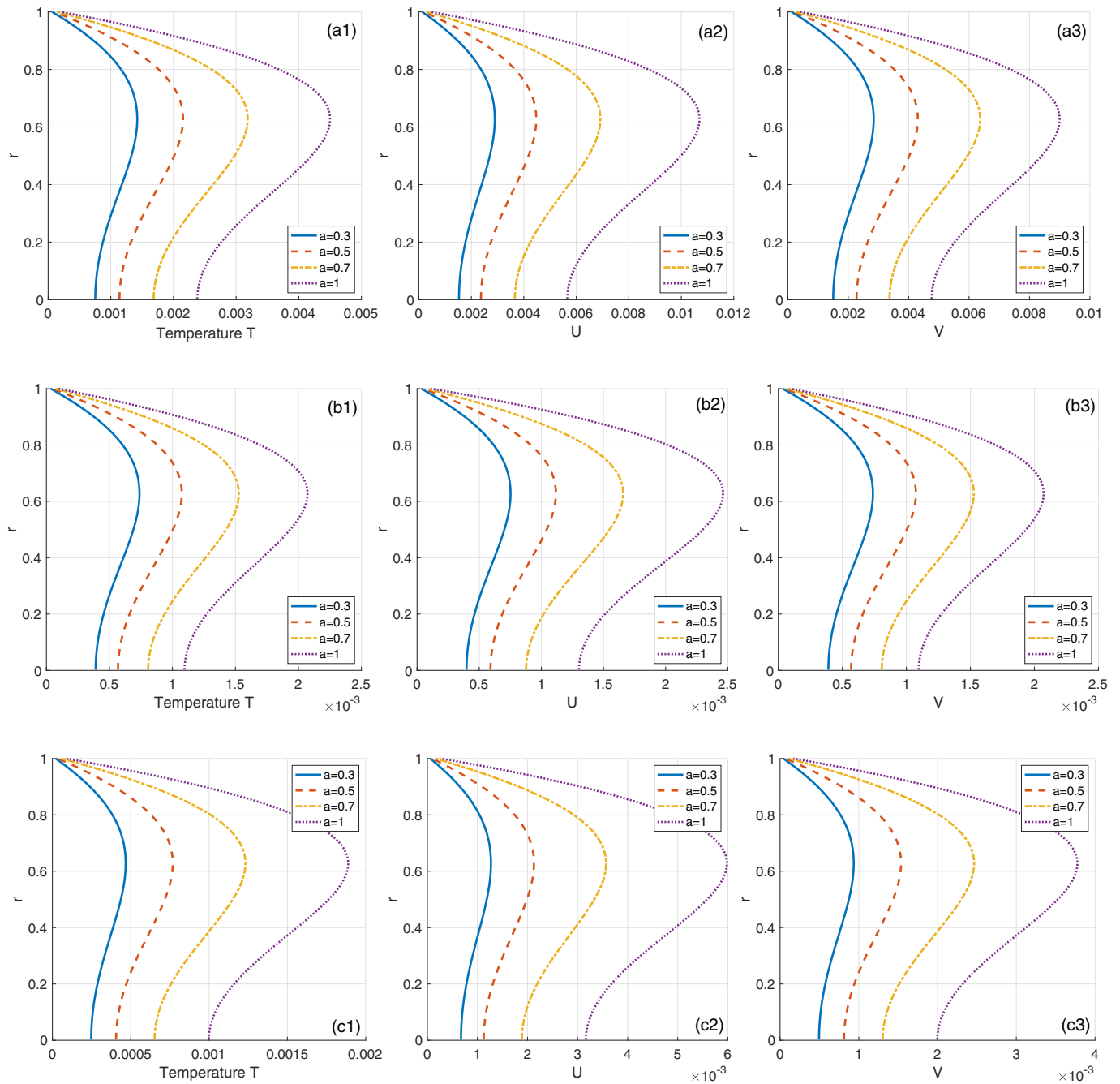
Fig. 4. Profiles of blood temperature $T(r, t)$, axial velocity $u(r, t)$, and particle velocity $v(r, t)$ for different values of Reynold number Re, at $t = 0.2$ (small value of time), with $S = 0.01$, $A_0 = 10^{-7}$, $A_1 = 10^{-7}$, $\omega = \pi/4$, $\beta = 0.5$, $\lambda = 0.5$, $G = 1.5$, $R = 0.2$ and $\mathcal{H} = 1$. Panels $(aj)_{j=1,2,3}$ correspond to $Re = 3$, panels $(bj)_{j=1,2,3}$ give results for $Re = 4$ and panels $(cj)_{j=1,2,3}$ correspond to $Re = 5$. In all the panels, the fractional parameter takes the values $a = 0.3$, 0.5, 0.7 and 1.

where $F_a(., .)$ is the Robotnov-Hartley's function, and $R_{a,\gamma}(., .)$ is the Lorenzo-Hartly's function [50]. For the particular case $a = 1$, Eq. (23) become

$$F_1(-m, t) = e^{-mt} \quad \text{and} \quad R_{1,-1}(-m, t) = \frac{1 - e^{-mt}}{m}. \tag{24}$$

Based on the fact that $T(r, t) = T_1(r, t) + T_2(r, t)$, the inverse Hankel transform of Eqs. (16) and (21) leads to the solutions

$$U(r, t) = 2 \sum_{n=1}^{\infty} \frac{J_0(rr_n)}{r_n J_1(r_n)} [F_{1n}(t) + F_{2n}(t)],$$

$$T_1(r, t) = 2 \sum_{n=1}^{\infty} \left(\frac{J_0(rr_n)}{r_n J_1(r_n)} [F_{3n}(t) + F_{4n}(t)] + \frac{J_0(rr_n)J_2(r_n)}{r_n J_1^2(r_n)} [F_{5n}(t) + F_{6n}(t)] \right),$$

$$T_2(r, t) = 2 \sum_{n=1}^{\infty} \frac{J_0(rr_n)}{r_n J_1(r_n)} [F_{7n}(t) + F_{8n}(t) + F_{9n}(t) + F_{10n}(t)], \quad \text{for} \quad 0 < a < 1$$

$$U(r, t) = 2 \sum_{n=1}^{\infty} \frac{J_0(rr_n)}{r_n J_1(r_n)} [A_{1n}(t) + A_{2n}(t)], \tag{25a}$$

$$T_1(r, t) = 2 \sum_{n=1}^{\infty} \left(\frac{J_0(rr_n)}{r_n J_1(r_n)} [A_{3n}(t) + A_{4n}(t)] + \frac{J_0(rr_n)J_2(r_n)}{r_n J_1^2(r_n)} [A_{5n}(t) + A_{6n}(t)] \right),$$

$$T_2(r, t) = 2 \sum_{n=1}^{\infty} \frac{J_0(rr_n)}{r_n J_1(r_n)} [A_{7n}(t) + A_{8n}(t) + A_{9n}(t) + A_{10n}(t)], \quad \text{for} \quad a = 1 \tag{25b}$$

where F_{in} and A_{in} $(i = 1, \dots, 10)$ are given in Appendices A and B, respectively.

4. Results and discussion

In this section, we collect the information due to the fractional-order parameter a and the other flow parameters, on temperature
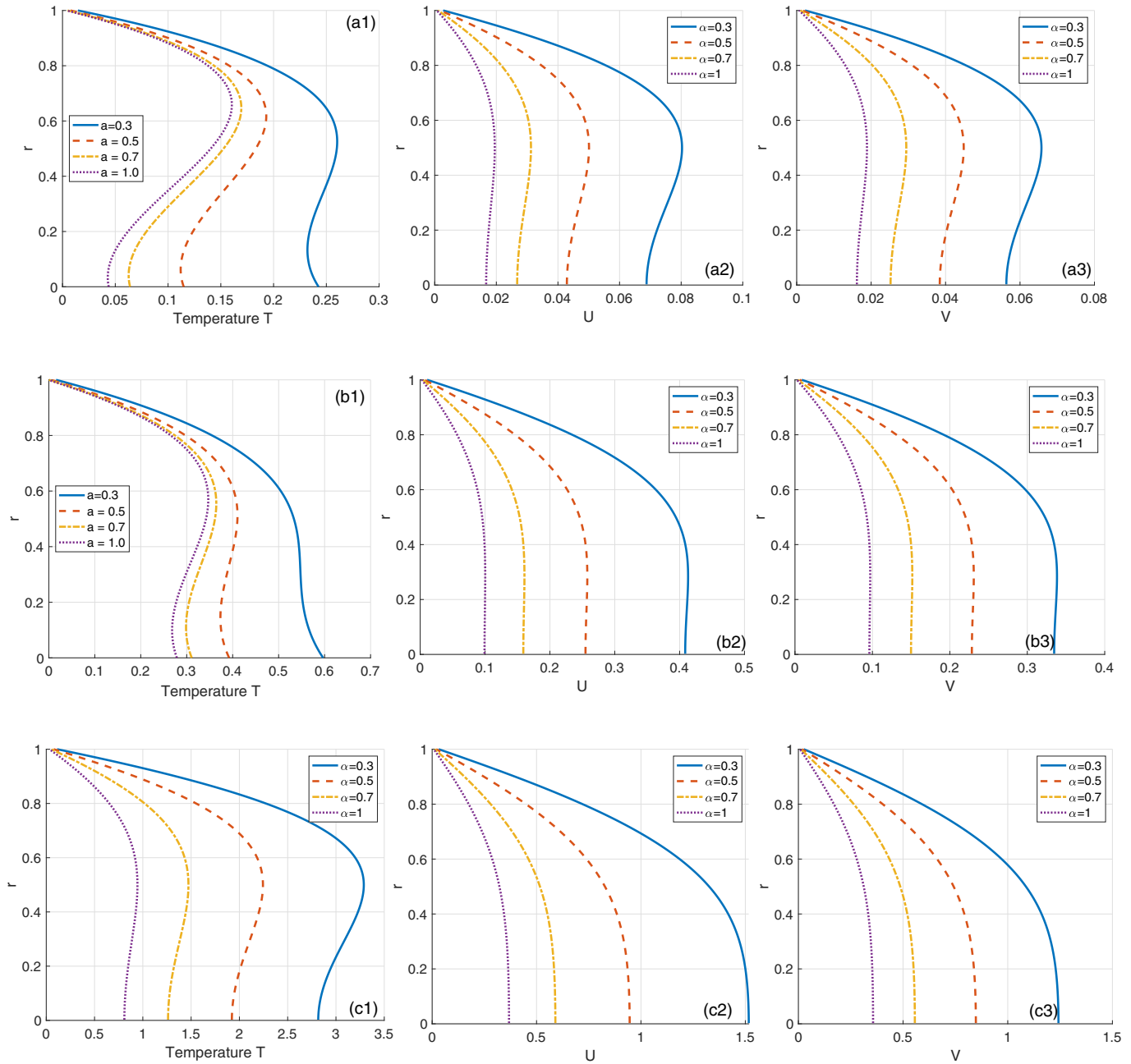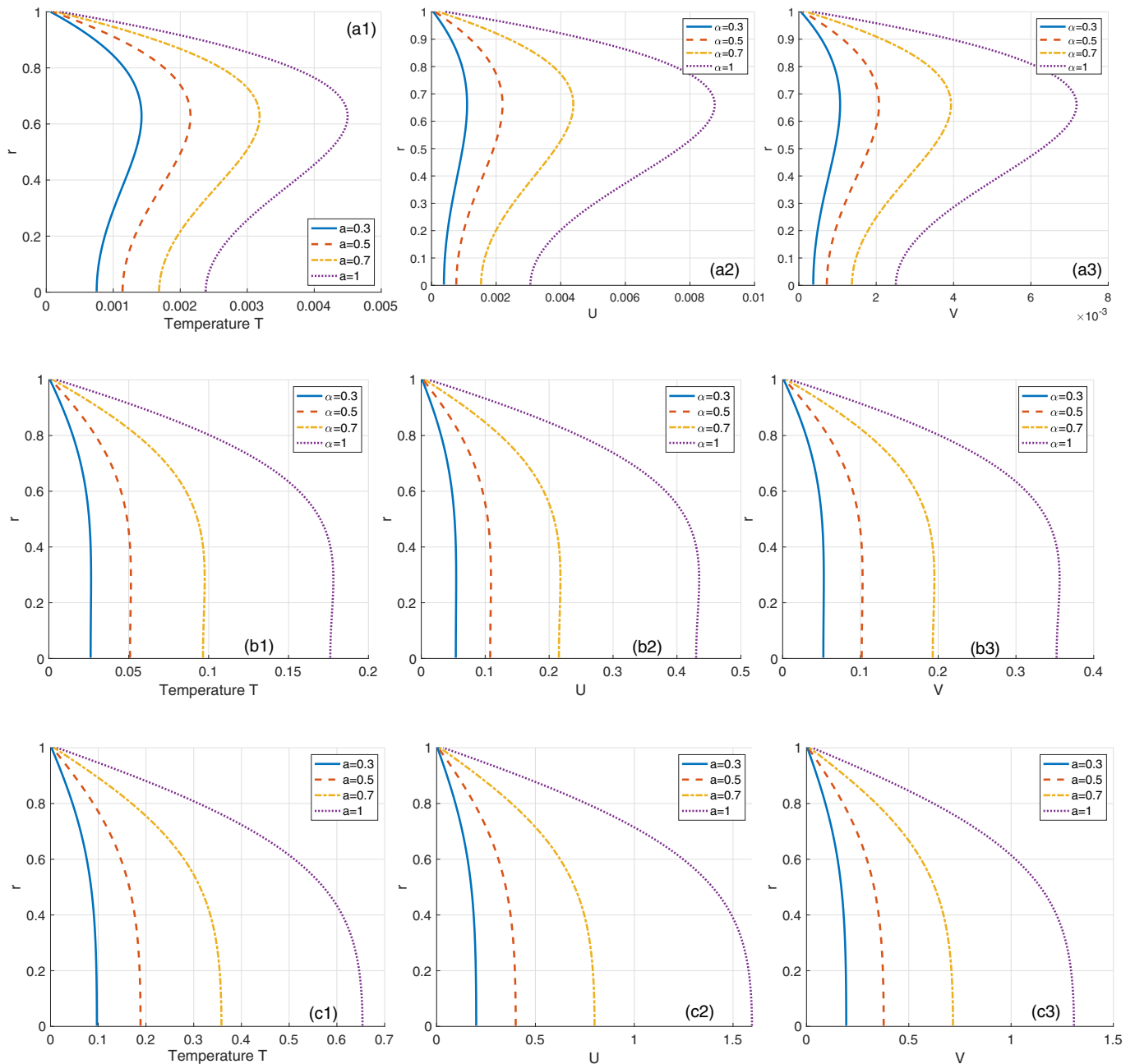
Fig. 5. Profiles of blood temperature $T(r, t)$, axial velocity $u(r, t)$, and particle velocity $v(r, t)$ for different values of Reynold number Re, at $t = 3$ (large value of time), with $S = 0.01$, $A_0 = 10^{-7}$, $A_1 = 10^{-7}$, $\omega = \pi/4$, $\beta = 0.5$, $\lambda = 0.5$, $G = 1.5$, $R = 0.2$ and $\mathcal{H} = 1$. Panels $(aj)_{j=1,2,3}$ correspond to $Re = 3$, panels $(bj)_{j=1,2,3}$ give results for $Re = 4$ and panels $(cj)_{j=1,2,3}$ correspond to $Re = 5$. In all the panels, the fractional parameter takes the values $a = 0.3$, 0.5, 0.7 and 1.

T, fluid velocity U and particle velocity V using numerical simulations and solutions (25). In that respect, we need positive solutions of the equation $J_0(x) = 0$. The corresponding results are recorded in Figs. 2–7, where the effect of a is studied in different situations related to changes in the Reynolds number (Re) and the Hartmann number ($\mathcal{H}$). For the rest of the calculations, other parameter values have been considered as: $A_0 = 10^{-7}$, $A_1 = 10^{-7}$, S=0.01, $\omega = \pi/4$, $R = 0.2$, $\lambda = 0.5$ $\beta = 0.5$ and $G = 0.8$.

In Figs. 2 and 3, we represent flow characteristics at small and high values of the time t, respectively. For the two cases, the temperature generally increases from the center of the vessel and drops near the wall. With the help of the fractional parameter, it is possible to control the increase of T, which is lower for $a = 1$. We should however stress that blood temperature is higher for larger

time. The same remark is made for the velocities, where the velocity of blood is higher than that of magnetic particles. This is different from the study proposed by Ali et al. [27], where the fractional parameter was controlling only the velocities, while it controls both the velocities and the temperature in our case.

Fig. 4 gives results for small values of time, i.e., $t = 0.2$, with changing the Reynolds number Re. For any of the values of the latter, the temperature, the blood velocity and particle velocity decrease with increasing the fractional parameter. Otherwise, the increase in velocity simply implies a decrease in the blood viscosity. Also, the velocity in general is an increasing function of the fractional parameter as supported by the calculations. On the contrary, temperature decreases with a, although changing the value of Re does not really have a significant effect on the blood temperature

Fig. 6. Profiles of blood temperature $T(r, t)$, axial velocity $u(r, t)$, and particle velocity $v(r, t)$ for different values of Hartmann number $\mathcal{H}$, at $t = 0.2$ (large value of time), with $S = 0.01$, $A_0 = 10^{-7}$, $A_1 = 10^{-7}$, $\omega = \pi/4$, $\beta = 0.5$, $\lambda = 0.5$, $G = 1.5$, $R = 0.2$ and $Re = 3$. Panels (aj)$_{j=1,2,3}$ correspond to $\mathcal{H} = 1$, panels (bj)$_{j=1,2,3}$ give results for $\mathcal{H} = 2$ and panels (cj)$_{j=1,2,3}$ correspond to $\mathcal{H} = 3$. In all the panels, the fractional parameter takes the values $a = 0.3$, 0.5, 0.7 and 1.

inside the vessel. One also clearly notices that blood temperature is lower near the tissues and increases progressively near the centerline. However, the temperature profile is such that there is a peak inside the vessel, which is significantly important in keeping the tissues safe. For large values of time, i.e., $t = 3$ (see Fig. 5), Re also takes the same values as in Fig. 4, but one notices small temperatures even though they still decreases with increasing a. The velocities of blood and particles also increase when Re changes, except that they are very small compared to what was obtained in Fig. 4. This confirms the results obtained in Ref. [35], where particle were not included in the model. Moreover, such a behavior was described by Shah et al. [51], who also obtained that the Reynolds number, coupled to an increasing fractional parameter, can contribute to increase considerably the speed of blood and cause an acceleration of the magnetic particles. The influence of the magnetic field on the blood temperature, blood velocity and particles velocity is depicted in Figs. 6 and 7. In Fig. 6, temperature and velocity profiles are recorded for a small value of time ($t = 0.5$) and columns from left to right correspond to $\mathcal{H}=1$, 2 and 3 (Hartmann number). One notice that the velocities of the blood and the particles are reduced with increasing $\mathcal{H}$. This becomes more predominant over long exposure time $t = 3$ as depicted in Fig. 7. In this last case, the temperature rather increases, which to our opinion has an impact not only on the blood viscosity, but also on the velocity of blood and the conveyed particles. Such a result is not surprising because, when a moving electrically conducting fluid is exposed to a magnetic field, there is electric induction in the fluid, and this is pronounced when magnetic particles are present.

For example, numerical and experimental works by Sharma et al. [12,52,53] revealed that Fe_3O_4 Magnetic particles can be efficiently captured when the applied magnetic field intensity is increased, with important applications in targeted drug delivery.
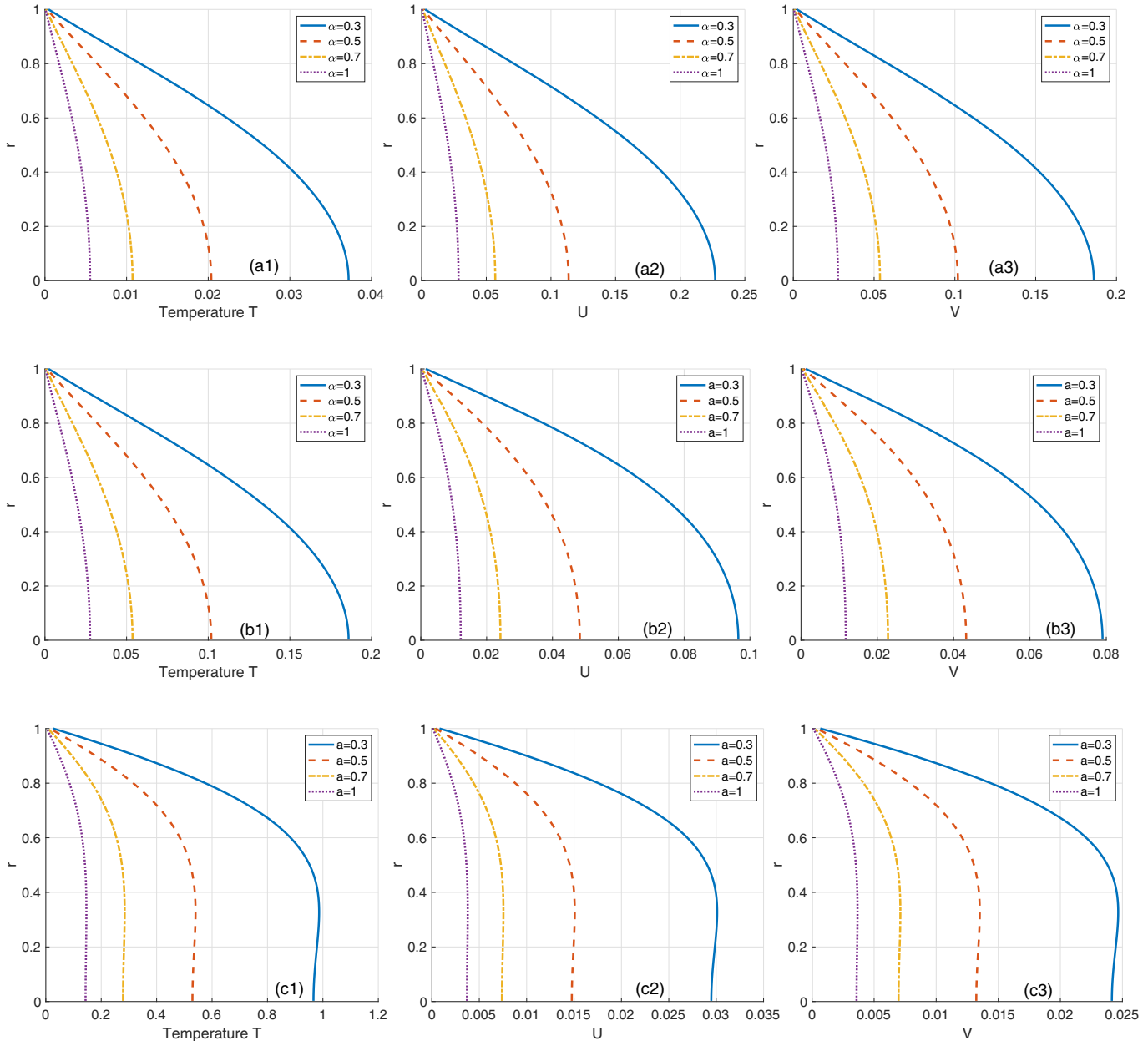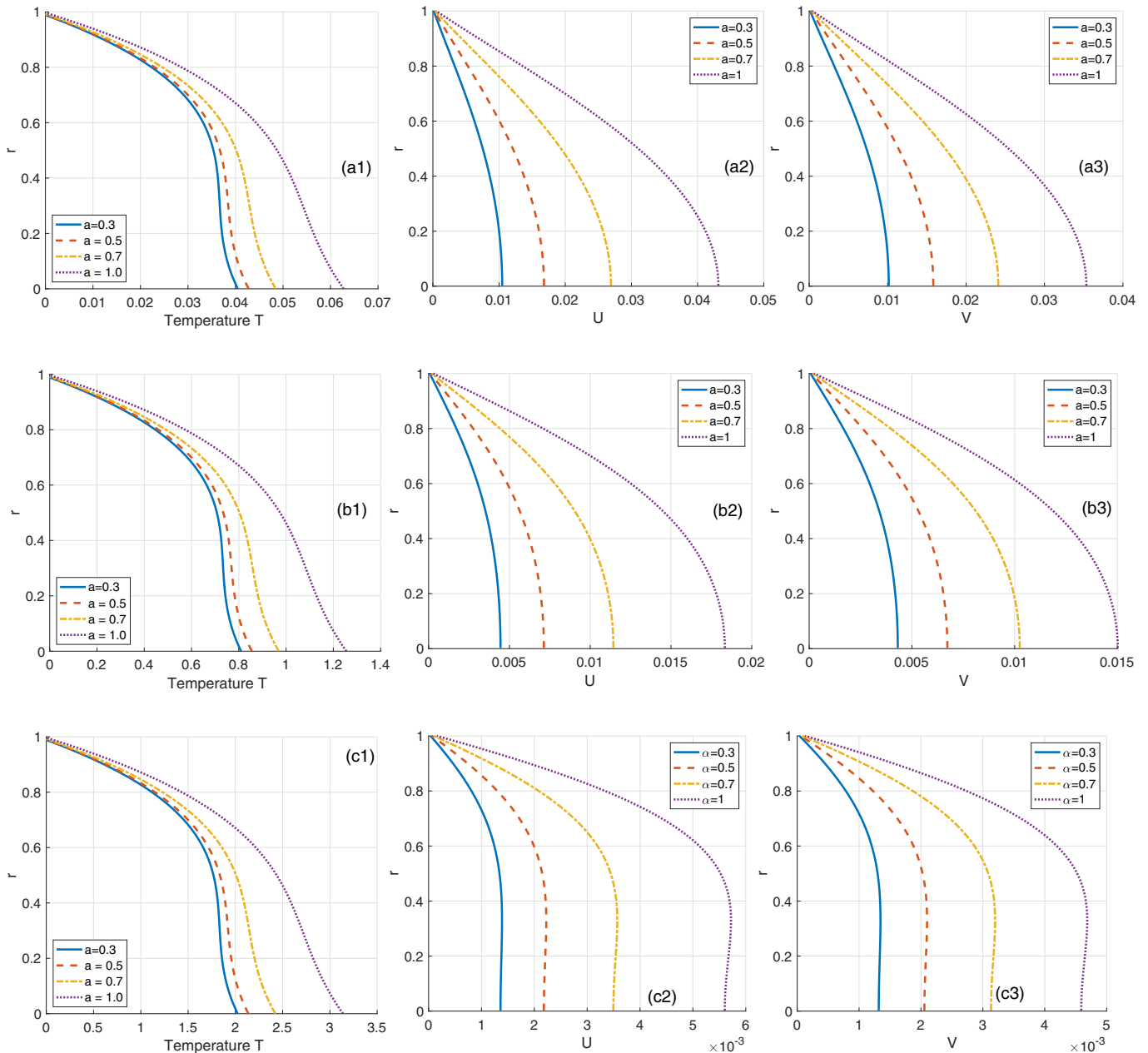
Fig. 7. Profiles of blood temperature $T(r, t)$, axial velocity $u(r, t)$, and particle velocity $v(r, t)$ for different values of Hartmann number $\mathcal{H}$, at $t = 3$ (large value of time), with $S = 0.01$, $A_0 = 10^{-7}$, $A_1 = 10^{-7}$, $\omega = \pi/4$, $\beta = 0.5$, $\lambda = 0.5$, $G = 1.5$, $R = 0.2$ and $Re = 3$. Panels (aj)$_{j=1,2,3}$ correspond to $\mathcal{H} = 1$, panels (bj)$_{j=1,2,3}$ give results for $\mathcal{H} = 2$ and panels (cj)$_{j=1,2,3}$ correspond to $\mathcal{H} = 3$. In all the panels, the fractional parameter takes the values $a = 0.3$, 0.5, 0.7 and 1.

Sheikholeslami and Shehzad [54] showed that in such conditions, an augmentation of the nanoparticles may deeply affect the thermal conduction of blood, and the whole process may be favorable in slowing down the blood flow as a result of a Lorentz force that is created and retards the flow of blood. At that stage, the temperature of blood may be enhanced as observed by Akbar et al. [55,56], while the opposite trend is observed in the case of velocities of fluid and particles. In the meantime, the fractional parameter that varies also plays a role in controlling the flow characteristics. One can for example notice that temperature and both velocities are lower for the classical value of the fractional parameter, i.e., $a = 1$. The various values that can be attributed to a make the model under our study flexible in the sense that it can be applied to a broad range of problems, each having specific applications either in technology or biomedicine.

5. Conclusion

The paper was devoted to the theoretical investigation of the motion of magnetic particles and blood flow in the presence of temperature and Caputo's fractional derivative. Considering the blood vessel as a cylindrical elastic tube, analytical solutions for the nonlinear fractional equations have been obtained through the Laplace transform, with respect to the time variable, and finite Hankel transform. Numerical calculations have been conducted, where information have been recorded for the blood temperature and both the blood and magnetic particle velocities. In general, for short intervals of time the blood flows faster that the particles, while the inverse is observed for large values of time, with magnetic particles being accelerated. The temperature increases from the center of the vessel and drops near the wall and all

the flow characteristics remain very sensitive to the change in the fractional-order parameter. The same results are obtained when the Reynolds number changes, since the temperature, the blood velocity and particle velocity decrease with increasing the fractional parameter. One also notices that the velocities of blood and particles are reduced with increasing $\mathcal{H}$, while the temperature remains an increasing function for both short and long time periods.

Declaration of Competing Interest

None.

Acknowledgments

Appendix A. Coefficients $F_{1n}(t)$ of Eq. (25a)

$$F_{1n}(t) = \frac{b_0 Re}{c_n}[(1-Ga_{1n})R_{a,-1}(-a_{1n},t) - (1-Ga_{2n})R_{a,-1}(-a_{2n},t)],$$

$$F_{2n}(t) = \frac{b_1 Re \cos(\omega t)}{c_n}[(1-Ga_{1n})F_a(-a_{1n},t) - (1-Ga_{2n})F_a(-a_{2n},t)],$$

$$F_{3n}(t) = \frac{\gamma b_0 c'_n}{c_n^2}[R_{\alpha,-1}(-l_{2n},t)F_\alpha(-l_{1n},t)(1-a_{2n}G) - R_{\alpha,-1}(-k_{2n},t)F_\alpha(-k_{1n},t)(1-a_{1n}G)]$$

$$F_{4n}(t) = \frac{\gamma b_1 c'_n \cos(\omega t)}{c_n^2}[F_\alpha(-l_{2n},t)F_\alpha(-l_{1n},t)(1-a_{2n}G) - F_\alpha(-k_{1n},t)F_\alpha(-k_{2n},t)(1-a_{1n}G)]$$

$$F_{5n}(t) = \frac{\gamma b_0}{c_n}[R_{\alpha,-1}(-l_{2n},t)F_\alpha(-l_{1n},t)(1-a_{2n}G) - R_{\alpha,-1}(-k_{2n},t)F_\alpha(-k_{1n},t)(1-a_{1n}G)]$$

$$F_{6n}(t) = \frac{\gamma b_1 \cos(\omega t)}{c_n}[F_\alpha(-l_{2n},t)F_\alpha(-l_{1n},t)(1-a_{2n}G) - F_\alpha(-k_{2n},t)F_\alpha(-k_{1n},t)(1-a_{1n}G)]$$

$$F_{7n}(t) = \frac{\gamma b_0 G}{c_n}[a'_{2n}R_{\alpha,-1}(-l_{2n},t)F_\alpha(-l_{1n},t) - a'_{1n}R_{\alpha,-1}(-k_{2n},t)F_\alpha(-k_{1n},t)]$$

$$F_{8n}(t) = \frac{\gamma b_0}{c_n}[a'_{2n}(1-a_{2n}G)F_\alpha(-a_{2n},t)(R_{\alpha,-1}(-l_{2n},t)F_\alpha(-l_{1n},t)) - a'_{1n}(1-a_{1n}G)F_\alpha(-a_{1n},t)(R_{\alpha,-1}(-k_{2n},t)F_\alpha(-k_{1n},t))]$$

$$F_{9n}(t) = \frac{\gamma b_1 G \cos(\omega t)}{c_n}[a'_{2n}F_\alpha(-l_{2n},t)F_\alpha(-l_{1n},t) - a'_{1n}F_\alpha(-k_{2n},t)F_\alpha(-k_{1n},t)]$$

$$F_{10n}(t) = \frac{\gamma b_1 \cos(\omega t)}{c_n}[a'_{2n}(1-a_{2n}G)F_\alpha(-a_{2n},t)(F_\alpha(-l_{2n},t)F_\alpha(-l_{1n},t)) - a'_{1n}(1-a_{1n}G)F_\alpha(-a_{1n},t)(F_\alpha(-k_{2n},t)F_\alpha(-k_{1n},t))]$$

Appendix B. Coefficients $A_{1n}(t)$ of Eq. (25b)

$$A_{1n}(t) = \frac{b_0 Re}{c_n}\left[\frac{c_n}{r_n^2 - Re\mathcal{H}^2} - \frac{(1-Ga_{1n})e^{-a_{1n}t}}{a_{1n}} + \frac{(1-Ga_{2n})e^{-a_{2n}t}}{a_{2n}}\right]$$

$$A_{2n}(t) = \frac{b_1 Re}{c_n}\left[\frac{(1-Ga_{1n})}{a_{1n}^2 + \omega^2}(a_{1n}\cos(\omega t) + \omega\sin(\omega t) - a_{1n}e^{-a_{1n}t}) + \frac{(1-Ga_{2n})}{a_{2n}^2 + \omega^2}(a_{2n}\cos(\omega t) + \omega\sin(\omega t) - a_{2n}e^{-a_{2n}t})\right]$$

$$A_{3n}(t) = \frac{\gamma b_0 c'_n}{c_n^2}\left[(1-a_{2n}G)\left(\frac{1-e^{-l_{1n}t}}{l_{2n}l_{1n}} + \frac{e^{-l_{1n}t}-e^{-l_{2n}t}}{l_{2n}(l_{1n}-l_{2n})}\right) - (1-a_{1n}G)\left(\frac{1-e^{-k_{1n}t}}{k_{2n}k_{1n}} + \frac{e^{-k_{1n}t}-e^{-k_{2n}t}}{k_{2n}(k_{1n}-k_{2n})}\right)\right]$$

$$A_{4n}(t) = \frac{\gamma b_1 c'_n \cos\omega t}{c_n^2}\left[\frac{(1-a_{2n}G)(e^{-l_{2n}t}-e^{-l_{1n}t})}{(l_{1n}-l_{2n})} - \frac{(1-a_{1n}G)(e^{-k_{2n}t}-e^{-k_{1n}t})}{(k_{1n}-k_{2n})}\right]$$

$$A_{5n}(t) = \frac{\gamma b_0}{c_n}\left[(1-a_{2n}G)\left(\frac{1-e^{-l_{1n}t}}{l_{2n}l_{1n}} + \frac{e^{-l_{1n}t}-e^{-l_{2n}t}}{l_{2n}(l_{1n}-l_{2n})}\right) - (1-a_{1n}G)\left(\frac{1-e^{-k_{1n}t}}{k_{2n}k_{1n}} + \frac{e^{-k_{1n}t}-e^{-k_{2n}t}}{k_{2n}(k_{1n}-k_{2n})}\right)\right]$$

$$A_{6n}(t) = \frac{\gamma b_1 \cos\omega t}{c_n}\left[\frac{(1-a_{2n}G)(e^{-l_{2n}t}-e^{-l_{1n}t})}{(l_{1n}-l_{2n})} - \frac{(1-a_{1n}G)(e^{-k_{2n}t}-e^{-k_{1n}t})}{(k_{1n}-k_{2n})}\right]$$

$$A_{7n}(t) = \frac{\gamma b_0 G}{c_n}\left[a'_{2n}\left(\frac{1-e^{-l_{1n}t}}{l_{2n}l_{1n}} + \frac{e^{-l_{1n}t}-e^{-l_{2n}t}}{l_{2n}(l_{1n}-l_{2n})}\right) - a'_{1n}\left(\frac{1-e^{-k_{1n}t}}{k_{2n}k_{1n}} + \frac{e^{-k_{1n}t}-e^{-k_{2n}t}}{k_{2n}(k_{1n}-k_{2n})}\right)\right]$$

$$A_{8n}(t) = \frac{\gamma b_0}{c_n}\left[\begin{array}{l} a'_{2n}(1-a_{2n}G)\left(\frac{1}{l_{2n}l_{1n}}\left(\frac{1-e^{-a_{2n}t}}{a_{2n}l_{1n}} + \frac{e^{-a_{2n}t}-e^{-l_{1n}t}}{l_{1n}(a_{2n}-l_{1n})}\right)\right. \\ \left. + \frac{1}{l_{2n}(l_{1n}-l_{2n})}\left(\frac{e^{-a_{2n}t}-e^{-l_{1n}t}}{l_{1n}-a_{2n}}\right) - \frac{1}{l_{2n}(l_{1n}-l_{2n})}\left(\frac{e^{-a_{2n}t}-e^{-l_{2n}t}}{l_{2n}-a_{2n}}\right)\right) \\ -a'_{1n}(1-a_{1n}G)\left(\frac{1}{k_{2n}k_{1n}}\left(\frac{1-e^{-a_{1n}t}}{a_{1n}k_{1n}} + \frac{e^{-a_{1n}t}-e^{-k_{1n}t}}{k_{1n}(a_{1n}-k_{1n})}\right)\right. \\ \left. + \frac{1}{k_{2n}(k_{1n}-k_{2n})}\left(\frac{e^{-a_{1n}t}-e^{-k_{1n}t}}{k_{1n}-a_{1n}}\right) - \frac{1}{k_{2n}(k_{1n}-k_{2n})}\left(\frac{e^{-a_{1n}t}-e^{-k_{2n}t}}{k_{2n}-a_{1n}}\right)\right) \end{array}\right]$$

$$A_{9n}(t) = \frac{\gamma b_1 \, G\cos\omega t}{c_n}\left[a'_{2n}\frac{e^{-l_{2n}t}-e^{-l_{1n}t}}{(l_{1n}-l_{2n})} - a'_{1n}\frac{e^{-k_{2n}t}-e^{-k_{1n}t}}{(k_{1n}-k_{2n})}\right]$$

$$A_{10n}(t) = \frac{\gamma b_1 \cos\omega t}{c_n}\left[\begin{array}{l} \frac{a'_{2n}(1-a_{2n}G)}{l_{1n}-l_{2n}}\left(\frac{e^{-a_{2n}t}-e^{-l_{2n}t}}{l_{2n}-a_{2n}} - \frac{e^{-a_{2n}t}-e^{-l_{1n}t}}{l_{1n}-a_{2n}}\right) \\ - \frac{a'_{1n}(1-a_{1n}G)}{k_{1n}-k_{2n}}\left(\frac{e^{-a_{1n}t}-e^{-k_{2n}t}}{k_{2n}-a_{1n}} - \frac{e^{-a_{1n}t}-e^{-k_{1n}t}}{k_{1n}-a_{1n}}\right) \end{array}\right]$$

References

[1] Voltairas PA, Fotiadis DI, Michalis LK. Hydrodynamics of magnetic drug targeting. J Biomech 2002;35:813.

[2] Plavins J, Lauva M. Study of colloidal magnetite binding erythrocytes: prospects for cell separation. J Magn Magn Mater 1993;122:349.

[3] Andra W, Nowak H. Magnetism in medicine. Berlin: Wiley VCH; 1998.

[4] Chinyoka T, Makinde OD. Computational dynamics of arterial blood flow in the presence of magnetic field and thermal radiation therapy. Adv Math Phys 2014;2014:915640. ID.

[5] Tabi CB, Motsumi TG, Bansi CDK, Mohamadou A. Nonlinear excitations of blood flow in large vessels under thermal radiations and uniform magnetic field. Commun Nonlinear Sci Numer Simul 2017;49:1.

[6] Mondal A, Shit GC. Transport of magneto-nanoparticles during electro-osmotic flow in a micro-tube in the presence of magnetic field for drug delivery application. J Magn Magn Mater 2017;442:319.

[7] Haik Y, Chen JC, Pai VM. Development of biomagnetic fluid dynamics. In: Proceedings of IX international symposium on transport phenomena in thermal fluids engineering, Singapore. Hawaii, USA: Pacific Centre in Thermal Fluids Engineering; 1996. pp. 25–28

[8] Frewer RA. The electrical conductivity of flowing blood. Biomed Eng 1974;9:552.

[9] Jaspard F, Nadi M. Dielectric properties of blood: an investigation of temperature dependence. Physiol Meas 2002;23:547.

[10] Cramer KR, Pai SI. Magnetofluid dynamics for engineers and applied physicists. Washington: McGraw-Hill; 1973.

[11] Davidson PA. An introduction to magnetohydrodynamics. Cambridge: Cambridge University Press; 2001.

[12] Sharma S, Singh U, Katiyar VK. Magnetic field effect on flow parameters of blood along with magnetic particles in a cylindrical tube. J Magn Magn Mater 2015;377:395.

[13] Bose S, Banerjee M. Magnetic particle capture for biomagnetic fluid flow in stenosed aortic bifurcation considering particle-fluid coupling. J Magn Magn Mater 2015;385:32.

[14] Kefayati GHR. Simulation of magnetic field effect on non-newtonian blood flow between two-square concentric duct annuli using FDLBM. J Taiwan Inst Chem Eng 2014;45:1184.

[15] Kefayati GHR. FDLBM simulation of magnetic field effect on non-newtonian blood flow in a cavity driven by the motion of two facing lids. Powder Tech 2014;253:325.

[16] Chen LC, Wang WH, Li ZS, Zhu WQ. Stationary response of duffing oscillator with hardening stiffness and fractional derivative. Int J Non-Linear Mech 2013;48:44.

[17] Shen Y, Yang S, Xing H, Gao G. Primary resonance of duffing oscillator with fractional-order derivative. Commun Nonlinear Sci Numer Simul 2012;17:3092.

[18] Tabi CB. Dynamical analysis of the Fitzhugh-Nagumo oscillations through a modified van der Pol equation with fractional-order derivative term. Int J Non–Linear Mech 2018;105:173.

[19] Doungmo EFG, Tabi CB. On the chaotic pole of attraction for Hindmarsh-Rose neuron dynamics with external current input. Chaos 2019;29:023104.

[20] Tabi CB. Fractional unstable patterns of energy in $\alpha-$helix proteins with long-range interactions. Chaos Solit Fract 2018;116:386.

[21] Njagarah JBH, Tabi CB. Spatial synchrony in fractional order metapopulation cholera transmission. Chaos Solit Fract 2018;117:37.

[22] Sumelka W, Blaszczyk T, Liebold C. Fractional euler-bernoulli beams: theory, numerical study and experimental validation. Eur J Mech-A/Solids 2015;54:243.

[23] Paola MD, Heuer R, Pirrotta A. Fractional visco-elastic euler-bernoulli beam. Int J Solids Struct 2013;50:3505.

[24] Kulish VV, Lage JL. Application of fractional calculus to fluid mechanics. J Fluids Eng 2002;124:803.

[25] Kumar D, Singh J, Kumar S. A fractional model of Navier-Stokes equation arising in unsteady flow of a viscous fluid. J Assoc Arab Univ Basic Appl Sci 2015;17:14.

[26] Nahad AS, Dumitru V, Constantin F. Effect of the fractional order and magnetic field on the blood flow in cylindrical domains. J Magn Magn Mater 2016;409:10.

[27] Ali F, Sheikh NA, Khan I, Saqib M. Magnetic field effect on blood flow of Casson fluid in axisymmetric cylindrical tube: a fractional model. J Magn Magn Mater 2017;423:327.

[28] Mandal PK. An unsteady analysis of non-newtonian blood flow through tapered arteries with a stenosis. Int J Non-Linear Mech 2005;40:151.

[29] Sharma MK, Sharma PR, Nasha V. Pulsatile MHD arterial blood flow in the presence of double stenoses. J Appl Fluid Mech 2013;6:331.

[30] Wang S, Xu M. Axial Couette flow of two kinds of fractional viscoelastic fluids in an annulus. Nonlinear Anal 2009;10:1087.

[31] Sutton WG, Sheman A. Engeneering magnetohydrodynamics. New York: Mc Graw-Hill; 1965.

[32] Bourhan A, Magableh T. Magnetic field effect on heat transfer and fluid flow characteristic of blood flow in mutli-stenosis arteries. Heat Mass Transf 2008;44:297.

[33] Sheikh NA, Ali F, Khan I, Saqib M. A modern approach of Caputo-Fabrizio time-fractional derivative to MHD free convection flow of generalized second–grade fluid in a porous medium. Neural Comput Appl 2018;30:1865.

[34] Imran M, Khan I, Ahmad M, Shah N, Nazar M. Heat and mass transport of differential type fluid with non-integer order time-fractional Caputo derivatives. J Mol Liq 2017;229:67.

[35] Bansi CDK, Tabi CB, Motsumi TG, Mohamadou A. Fractional blood flow in oscillatory arteries with thermal radiation and magnetic field effects. J Magn Magn Mater 2018;456:38.

[36] Ali F, Imtiaz A, Khan I, Sheikh NA. Flow of magnetic particles in blood with isothermal heating: a fractional model for two-phase flow. J Magn Magn Mater 2018;456:413.

[37] Baleanu D, Agrawal O. Hamilton formalism within Caputo's derivative. C J Phys 2006;56:1087.

[38] Odibat Z. Approximations of fractional integrals and Caputo fractional derivatives. Appl Math Comput 2006;178:527.

[39] Srinivas S, Kothandapani M. The influence of heat and mass transfer on MHD peristaltic flow through a porous space with compliant walls. Appl Math Comput 2009;213:197.

[40] Tzirtzilakis EE. A mathematical model for blood flow in magnetic field. Phys Fluids A 2005;17:077103.

[41] Cogley ACL, Vincenti WG, Giles ES. Differential approximation for radiative heat transfer in a non-grey gas near equilibrium. Am Inst Aeronaut Astronaut 1968;6:551.

[42] Caputo M, Fabrizio M. A new definition of fractional derivative without singular kernel. Progr Fract Differ Appl 2015;1:73.

[43] Doungmo EFG, Kumar S, Mugisha SB. Similarities in a fifth-order evolution equation with and with no singular kernel. Chaos Solit Fract 2020;130:109467.

[44] Atangana A, Doungmo EFG. Onservatory of Kaup-Kupershmidt equation to the concept of fractional derivative with and without singular kernel. Acta Math Appl Sin 2018;34:351. C

[45] Atangana A, Koca I. Chaos in a simple nonlinear system with Atangana-Baleanu derivatives with fractional order. Chaos Solit Fract 2016;89:447.

[46] Doungmo EFG. Strange attractor existence for non-local operators applied to four-dimensional chaotic systems with two equilibrium points. Chaos 2019;29:023117.

[47] Doungmo EFG. Chaotic processes using the two-parameter derivative with non-singular and non-local kernel: basic theory and applications. Chaos 2016;26:084305.

[48] Everitt WN, Kalf H. The bessel differential equation and the Hankel transform. JAMP Appl Math 2007;208:3.

[49] Li XJ. On the Hankel transform of order zero. J Math Anal Appl 2007;335:935.

[50] Rubinsky B. Microscale heat transfer in biological systems at low temperatures. Exp Heat Transf Int J 1997;10:1.

[51] Ali N, Vieru D, Fetecau C. Effects of the fractional order and magnetic field on the blood flow in cylindrical domains. J Magn Magn Mater 2016;409. Shah, 19.

[52] Sharma S, Gaur A, Singh U, Katiyar VK. Capture efficiency of magnetic nanoparticles in a tube under magnetic field. Procedia Mater Sci 2015;10:64–9.

[53] Sharma S, Kumar R, Gaur A. A model for magnetic nanoparticles transport in a channel for targeted drug delivery. Procedia Mater Sci 2015;10:44.

[54] Sheikholeslami M, Shehzad SA. Magnetohydrodynamic nanofluid convection in a porous enclosure considering heat flux boundary condition. Int J Heat Mass Transf 2017;106:1261.

[55] Akbar NS, Raza M, Ellahi R. Endoscopic effects with entropy generation analysis in peristalsis for the thermal conductivity of nanofluid. J Appl Fluid Mech 2016;9:1721.

[56] Akbar NS, Butt AW. Bio-mathematical venture for the metallic nanoparticles due to ciliary motion. Comput Methods Program Biol 2016;134:43.

P. A. Ndjawa Yomi, C. D. Bansi Kamdem, T. Nkoa Nkomom, C. B. Tabi, A. Mohamadou, T. C. Kofane, et al.

View Online   Export Citation   CrossMark

Fractional blood flow in rotating nanofluid with different shapes nanoparticles in the influence of activation energy and thermal radiation

P. A. Ndjawa Yomi,[1,a] ID C. D. Bansi Kamdem,[1,b] ID T. Nkoa Nkomom,[2,c] C. B. Tabi,[3,d] A. Mohamadou,[4,e]
and T. C. Kofane[5,f]

AFFILIATIONS

[1] Laboratory of Biophysics, University of Yaounde I, B.P. 812 Yaounde, Cameroon
[2] Department of Physics, Higher Teacher Training College of Bertoua, B.P. 652 Bertoua, Cameroon
[3] Botswana International University of Science and Technology, Private Bag 16 Palapye, Botswana
[4] Department of Physics, Faculty of Science, University of Maroua, B.P. 814 Maroua, Cameroon
[5] Laboratory of Mechanics, University of Yaounde I, B.P. 812 Yaounde, Cameroon

[a] Electronic mail: ndjawa.pavel@yahoo.fr
[b] Author to whom correspondence should be addressed: bansidelphin@yahoo.fr
[c] Electronic mail: theodulenkoa@yahoo.fr
[d] Electronic mail: tabic@biust.ac.bw
[e] Electronic mail: mohdoufr@yahoo.fr
[f] Electronic mail: tckofane@yahoo.com

ABSTRACT

A fractional blood flow model, in the presence of magnetic nanoparticles, is considered in this work. The effects of activation energy and thermal radiation on the blood flowing in the oscillating elastic tube are studied. The nanofluid inside the tube is activated by the rotating effect of the charged particles, a constant external magnetic field, and the activation energy. The blood is assumed to be at a temperature and a concentration that vary with the speed of the particles. The study takes advantage of a model, which includes a fractional-order derivative of Caputo's type. The shape of nanoparticles and the speed of blood and the distributions of temperature and concentration are assimilated to Brownian motion and thermophoresis. They are calculated numerically using the L_1-algorithm method. The results show that the applied magnetic field and the effects of the fractional-order parameter reduce the velocity of the nanofluid and nanoparticles, which considerably affects the temperature and concentration of the fluid. It is also found that the particle shape and fractional derivative parameters significantly influence velocities and heat transfer.

Published under an exclusive license by AIP Publishing. https://doi.org/10.1063/5.0053149

Blood flow is fundamental in any human being and constitutes the right channel to treat illnesses like cancer. This brings into play the incredible role of magnetic particles used to transport drugs and any other nutrient to targeted organs in a process known as intelligent drug delivery. The exact process is also used to increase the concentration of drugs in some parts of the body relative to others, specifically diseased tissue, thereby smartly preventing interaction with healthy tissue. This paper addressed the interaction of such nanoparticles of different structures and shapes with blood flowing in vessels when Caputo's fractional-order derivative is considered, under the influence of some important factors such as the magnetic field, activation energy, and thermal radiation. The subsequent full numerical results show that velocity, temperature, and concentration distributions are highly influenced by such factors under the finite-element scheme and the L_1-algorithm method.

I. INTRODUCTION

Nanotechnology is an ancient science that humans keep improving over the years. Since its introduction by the American

physicist and Nobel Prize laureate Feynman in 1959,[1] the concept of nanotechnology has become an active research area with impact in different industrial contexts, including pharmacology, petroleum, communication, astronomy, and so on.[2] Along the same line, several studies have been undertaken in the field of bio-nanotechnology, a new research direction bringing together natural sciences and medicine that allows creating new materials and products at the nanometer scale (10^{-9} m).[3] These feats allow researchers to better interpret molecular metabolisms in the context of the diagnosis, treatment, and prognosis of diseases facing humanity, such as cancers, tumors, cardiovascular diseases, and, recently, the coronavirus (Covid-19). Blood is a fluid with electrical properties that allows it to conduct current and gives it this aspect of magnetohydrodynamic fluid. In the presence of a magnetic field, its velocity tends to decrease due to the existence of the Lorentz force, which is the product of the interaction between electric and magnetic field.[4] Choi et al.[5] were the first to use the word nanofluid, which is a study of nanoparticles in the form of metals: Cu, Ag; nitride metals such as SiN and AlN; oxide ceramics such as PbO and CuO; to name just a few.[6] It emerged that nanofluids have thermal properties, which were investigated by several researchers like Aaiza et al.[7] and Lomascolo et al.[8] They experimentally demonstrated the link between thermal conductivity, the concentration of the medium, and the shape and size of nanoparticles: the smaller they are, the more they can cause enormous damage by inhalation by humans.

Many scientists have investigated non-Newtonian Casson fluids,[9] which have the same behavior as blood. Blood transport nutrients and oxygen through the tissues and organs. It moves at a certain velocity, allowing the body's heat, which is transmitted below the skin surface into tissues and muscles. It is the reason that one of the ways to treat some diseases is by using thermal radiation therapy, and Ogulu and Bestman[10] theoretically addressed this heat effect. Mekheimer and Kot,[11] Majee and Shit,[4] Craciunescu and Clegg,[12] and Horng et al.[13] studied the behavior of arteries during thermal therapy under the pulsatile blood flow effects. In general, the presence of erythrocytes makes the blood to be a biomagnetic fluid, which creates a magnetic field on the vessel wall.[14,15] Vajravelu et al.[16] discussed the diffusion of chemically reactive species in Casson fluid flow over an unsteady permeable stretching surface. Kandasamy et al.[17] investigated a single-walled carbon nanotube (SWCNT), alumina (Al_2O_3), and copper (Cu) nanoparticles on convective mass transfer in the presence of base fluid (water) over a horizontal plate. Pramanik,[18] in turn, looked for the presence of thermal radiation, Casson fluid, and heat transfer past an exponentially porous stretching surface. Reid et al.[19] and Qayyum and Khan[20] introduce the effects of magneto-hydrodynamics through a porous medium. Moreover, in 2018, Khalid et al.[21] combined those ideas to come out with some results. Most of these researchers have ignored the effects of nonlinear convection and have only dealt with cases where the governing equations are linear. For example, Ali et al.[22] expressed the magnetohydrodynamic effects on the transient rotational flow of Maxwell nanofluids, where temperature and concentration distributions were associated with Cattaneo–Christove double diffusion, Brownian motion, and thermophoresis. Until now, several papers published on fractional-order derivatives propose to solve different
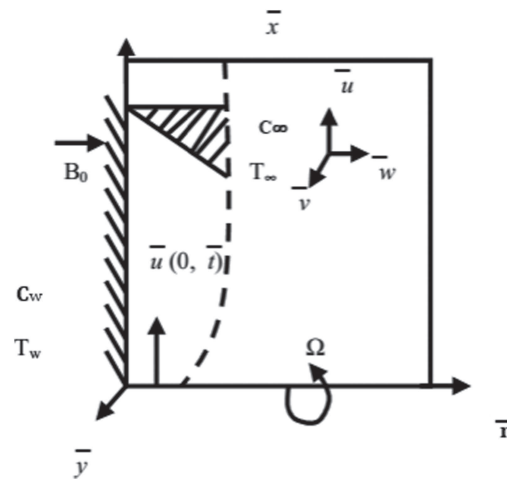

FIG. 1. Schematic representation of the physical system.

problems in applied mathematics, sciences, engineering, and industry, especially in the extraction of crude oil from petroleum products (see, for example, Refs. [23–25]). This idea helps us to study heat transfer enhancement in engine oil-based nanofluid with suspended nanoparticles.[26] This kind of fluid is a non-Newtonian fluid, which is a counterexample of the Casson fluid.[9,27]

In addition, Cao et al.[28] report that the convection flow and the heat transfer are enhanced where the average Nusselt number increases with the rise of fractional derivative parameters, while the average skin friction coefficient is only affected by the velocity fractional derivative parameter. Also, Pan et al.[29] show the inverse correlation between thermal transfer ability of nanofluid with fractional derivatives. Other nanofluids were been studied, like Sisko nanofluid,[30] where for both cases of shear thinning and thickening the temperature fractional derivative parameter reduced the heat and mass transfer ability of Sisko nanofluid. The effect and physical meanings of fractional derivative are also reported by Zhang et al.;[31] for the case of stronger memory characteristic, it is found by numerical computations that the heat transfer is enhanced by the time and spatial fractional heat conduction model.

Recently, Bansi et al.[32] studied the fractional blood flow in oscillatory arteries with thermal radiation and magnetic field effects. Tabi et al.[33] addressed the effect of thermal radiation in the presence of fractional-order derivative, assuming that the body has as a temperature due to the agitation of the particles which seem to be accelerated, with their velocity being suitably controlled by the

TABLE I. Sphericity ψ for different shapes nanoparticles.

Model	Platelets	Blades	Cylinders	Bricks
ψ	0.36	0.52	0.62	0.81

TABLE II. Thermo-physical properties of Blood and nanoparticles.

Physical properties	Blood/base fluid	SWCNTs	Al_2O_3 (alumina)	TiO_2 (tin)	Cu (copper)
ρ (kg/m^3)	1080	2600	3970	4250	8933
C_p (J/kg K)	3500	425	765	686.2	385
k (W/mK)	0.59	6600	40	8.953	401
σ (s/m)	0.6	10^6–10^7	35×10^6	2.6×10^6	59.5×10^6
$\beta \times 10^{-5}$ (1/K)	0.18	27	0.85	0.9	1.67

fractional-order parameter. Zhao et al.[34,35] formulated and derived new equations governing the fractional boundary layer, which are nonlinear coupled equations with a mixed derivative of space–time in convection terms. In addition, they provided a newly developed finite difference method combined with an L_1-algorithm to solve the nonlinear equations of the fractional boundary layer.

Also, the effects of memory and the hereditary properties of materials are suitably described by the fractional calculus through the fractional-order differential operator who is non-local.[36,37] Shen et al.[38] explored the flow and heat transfer characteristics of fractional MHD Maxwell viscoelastic nanofluid by using the Hamilton and Crosser model, which has extensive applications in the medical analysis of biological fluids, nuclear reactors, and MHD-generators with the fractional Cattaneo model of heat conduction to investigate the heat transfer in the temperature boundary layer. Timofeeva et al.[39] showed that for EG/H_2O suspensions of nonspherical alumina particles, overall thermal conductivity starts decreasing below sphericity of 0.6, while the viscosities of nanofluids are shown to depend on both particle shapes and surface properties of nanoparticles.

Being motivated by the discussions as mentioned above, in this problem, we have investigated the blood flow numerically as a base fluid and heat transfer through along activation energy effects for different shapes of particles like Single Walls Carbon Nanotubes (SWCNTs), Cu (copper), TiO_2, and Al_2O_3 (alumina) using the finite element of Caputo fractional derivative order operator.

II. MODEL EQUATIONS AND MATHEMATICAL FORMULATION OF THE PROBLEM

We consider an unstable viscous transient one-dimensional MHD blood and incompressible nanofluid flow on an extended sheet with a rotating frame. The plate has an oscillatory movement on time t and frequency n with velocity. $u(0, t)$, which is given by $\bar{u}(0, \bar{t}) = U_0 \sin(\bar{n}\bar{t})$, with U_0 a space-dependent Gaussian form.[44] Physically, we assume that the whole frame is at rest in time $t < 0$; however, for $t = 0$ ($\bar{u}(0, 0) = 0$), the sheet is stretched along the x direction at $r = 0$ with angular velocity (Ω). The viscoelastic liquid model is created through types of species that incorporate chemical reactions and Arrhenius activating energy. B_0 is a uniform (magnetic field) and applied with direction r, which is taken normal to y axis and crossing an exponential accelerated infinite vertical plate in x axis. Initially, at $t \leq 0$, the fluid and plate are stable, with temperature and concentration being constant. When $t > 0$, the plate is exponentially accelerated with $u = U_0 \sin wt$; the surface temperature and concentration are raised to T_w and C_w, from their respective equilibrium values C_∞ and T_∞. The schematic representation of the configuration, with the coordinate system related to the problem, is given in Fig. 1.

The modified model proposed in this paper is inspired by the seminal contributions from Refs. 3, 22, 32, and 40. In fact, we make use of the usual approximation and propose the flow to be governed by the following equations:

$$
\begin{cases}
\dfrac{\partial w^*}{\partial r^*} = 0, \\[2mm]
\dfrac{\partial u^*}{\partial t^*} + w^* \dfrac{\partial u^*}{\partial r^*} - 2\Omega v^* = \dfrac{1}{\rho_{nf}}\left[\nu_{nf}\dfrac{\partial^2 u^*}{\partial r^{*2}} - \dfrac{\nu_{nf}}{k^*}u^* - (\sigma_{nf}B_0^2)u^* \right. \\[2mm]
\left. \qquad + g\rho_{nf}(\beta_T)_{nf}(T^* - T_\infty^*) + g\rho_{nf}(\beta_C)_{nf}(C^* - C_\infty^*) \right], \\[2mm]
\dfrac{\partial v^*}{\partial t^*} + w^* \dfrac{\partial v^*}{\partial r^*} + 2\Omega u^* = \dfrac{1}{\rho_{nf}}\left[\nu_{nf}\dfrac{\partial^2 v^*}{\partial r^{*2}} - \dfrac{\nu_{nf}}{k^*}v^* - (\sigma_{nf}B_0^2)v^* \right], \\[2mm]
\dfrac{\partial T^*}{\partial t^*} + w^* \dfrac{\partial T^*}{\partial r^*} = \dfrac{k_{nf}}{(\rho C_t)_{nf}}\dfrac{\partial^2 T^*}{\partial r^{*2}} - \dfrac{1}{(\rho C_t)_{nf}}\dfrac{\partial q_r}{\partial r^*} \\[2mm]
\qquad - \dfrac{Q_H}{(\rho C_t)_{nf}}(T^* - T_\infty^*), \\[2mm]
\dfrac{\partial C^*}{\partial t^*} + w^* \dfrac{\partial C^*}{\partial r^*} = D_B \dfrac{\partial^2 C^*}{\partial r^{*2}} + \dfrac{D_T}{T_\infty}\dfrac{\partial^2 T^*}{\partial r^{*2}} \\[2mm]
\qquad - K_r^2(C^* - C_\infty^*)\left(\dfrac{T^*}{T_\infty^*}\right)^m \exp\left(\dfrac{-E_a}{K_B T^*}\right),
\end{cases}
\tag{1}
$$

where u^* represents the axial velocity, T^* and C^* are, respectively, the temperature and the concentration of the solute, B_0 is the applied magnetic field, g, σ_{nf}, and ρ_{nf} are, respectively, the acceleration due to the gravity, electrical conductivity, and density of blood, $C_{t_{nf}}$, k_{nf}, and ν_{nf} represent, respectively, the specific heat at constant pressure, thermal conductivity and kinematic viscosity, D_B is the molecular diffusivity, k^* is the permeability of the porous medium, K_r^2 is the reaction rate, m is a fitted rate constant, $k_{t_{nf}}$ is the thermal diffusion ratio, $k_{c_{nf}}$ is the chemical reaction parameter, and T_m is the mean fluid temperature.

Table I shows us the contribution of the shape of different nanoparticles represented by sphericity ψ in Refs. 7, 39, and 56. In this study, the base fluid is blood with SWCNTs, Al_2O_3, T_iO_2, and Cu based nanoparticles. The thermophysical properties of the nanofluids are presented in Table II.[7,41,56] The coefficient of thermal
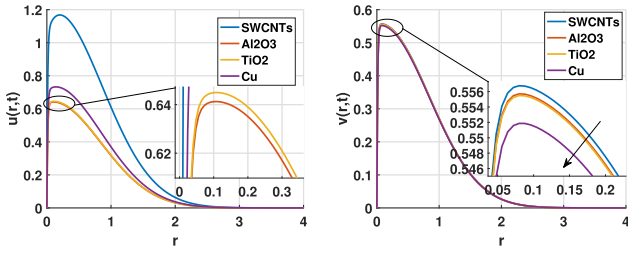
FIG. 2. Velocities of different nanoparticles for $\psi = 0.05$.

expansion and the density of nanofluid are taken to be[45,46]

$$v_{nf} = \frac{v_f}{(1-\psi)^{2.5}}, \quad (\rho\beta)_{nf} = (1-\psi)(\rho\beta)_f + \psi(\rho\beta)_p,$$

$$\rho_{nf} = (1-\psi)\rho_f + \psi\rho_p,$$

$$(\rho C_t)_{nf} = (1-\psi)(\rho C_t)_f + \psi(\rho C_t)_p,$$

$$\frac{\sigma_{nf}}{\sigma_f} = 1 + \frac{3\left(\frac{\sigma_p}{\sigma_f} - 1\right)\psi}{\left(\frac{\sigma_p}{\sigma_f} + 2\right) - \psi\left(\frac{\sigma_p}{\sigma_f} - 1\right)}, \quad (2)$$

$$\frac{k_{nf}}{k_f} = \frac{(k_p + (m-1)k_f) - (m-1)\psi(k_f - k_p)}{(k_p + (m-1)k_f) + \psi(k_f - k_p)},$$

where ψ is the solid volume fraction. The indexes nf, f, and p denote, respectively, the nanofluid, fluid, and nanosolid particles.

The initial and boundary conditions for the problem are

$$t^* < 0: \quad u^* = 0, \quad v^* = 0, \quad T^* = T_w^* + (T_w^* - T_\infty^*),$$
$$C^* = C_w^* + (C_w^* - C_\infty^*) \quad \text{for all } r^*;$$
$$t^* \geq 0: \quad u^* = 0, \quad v^* = 0, \quad T^* = T_w^*, \quad C^* = C_w^*, \quad \text{at } r^* = 0;$$
$$(3)$$
$$t^* > 0: \quad u^* \longrightarrow 0, \quad v^* \longrightarrow 0, \quad T^* \longrightarrow T_\infty^*,$$
$$C^* \longrightarrow C_\infty^*, \quad \text{as } r^* \longrightarrow \infty.$$

Using the Rosseland approximation for radiation,[3,22] the radiative heat flux is simplified as $q_r = -\frac{4\sigma^*}{3\beta_R}\frac{\partial T^{*'4}}{\partial r^*}$, where σ^* is the Stefan–Boltzman fluid constant and β_R is the coefficient of mean absorption.
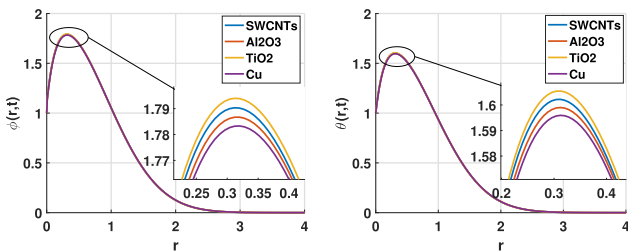

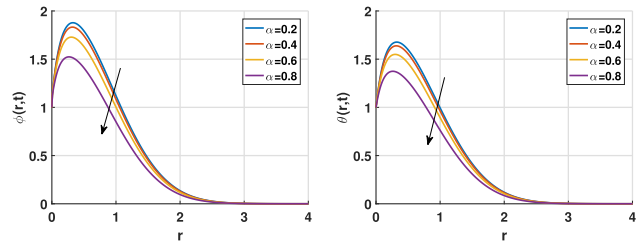**FIG. 3.** Concentration and temperature of different nanoparticles for $\psi = 0.05$.

FIG. 4. Effect of the fractional parameter for the concentration and the temperature.

It is assumed that $T^{*'4} = 4T_\infty^{*3}T^* - 3T_\infty^{*4}$; then, $\frac{\partial q_r}{\partial r} = -\frac{16\sigma^* T_\infty^{*3}}{3\beta_R}\frac{\partial^2 T^*}{\partial r^{*2}}$.

Substituting the above into the equation of temperature in system (1), we obtain

$$\frac{\partial T^*}{\partial t} + w^*\frac{\partial T^*}{\partial r} = \frac{k_{nf}}{(\rho C_t)_{nf}}\frac{\partial^2 T^*}{\partial r^{*2}} + \frac{16\sigma_{nf}^* T_\infty^{*3}}{3(\rho C_t)_{nf}\beta_R}\frac{\partial^2 T^*}{\partial r^{*2}}$$
$$- \frac{Q_H(T^* - T_\infty^*)}{(\rho C_t)_{nf}}. \quad (4)$$

Our study will mainly focus on velocities perpendicular to the applied magnetic field; then, we consider the solution of Eq. (1) as $w^* = -w_0$. We introduce the following dimensionless variables and parameters:

$$r = \frac{r^* U_0}{v_f}, \quad t = \frac{U_0^2 t^*}{v_f}, \quad u = \frac{u^*}{U_0}, \quad v = \frac{v^*}{U_0}, \quad \Omega^* = \frac{K_r^2}{U_0^2},$$
$$n = n^*\frac{v_f}{U_0^2}, \quad (5)$$
$$\theta = \frac{T^* - T_\infty^*}{T_w^* - T_\infty^*}, \quad \phi = \frac{C^* - C_\infty^*}{C_w^* - C_\infty^*},$$

where Ω^* is an adimensional form of reaction rate K_r^2. These equations and conditions are obtained after the transformations

$$\frac{\partial u}{\partial t} - S\frac{\partial u}{\partial r} - Rv = \frac{1}{E_1 E_3}\frac{\partial^2 u}{\partial r^2} - \frac{K_p}{E_1 E_3}u - \frac{E_6 M^2}{E_3}u$$
$$+ \frac{E_4 G_r}{E_3}\theta + \frac{E_4 G_m}{E_3}\phi,$$

$$\frac{\partial v}{\partial t} - S\frac{\partial v}{\partial r} + Ru = \frac{1}{E_1 E_3}\frac{\partial^2 v}{\partial r^2} - \frac{K_p}{E_1 E_3}v - \frac{E_6 M^2}{E_3}v,$$
$$(6)$$
$$\frac{\partial \theta}{\partial t} - S\frac{\partial \theta}{\partial r} = \frac{1}{P_r}\left[\frac{E_2}{E_5}\frac{\partial^2 \theta}{\partial r^2} - \frac{Q}{E_5}\theta\right],$$

$$\frac{\partial \phi}{\partial t} - S\frac{\partial \phi}{\partial r} = \frac{1}{L_e}\left[\frac{\partial^2 \phi}{\partial r^2} - \frac{N_t}{N_b}\frac{\partial^2 \theta}{\partial r^2}\right]$$
$$- Le\lambda^*(1 + \gamma\theta)^m \exp\left(\frac{-EE}{1 + \gamma\theta}\right),$$
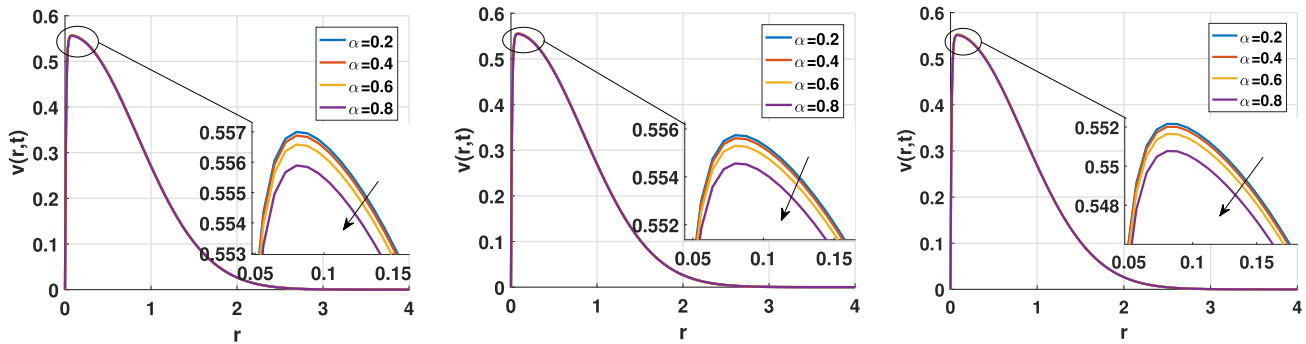
FIG. 5. Effect of the fractional parameter on velocity of nanoparticles: SWCNTs, TiO$_2$, and Cu.

where $\lambda^* = \Omega^* D_B$ is the chemical reaction rate, $P_r = \dfrac{(\rho C_t)_f \nu_f}{k_f}$ is the Prandtl number, $S = \dfrac{w_0}{U_0}$ is the suction parameter, $M = \dfrac{\sigma_f B_0^2 \nu_f}{\rho_f U_0^2}$ is the magnetic parameter, $R_e = \dfrac{U_0^2}{\nu_{nf}}$ is the Reynold number, $R = \dfrac{2\Omega}{Re}$ is the rotating parameter, $G_r = \dfrac{g\beta_{Tf}\nu_f(T_w^* - T_\infty^*)}{U_0^3}$ is the thermal Grashof number, $G_m = \dfrac{g\beta_{Cf}\nu_f(C_w^* - C_\infty^*)}{U_0^3}$ is the mass Grashof number, $Q = \dfrac{Q_H \nu_f^2}{k_f U_0^2}$ is the heat source, $Le = \dfrac{\nu_f}{D_B}$ is the Lewis number, $N_b = \dfrac{\tau D_B(C_w^* - C_\infty^*)}{\nu_f C_\infty^*}$ is the Brownian motion, $N_t = \dfrac{\tau D_T(T_w^* - T_\infty^*)}{\nu_f T_\infty^*}$ is the thermophoresis parameter, $\gamma = \dfrac{T_w^* - T_\infty^*}{T_\infty^*}$ is the thermal relaxation parameter, $EE = \dfrac{E_a}{K_B T_\infty}$ is an activation energy, $K_p = \dfrac{1}{k^* U_0^2}$ is the porosity parameter, and $F = \dfrac{4\sigma^* T_\infty^{*3}}{\beta_R k_f}$ is the radiation parameter, with

$$E_1 = (1 - \psi)^{2.5}, \quad E_2 = \frac{k_{nf}}{k_f} + \frac{4F}{3}, \quad E_3 = 1 - \psi + \psi\left(\frac{\rho_p}{\rho_f}\right),$$

$$E_4 = 1 - \psi + \psi\left(\frac{(\rho\beta)_p}{(\rho\beta)_f}\right), \quad E_5 = 1 - \psi + \psi\left(\frac{(\rho C_t)_p}{(\rho C_t)_f}\right),$$

$$E_6 = 1 + \frac{3\left(\dfrac{\sigma_p}{\sigma_f} - 1\right)\psi}{\left(\dfrac{\sigma_p}{\sigma_f} + 2\right) - \psi\left(\dfrac{\sigma_p}{\sigma_f} - 1\right)}.$$

To generalize (6), we have applied the definition of Caputo fractional derivate operator. Then, the corresponding fractional model is formulated as
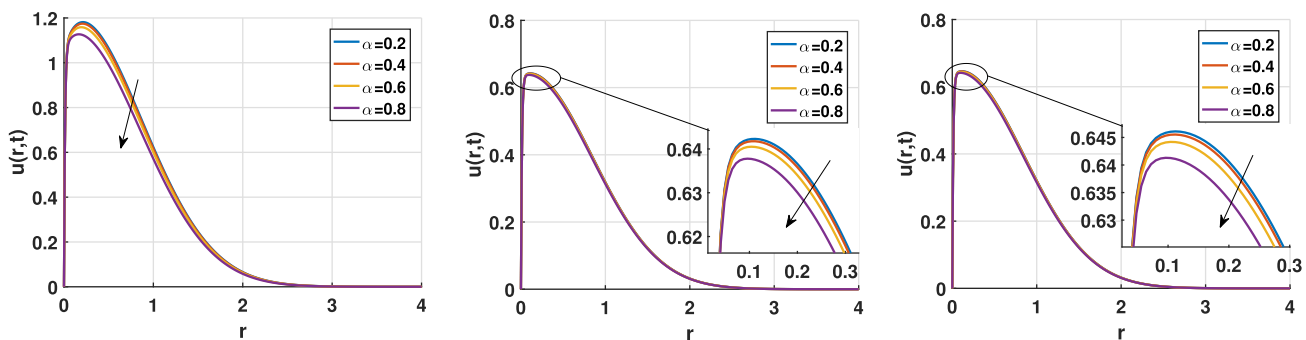
FIG. 6. Effect of the fractional parameter on the velocity of nanofluid for SWCNTs, Al$_2$O$_3$, and TiO$_2$.
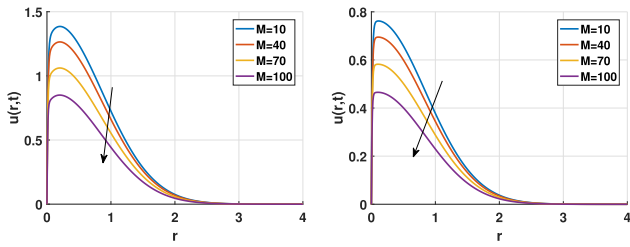
FIG. 7. Effect of the magnetic parameter on velocities for SWCNTs and Al_2O_3.
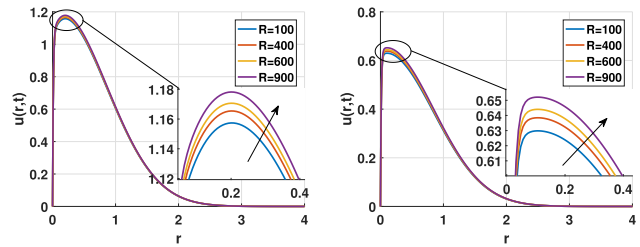
FIG. 8. Effect of the thermal Grashof number for SWCNTs and Al_2O_3.

FIG. 9. Effect of the mass Grashof number for SWCNTs and Al_2O_3.

FIG. 10. Effect of the Brownian motion and the thermophoresis parameter.
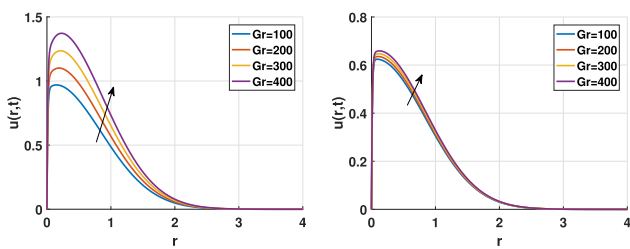
FIG. 11. Effect of the rotating parameter on the nanofluid velocity for SWCNTs and Al_2O_3.

FIG. 12. Effect of the rotating parameter on the nanoparticle velocity for SWCNTs and Al_2O_3.

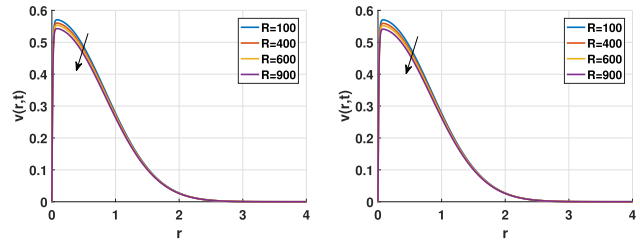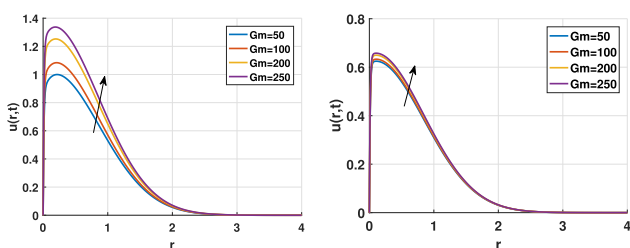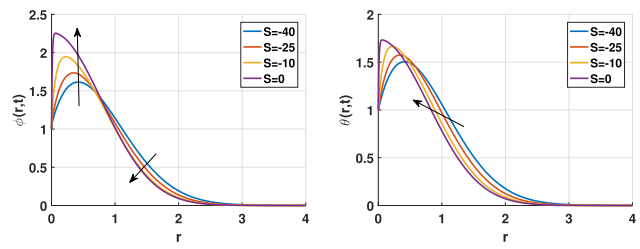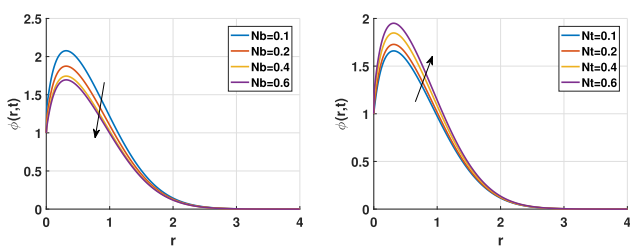**FIG. 13.** Effect of the suction parameter on the concentration and the temperature case of SWCNTs.
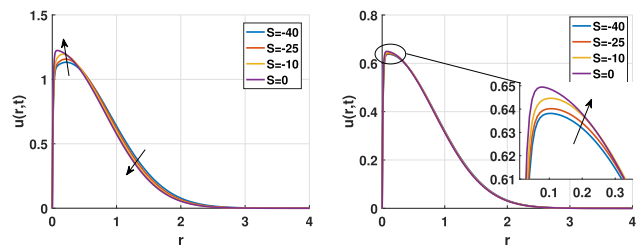

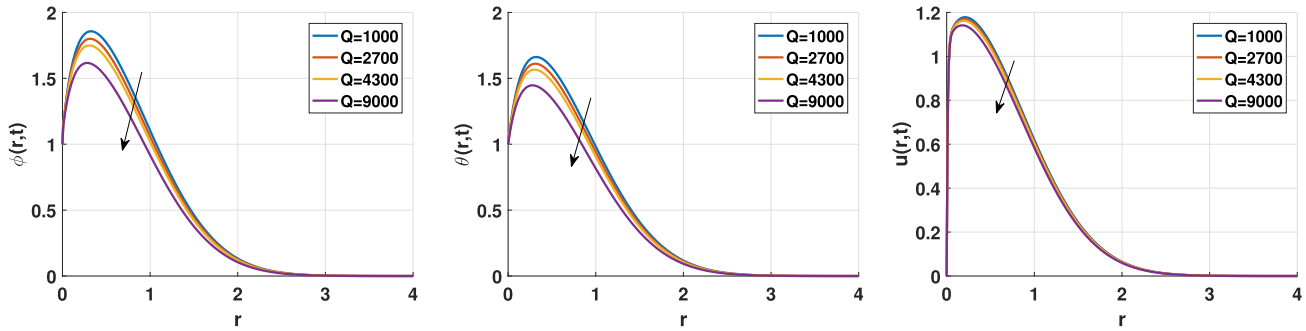**FIG. 14.** Effect of suction parameter on the nanofluid velocity for SWCNTs and Al_2O_3.

FIG. 15. Effect of the heat source parameter case of SWCNTs.

$$_cD_t^\alpha u = \frac{1}{E_1 E_3}\frac{\partial^2 u}{\partial r^2} - \frac{K_p}{E_1 E_3}u - \frac{E_6 M^2}{E_3}u + \frac{E_4 G_r}{E_3}\theta$$
$$+ \frac{E_4 G_m}{E_3}\phi + S\frac{\partial u}{\partial r} + Rv,$$

$$_cD_t^\alpha v = \frac{1}{E_1 E_3}\frac{\partial^2 v}{\partial r^2} - \frac{K_p}{E_1 E_3}v - \frac{E_6 M^2}{E_3}v + S\frac{\partial v}{\partial r} - Ru,$$

$$_cD_t^\alpha \theta = \frac{1}{P_r}\left[\frac{E_2}{E_5}\frac{\partial^2 \theta}{\partial r^2} - \frac{Q}{E_5}\theta\right] + S\frac{\partial \theta}{\partial r},$$

$$_cD_t^\alpha \phi = \frac{1}{L_e}\left[\frac{\partial^2 \phi}{\partial r^2} - \frac{N_t}{N_b}\frac{\partial^2 \theta}{\partial r^2}\right] - Le\lambda^*(1 + \gamma\theta)^m \exp\left(\frac{-EE}{1 + \gamma\theta}\right)$$
$$+ S\frac{\partial \phi}{\partial r},$$

(7)

where

$$D_t^\alpha f(r,t) = \begin{cases} \frac{1}{\Gamma(1-\alpha)}\int_0^t \frac{1}{(t-\tau)^\alpha}\frac{\partial f(r,\tau)}{\partial \tau}d\tau, & 0 < \alpha < 1, \\ \frac{\partial f(r,\tau)}{\partial \tau}, & \alpha = 1 \end{cases}$$

(8)

is the Caputo fractional derivative operator of order $0 < \alpha \le 1$.[47–49] The corresponding boundary conditions become

$$t < 0: \quad u = 0, \quad v = 0, \quad \theta = 0, \quad \phi = 0, \quad \text{at } r \ge 0,$$

$$t \ge 0: \quad u = 0, \quad v = 0, \quad \theta = 1, \quad \phi = 1, \quad \text{at } r = 0,$$

(9)

$$t > 0: \quad u \longrightarrow 0, \quad v \longrightarrow 0, \quad \theta \longrightarrow 0, \quad \phi \longrightarrow 0, \quad \text{as } r \longrightarrow \infty.$$

III. COMPUTATIONAL SCHEME

By using the L_1-algorithm method, the time fractional derivate $(0 < \alpha < 1)$ is discretized through a finite difference approximation scheme[50]

$$\left[cD_t^\alpha f(t)\right]_{t=t_k} = \sum_{s=0}^{k-1} b_{k-s-1}\left[f(t_{s+1} - f(t_s))\right], \quad 0 < \alpha < 1, \quad (10)$$

where $k = 1, 2, \ldots, N$, $s = 0, 1, \ldots, k-1$, and $b_A = \frac{\Delta t^{-\alpha}}{\Gamma(2-\alpha)}$ $\left[(A+1)^{1-\alpha} - (A)^{1-\alpha}\right]$. Applying the forward central difference

FIG. 16. Effect of the radiation parameter case of SWCNTs.

FIG. 17. Effect of the radiation parameter case of TiO_2.
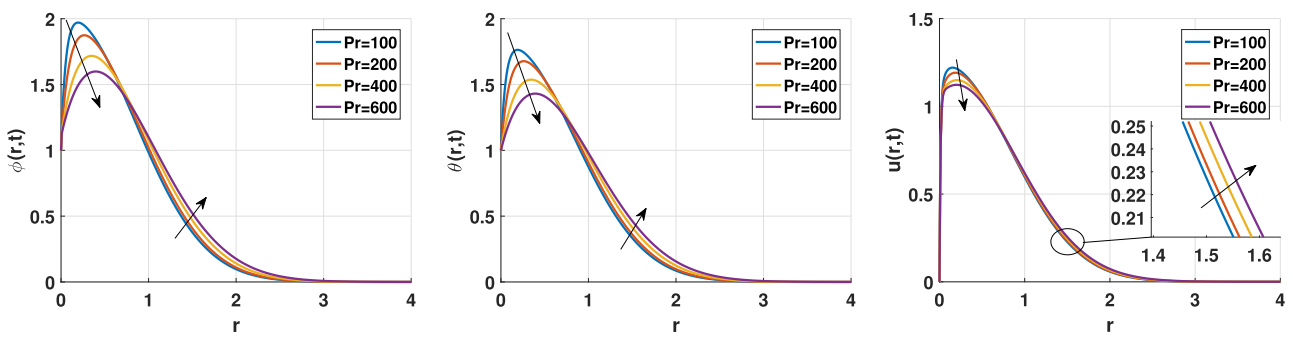
FIG. 18. Effect of the Prandtl number.
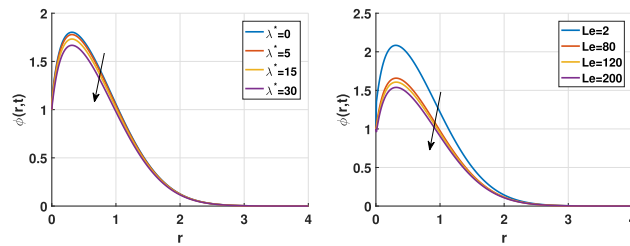
FIG. 19. Effect of the chemical reaction rate and the Lewis number.
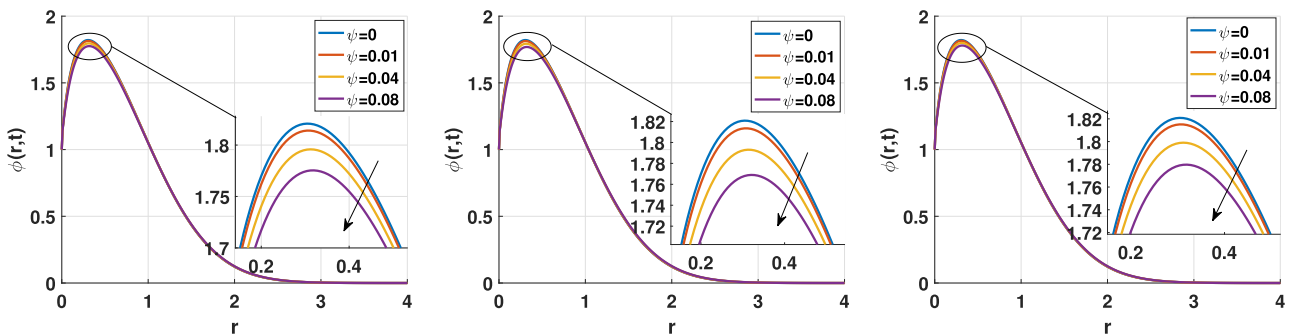
FIG. 20. Concentration of SWCNTs, Al_2O_3, and TiO_2 for $\psi < 0.1$.
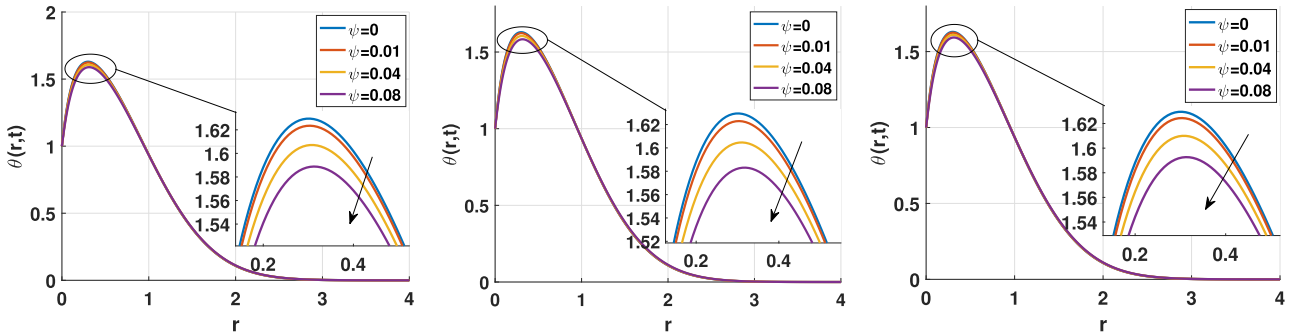
FIG. 21. Temperature of SWCNTs, Al_2O_3, and TiO_2 for $\psi < 0.1$.
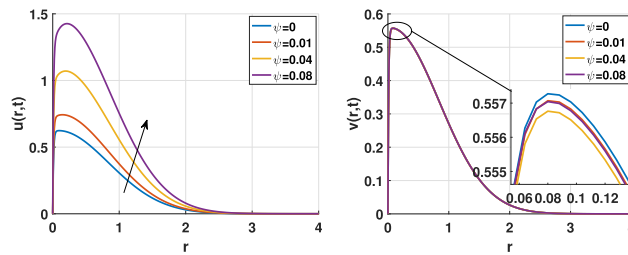
FIG. 22. Velocity of SWCNTs for $\psi < 0.1$.
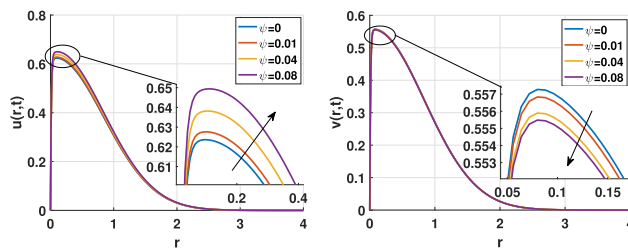
FIG. 23. Velocity of Al_2O_3 for $\psi < 0.1$.

FIG. 24. Concentration of SWCNTs, Al_2O_3, and TiO_2 for $\psi \in [0.05, 0.4]$.

FIG. 25. Temperature of SWCNTs, Al$_2$O$_3$, and TiO$_2$ for $\psi \in [0.05, 0.4]$.

method, one gets the discretized expressions

$$\left.\frac{\partial u}{\partial t}\right|_{t=t_k} = \frac{u(r_i, t_k) - u(r_i, t_{k-1})}{\Delta t} + O(\Delta t),$$

$$\left.\frac{\partial u}{\partial r}\right|_{t=t_k} = \frac{u(r_i, t_k) - u(r_{i-1}, t_k)}{\Delta t} + O(\Delta r), \quad (11)$$

$$\left.\frac{\partial^2 u}{\partial r^2}\right|_{t=t_k} = \frac{u(r_{i+1}, t_k) - 2u(r_i, t_k) + u(r_{i-1}, t_k)}{\Delta r^2} + O(\Delta r^2),$$

in which Δr is a space step, and Δt is the time step. With $t_k = (k-1)\Delta t$ and $r_i = (i-1)\Delta r$, $i = 1, 2, \ldots, M$. Therefore, the problem to solve reduces to the following discretized equations obtained from Eq. (7):

$$u(r_i, t_k) = \frac{1}{Y_1}\left[e_0 Z_1 + \frac{E_4}{E_3}\left(G_r\theta(r_i, t_k) + G_m\phi(r_i, t_k)\right) + Rv(r_i, t_k)\right.$$
$$\left. + \frac{u(r_{i+1}, t_k)}{E_1 E_3 \Delta r^2} + \left(\frac{1}{E_1 E_3 \Delta r^2} - \frac{S}{\Delta r}\right)u(r_{i-1}, t_k)\right],$$

$$v(r_i, t_k) = \frac{1}{Y_1}\left[e_0 Z_2 - Ru(r_i, t_k) + \frac{v(r_{i+1}, t_k)}{E_1 E_3 \Delta r^2}\right.$$
$$\left. + \left(\frac{1}{E_1 E_3 \Delta r^2} - \frac{S}{\Delta r}\right)v(r_{i-1}, t_k)\right],$$

$$\theta(r_i, t_k) = \frac{1}{Y_2}\left[e_0 Z_3 + \frac{E_2}{P_r E_5 \Delta r^2}\theta(r_{i+1}, t_k)\right.$$
$$\left. + \left(\frac{E_2}{P_r E_5 \Delta r^2} - \frac{S}{\Delta r}\right)\theta(r_{i-1}, t_k)\right],$$

$$\phi(r_i, t_k) = \frac{1}{Y_3}\left[e_0 Z_4 + \left(\frac{1}{L_e \Delta r^2} + \frac{N_t}{L_e N_b \Delta r^2}\right)\phi(r_{i+1}, t_k)\right.$$
$$\left. + \left(\frac{1}{L_e \Delta r^2} + \frac{N_t}{L_e N_b \Delta r^2} - \frac{S}{\Delta r}\right)\phi(r_{i-1}, t_k)\right], \quad (12)$$

where

$$Z_1 = \lambda_{k-1}u(r_i, t_0) + \sum_{A=1}^{k-1}(\lambda_{A-1} - \lambda_A)u(r_i, t_{k-A}),$$

$$Z_2 = \lambda_{k-1}v(r_i, t_0) + \sum_{A=1}^{k-1}(\lambda_{A-1} - \lambda_A)v(r_i, t_{k-A}),$$

$$Z_3 = \lambda_{k-1}\theta(r_i, t_0) + \sum_{A=1}^{k-1}(\lambda_{A-1} - \lambda_A)\theta(r_i, t_{k-A}),$$

$$Z_4 = \lambda_{k-1}\phi(r_i, t_0) + \sum_{A=1}^{k-1}(\lambda_{A-1} - \lambda_A)\phi(r_i, t_{k-A}),$$

$$Y_1 = \frac{\Delta t^{-\alpha}}{\Gamma(2-\alpha)} + \frac{2}{E_1 E_3 \Delta r^2} + \frac{E_6}{E_3}M^2 - \frac{S}{\Delta r} + \frac{K_p}{E_1 E_3},$$

$$Y_2 = \frac{\Delta t^{-\alpha}}{\Gamma(2-\alpha)} + \frac{2E_2}{P_r E_5 \Delta r^2} + \frac{Q}{P_r E_5} - \frac{S}{\Delta r},$$

$$Y_3 = \frac{\Delta t^{-\alpha}}{\Gamma(2-\alpha)} + \frac{2}{L_e \Delta r^2} + \frac{N_t}{L_e N_b \Delta r^2} - \frac{S}{\Delta r}$$
$$+ L_e\lambda^*(1 + \gamma\theta(r_i, t_k))^m\left(-\frac{EE}{1 + \gamma\theta(r_i, t_k)}\right),$$

$$e_0 = \frac{\Delta t^{-\alpha}}{\Gamma(2-\alpha)},$$

$$\lambda_A = (A+1)^{1-\alpha} - (A)^{1-\alpha}.$$

IV. RESULTS AND DISCUSSION

The numerical solutions for the velocity, temperature, and concentration are obtained by means of the above developed finite difference method combined with an L_1-algorithm. The effects of the nanoparticle volume fraction ψ, fractional derivative parameters α, magnetic parameter M together with nanoparticle shape factor $q = \frac{3}{\eta}$, with η being the sphericity of nanoparticles on flow and heat transfer, are analyzed. The numerical results are addressed for $\alpha = 0.5, M = 55, Gr = 250, Gm = 150, F = 1, Pr = 300, R = 500, m = 1, Kp = 500, \lambda^* = 2.5, Le = 30, \gamma = 1.5,$
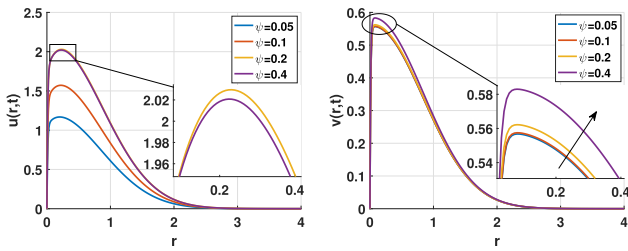
FIG. 26. Velocity of SWCNTs for $\psi \in [0.05, 0.4]$.
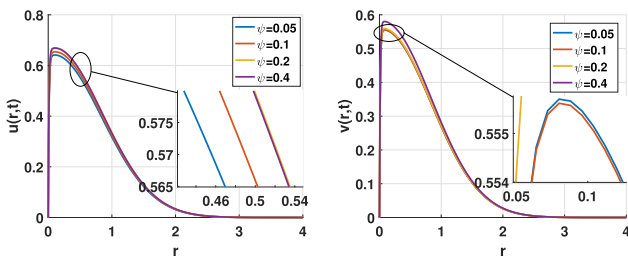
FIG. 27. Velocity of Al$_2$O$_3$ for $\psi \in [0.05, 0.4]$.

FIG. 28. Velocities of different nanoparticles for $\psi = 0.4$.

FIG. 29. Concentration and temperature of different nanoparticles for $\psi = 0.4$.

FIG. 30. Effect of the porosity parameter for SWCNTs and Al$_2$O$_3$.

FIG. 31. Effect of activation energy for SWCNTs and Cu.
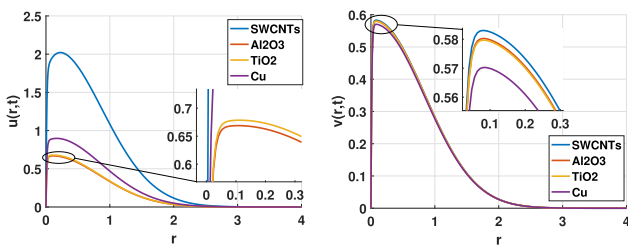
$Nt = 0.3, Nb = 0.3, EE = 1, Q = 3000$, and $S = -20$. In Fig. 2, the variation of nanoparticles for the value of $\psi = 0.05$ shows us that the SWCNTs particles accelerate the movement of the nanofluid the most compared to the others: Cu, TiO$_2$, and Al$_2$O$_3$, respectively. Moreover, the Cu particles have a higher velocity than the Al$_2$O$_3$ particles in the blood nanofluid, represented here by the first figure on the left. This behavior has also been observed in Ref. 3. The right panel of Fig. 2 explains the movement of the nanoparticles in rotation, we observe a decrease in the velocities of Cu, which has the lowest velocity followed by TiO$_2$, Al$_2$O$_3$, and SWCNTs, respectively, in an increasing manner. Figure 3 shows the evolution of the concentration and the temperature in the medium. We notice that TiO$_2$ has the highest temperature and concentration, followed, respectively, by SWCNTs, Al$_2$O$_3$, and Cu. This has been extensively studied by Hady et al.[42] who obtained results contrary to those found in this work. This is probably due to the fact that TiO$_2$ nanoparticles are proved to have better cooling performance for this problem than the other two types of nanoparticles Cu and Al$_2$O$_3$.

In Figs. 4–6, the impact of the fractional-order parameter is studied. We observe that the increase of α causes a decrease in the concentration, temperature, particle velocity, and even fluid velocity. This parameter reacts more significantly in the case of SWCNTs compared to the various other nanoparticles, which is illustrated in Fig. 6.

The fractional-order parameter plays a very important role in the calibration of velocity, concentration, and temperature distributions.[32,33,51,52] It allows an initialization of the system according to the study and treatment carried out, generally observed during surgical interventions, on the optimization or stability of energy transport in many dynamic systems. In Fig. 7, the increase of the magnetic field also causes the decrease of different velocities, thus making the medium more viscous which produces forces of resistance making the velocity to slow down.[53]

The very low values of the magnetic field in the two nanoparticle cases considered in Fig. 7 increasingly boost the velocity distributions initially obtained in Fig. 2.
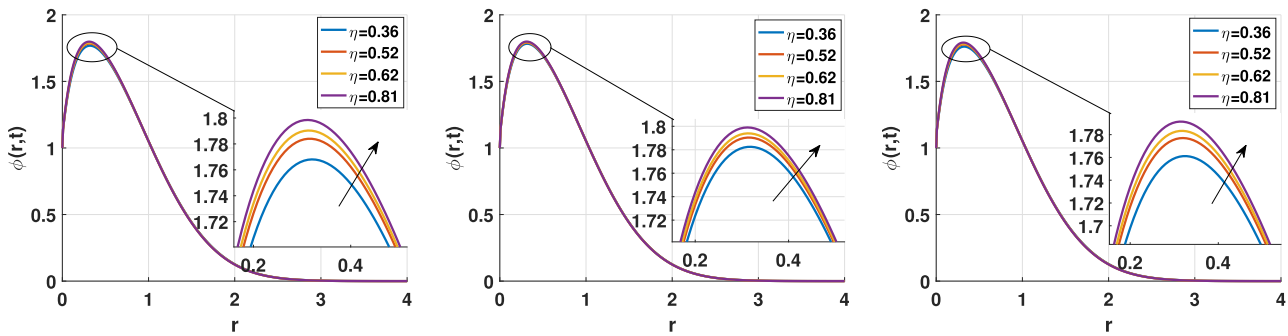
FIG. 32. Effect of different sphericity parameters for SWCNTs, TiO₂, and Cu.

The Grashof parameters in Figs. 8 and 9 contribute to the increase of the velocity of nanofluid when they also increase. The concentration of the medium grows with increasing values of the thermophoresis parameter, as shown by Fig. 10. This parameter is greater than the noise parameter, which causes the decrease of concentration. The thermophoretic force causes the concentration layer to move from the lower region to the higher one. Similarly, the faster random motion of particles in nanofluids elevates the Brownian forces to boost the concentration layer. For the rotation parameter, Figs. 11 and 12 show us that the more the rotational movement of the nanoparticles accelerates, the more the velocity of the nanofluid increases and the nanoparticles decreases. So, the rotational motion allows the particles to calibrate their velocities and move either slowly or quickly.[22,54] Figures 13 and 14 give us the evolution of the parameter of the velocity of the global transport. For increasing values of this parameter, the concentration has two domains. The first one increases with the amplitude of the concentrations. For the second one, the more the parameter increases, the more the concentration decreases. This marks an inflection zone between the central lines and the walls of the tube. Thus, as the suction parameter increases, the temperature increases, creating a bifurcation in the spatial evolution of the concentration for the different particles and the blood-nanofluid velocity distribution, as noticed for SWCNTs, while for Al₂O₃, the increase of the suction parameter increases with the ensembled velocity and does not produce any bifurcation.

For the temperature, the evolution of this number increases the amplitude. The increase of the heat source variable in Fig. 15 contributes to the decrease of the system.

The same remarks are valuable for the case of SWCNTs, whose concentration, temperature, and velocity distributions are decreasing. This also applied to the other nanoparticles, Al₂O₃, TiO₂, and Cu, which also decrease with the heat source parameter. This is in line with the study done by Choi and Eastman,[5,43] where nanoparticles were not taken into account.

The radiation parameter F is investigated in Figs. 16 and 17, respectively, for the cases of SWCNTs and T$_i$O₂. Bifurcations are created in all distributions of the system where the values are increasing in the central lines and decreasing near the vessel walls for increasing values of the radiative parameter as shown in Figs. 16 and 17. An increase in F leads to an enhancement in the velocity, temperature, and concentration distributions across the boundary layer.

The effect of thermal radiation is to enhance heat transfer; this is because thermal boundary layer thickness increases with an increase in the thermal radiation.

FIG. 33. Effect of different sphericity parameters for SWCNTs, TiO₂, and Cu.
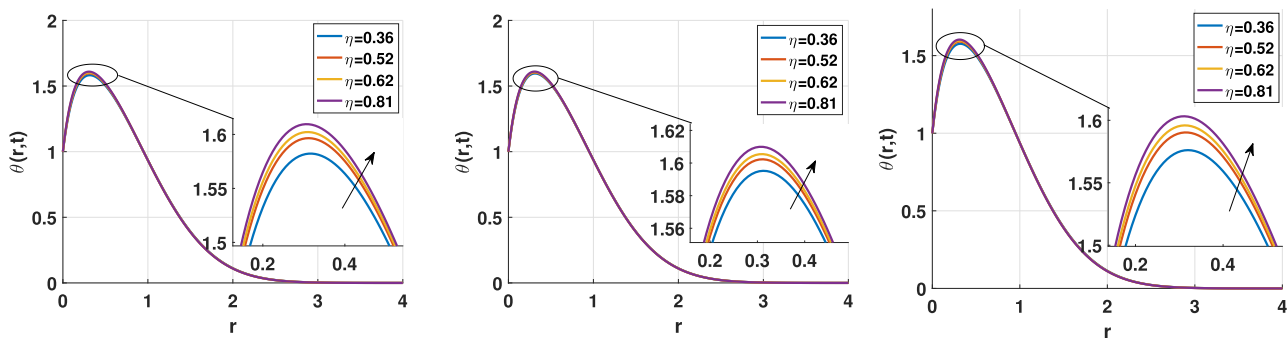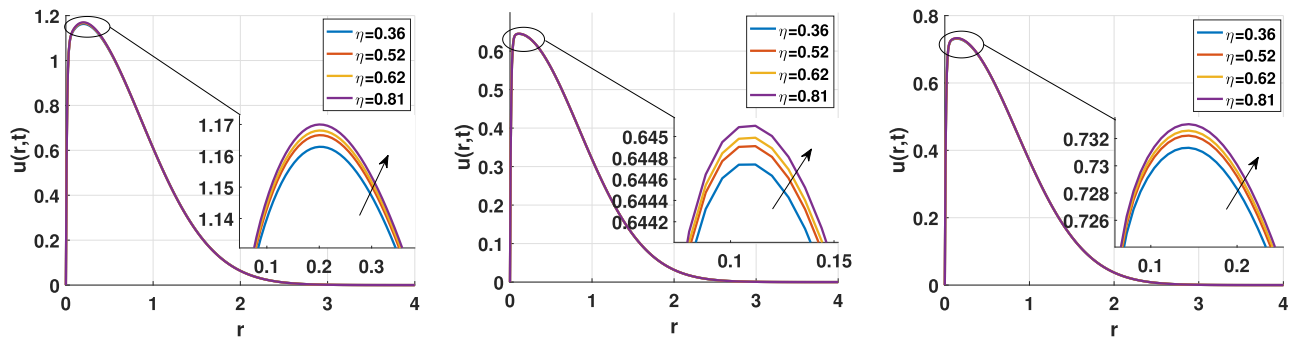
FIG. 34. Effect of different sphericity parameters for SWCNTs, TiO$_2$, and Cu.

The Prandtl number, as shown in Fig. 18, also gives rise to an inflection zone in the system. The more this number increases, the more the amplitude of the system decreases and the first zone decreases up to a certain distance. Then, we observe the growth of the system.

These parameters in Figs. 15–18 allow us to better control the problems related to thermoregulation during hyperthermia in the presence of a heat source.

Figure 19 displays the chemical reaction rate; when it increases, the concentration in the medium also decreases, and for the Lewis number, the more it increases, the less are the concentration, which makes the medium less viscous.

So, for a small value of L_e, the concentration tends to be very high and we have high mass diffusivity. Figures 20 and 21 show the concentration and temperature, respectively, of the solid volume fraction of nanoparticles for the values $\psi < 0.1$. Then, for the case of SWCNTs and Al$_2$O$_3$, the velocities are represented in Figs. 22 and 23, where the overall velocity of the nanofluid increases with the increase of the solid volume fraction parameter. On the other hand, the velocity of the nanoparticles decreases for the case of Al$_2$O$_3$. Moreover, for the case of SWCNTs, we observe a random decrease of the nanoparticles velocity with the increase of ψ. This is similar to the study by Zahir *et al.*[56]

We notice a decrease of both the concentration and the temperature for the increasing values of ψ, and for Figs. 24 and 25, the solid volume fraction evolves in an increasing manner and higher than the value 0.1, to observe its evolution for different structures. It is observed, for the concentration and the temperature, a birth of an inflection zone for which of an initial time until a certain time, we have a decrease of the parameters of distributions. After that time, growth of the system is observed. So, for small values of ψ, we observe a certain order of the system, and for large values of ψ, a certain disorder is observed. This is illustrated by Figs. 26 and 27, which led us to study the evolution of nanoparticles for larges values of ψ. We note the drop in concentration and temperature of TiO$_2$ up to the inflection point, while for the velocities, it turns out that the SWCNT particle has to be able to move faster in the medium and to accelerate the dynamics of the nanofluid, as shown in Fig. 28. As far as Cu is concerned, it moves slowly but with the ability to speed up the velocity of the nanofluid compared to Al$_2$O$_3$ and TiO$_2$ for a large ψ. In Fig. 29, the evolution of concentration and

temperature has been expressed. We realize that for a big value of ψ, the nanoparticle TiO$_2$ reduced considerably compared to the small value of ψ; then, in this case, when the viscosity of the nanofluid increases, the concentration and the temperature of the medium tend to decrease. Figure 30 gives us the evolution of the velocity of the fluid for the increasing porosity parameter; it allows the decrease of the velocity and thus makes the medium more viscous. So, we observe in Fig. 31 an increase in the activation energy allowing the growth of the concentration characterizing the presence of several nanoparticles. Figures 32–34 show the behavior of the sphericity parameter of the nanoparticle shapes in the case of SWCNTs, TiO$_2$, and Cu, the more this parameter increases, the more the concentration, the temperature, and the velocity of the nanofluid evolve, thus adding to this type of study, which was carried out by Timofeeva *et al.*[39] who were interested in the effects of particle shape on the thermophysical properties of alumina nanofluids considered as base fluid.

V. CONCLUSION

In the present study, we focused on the effect of the thermal radiation, chemical reaction, and magnetic field through a magneto-hydrodynamic blood flow in the presence of nanoparticles stressing an exponentially accelerated infinite vertical plate. To solve the equation governed by this problem, we used the numerical L_1-algorithm method of Caputo fractional-order derivative operator. The results were plotted by using a Matlab code with different parameters, such as magnetic (M), solid volume fraction (ψ), sphericity (η), etc., to observe their influence in the velocity, temperature, and concentration. We concluded that mass transfer of blood, alumina, tin and copper SWCNTs onto a flat plate in the presence of a chemical reaction produces a bifurcated system for high values of sphericity ψ for different forms of nanoparticles between the central line and the vessel walls with oscillating flow. The presence of Cu–blood and SWCNT–blood plays a dominant role in the flow field.

Thermal radiation can influence the effective viscosity of the fluid, which indirectly affects the velocity profile and increases the temperature at the vessel centerline, which is very important during hyperthermia. This study improves on the one proposed by Asifa

et al.,[55] where the model was a compressible form of heat transfer with a nanofluid hybrid flowing over a rotating disk, and gives an idea of the influence of the shape of the nanoparticles in the fractional blood flow model.

DATA AVAILABILITY

The data that support the findings of this study are available within the article.

REFERENCES

[1] R. Feynman, "Nanotechnology," Caltech Eng. Sci. **23**, 22–36 (1960).
[2] S. Bayda, M. Adeel, T. Tuccinardi, M. Cordani, and F. Rizzolio, "The history of nanoscience and nanotechnology: From chemical–physical applications to nanomedicine," Molecules **25**, 112 (2020).
[3] K. S. R. Vani and D. Rao, "Effect of thermal radiation on unsteady convective heat transfer flow of a rotating nano-fluid past a vertical plate," Adv. Appl. Sci. Res. 7, 83–94 (2016).
[4] S. Majee and G. C. Shit, "Numerical investigation of MHD flow of blood and heat transfer in a stenosed arterial segment," J. Magn. Magn. Mater. **424**, 137–147 (2017).
[5] S. U. S. Choi and J. A. Eastman, *Enhancing Thermal Conductivity of Fluids with Nanoparticles* (Argonne National Laboratory, Illinois, 1995).
[6] F. Shahzad, M. Sagheer, and S. Hussain, "Numerical simulation of magnetohydrodynamic Jeffrey nanofluid flow and heat transfer over a stretching sheet considering Joule heating and viscous dissipation," AIP Adv. **8**, 065316 (2018).
[7] G. Aaiza, I. Khan, and S. Shafie, "Energy transfer in mixed convection MHD flow of nanofluid containing different shapes of nanoparticles in a channel filled with saturated porous medium," Nanoscale Res. Lett. **10**, 490 (2015).
[8] M. Lomascolo, G. Colangelo, M. Milanese, and A. De Risi, "Review of heat transfer in nanofluids: Conductive, convective and radiative experimental results," Renew. Sustain. Energy Rev. **43**, 1182–1198 (2015).
[9] N. Casson, "A flow equation for pigment-oil suspensions of the printing ink type," in Rheol. Disperse Syst., edited by C. C. Mills (Pergamon Press, Oxford, 1959), pp. 84–104.
[10] A. Ogulu and A. R. Bestman, "Deep heat muscle treatment a mathematical model-II," Acta Phys. Hun. **73**, 17 (1993).
[11] K. S. Mekheimer and M. A. El Kot, "Suspension model for blood flow through catheterized curved artery with time-variant overlapping stenosis," Eng. Sci. Technol. Int. J. **18**, 452–462 (2015).
[12] O. I. Craciunescu and S. T. Clegg, "Pulsatile blood flow effects on temperature distribution and heat transfer in rigid vessels," J. Biomech. Eng. **123**, 500–505 (2001).
[13] T.-L. Horng, W.-L. Lin, C.-T. Liauh, and T.-C. Shih, "Effects of pulsatile blood flow in large vessels on thermal dose distribution during thermal therapy," Med. Phys. **34**, 1312–1320 (2007).
[14] T. Higashi, A. Yamagishi, T. Takeuchi, N. Kawaguchi, S. Sagawa, S. Onishi *et al.*, "Orientation of erythrocytes in a strong static magnetic field," Blood **82**, 1328–1334 (1993).
[15] A. Yamagishi, "Biological systems in high magnetic field," J. Magn. Magn. Mater. **90**, 43–46 (1990).
[16] K. Vajravelu, K. V. Prasad, and C.-O. Ng, "Unsteady convective boundary layer flow of a viscous fluid at a vertical surface with variable fluid properties," Nonlinear Anal.: Real World Appl. **14**, 455–464 (2013).
[17] R. Kandasamy, R. Mohamad, and M. Ismoen, "Impact of chemical reaction on Cu, Al_2O_3 and SWCNTs–nanofluid flow under slip conditions," Eng. Sci. Technol. Int. J. **19**, 700–709 (2016).
[18] S. Pramanik, "Casson fluid flow and heat transfer past an exponentially porous stretching surface in presence of thermal radiation," AIN Shams Eng. J. **5**, 205–212 (2014).
[19] P. C. Reid, R. E. Hari, G. Beaugrand, D. M. Livingstone, C. Marty, D. Straile, J. Barichivich, E. Goberville, R. Adrian, Y. Aono *et al.*, "Global impacts of the 1980s regime shift," Glob. Chang. Biol. **22**, 682–703 (2016).
[20] M. Qayyum and H. Khan, "Behavioral study of unsteady squeezing flow through porous medium," J. Porous Media **19**, 83–94 (2016).

[21] A. Khalid, I. Khan, A. Khan, and S. Shafie, "Unsteady MHD free convection flow of Casson fluid past over an oscillating vertical plate embedded in a porous medium," Eng. Sci. Technol. Int. J. **18**, 309–317 (2015).
[22] B. Ali, Y. Nie, S. Hussain, A. Manan, and M. T. Sadiq, "Unsteady magnetohydrodynamic transport of rotating Maxwell nanofluid flow on a stretching sheet with Cattaneo–Christov double diffusion and activation energy," Therm. Sci. Eng. Prog. **20**, 100720 (2020).
[23] B. S. T. Alkahtani and A. Atangana, "Analysis of non-homogeneous heat model with new trend of derivative with fractional order," Chaos Soliton. Fract. **89**, 566–571 (2016).
[24] D. Baleanu and A. Fernandez, "On some new properties of fractional derivatives with Mittag-Leffler kernel," Commun. Nonlinear Sci. Numer. Simul. **59**, 444–462 (2018).
[25] A. Khan, K. Ali Abro, A. Tassaddiq, and I. Khan, "Atangana–Baleanu and Caputo Fabrizio analysis of fractional derivatives for heat and mass transfer of second grade fluids over a vertical plate: A comparative study," Entropy **19**, 279 (1980).
[26] W. A. Azhar, D. Vieru, and C. Fetecau, "Free convection flow of some fractional nanofluids over a moving vertical plate with uniform heat flux and heat source," Phys. Fluids **29**, 082001 (2017).
[27] S. Mukhopadhyay, "Casson fluid flow and heat transfer over a nonlinearly stretching surface," Chin. Phys. B **22**, 074701 (2013).
[28] Z. Cao, J. Zhao, Z. Wang, F. Liu, and L. Zheng, "MHD flow and heat transfer of fractional Maxwell viscoelastic nanofluid over a moving plate," J. Mol. Liq. **222**, 1121–1127 (2016).
[29] M. Zhang, M. Shen, F. Liu, and H. Zhang, "Modeling heat transport in nanofluids with stagnation point flow using fractional calculus," Appl. Math. Model. **40**, 8974–8984 (2016).
[30] M. Shen, L. Chen, M. Zhang, and F. Liu, "A renovated Buongiorno's model for unsteady Sisko nanofluid with fractional Cattaneo heat flux," Int. J. Heat Mass Transf. **126**, 277–286 (2018).
[31] M. Zhang, M. Shen, F. Liu, and H. Zhang, "A new time and spatial fractional heat conduction model for Maxwell nanofluid in porous medium," Comput. Math. Appl. **78**, 1621–1636 (2019).
[32] C. D. K. Bansi, C. B. Tabi, T. G. Motsumi, and A. Mohamadou, "Fractional blood flow in oscillatory arteries with thermal radiation and magnetic field effects," J. Magn. Magn. Mater. **456**, 38–45 (2018).
[33] C. B. Tabi, P. A. Y. Ndjawa, T. G. Motsumi, C. D. K. Bansi, and T. C. Kofané, "Magnetic field effect on a fractionalized blood flow model in the presence of magnetic particles and thermal radiations," Chaos Soliton. Fract. **131**, 109540 (2019).
[34] J. Zhao, L. Zheng, X. Zhang, and F. Liu, "Unsteady natural convection boundary layer heat transfer of fractional Maxwell viscoelastic fluid over a vertical plate," Int. J. Heat Mass Transf. **97**, 760–766 (2016).
[35] J. Zhao, L. Zheng, X. Zhang, and F. Liu, "Convection heat and mass transfer of fractional MHD Maxwell fluid in a porous medium with Soret and Dufour effects," Int. J. Heat Mass Transf. **103**, 203–210 (2016).
[36] D. Baleanu, B. Agheli, and M. M. Al Qurashi, "Fractional advection differential equation within Caputo and Caputo–Fabrizio derivatives," Adv. Mech. Eng. **8**, 1687814016683305 (2016).
[37] X.-J. Yang, F. Gao, and H. M. Srivastava, "Exact travelling wave solutions for the local fractional two-dimensional Burgers-type equations," Comput. Math. Appl. **73**, 203–210 (2017).
[38] M. Shen, S. Chen, and F. Liu, "Unsteady MHD flow and heat transfer of fractional Maxwell viscoelastic nanofluid with Cattaneo heat flux and different particle shapes," Chin. J. Phys. **56**, 1199–1211 (2018).
[39] E. V. Timofeeva, J. L. Routbort, and D. Singh, "Particle shape effects on thermophysical properties of alumina nanofluids," J. Appl. Phys. **106**, 014304 (2009).
[40] F. Ali, S. Murtaza, N. A. Sheikh, and I. Khan, "Heat transfer analysis of generalized Jeffery nanofluid in a rotating frame: Atangana–Baleanu and Caputo–Fabrizio fractional models," Chaos Soliton. Fract. **129**, 1–15 (2019).
[41] K. Ilyas, "New idea of Atangana and Baleanu fractional derivatives to human blood flow in nanofluids," Chaos **29**, 013121 (2019).

[42] F. M. Hady, F. S. Ibrahim, S. M. Abdel-Gaied, and M. R. Eid, "Radiation effect on viscous flow of a nanofluid and heat transfer over a nonlinearly stretching sheet," Nanoscale Res. Lett. **7**, 1–13 (2012).

[43] C. B. Tabi, T. G. Motsumi, C. D. K. Bansi, and A. Mohamadou, "Nonlinear excitations of blood flow in large vessels under thermal radiations and uniform magnetic field," Commun. Nonl. Sci. Numer. Simul. **49**, 1 (2017).

[44] A. N. Brooks and T. J. R. Hughes, "Streamline upwind/Petrov-Galerkin formulations for convection dominated flows with particular emphasis on the incompressible Navier-Stokes equations," Comput. Methods Appl. Mech. Eng. **32**, 199–259 (1996).

[45] A. Atangana and D. Baleanu, "New fractional derivatives with nonlocal and non-singular kernel: Theory and application to heat transfer model," arXiv:1602.03408 (2016).

[46] A. I. Aliyu, M. Inc, A. Yusuf, and D. Baleanu, "A fractional model of vertical transmission and cure of vector-borne diseases pertaining to the Atangana–Baleanu fractional derivatives," Chaos Soliton. Fract. **116**, 268–277 (2018).

[47] M. Caputo, "Linear models of dissipation whose Q is almost frequency independent-II," Geophys. J. Int. **13.5**, 529–539 (1967).

[48] A. A. Kilbas, H. M. Srivastava, and J. J. Trujillo, *Theory and Applications of Fractional Differential Equations* (Elsevier Science Limited, 2006), Vol. 204.

[49] M. Caputo, *Elasticita e Dissipazione* (Zanichelli, 1969).

[50] F. Liu, P. Zhuang, V. Anh, I. Turner, and K. Burrage, "Stability and convergence of the difference methods for the space–time fractional advection–diffusion equation," Appl. Math. Comput. **191**, 12–20 (2007).

[51] A. Farhad, A. S. Nadeem, I. Khan, and M. Saqid, "Magnetic field effect on blood flow of Casson fluid in axisymmetric cylindrical tube: A fractional model," J. Magn. Magn. Mater. **423**, 327–336 (2017).

[52] S. Ijaz, Z. Iqbal, E. N. Maraj, and S. Nadeem, "Investigation of Cu-CuO/blood mediated transportation in stenosed artery with unique features for theoretical outcomes of hemodynamics," J. Mol. Liq. **254**, 421–432 (2018).

[53] A. S. Nahad, V. Dumitru, and F. Constantin, "Effect of the fractional order and magnetic field on the blood flow in cylindrical domains," J. Magn. Magn. Mater. **409**, 10–19 (2016).

[54] R. Sharma, S. M. Hussain, H. Joshi, and G. S. Seth, "Analysis of radiative magneto-nanofluid over an accelerated plate in a rotating medium with Hall effects," Trans. Tech. Publ. **11**, 129–145 (2017).

[55] A. Tassaddiq, S. Khan, M. Bilal, T. Gul, S. Mukhtar, Z. Shah, and E. Bonyah, "Heat and mass transfer together with hybrid nanofluid flow over a rotating disk," AIP Adv. **10**, 055317 (2020).

[56] Z. Shah, E. Bonyah, S. Islam, and T. Gul, "Impact of thermal radiation on electrical MHD rotating flow of Carbon nanotubes over a stretching sheet," AIP Adv. **9**, 015115 (2019).

Erratum: "Fractional blood flow in rotating nanofluid with different shapes nanoparticles in the influence of activation energy and thermal radiation" [Chaos 31, 093109 (2021)]

P. A. Ndjawa Yomi, C. D. Bansi Kamdem, T. Nkoa Nkomom, et al.

View Online   Export Citation   CrossMark

Erratum: "Fractional blood flow in rotating nanofluid with different shapes nanoparticles in the influence of activation energy and thermal radiation" [Chaos 31, 093109 (2021)]

P. A. Ndjawa Yomi,[1] [ID] C. D. Bansi Kamdem,[1,a)] [ID] T. Nkoa Nkomom,[2] C. B. Tabi,[3] A. Mohamadou,[4] and T. C. Kofane[5]

AFFILIATIONS

[1] Laboratory of Biophysics, University of Yaounde I, B.P. 812, Yaounde, Cameroon
[2] Department of Physics, Higher Teacher Training College of Bertoua, B.P. 652, Bertoua, Cameroon
[3] Botswana International University of Science and Technology, Private Bag 16, Palapye, Botswana
[4] Department of Physics, Faculty of Science, University of Maroua, B.P. 814, Maroua, Cameroon
[5] Laboratory of Mechanics, University of Yaounde I, B.P. 812, Yaounde, Cameroon

a) **Author to whom correspondence should be addressed:** bansidelphin@yahoo.fr

https://doi.org/10.1063/5.0085998

Through this Erratum, we are correcting the reference 19 in the introduction with Kataria and Patel [H. R. Kataria and H. R. Patel, "Radiation and chemical reaction effects on MHD Casson fluid flow past an oscillating vertical plate embedded in porous medium," Alexandria Eng. J. **55**, 583–595 (2016).]

Let us consider the modified model proposed in our previously published paper:[1]

$$
\begin{cases}
\dfrac{\partial w^*}{\partial r^*} = 0, \\[2mm]
\dfrac{\partial u^*}{\partial t^*} + w^* \dfrac{\partial u^*}{\partial r^*} - 2\Omega v^* = \dfrac{1}{\rho_{nf}} \left[v_{nf} \dfrac{\partial^2 u^*}{\partial r^{*2}} - \dfrac{v_{nf}}{k^*} u^* - (\sigma_{nf} B_0^2) u^* + g\rho_{nf}(\beta_T)_{nf}(T^* - T_\infty^*) + g\rho_{nf}(\beta_C)_{nf}(C^* - C_\infty^*) \right], \\[2mm]
\dfrac{\partial v^*}{\partial t^*} + w^* \dfrac{\partial v^*}{\partial r^*} + 2\Omega u^* = \dfrac{1}{\rho_{nf}} \left[v_{nf} \dfrac{\partial^2 v^*}{\partial r^{*2}} - \dfrac{v_{nf}}{k^*} v^* - (\sigma_{nf} B_0^2) v^* \right], \\[2mm]
\dfrac{\partial T^*}{\partial t^*} + w^* \dfrac{\partial T^*}{\partial r^*} = \dfrac{k_{nf}}{(\rho C_t)_{nf}} \dfrac{\partial^2 T^*}{\partial r^{*2}} - \dfrac{1}{(\rho C_t)_{nf}} \dfrac{\partial q_r}{\partial r^*} - \dfrac{Q_H}{(\rho C_t)_{nf}}(T^* - T_\infty^*), \\[2mm]
\dfrac{\partial C^*}{\partial t^*} + w^* \dfrac{\partial C^*}{\partial r^*} = D_B \dfrac{\partial^2 C^*}{\partial r^{*2}} + \dfrac{D_T}{T_\infty^*} \dfrac{\partial^2 T^*}{\partial r^{*2}} - K_r^2 (C^* - C_\infty^*) \left(\dfrac{T^*}{T_\infty^*} \right)^m \exp\left(\dfrac{-E_a}{K_B T^*} \right),
\end{cases}
\tag{1}
$$

where ν_{nf} represents dynamic viscosity. The modified dimensionless variables and parameters follow:

$$t = \frac{U_0^2 t^*}{\nu_f \rho_f}, \quad u = \frac{u^*}{U_0 \rho_f^2}, \quad v = \frac{v^*}{U_0 \rho_f^2}, \quad n = n^* \frac{\nu_f \rho_f}{U_0^2},$$

$$\theta = \frac{T^* - T^*_\infty}{T^*_w - T^*_\infty}, \quad \phi = \frac{C^* - C^*_\infty}{C^*_w - C^*_\infty}, \quad r = \frac{r^* U_0}{\nu_f}. \tag{2}$$

Then, after introducing the dimensionless variables, we replace the nanofluid and equivalent fluid expressions given by Eq. (3):

$$\nu_{nf} = \frac{\nu_f}{(1-\psi)^{2.5}}, \quad (\rho\beta)_{nf} = (1-\psi)(\rho\beta)_f + \psi(\rho\beta)_p,$$

$$\rho_{nf} = (1-\psi)\rho_f + \psi\rho_p,$$

$$(\rho C_t)_{nf} = (1-\psi)(\rho C_t)_f + \psi(\rho C_t)_p,$$

$$\frac{\sigma_{nf}}{\sigma_f} = 1 + \frac{3\left(\frac{\sigma_p}{\sigma_f} - 1\right)\psi}{\left(\frac{\sigma_p}{\sigma_f} + 2\right) - \psi\left(\frac{\sigma_p}{\sigma_f} - 1\right)}, \tag{3}$$

$$\frac{k_{nf}}{k_f} = \frac{(k_p + (m-1)k_f) - (m-1)\psi(k_f - k_p)}{(k_p + (m-1)k_f) + \psi(k_f - k_p)}.$$

By considering the Rosseland approximation for radiation in the temperature distribution equation $q_r = -\frac{4\sigma^*}{3\beta_R}\frac{\partial T^{*'4}}{\partial r^*}$, where σ^* is the Stefan-Boltzman fluid constant and β_R is the coefficient of mean absorption.

It is assumed that $T^{*'4} = 4T^{*3}_\infty T^* - 3T^{*4}_\infty$ then, $\frac{\partial q_r}{\partial r^*} = -\frac{16\sigma^* T^{*3}_\infty}{3\beta_R} \times \frac{\partial^2 T^*}{\partial r^{*2}}$. Substituting the above into the equation of temperature in system (1), we arrive at Eq. (4):

$$\frac{\partial T^*}{\partial t^*} + w^* \frac{\partial T^*}{\partial r^*} = \frac{k_{nf}}{(\rho C_t)_{nf}}\frac{\partial^2 T^*}{\partial r^{*2}} + \frac{16\sigma^*_{nf} T^{*3}_\infty}{3(\rho C_t)_{nf}\beta_R}\frac{\partial^2 T^*}{\partial r^{*2}}$$

$$- \frac{Q_H(T^* - T^*_\infty)}{(\rho C_t)_{nf}}. \tag{4}$$

On page 4 of our previously published paper,[1] the expression of $\frac{\partial q_r}{\partial r}$ should be $\frac{\partial q_r}{\partial r^*}$. Also, $\frac{\partial T^*}{\partial t}$ and $\frac{\partial T^*}{\partial r}$ should be $\frac{\partial T^*}{\partial t^*}$ and $\frac{\partial T^*}{\partial r^*}$.

In addition, the scaling of time and velocities in Eq. (5) of our previously published paper[1] has been modified subsequently, including the presence of the fluid density in many of the scaled parameters and making no changes to Eq. (6) and the rest of the work in Ref. 1.

The system as follows:

$$\frac{\partial u}{\partial t} - S\frac{\partial u}{\partial r} - Rv = \frac{1}{E_1 E_3}\frac{\partial^2 u}{\partial r^2} - \frac{K_p}{E_1 E_3}u - \frac{E_6 M^2}{E_3}u$$

$$+ \frac{E_4 G_r}{E_3}\theta + \frac{E_7 G_m}{E_3}\phi,$$

$$\frac{\partial v}{\partial t} - S\frac{\partial v}{\partial r} + Ru = \frac{1}{E_1 E_3}\frac{\partial^2 v}{\partial r^2} - \frac{K_p}{E_1 E_3}v - \frac{E_6 M^2}{E_3}v,$$

$$\frac{\partial \theta}{\partial t} - S\frac{\partial \theta}{\partial r} = \frac{1}{P_r}\left[\frac{E_2}{E_5}\frac{\partial^2 \theta}{\partial r^2} - \frac{Q}{E_5}\theta\right], \tag{5}$$

$$\frac{\partial \phi}{\partial t} - S\frac{\partial \phi}{\partial r} = \frac{1}{L_e}\left[\frac{\partial^2 \phi}{\partial r^2} + \frac{N_t}{N_b}\frac{\partial^2 \theta}{\partial r^2}\right]$$

$$- Le\lambda^*(1+\gamma\theta)^m \exp\left(\frac{-EE}{1+\gamma\theta}\right)\phi,$$

where $\lambda^* = \Omega^* D_B$ is the chemical reaction rate, with $\Omega^* = \frac{K_r^2 \rho_f^2}{U_0^2}$, a function of reaction rate K_r^2, $P_r = \frac{(C_t)_f \nu_f}{k_f}$ is the Prandtl number, $S = \frac{w_0 \rho_f}{U_0}$ is the suction parameter, $M = \sqrt{\frac{\sigma_f B_0^2 \nu_f}{U_0^2}}$ is the magnetic parameter, $R_e = \frac{U_0^2}{\nu_f \rho_f}$ is the Reynold number, $R = \frac{2\Omega}{Re}$ is the rotating parameter, $G_r = \frac{g(\beta_T)_f \nu_f(T^*_w - T^*_\infty)}{U_0^3 \rho_f}$ is the thermal Grashof number, $G_m = \frac{g(\beta_C)_f \nu_f(C^*_w - C^*_\infty)}{U_0^3 \rho_f}$ is the mass Grashof number, $N_b = \frac{\tau D_B(C^*_w - C^*_\infty)}{\nu_f}$ is the Brownian motion, $N_t = \frac{\tau D_T(T^*_w - T^*_\infty)}{\nu_f T^*_\infty}$ is the thermophoresis parameter, $Le = \frac{\nu_f}{D_B \rho_f}$ is the Lewis number, $K_p = \frac{\nu_f^2}{k^* U_0^2}$ is the porosity parameter, $EE = \frac{E_a}{K_B T^*_\infty}$ is the activation parameter, $F = \frac{4\sigma^* T^{*3}_\infty}{\beta_R k_f}$ is the radiation parameter, $\gamma = \frac{T^*_w - T^*_\infty}{T^*_\infty}$ is the thermal relaxation parameter, with

$$E_1 = (1-\psi)^{2.5}, \quad E_2 = \frac{k_{nf}}{k_f} + \frac{4F}{3}, \quad E_3 = 1 - \psi + \psi\left(\frac{\rho_p}{\rho_f}\right),$$

$$E_4 = 1 - \psi + \psi\left(\frac{(\rho\beta_T)_p}{(\rho\beta_T)_f}\right), \quad E_5 = 1 - \psi + \psi\left(\frac{(\rho C_t)_p}{(\rho C_t)_f}\right),$$

$$E_6 = 1 + \frac{3\left(\frac{\sigma_p}{\sigma_f} - 1\right)\psi}{\left(\frac{\sigma_p}{\sigma_f} + 2\right) - \psi\left(\frac{\sigma_p}{\sigma_f} - 1\right)},$$

$$E_7 = 1 - \psi + \psi\left(\frac{(\rho\beta_C)_p}{(\rho\beta_C)_f}\right).$$

$\rho_{nf} \times (\beta)_{nf}$ is equivalent to $(\rho\beta)_{nf}$ because we consider (nf) as the index of notations of nanofluids and we have two cases:

$$\rho_{nf}(\beta_T)_{nf} = (\rho\beta_T)_{nf} = (1 - \psi)(\rho\beta_T)_f + \psi(\rho\beta_T)_p,$$

$$\rho_{nf}(\beta_C)_{nf} = (\rho\beta_C)_{nf} = (1 - \psi)(\rho\beta_C)_f + \psi(\rho\beta_C)_p,$$

where (f) is the index of notation of fluids, and (p) the index for particles: TiO_2, Al_2O_3, etc.

$(\beta_T)_{nf}$, $(\beta_T)_f$, $(\beta_C)_{nf}$, $(\beta_C)_f$ are just notations of the thermal expansion to distinguish the Grashof case temperature and concentration in the system, for reasons of transformations and equivalence. But thereafter, they are taken identical in the numerical program since a particle has a unique β, the values of the parameter $(\beta_C)_p$ not being given in the literature.

The thermal expansion parameters in the notation of the temperature and concentration case have been considered as thermal expansion parameters of the studied chemical particle or nanoparticle whose properties have been introduced in Table II of our previously published paper.[1]

$(\rho C_t)_f$ is the product of density and the specific heat for the case of base fluid, ρ_f is the density of base fluid, $(C_t)_f$ is the specific heat for the case of base fluid, T_∞^* is temperature of the ambient fluid, C_∞^* is concentration of the ambient fluid, w^* is a velocity component along z axe, v^* is a velocity component along y axe, D_T is the thermal diffusivity.

Moreover, the input error of the sign in Eqs. (6) and (7), respectively, of our previously published paper[1] for the concentration distribution equation,

$$_cD_t^\alpha u = \frac{1}{E_1 E_3}\frac{\partial^2 u}{\partial r^2} - \frac{K_p}{E_1 E_3}u - \frac{E_6 M^2}{E_3}u + \frac{E_4 G_r}{E_3}\theta$$

$$+ \frac{E_7 G_m}{E_3}\phi + S\frac{\partial u}{\partial r} + Rv,$$

$$_cD_t^\alpha v = \frac{1}{E_1 E_3}\frac{\partial^2 v}{\partial r^2} - \frac{K_p}{E_1 E_3}v - \frac{E_6 M^2}{E_3}v + S\frac{\partial v}{\partial r} - Ru,$$

$$\quad (6)$$

$$_cD_t^\alpha \theta = \frac{1}{P_r}\left[\frac{E_2}{E_5}\frac{\partial^2 \theta}{\partial r^2} - \frac{Q}{E_5}\theta\right] + S\frac{\partial \theta}{\partial r},$$

$$_cD_t^\alpha \phi = \frac{1}{L_e}\left[\frac{\partial^2 \phi}{\partial r^2} + \frac{N_t}{N_b}\frac{\partial^2 \theta}{\partial r^2}\right] - Le\lambda^*(1 + \gamma\theta)^m \exp\left(\frac{-EE}{1 + \gamma\theta}\right)\phi$$

$$+ S\frac{\partial \phi}{\partial r}.$$

REFERENCES

[1] P. A. Ndjawa Yomi, C. D. Bansi Kamdem, T. Nkoa Nkomom, C. B. Tabi, A. Mohamadou, and T. C. Kofane, "Fractional blood flow in rotating nanofluid with different shapes nanoparticles in the influence of activation energy and thermal radiation," Chaos **31**, 093109 (2021).

Regular Article

Modulated blood waves in the coupled complex Ginzburg–Landau equations of Jeffrey fluids in arteries

C. D. Bansi Kamdem[1,2,a] , **P. A. Ndjawa Yomi**[1,2,b], **C. B. Tabi**[3,c], **A. Mohamadou**[4,d]

[1] Laboratory of Biophysics, Department of Physics, Faculty of Science, University of Yaounde, I, P.O. Box 812, Yaounde, Cameroon
[2] African Centre for Advanced Studies, P.O. Box 4477, Yaounde, Cameroon
[3] Botswana International University of Science and Technology, Private Bag 16 , Palapye, Botswana
[4] National Advanced School of Engineering of Maroua, University of Maroua, P.O. Box 46, Maroua, Cameroon

Abstract Modulational instability of continuous-wave solutions is investigated in Jeffrey fluids with application to blood flow in arteries. The multiple-scale expansion is used to show that backward propagating dissipative blood waves can be studied through a set of nonlinearly coupled complex Ginzburg–Landau equations. Characteristics of the modulational instability are produced, where the instability gain spectrum is investigated under both low and high viscous effects. In the two regimes, the most obvious effect is the enlargement of the instability bandwidth while increasing the viscosity coefficient.

1 Introduction

Understanding the various behaviors of blood waves has become a subject of deep interest, as they can be used to test the hypothesis of disease formation, assess and diagnose cardiovascular diseases. These waves mainly give important information about the blood pressure which should be self-regulated for a better functioning of vital organs. In general, highly localized blood pulses indicate an enhancement of the blood pressure (BP), due to the increases of the heart rate, in either normal or pathological situations [1–3]. In the particular case of cardiovascular diseases, the uncontrolled increase in the *BP* exposes individuals to some fatal heart attack and stroke possibilities. One of the main factors that is sometimes ignored or considered in critical case decision is the viscosity of blood [4], which describes the resistance to flow and gives the pressure drop and the wall shear stress. Its increase requires the heart to work harder in pushing the viscous blood out at even higher pressures, therefore affecting the intimal layer of the vessel, which results to the formation of diseases like atherosclerosis, aneurism and stenoses [5–8]. Of course, some solutions to these vascular diseases include the use of prostheses, whose properties should be similar to those of real arterial walls. In order to model such elastic tubes and the fluid flowing inside, many models have been proposed, all of them converging to the fact that the profile of the blood pressure have solitonic characteristics, as found from solving the KdV and nonlinear Schrödinger (NLS) equations [9–15]. Although they effectively illustrate the pulsatile nature of blood flow, none of the above models inherently include viscous effects. One of the major reasons might be that they apply to large vessels and are mainly based on the theory of Navier–Stokes fluids [9–15]. Objectively, blood is mainly made of red blood cells, platelets and leukocytes, which makes it a non-Newtonian fluid [16]. Furthermore, when the diameter of the blood vessel reduces to the same order of magnitude as red blood cells, the non-Newtonian character of blood should be considered [17]. More explanations on this aspect can be found in the works Majhi and Nair [18], Prakash and Ogulu [19], Akbar et al. [20], where the simplest way to describe such fluids is through the Jeffrey model [21–24]. It is, in fact, the simplest form of non-newtonian fluids, which include straightforwardly the viscosity of blood. It has been applied to unsteady flow of fluid through tapered elastic aorta with stenosis [25]. The problem of peristaltic transport of Jeffrey fluids has been addressed by Vajravelu et al. [26] using a vertical porous stratum. Blood has also been modelled, by Akbar and Nadeem [27], as Jeffrey fluid with variable viscosity, flowing into a tapered artery with stenosis. An oscillatory flow of a jeffrey fluid in an elastic tube of variable cross section was studied by Narayana et al. [28]. It appears that, without taking into account the viscosity of the medium, the effect of the nonlinear parameter during the flow of a Jeffrey fluid in a conical tube is linearly localized and narrowed

Using the same model, we first want to show that the global dynamics of blood can be reduced to a set of nonlinearly coupled complex Ginzburg– Landau (CGL) equations. CGL equations arise in any dissipative nonlinear model [29], including fluid dynamics

---

[a] e-mail: bansidelphin@yahoo.fr (corresponding author)

[b] emails: ndjawa.pavel@yahoo.fr; pavel.ndjawa@acas-yde.org

[c] e-mail: contab408@yahoo.com

[d] e-mail: amohamad@ictp.it

[30], nonlinear optics [31, 32], laser physics [33, 34], theory of phase transitions [35], nonlinear transmission line [36–38] and in the stick-slip motion [39]. Generalized solutions can be obtained through the activation of modulational instability (MI), which suggests that plane wave profiles $\phi(x, t) \sim e^{i(kx-\omega t)}$ become unstable under modulation as a result of the competitive nonlinear and dispersive effects [32, 40, 41]. This results to an exponential growth rate of some unstable modes, such that the plane wave solution breaks up into trains of waves with solitonic profiles. This has been addressed in a broad range of disciplines ranging from fluid dynamics [40], nonlinear optics [32, 42], biophysics and plasma physics [43–47] and so on.

More recently, the same technique has been used to show, analytically and numerically, the existence of Mayer's waves in a modified Yomosa's model [45] for large elastic blood vessels, in the absence of viscosity. In the presence of viscosity, we observe the propagation of dissipative Mayer waves in viscoelastic tubes filled with blood fluid [48]. Then, we may associate such effects to the present model and study their impact on the emergence of Mayer's waves

This is also implemented in this letter, to bring out the possibility of the Jeffrey fluid model to exhibit modulated or Mayer's waves, arterial pressure oscillations slower than respiration, originating from oscillations induced in sympathetic nerve activation of peripheral resistance vessels [49]. To efficiently address this issue, we first reduce the constitutive equations, via the multiple-scale expansion, to a set of CGL equations. Analytical calculations on the theory of MI then follow, where we propose the condition for modulated localized soliton-like structures to be observed. Particularly, numerical calculations of the gain are made, where the impact of low and high viscous effects is discussed. Some concluding remarks are finally given (Fig. 1).

2 The coupled CGL equations for Jeffrey fluids

We consider a thin elastic tube, filled with an incompressible fluid. The radius of the cross section of the tube is $r = a(z)$, with $r = 0$ being the axis of the tube. If $\overline{P}$ is the pressure, λ_1 the ration of relaxation to retardation time, λ_2 the delay time. The Cauchy and extra stress tensors $\overline{T}$ and $\overline{s}$ respectively are given by the constitutive equations:

$$\overline{T} = -\overline{p}\overline{I} + \overline{s}, \qquad \overline{s} = \frac{\mu}{1+\lambda_1}(\dot{\gamma} + \lambda_2\ddot{\gamma}), \tag{1}$$

where $\overline{I}$ is the identity tensor and γ is the shear rate, with $\dot{\gamma} = \frac{\partial \gamma}{\partial t}$. When the Jeffrey fluid described above flows through the elastic tube, the equations that describe the motion of the fluid are written as follows:

$$\frac{\partial u^*}{\partial t^*} + u^*\frac{\partial u^*}{\partial r^*} + w^*\frac{\partial u^*}{\partial z^*} = -\frac{1}{\rho_0}\frac{\partial p^*}{\partial r^*} + \nu\left[\frac{1}{1+\lambda_1}\frac{\partial}{\partial r^*}\left(\frac{u^*}{r^*} + \frac{\partial u^*}{\partial r^*}\right) + \frac{\partial^2 u^*}{\partial z^{*2}}\right],$$
$$\frac{\partial w^*}{\partial t^*} + u^*\frac{\partial w^*}{\partial r^*} + w^*\frac{\partial w^*}{\partial z^*} = -\frac{1}{\rho_0}\frac{\partial p^*}{\partial z^*} + \nu\left[\frac{1}{r^*}\frac{\partial}{\partial r^*}\left(\frac{r^*}{1+\lambda_1}\frac{\partial w^*}{\partial r^*}\right) + \frac{\partial^2 w^*}{\partial z^{*2}}\right], \tag{2}$$

where u^* and w^* are the velocity components in r^* and z^* direction respectively. ρ_0 is the density of the fluid and ν is its dynamic viscosity coefficient. The pressure P^* is related to the radial displacement of the wall ψ, via the equation

$$\rho_0\frac{\partial^2\psi^*}{\partial t^{*2}} = \frac{p^* - p_e^*}{H_0}\left(1 + \frac{\psi^*}{\epsilon a_0}\right) - \frac{h_0 E\psi^*(1 + a\psi^*/\epsilon a_0)}{H_0\epsilon a_0^2(1 + \psi^*/\epsilon a_0)}, \tag{3}$$

with E being the Young's modulus and a the nonlinear coefficient of elasticity. a_0 denotes the equilibrium radius of the tube at rest, h_0 represents the thickness of the wall and H_0 is the effective inertial thickness of the wall. The velocities u^* and w^* satisfy the continuity equation, given by:

$$\frac{\partial u^*}{\partial r^*} + \frac{u^*}{r^*} + \frac{\partial w^*}{\partial z^*} = 0. \tag{4}$$

The dimensionless parameters $t^* = \omega_0 t$, $r^* = \frac{r}{a_0}$, $z^* = \frac{\epsilon z}{a_0}$, $u^* = \frac{u}{\epsilon u_0}$, $w^* = \frac{W}{u_0}$, $p^* - p_e^* = \frac{\epsilon a_0}{\rho_0 u_0 \nu}p$, $\psi^* = a_0\epsilon\psi$ are introduced into Eqs. (2), (3) and (4), so that the equations for the dynamics of the system become:

$$\epsilon^2\alpha^2\frac{\partial u}{\partial t} + \epsilon^3 R_e\left(u\frac{\partial u}{\partial r} + W\frac{\partial u}{\partial z}\right) = -\frac{\partial p}{\partial r} + \epsilon^2\left[\frac{1}{1+\lambda_1}\frac{\partial}{\partial r}\left(\frac{u}{r} + \frac{\partial u}{\partial r}\right)\right] + \epsilon^4\frac{\partial^2 u}{\partial z^2},$$
$$\alpha^2\frac{\partial W}{\partial t} + \epsilon R_e\left(u\frac{\partial W}{\partial r} + W\frac{\partial W}{\partial z}\right) = -\frac{\partial p}{\partial z} + \frac{1}{r}\frac{\partial}{\partial r}\left(\frac{r}{1+\lambda_1}\frac{\partial W}{\partial r}\right) + \epsilon^2\frac{\partial^2 W}{\partial z^2},$$
$$\frac{\partial u}{\partial r} + \frac{u}{r} + \frac{\partial W}{\partial z} = 0,$$
$$\rho_0(1-\psi)\omega_0^{-2}\epsilon a_0\frac{\partial^2\psi}{\partial t^2} = \frac{\epsilon a_0}{H_0\rho_0\nu u_0}P - \epsilon^3 h_0 H_0 Ea_0^3\psi(1 + a\psi)(1 - 2\psi), \tag{5}$$

with the boundary conditions $u = S_t\frac{\partial\psi}{\partial t}, W = 0$, on $r = S$.

$\alpha = a_0(\frac{\omega_0}{\nu})^{1/2}$ is the Womersley parameter and $R_e = \frac{u_0 a_0}{\nu}$ (is the Reynolds number). $S_t = \frac{\omega_0 a_0}{u_0}$ is the Strouhal number,

Fig. 1 Geometry of the problem
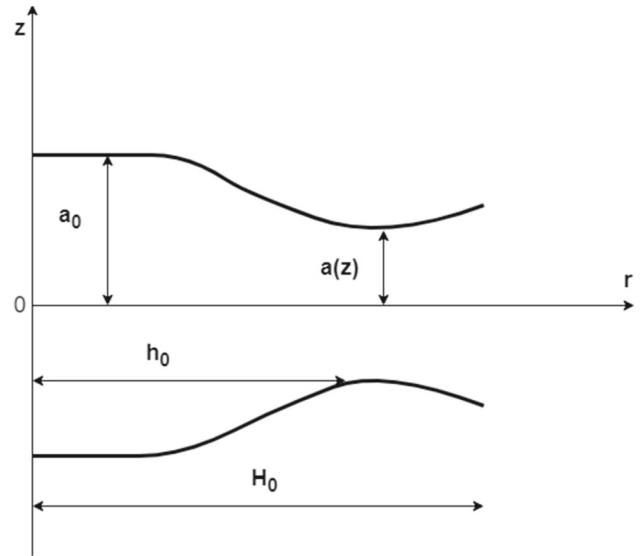
with u_0 being the characteristic velocity and w_0 the frequency of oscillatory flow. The terms in ϵ and higher order terms can be neglected, and additionally to the boundary conditions and the continuity equation, the following equations for the fluid-tube dynamics can be obtained:

$$r\frac{\partial^2 W}{\partial r^2} + \frac{\partial W}{\partial r} - (1+\lambda_1)r\frac{\partial P}{\partial z} - \alpha^2(1+\lambda_1)r\frac{\partial W}{\partial t} = 0,$$

$$\frac{s_t}{r}\frac{\partial \psi}{\partial t} + s_t\frac{\partial^2 \psi}{\partial t \partial r} + \frac{\partial W}{\partial z} = 0, \tag{6}$$

$$\beta_1(1-\psi)\frac{\partial^2 \psi}{\partial t^2} = P,$$

where $\beta_1 = \omega_0^{-2}\rho_0^2 H_0 \nu u_0$.

We are interested in modulated waves, and it is most suitable to make use of the multiple-scaling expansion by considering the stretched coordinates

$$r_n = \epsilon^n r, \qquad z_n = \epsilon^n z, \qquad t_n = \epsilon^n t, \qquad (n = 0, 1, 2, 3, ...), \tag{7}$$

and the derivative expansions:

$$\frac{\partial}{\partial r} = \sum_{n=0}^{N}\epsilon^n\frac{\partial}{\partial r_n}, \qquad \frac{\partial}{\partial z} = \sum_{n=0}^{N}\epsilon^n\frac{\partial}{\partial z_n}, \qquad \frac{\partial}{\partial t} = \sum_{n=0}^{N}\epsilon^n\frac{\partial}{\partial t_n}. \tag{8}$$

In what follows, the field variables are assumed to be functions of the stretched variables, and we expand them into asymptotic series of ϵ as follows:

$$\psi = \sum_{n=1}^{\infty}\epsilon^n\psi_n(r_0, r_1, r_2, ...; \quad z_0, z_1, z_2, ...; \quad t_0, t_1, t_2, ...),$$

$$W = \sum_{n=1}^{\infty}\epsilon^n W_n(r_0, r_1, r_2, ...; \quad z_0, z_1, z_2, ...; \quad t_0, t_1, t_2, ...), \tag{9}$$

$$P = \sum_{n=1}^{\infty}\epsilon^n P_n(r_0, r_1, r_2, ...; \quad z_0, z_1, z_2, ...; \quad t_0, t_1, t_2, ...).$$

Fig. 2 Dispersion relation for $s_t = 0.2$, $a = 1$, $r_0 = 0.35$
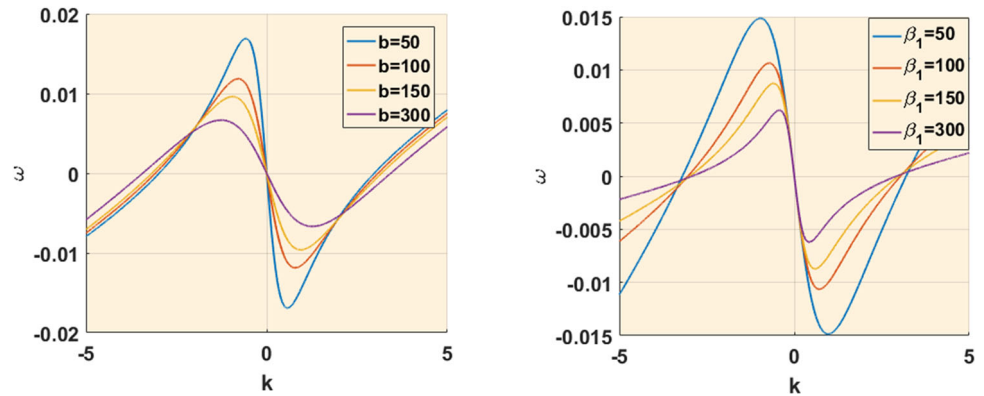
(a) Effect of b, with $\beta_1 = 80$ in the dispersion relation.   (b) Effect of β_1, with $b = 100$ in the dispersion relation.

On this basis, we can gather the different terms, and coefficients of the powers of the small parameter ϵ, hence the main order $O(\epsilon)$, after having inserted : $a = 1 + \lambda_1$ and $b = \alpha^2(1 + \lambda_1)$, we get the set of equations:

$$P_1 - \beta_1 \frac{\partial^2 \psi_1}{\partial t_0^2} = 0,$$

$$s_t \frac{\partial \psi_1}{\partial t_0} + s_t r_0 \frac{\partial^2 \psi_1}{\partial t_0 \partial r_0} + r_0 \frac{\partial W_1}{\partial z_0} = 0, \tag{10}$$

$$r_0 \frac{\partial^2 W_1}{\partial r_0^2} + \frac{\partial W_1}{\partial r_0} - a r_0 \frac{\partial P_1}{\partial z_0}, \ -b r_0 \frac{\partial W_1}{\partial t_0} = 0.$$

One of the most fascinating phenomena in the process of blood flow is the coexistence of forward and backward propagating waves. They are assumed to propagate with the same angular frequency ω, and opposite wavenumbers k and $-k$. One can then consider trial solutions for Eq. (10), in the generalized forms

$$\psi_1 = \psi e^{i\theta} + \psi' e^{i\theta'} + c.c., \quad W_1 = W_1^{(1)} e^{i\theta} + W_1'^{(1)} e^{i\theta'} + c.c., \quad P_1 = P_1^{(1)} e^{i\theta} + P_1'^{(1)} e^{i\theta'} + c.c, \tag{11}$$

where $\theta = \omega t_0 - k z_0 - k r_0$ and $\theta' = \omega t_0 + k z_0 + k r_0$ are two phases for the carrier waves, with $\omega' = \omega$. Plugging solutions (11) into Eq. (10) leads to a set of inhomogeneous equations in ψ, ψ', $W_1'^{(1)}$, $W_1^{(1)}$, $P_1'^{(1)}$, and $P_1^{(1)}$ whose nontrivial solutions exist, if its determinant is zero. This leads to the dispersion relation

$$\omega = \frac{k s_t [a r_0 k^2 \beta_1 (r_0^2 k^2 - 1) - b s_t (1 + k^2 r_0^2)]}{r_0 [b^2 s_t^2 (1 + k^2 r_0^2) + a r_0 k^2 \beta_1 (2 b s_t + a r_0 k^2 \beta_1)]}$$
$$- i \frac{k^2 s_t [b s_t (1 + k^2 r_0^2) + 2 a r_0 k^2 \beta_1]}{[b^2 s_t^2 (1 + k^2 r_0^2) + a r_0 k^2 \beta_1 (2 b s_t + a r_0 k^2 \beta_1)]} = \omega_r + i \omega_i \tag{12}$$

Figure 2 shows us the dispersion relation as a function of the wave number (k), for different values of "b" and "β_1" increasing. It is observed a decrease in the frequency during the increase of "b" and "β_1". This dispersion relation obtained admits a trivial solution, which is influenced by the parameters "b" and "β_1", depend strongly on the viscosity of the medium and where "b" depends jointly on "λ_1" and the viscosity. This is observed in Fig. 2a, b respectively. The variation of these two parameters imposes a very fast vibration, that decreases with the increase in each of them, while keeping a stable inflection point in zero.

So that, $W_1'^{(1)}$, $W_1^{(1)}$, $P_1'^{(1)}$, and $P_1^{(1)}$ are written as:

$$W_1^{(1)} = \left(\frac{1}{k r_0} + i\right) \omega s_t \psi; \qquad W_1^{'(1)} = \left(\frac{1}{k r_0} - i\right) \omega s_t \psi',$$

$$P_1^{(1)} = \left\{ \frac{\omega s_t (k - \omega b r_0 - k^3 r_0^2)}{k^2 r_0^2 a} + i \frac{\omega s_t (b r_0 \omega - 2k)}{k a r_0} \right\} \psi, \tag{13}$$

$$P_1^{'(1)} = \left\{ \frac{\omega s_t (k + \omega b r_0 - k^3 r_0^2)}{k^2 r_0^2 a} + i \frac{\omega s_t (b r_0 \omega + 2k)}{k a r_0} \right\} \psi'.$$

Fig. 3 Group velocity for $s_t = 0.2$, $a = 1$, $r_0 = 0.35$
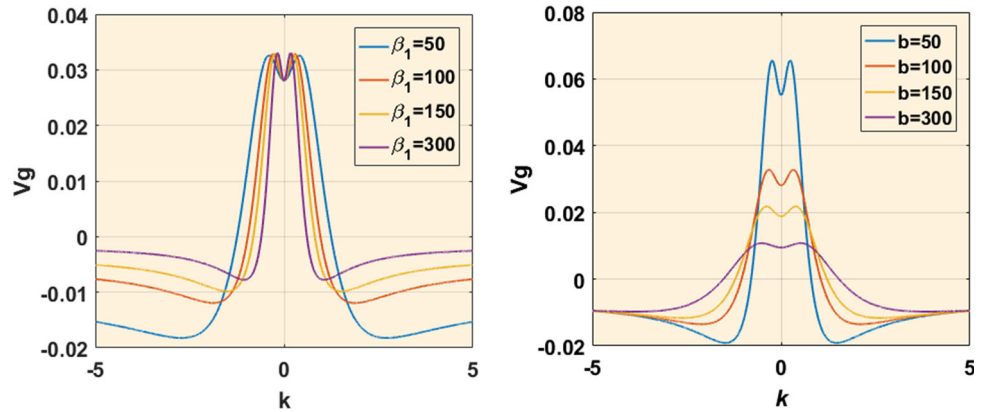
(a) Effect of b, with $\beta_1 = 80$ in the group velocity.

(b) Effect of β_1, with $b = 100$ in the group velocity.

As functions of ψ and ψ', the same procedure can be adopted for the order $O(\epsilon^2)$, whose solutions can be investigated in the form

$$\psi_2 = \overline{\psi_2}^{(0)} + \psi_2^{(1)}e^{i\theta} + \psi_2^{'(1)}e^{i\theta'} + \psi_2^{(2)}e^{2i\theta} + \psi_2^{'(2)}e^{2i\theta'} + \psi_2^{(+)}e^{i(\theta+\theta')} + \psi_2^{(-)}e^{i(\theta-\theta')} + cc$$

$$W_2 = \overline{W_2}^{(0)} + W_2^{(1)}e^{i\theta} + W_2^{'(1)}e^{i\theta'} + W_2^{(2)}e^{2i\theta} + W_2^{'(2)}e^{2i\theta'} + W_2^{(+)}e^{i(\theta+\theta')} + W_2^{(-)}e^{i(\theta-\theta')} + cc \quad (14)$$

$$P_2 = \overline{P_2}^{(0)} + P_2^{(1)}e^{i\theta} + P_2^{'(1)}e^{i\theta'} + P_2^{(2)}e^{2i\theta} + P_2^{'(2)}e^{2i\theta'} + P_2^{(+)}e^{i(\theta+\theta')} + P_2^{(-)}e^{i(\theta-\theta')} + cc,$$

Replacing the above into the corresponding equations and letting the coefficients of $e^{-i\theta}$, $e^{-2i\theta}$, $e^{-i\theta'}$, $e^{-2i\theta'}$, $e^{-i(\theta+\theta')}$, and $e^{-i(\theta-\theta')}$ equal to zero, we obtain the different terms for solutions (14) as given in "Appendix A" as functions of ψ, ψ', ψ_2^+ and $\psi_2^{'(1)}$. The solvability condition for the found systems give the group velocity

$$v_g = \frac{\partial\omega}{\partial k} = \frac{-s_t r_0^4 a^2 \beta_1^3 k^8 - l_1 k^6 + l_2 k^4 + l_3 k^2 + b^2 s_t^3 (bs_t - ar_0)}{r_0[a^2 r_0^2 \beta_1^2 k^4 + (b^2 s_t^2 r_0^2 + 2abr_0\beta_1 s_t)k^2 + b^2 s_t^2]^2}$$

$$- i \frac{2br_0^2 s_t^2(a\beta_1 + br_0 s_t)(3a\beta_1 + br_0 s_t)k^5 + 4b^2 s_t^3 r_0(br_0 s_t + 2a\beta_1)k^3 + 2b^3 s_t^4 k}{[a^2 r_0^2 \beta_1^2 k^4 + (b^2 s_t^2 r_0^2 + 2abr_0\beta_1 s_t)k^2 + b^2 s_t^2]^2} = v_r + i v_i, \quad (15)$$

where

$$l_1 = s_t r_0^2 a^2 \beta_1^3 + abs_t^2 r_0^3(ar_0 + 6)\beta_1^2 + 3s_t^3 r_0^4 b^2 \beta_1,$$

$$l_2 = s_t r_0 a[bs_t(2 - 3ar_0) + 3a^3 r_0^2]\beta_1^2 + s_t^4 r_0^3 b^2 a(2ar_0 - 4)\beta_1 + s_t^5 r_0^5 b^3 a,$$

$$l_3 = [s_t^3 b^2(3 - 2ar_0) + 2bs_t^2 a^2 r_0^2]\beta_1 + s_t^3 b^2 r_0^2(ar_0 + 2bs_t).$$

Figure 3 shows the group velocity as a function of wavenumber (k). Fig. (3)a highlights the group velocity for an increase in "b". We observe that, the Jeffrey fluid has the ability to have a very high viscosity for large values of "b". Fig. (3)b shows us for an increase in "β_1", a clearer localization of the wave. Also, Fig. (3) shows inflection points between group velocity and wave number.

In the basic models proposed by Yomosa [9], the study on viscosity is not taken into account. On the other hand, the modified model of Yomosa proposed by Bansi et al. [48], it is observed that, the dispersion relation is entirely dependent on the thickness of the artery structure, whose study shows that the frequency waves decrease with them. Now, we realize that taking into account the viscosity in this new model, we present the vibratory modes of frequency waves by varying the coefficients "b" and "β_1", which are very strongly dependent on the viscosity.

In order to get the coupled amplitude equations, we finally consider the order $O(\epsilon^3)$ and we make use of the solutions obtained for $O(\epsilon)$ and $O(\epsilon^2)$. On collecting the coefficients of $e^{-i\theta}$ and $e^{-i\theta'}$ and setting them to zero, we finally obtain the following set of coupled equations:

$$i\frac{\partial\psi}{\partial\tau} + P\frac{\partial^2\psi}{\partial\xi^2} + [Q_1|\psi|^2 + Q_2|\psi'|^2]\psi = -\left\{R\frac{\partial^2\psi}{\partial\xi\partial\tau} + M\frac{\partial^3\psi}{\partial\xi^2\partial\tau} + S\frac{\partial^3\psi}{\partial\xi^3} + T\frac{\partial^4\psi}{\partial\xi^4}\right\},$$

$$i\frac{\partial\psi'}{\partial\tau} + P'\frac{\partial^2\psi'}{\partial\xi^2} + [Q_1'|\psi'|^2 + Q_2'|\psi|^2]\psi' = -\left\{R'\frac{\partial^2\psi'}{\partial\xi\partial\tau} + M'\frac{\partial^3\psi'}{\partial\xi^2\partial\tau} + S'\frac{\partial^3\psi'}{\partial\xi^3} + T'\frac{\partial^4\psi'}{\partial\xi^4}\right\}, \quad (16)$$

for ψ and ψ'. The coefficients $P = P_r + iP_i$, $Q_1 = Q_{1r} + iQ_{1i}$, $Q_2 = Q_{2r} + iQ_{2i}$, $M = M_r + iM_i$, $R = R_r + iR_i$, $S = S_r + iS_i$ and $T = T_r + iT_i$, and their equivalents with the prime for Eq. (16), are all complex and given in "Appendix B". These are modified *CGL* equations, that are nonlinearly coupled via the coefficients Q_2 and Q_2', with third and fourth order spatial derivatives. When $R = M = S = T = R' = M' = S' = T' = 0$, we recover the standard CGL equations, as written on the left-hand side of Eq. (16),

Fig. 4 (color online) The panels show the coefficients for the standard coupled *CGL* equations versus the wavenumber k
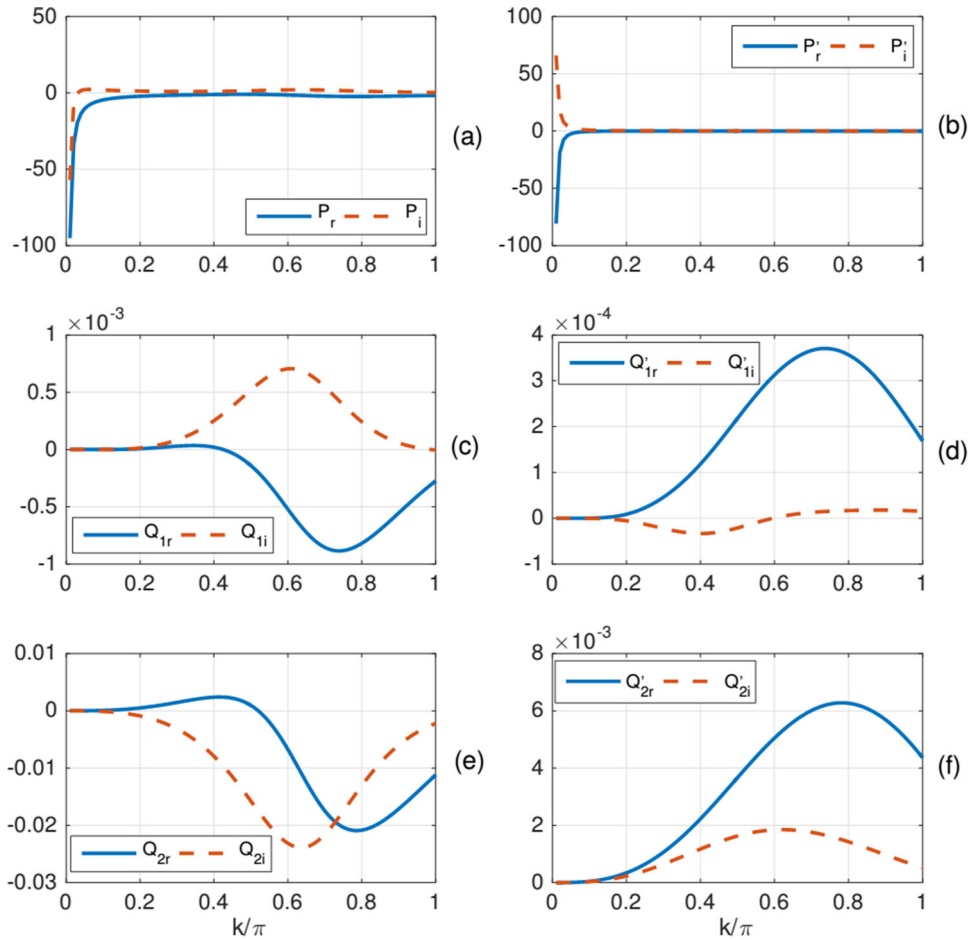
whose coefficients are represented versus the wavenumber k in Fig. 4, with the real and imaginary parts of each coefficient being plotted on the same diagram. The terms on the right-hand side are modified terms that are brought by the complexity of the studied system. They are plotted in Fig. 5 versus the wavenumber k. One of the most interesting aspects in all these figures is that they all depend on the viscosity coefficient ν, which is the main concern of this letter. However, as introduced here, these equations display the original features of having third- and fourth-order spatial derivatives, which, to our knowledge, have not yet been obtained in the case of blood flow dynamics. Coupled *CGL* equations, with different features, were obtained by Ndzana et al. [50] and by Kengne and Vaillancourt [51] in the context of signal transport in electrical transmission lines.

In the rest of this work, we would be focusing on how these highly dispersive terms compete with nonlinear effects in the process of nonlinear modulated wave formation in Jeffrey fluids.

3 Modulational instability

Plane wave solutions are very sensitive to small perturbations, and might become unstable when some characteristic parameters fall inside some intervals. When this is the case, the plane wave is expected to break up into trains of waves with soliton-like shape. For the set of Eq. (16), let us assume the plane wave solutions $\psi(\xi, \tau) = U_0 e^{[i(k_1\xi - \Omega_1\tau)]}$, and $\psi'(\xi, \tau) = V_0 e^{[i(k_2\xi - \Omega_2\tau)]}$, where the wavenumbers k_1 and k_2 and the frequencies Ω_1 and Ω_2 satisfy the dispersion relations

$$
\begin{aligned}
(1 + k_1 R_r + M_i k_1^2)\Omega_1 - k_1^2 P_r + k_1^3 S_i + k_1^4 T_r + Q_{1_r}|U_0|^2 + Q_{2_r}|V_0|^2 = 0, \\
(1 + k_2 R_r' + M_i' k_2^2)\Omega_2 - k_2^2 P_r' + k_2^3 S_i' + k_2^4 T_r' + Q_{1_r}'|V_0|^2 + Q_{2_r}'|U_0|^2 = 0,
\end{aligned}
\tag{17}
$$

for the real part, and

$$
\begin{aligned}
(k_1 R_i - M_r k_1^2)\Omega_1 - k_1^2 P_i - k_1^3 S_r + k_1^4 T_i + Q_{1_i}|U_0|^2 + Q_{2_i}|V_0|^2 = 0, \\
(k_2 R_i' - M_r' k_2^2)\Omega_2 - k_2^2 P_i' - k_2^3 S_r' + k_2^4 T_i' + Q_{1_i}'|V_0|^2 + Q_{2_i}'|U_0|^2 = 0,
\end{aligned}
\tag{18}
$$

Fig. 5 (Color online) Additional coefficients for the coupled CGL equations versus the wavenumber k
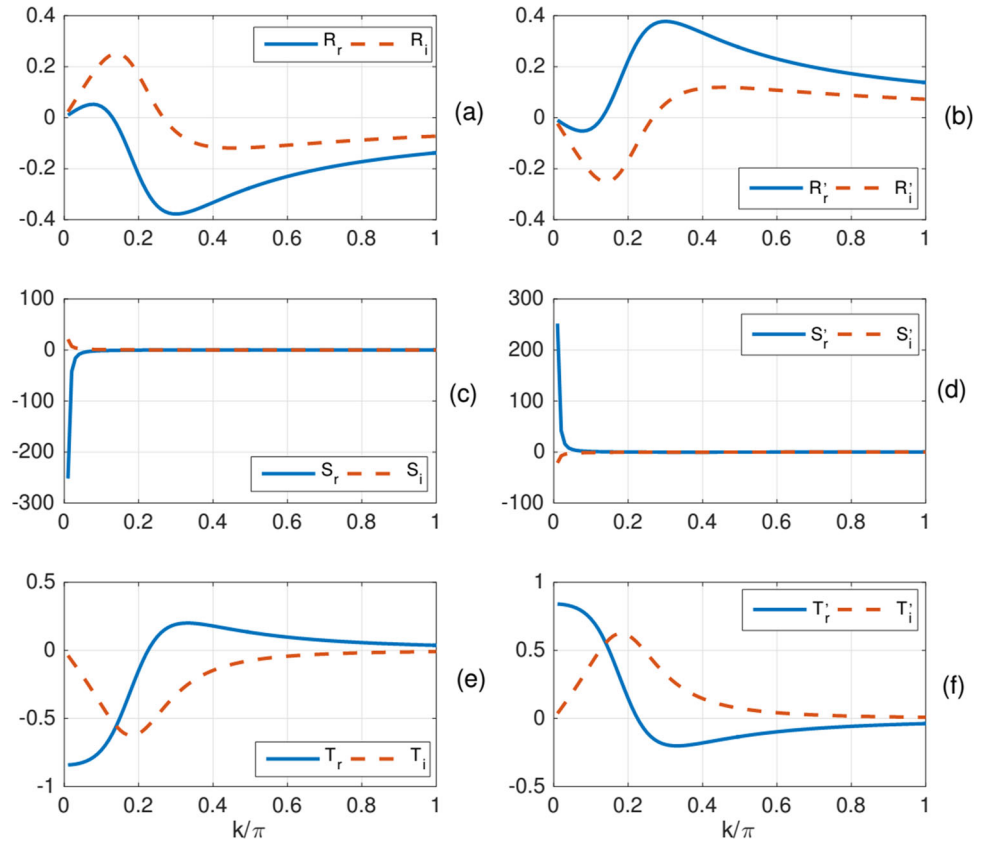
for the imaginary part. If we consider the physically symmetric case, i.e., $\Omega_1 = \Omega_2 = \Omega$ and $k_1 = k_2 = K$, it will be possible to find straightforward expressions for U_0 and V_0 as follows:

$$|U_0|^2 = \left| \frac{(\delta_1' \delta_2 - \delta_1 \delta_2')(\delta_3 Q_{1i}' - \delta_3' Q_{2i}) - (\delta_3' \delta_4 - \delta_3 \delta_4')(\delta_1' Q_{2r} - \delta_1 Q_{1r}')}{(\delta_3 Q_{1i}' - \delta_3' Q_{2i})(\delta_1 Q_{2r} - \delta_1 Q_{1r}')(\delta_3 Q_{2i}' - \delta_3' Q_{1i})} \right|,$$

$$|V_0|^2 = \left| \frac{(\delta_4' \delta_3 - \delta_4 \delta_3')(\delta_1' Q_{1r} - \delta_1 Q_{2r}) - (\delta_4' \delta_3 - \delta_3' \delta_4)(\delta_1' Q_{1r} - \delta_1 Q_{2r}')}{(\delta_3 Q_{1i}' - \delta_3' Q_{2i})(\delta_1 Q_{2r} - \delta_1 Q_{1r}')(\delta_3 Q_{2i}' - \delta_3' Q_{1i})} \right|,$$

(19)

with $\delta_1 = 1 + K R_r + M_i K^2$, $\delta_1' = 1 + K R_r' + M_i' K^2$, $\delta_2 = K^2 P_r - K^3 S_i - K^4 T_r$, $\delta_2' = K^2 P_r' - K^3 S_i' - K^4 T_r'$, $\delta_3 = K R_i - K^2 M_r$, $\delta_3' = K R_i' - K^2 M_r'$, $\delta_4 = K^2 P_i + K^3 S_r - K^4 T_i$ and $\delta_4' = K^2 P_i' + K^3 S_r' - K^4 T_i'$. Studying the stability of a solution, implies introducing some perturbation and observe how they could affect the unperturbed solution. In the case at hand, perturbations are introduced in the amplitudes of the uniform waves, i.e., $\psi(\xi, \tau) = [U_0 + U(\xi, \tau)]e^{[i(k\xi - \Omega_0 \tau)]}$ and $\psi'(\xi, \tau) = [V_0 + V(\xi, \tau)]e^{[i(k\xi - \Omega_0 \tau)]}$, where U and V are the perturbations, governed by the linearized equations

$$[-k^2 M + i(1 + Rk)]\frac{\partial U}{\partial \tau} - [3k^2 S - 2kM\Omega_0 + i(R\Omega_0 - 2kT + 4k^3 T)]\frac{\partial U}{\partial \xi} + [P - 6k^2 T - i(3kS + M\Omega_0)]\frac{\partial^2 U}{\partial \xi^2}$$

$$+ Q_1 |U_0|^2 (U + U^*) + Q_2 |V_0|^2 (V + V^*) + (R + 2ikM)\frac{\partial^2 U}{\partial \xi \partial \tau} + M\frac{\partial^3 U}{\partial \xi^2 \partial \tau} + [S + 4ikT]\frac{\partial^3 U}{\partial \xi^3} + T\frac{\partial^4 U}{\partial \xi^4} = 0,$$

$$[-k^2 M' + i(1 + R'k)]\frac{\partial V}{\partial \tau} - [3k^2 S - 2kM'\Omega_0 + i(R'\Omega_0 - 2kT' + 4k^3 T')]\frac{\partial V}{\partial \xi} + [P' - 6k^2 T' - i(3kS' + M\Omega_0)]\frac{\partial^2 V}{\partial \xi^2}$$

(20)

$$+ Q_1' |V_0|^2 (V + V^*) + Q_2' |U_0|^2 (U + U^*) + (R' + 2ikM)\frac{\partial^2 V}{\partial \xi \partial \tau} + M'\frac{\partial^3 V}{\partial \xi^2 \partial \tau} + [S' + 4ikT']\frac{\partial^3 V}{\partial \xi^3} + T'\frac{\partial^4 V}{\partial \xi^4} = 0,$$

whose generalized solutions can be taken in the forms:

$U(\xi, \tau) = ae^{[i(q\xi + \Omega\tau)]} + b^* e^{[-i(q\xi + \Omega\tau)]}$ and $V(\xi, \tau) = ce^{[i(q\xi + \Omega\tau)]} + d^* e^{[-i(q\xi + \Omega\tau)]}$, where q and Ω are respectively, an arbitrary real wavenumber of the perturbation and the corresponding propagation frequency; which is complex in general.

Replacing these into Eq. (20) leads to a set of four homogeneous equation for a, b, c, d i.e.,

$$\begin{pmatrix} m_{11} - i\Omega & m_{12} & m_{13} & m_{14} \\ m_{21} & m_{22} + i\Omega & m_{23} & m_{24} \\ m_{31} & m_{32} & m_{33} - i\Omega & m_{44} \\ m_{41} & m_{42} & m_{43} & m_{44} + i\Omega \end{pmatrix} \begin{pmatrix} a \\ b \\ c \\ d \end{pmatrix} = \begin{pmatrix} 0 \\ 0 \\ 0 \\ 0 \end{pmatrix}, \tag{21}$$

where the complex coefficients $m_{ij}(i, j = 1, 2, 3, 4)$, of the system matrix are given by:

$$m_{11} = \frac{q^4 T + 4q^3 kT + q^2(6k^2 T - P) + q(R\Omega_0 + 4k^3 T + 2kT) + Q_1|U_0|^2 -}{-q^2 M + 2qkM + k^2 M - i(qR + kR + 1)}$$
$$- i\frac{[q^3 S + q^2(3kS + M\Omega_0) - q(2kM\Omega_0 - 3k^2 S)]}{-q^2 M + 2qkM + k^2 M - i(qR + kR + 1)},$$

$$m_{12} = \frac{Q_1|U_0|^2}{-q^2 M + 2qkM + k^2 M - i(qR + kR + 1)},$$

$$m_{13} = m_{14} = \frac{Q_2|V_0|^2}{-q^2 M + 2qkM + k^2 M - i(qR + kR + 1)},$$

$$m_{21} = \frac{Q_1^*|U_0|^2}{-q^2 M^* + 2qkM^* + k^2 M^* - i(qR^* + kR^* + 1)},$$

$$m_{23} = m_{24} = \frac{Q_2^*|V_0|^2}{-q^2 M^* + 2qkM^* + k^2 M^* - i(qR^* + kR^* + 1)},$$

$$m_{22} = \frac{q^4 T^* - 4q^3 kT^* + q^2(6k^2 T^* - P^*) - q(R^*\Omega_0 + 4k^3 T^* - 2kT^*) + Q_1^*|U_0|^2}{-q^2 M^* + 2qkM^* + k^2 M^* - i(qR^* + kR^* + 1)}$$
$$- i\frac{[q^3 S^* + q^2(3kS^* + M^*\Omega_0) - q(2kM^*\Omega_0 - 3k^2 S^*)]}{-q^2 M^* + 2qkM^* + k^2 M^* - i(qR^* + kR^* + 1)}$$

$$m_{31} = m_{32} = \frac{Q_2'|U_0|^2}{-q^2 M' + 2qkM' + k^2 M' - i(qR' + kR' + 1)},$$

$$m_{34} = \frac{Q_1'|V_0|^2}{-q^2 M' + 2qkM' + k^2 M' - i(qR' + kR' + 1)},$$

$$m_{33} = \frac{q^4 T' + 4q^3 kT' + q^2(6k^2 T' - P') + q(R'\Omega_0 + 4k^3 T' + 2kT') + Q_1'|U_0|^2}{-q^2 M' + 2qkM' + k^2 M' - i(qR' + kR' + 1)}$$
$$- i\frac{[q^3 S' + q^2(3kS' + M'\Omega_0) - q(2kM'\Omega_0 - 3k^2 S')]}{-q^2 M' + 2qkM' + k^2 M' - i(qR' + kR' + 1)},$$

$$m_{41} = m_{42} = \frac{Q_2'^*|U_0|^2}{-q^2 M'^* + 2qkM'^* + k^2 M'^* - i(qR'^* + kR'^* + 1)},$$

$$m_{43} = \frac{Q_1'^*|V_0|^2}{-q^2 M'^* + 2qkM'^* + k^2 M'^* - i(qR'^* + kR'^* + 1)},$$

$$m_{44} = \frac{q^4 T'^* + 4q^3 kT'^* + q^2(6k^2 T'^* - P'^*) + q(R'^*\Omega_0 + 4k^3 T'^* + 2kT'^*) + Q_1'^*|U_0|^2}{-q^2 M'^* + 2qkM'^* + k^2 M'^* - i(qR'^* + kR'^* + 1)}$$
$$- i\frac{[q^3 S'^* + q^2(3kS'^* + M'^*\Omega_0) - q(2kM'^*\Omega_0 - 3k^2 S'^*)]}{-q^2 M'^* + 2qkM'^* + k^2 M'^* - i(qR'^* + kR'^* + 1)}. \tag{22}$$

The dispersion relation which gives q as a function of Ω is found through the solvability condition of system (21). In other words, system (21) will admit non-trivial solutions if its determinant is equal to zero. Therefore, for this specific case, $det(M) = 0$ amounts to a quartic equation for Ω. As introduced so far, the perturbation frequency is in the form $\Omega = \Omega_r + i\Omega_i$, and the term $e^{-\Omega_i \tau}$ is responsible for some perturbations. Therefore, the features of the wave instability depend on the sign of Ω_i. Otherwise, *MI* develops when the frequency possesses a non-zero imaginary part leading to an exponential growth rate of the perturbed amplitude. Its largest value gives the *MI* gain $\Gamma = |Im(\Omega)|$, from which the onset of *MI* can be detected.

4 Numerical results

Finding solutions for the quartic equation in Ω, obtained form the condition $det(M) = 0$, is quite cumbersome and requires at some points a few assumptions and simplifications. For that reason, we find the solutions numerically and extract essentially solutions for

Fig. 6 (Color online) Instability gain spectra under the effect of the viscous coefficient ν, versus the perturbation wavenumber and frequency, q and Ω. Panels (a1–c1) show the finite gains, with their corresponding density plots in panels (a2–c2), for $K = 0.35\pi$, U_0 and V_0 are given by Eq. (19)
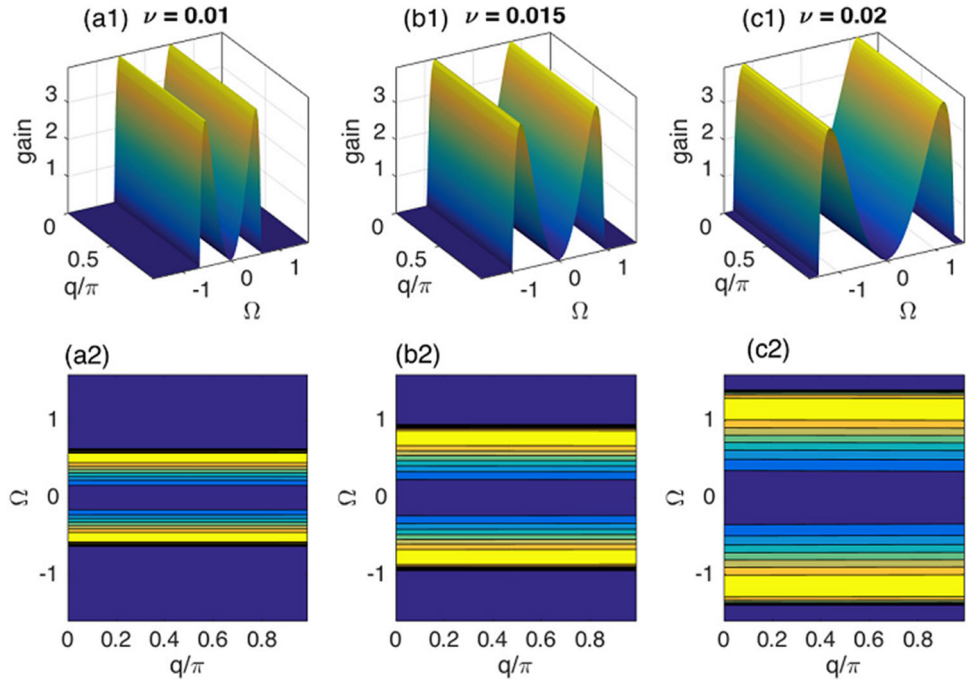
which $\Omega_i \neq 0$, in order for the MI gain to exist. Particular attention is paid to viscous effects, responsible for the complex character of the set of Eq. (16).

Firstly, we consider the unperturbed wavenumber to take the value $K = 0.35\pi$. Results for different values of ν are displayed in Fig. 6, where Fig. 6a1–c1 shows the gains and panels (a2–c2) show their corresponding density plots. The general aspect here is that increasing the viscosity coefficient ν enlarges the MI bandwidth. Also, localized blood waves will be expected for all $q \in [0, \pi]$. However, there is no MI for $\Gamma = 0$ and the highest value for the gain remains the same for for all q with increasing ν.

In the meantime, an interesting case arises when $K = 0.95\pi$, as displayed in Fig. 7. In fact, the general view is that the gain spectrum changes at $q = 0.5\pi$, leading to some wings of instability for $\nu = 0.01$. For $q < 0.5\pi$, the gain is quite high and gradually decreases for $q > 0.5\pi$.

Obviously, the MI bandwidth increases with increasing ν as portrayed in Fig. 7b1–c1, and b2–c2. When $\Omega = 1.5$, the window of instability created between $q = 0$ and $q = 0.5\pi$ enlarges too, while the MI gain gets enlarged.

Finally, for $K = 0.95\pi$ as in Fig. 7, we consider big viscosity of the blood flowing in the tube. The corresponding results are summarized in Fig. 8. In this case, the MI gain has zero value for $q > 0.5\pi$, all the contrary of the results from Fig. 7. With increasing ν, the instability region gets expanded,

The same behaviors around $q = 0.5\pi$ are visible. As a whole, the features of *MI* change with increasing the viscosity coefficient, showing that in heamodynamics, viscosity is an important factor that deserves to be seriously regarded.

In order to supply oxygen and nutrients to the tissues and organs, the contribution on blood viscosity should be effective [52]. This affectivity might be affected by several factors, including hematocrit and smoking [53, 54]. A broad range of experimental studies has come to the conclusion that, the higher the viscosity of blood, the higher the heart rate, which is mainly responsible for heart failure and its many consequences.

Nevertheless, high blood pressure importantly affects the characteristics of blood waves, which to some extent have solitonic features. In the regions of MI discussed in Figs. 6, 7 and 8, these solitons might be affected by viscosity, as it is the case in the diagrams.

5 Conclusion

In summary, we have addressed the characteristics of MI in coupled *CGL* equations, derived from Jeffrey's viscous fluid model. The influence of the viscosity have been studied for $K < 0.5\pi$ and $K > 0.5\pi$. In general, we have found that viscosity importantly affects the formation of blood waves and also restricts their onset to some regions of the gain spectra. Once more, the conclusion to this work converges to the fact that many of the arterial ailments are linked to uncontrolled blood viscosity, with direct consequences on solitonic blood waves, whose changes in behaviors affect the heart rate. This might give rise to some counter-propagating waves in vessels and eventually their death over a short distance of propagation as a result of high viscosity. The heart rate will then increase uncontrollably, trying to pump blood in tissues and organs and supply them with oxygen. The bandwidth of *MI* is therefore

Fig. 7 (Color online) The instability gain spectra versus the perturbation wavenumber and frequency, q and Ω respectively. The influence of the viscous coefficient ν is studied. Panels (a1–c1) show the gains of MI and their corresponding density plots in panels (a2–c2). The unperturbed wavenumber is $K = 0.95\pi$ and the initial amplitudes are such that U_0 and V_0 are given by Eq. (19)
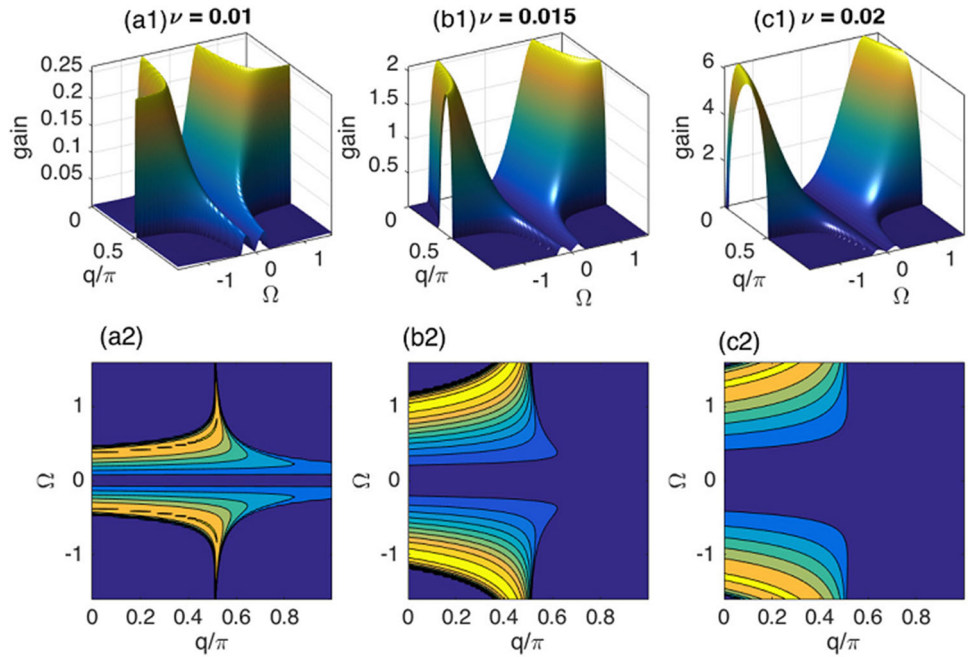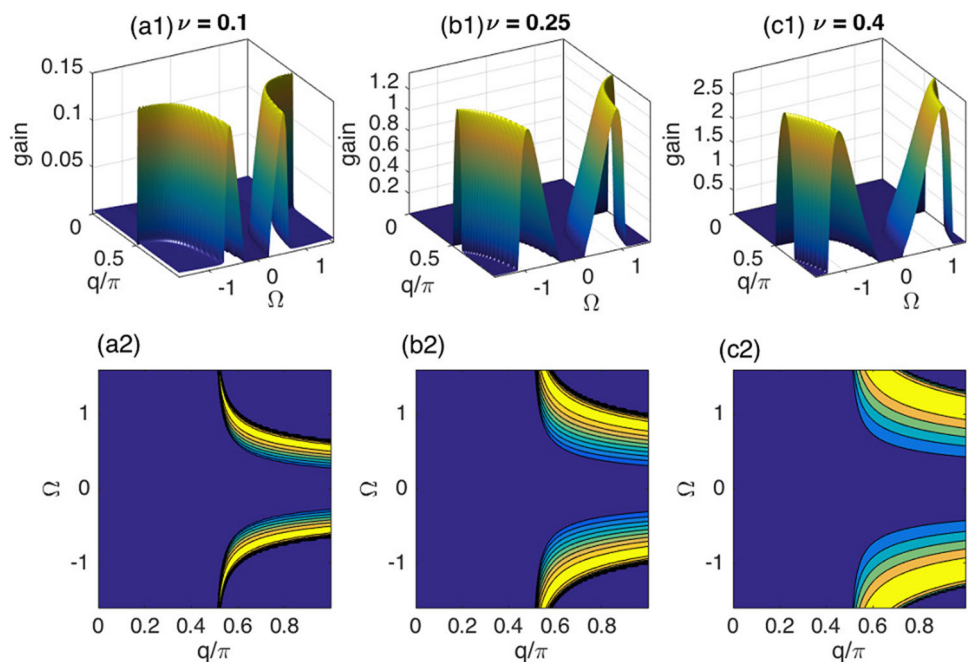

Fig. 8 (Color online) Instability gain spectra under the effect of a high viscous coefficient ν, versus the perturbation wavenumber and frequency, q and Ω. Panels (a1–c1) show the finite gains, with their corresponding density plots in panels (a2–c2), for $K = 0.95\pi$, U_0 and V_0 are given by Eq. (19)

an important factor to be controlled in this respect, for blood wave frequency to remain normal under physiological viscosity parameter. However, at this stage, nothing can be said on their longtime evolution, but interesting is the fact that we at least have some information on their onset. In an ongoing work, complete numerical simulations of such waves are performed and results will be submitted elsewhere for publication.

6 Appendix (A-1-48): Coefficients of order $O(\epsilon^2)$ of the multiple scales of equation (14), and Coefficients of the first member of equations (16).

$$W_2^{(1)} = \frac{\omega s_t(1 - ikr_0)}{kr_0}\psi_2^{(1)} + \frac{\omega s_t}{k}\frac{\partial \psi}{\partial r_1} + \left(\frac{\omega s_t}{k} - \frac{i\omega s_t}{k^2 r_0}\right)\frac{\partial \psi}{\partial z_1} - \left(s_t - \frac{is_t}{kr_0}\right)\frac{\partial \psi}{\partial t_1} - \frac{is_t r_1}{kr_0}\frac{\partial^2 \psi}{\partial r_1 \partial t_1}$$

$$W_2^{'(1)} = -\frac{\omega s_t(1-ikr_0)}{kr_0}\psi_2^{'(1)} - \frac{\omega s_t}{k}\frac{\partial \psi'}{\partial r_1} + \left(\frac{\omega s_t}{k} + \frac{i\omega s_t}{k^2 r_0}\right)\frac{\partial \psi'}{\partial z_1} + \left(s_t + \frac{is_t}{kr_0}\right)\frac{\partial \psi'}{\partial t_1} + \frac{is_t r_1}{kr_0}\frac{\partial^2 \psi'}{\partial r_1 \partial t_1}$$

$$P_2^{(1)} = \left[\omega s_t(2k+b\omega) + i\frac{k(1-k^2 r_0^2)+br_0\omega}{kr_0}\right]\psi_2^{(1)} + \left[\frac{s_t\omega(4k+br_0\omega)}{k^2 r_0 a} + i\frac{s_t\omega(k^2 r_0^2-1)}{k^2 r_0^2 a}\right]\frac{\partial \psi}{\partial r_1}$$

$$+ \left[\frac{s_t\omega(bkr_0\omega - br_0\omega + 2k)}{k^2 r_0 a} + i\frac{1-k(k^2 r_0^2+1)-r_0\omega(1+b)-k^2 r_0^2}{k^2 r_0^2 a}\right]\frac{\partial \psi}{\partial z_1}$$

$$- \left[\frac{2bs_t\omega}{ka} - i\frac{s_t(k(k^2 r_0^2+1)+2br_0\omega)}{k^2 r_0^2 a}\right]\frac{\partial \psi}{\partial t_1} - \left[\frac{r_1 s_t\omega}{kr_0 a} - i\frac{r_1 s_t\omega}{k^2 r_0^2 a}\right]\frac{\partial^2 \psi}{\partial r_1^2} - \left[\frac{r_1 s_t}{r_0 a} + i\frac{r_1 s_t(k+br_0\omega)}{k^2 r_0^2 a}\right]\frac{\partial^2 \psi}{\partial r_1 \partial t_1}$$

$$P_2^{'(1)} = \left[-br_0 s_t\omega^2 + i\frac{k(1+k^2 r_0^2)-br_0\omega}{kr_0}\right]\psi_2^{'(1)} + \left[\frac{s_t\omega(2k-br_0\omega)}{k^2 r_0 a} - i\frac{s_t\omega(k^2 r_0^2+1)}{k^2 r_0^2 a}\right]\frac{\partial \psi'}{\partial r_1}$$

$$+ \left[\frac{s_t\omega(bkr_0\omega - br_0\omega - 2k)}{k^2 r_0 a} + i\frac{s_t\omega(1-k(k^2 r_0^2+1)+r_0\omega(1+b)-k^2 r_0^2)}{k^2 r_0^2 a}\right]\frac{\partial \psi'}{\partial z_1}$$

$$+ i\frac{(k^2 r_0^2+1)}{kr_0^2 a}\frac{\partial \psi'}{\partial t_1} + \left[\frac{r_1 s_t\omega}{kr_0 a} + i\frac{r_1 s_t\omega}{k^2 r_0^2 a}\right]\frac{\partial^2 \psi'}{\partial r_1^2} + \left[\frac{r_1 s_t}{r_0 a} + i\frac{r_1 s_t(-k+br_0\omega)}{k^2 r_0^2 a}\right]\frac{\partial^2 \psi'}{\partial r_1 \partial t_1}$$

$$J_1 = \frac{ks_t\omega_r(1-2k^2 r_0^2) + (\omega_r^2-\omega_i^2)(bs_t r_0 + 4\beta_1 k^2 r_0^2) + s_t k^2 r_0\omega_i(2b\omega_r+3)}{k^2 r_0^2}$$

$$J_2 = \frac{ks_t\omega_i(k^2 r_0^2-1) - 2\omega_r\omega_i(bs_t r_0 + 4\beta_1 k^2 r_0^2) + bkr_0 s_t(\omega_r^2-\omega_i^2) + 3s_t k^2 r_0\omega_r}{k^2 r_0^2}$$

$$\theta_r = \frac{(\omega_r^2-\omega_i^2)J_1 + 2\omega_r\omega_i J_2}{J_1^2+J_2^2}, \quad \theta_i = \frac{(\omega_r^2-\omega_i^2)J_2 + 2\omega_r\omega_i J_1}{J_1^2+J_2^2}$$

$$\psi_2^{(2)} = (\theta_r - i\theta_i)\psi^2, \quad \psi_2^{'(2)} = \psi_2^{(2)},$$

$$W_2^{(2)} = \frac{2\omega s_t(1-ikr_0)}{kr_0}\psi_2^{(2)}, \quad W_2^{'(2)} = -\frac{2\omega s_t(1+ikr_0)}{kr_0}\psi'^2, \quad P_2^{(2)} = -4\beta_1\omega^2\psi_2^{(2)} + \omega^2\psi^2,$$

$$P_2^{'(2)} = -4\beta_1\omega^2\psi_2^{'(2)} + \omega^2\psi'^2, \quad \psi_2^{(+)} = \frac{1}{\beta_1}\psi\psi', \quad \psi_2^{(-)} = 2\omega^2\beta_1\psi\psi'^*, \quad W_2^{(+)} = 0, \quad W_2^{(-)} = 0,$$

$$P_2^{(+)} = 0, \quad P_2^{(-)} = 2\omega^2\beta_1\psi\psi'^*, \quad \psi_2^{(0)} = \frac{2r_0\omega^2 a}{r_1^2\vartheta s_t}|\psi|^2, \quad \psi_2^{'(0)} = \frac{2r_0\omega^2 a}{r_1^2\vartheta s_t}|\psi'|^2,$$

$$W_2^{(0)} = -2\beta_1 a|\psi|^2, \quad W_2^{'(0)} = 0, \quad P_2^{(0)} = 2\omega^2|\psi|^2 \quad P_2^{'(0)} = 2\omega^2|\psi'|^2 \tag{23}$$

$$\Delta = A^2 + B^2, \quad A = \frac{bs_t(r_0+1)(\omega_r-kr_0\omega_i) - ks_t r_0(1+k^2 r_0^2) - 2\beta_1\omega_r k^2 r_0^2 a}{k^2 r_0^2 a}, \quad B = \frac{bs_t(r_0+1)(\omega_i+kr_0\omega_r) + 2\beta_1\omega_i k^2 r_0^2 a}{k^2 r_0^2 a},$$

$$\Delta' = A'^2 + B'^2, \quad A' = \frac{bs_t kr_0\omega_i(1-r_0) + ks_t r_0(1+k^2 r_0^2) + s_t b\omega_r(1+r_0) - 2\beta_1\omega_r k^2 r_0^2 a}{k^2 r_0^2 a},$$

$$B' = \frac{bs_t kr_0\omega_i(r_0+1) - s_t bkr_0\omega_r(r_0-1) - 2\beta_1\omega_r k^2 r_0^2 a}{k^2 r_0^2 a},$$

$$X_p = -\frac{2bk^2 s_t r_0(1+2r_0)(\omega_r\vartheta_i+\omega_i\vartheta_r) + bs_t(\omega_i^2-\omega_r^2) + bk(r_0-1)(\omega_r\vartheta_r-\omega_i\vartheta_i) + 2bks_t(kr_0^2-2s_t)\omega_r\omega_i + k(k-1)}{ak^4 r_0^2}$$

$$- \frac{k^3 r_0^2(1+k) + k\omega_r[r_0(1+b)-s_t+k^2 s_t r_0(6r_0-r_1)] + k^2\vartheta_r[k^2 r_0^2(s_t+a\beta_1)-s_t(1+br_0)]}{ak^4 r_0^2}$$

$$- \frac{s_t k^3 r_0\vartheta_i(4+br_0) + s_t k^2\omega_i(r_1+8s_t)}{ak^4 r_0^2}$$

$$Y_p = -\frac{2bk^2 s_t r_0(1+2r_0)(\omega_i\vartheta_i-\omega_r\vartheta_r) + bks_t(kr_0^2+r_1-2s_t)(\omega_i^2-\omega_r^2) + bk(r_0-1)(\omega_r\vartheta_i+\omega_i\vartheta_r) - 2bs_t\omega_r\omega_i}{ak^4 r_0^2}$$

$$- \frac{k^2\vartheta_i[k^2 r_0^2(s_t+a\beta_1)-s_t(1+br_0)] - s_t k^3 r_0\vartheta_r(4+br_0) - s_t k^2\omega_r(r_1+8s_t) + k\omega_i[s_t(6k^2 r_0^2-1)+r_0(1+b)-k^2 r_0 s_t r_1]}{ak^4 r_0^2}$$

$$P_r = \frac{(AX_p + BY_p)}{\Delta}, \quad P_i = \frac{(AY_p - BX_p)}{\Delta}$$

$$X'_p = \frac{bs_t(\omega_i^2 - \omega_r^2) + bks_t(1+r_0)(\omega_i\vartheta_i - \omega_r\vartheta_r) - 2bks_t r_0(\omega_i\vartheta_r + \omega_r\vartheta_i) + 2s_t\omega_i\omega_r[kr_0^2(2-b) - kr_1 + 2br_0] - 2bs_t k^2 r_0^2\vartheta_i\vartheta_r}{k^3 r_0^2 a}$$

$$\frac{k\omega_r[r_0(b+s_t k^2 r_1) - s_t - k^2 r_0^2(4+r_0)] - k^2\vartheta_r(1+k^2 r_0^2) + s_t k\omega_i(r_1 - 2r_0)}{k^3 r_0^2 a}$$

$$Y'_p = \frac{s_t(\omega_r^2 - \omega_i^2)[kr_1 + r_0(kr_0 - 2) - 2kr_0^2] - bks_t(1+r_1)(\omega_r\vartheta_i + \omega_i\vartheta_r) + 2bks_t r_0(\omega_r\vartheta_r - \omega_i\vartheta_i) - 2bs_t\omega_i\omega_r}{k^3 r_0^2 a}$$

$$\frac{bs_t k^2 r_0^2(\vartheta_r^2 - \vartheta_i^2) + k\omega_i[k^2 r_0 s_t(r_1 - 4r_0) + r_0(b - k^2 r_0^2) - s_t] - k^2\vartheta_i(1+k^2 r_0^2) - 4s_t k^2 r_0^2\vartheta_r}{k^3 r_0^2 a}$$

$$P'_r = \frac{(A'X'_p + B'Y'_p)}{\Delta'}, \quad P'_i = \frac{(A'Y'_p - B'X'_p)}{\Delta'}$$

$$Q_{1r} = -\frac{(B-A)}{\Delta}\left[\frac{\beta_1(\vartheta_r + \vartheta_i)[2\omega_r\omega_i + (\omega_r^2 - \omega_i^2)][2ar_0(\omega_r^2 - \omega_i^2) + 5\theta_r r_1^2 s_t\vartheta_r]}{r_0^2 s_t(\vartheta_r^2 + \vartheta_i^2)}\right] + \frac{5\beta_1\theta_i(B+A)(\omega_r\omega_i)}{\Delta},$$

$$Q'_{1r} = -\frac{(B'-A')}{\Delta'}\left[\frac{\beta_1(\vartheta_r + \vartheta_i)[2\omega_r\omega_i + (\omega_r^2 - \omega_i^2)][2ar_0(\omega_r^2 - \omega_i^2) + 5\theta_r r_1^2 s_t\vartheta_r]}{r_0^2 s_t(\vartheta_r^2 + \vartheta_i^2)}\right] + \frac{5\beta_1\theta_i(B'+A')(\omega_r\omega_i)}{\Delta'},$$

$$Q_{1i} = -\frac{(B-A)}{\Delta}\left[\frac{\beta_1(\vartheta_r - \vartheta_i)[2\omega_r\omega_i - (\omega_r^2 - \omega_i^2)][2ar_0(\omega_r^2 - \omega_i^2) + 5\theta_r r_1^2 s_t\vartheta_r]}{r_0^2 s_t(\vartheta_r^2 + \vartheta_i^2)}\right] + \frac{10\beta_1\theta_i(B+A)(\omega_r^2 - \omega_i^2)}{\Delta},$$

$$Q'_{1i} = -\frac{(B'-A')}{\Delta'}\left[\frac{\beta_1(\vartheta_r - \vartheta_i)[2\omega_r\omega_i - (\omega_r^2 - \omega_i^2)][2ar_0(\omega_r^2 - \omega_i^2) + 5\theta_r r_1^2 s_t\vartheta_r]}{r_0^2 s_t(\vartheta_r^2 + \vartheta_i^2)}\right] + \frac{10\beta_1\theta_i(B'+A')(\omega_r^2 - \omega_i^2)}{\Delta},$$

$$Q_{2r} = \frac{-2\beta_1[(\omega_r^2 - \omega_i^2)A - 2\omega_r\omega_i B]}{\Delta}, \quad Q_{2i} = \frac{-2\beta_1[(\omega_r^2 - \omega_i^2)B - 2\omega_r\omega_i A]}{\Delta},$$

$$Q'_{2r} = \frac{-5[(\omega_r^2 - \omega_i^2)A' - 2\omega_r\omega_i B']}{\Delta'}, \quad Q'_{2i} = \frac{-5[(\omega_r^2 - \omega_i^2)B' - 2\omega_r\omega_i A']}{\Delta'}, .$$

$$(24)$$

7 Appendix (A-2-16): Coefficients of the second member of the equations (16).

$$R_r = -\frac{s_t r_1[bk^2 r_0\omega_r + b(1+2r_0)\omega_i + bkr_0(\vartheta_i + k^2\vartheta_r) + k^5 r_0^2]A + s_t r_1[b(1+2r_0)\omega_r - bk^2 r_0\omega_i + bkr_0(\vartheta_r - k^2\vartheta_i) + kr_0]B}{\Delta k^2 r_0^2 a},$$

$$R'_r = \frac{s_t r_1[bk^2 r_0\omega_r + 2b\omega_i + bkr_0(\vartheta_i + k^2\vartheta_r) + k^5 r_0^2]A' - s_t r_1[-2b\omega_r + bk^2 r_0\omega_i - bkr_0(\vartheta_r - k^2\vartheta_i) + kr_0]B'}{\Delta' k^2 r_0^2 a},$$

$$R_i = -\frac{s_t r_1 b[2b(1+2r_0)\omega_r - bk^2 r_0\omega_i + bkr_0(\vartheta_r - k^2\vartheta_i) + kr_0]A - s_t r_1[bk^2 r_0\omega_r + b(1+2r_0)\omega_i + bkr_0(\vartheta_i + k^2\vartheta_r) + k^5 r_0^2]B}{\Delta k^2 r_0^2 a},$$

$$R'_i = \frac{s_t r_1 b[-2b\omega_r + bk^2 r_0\omega_i - bkr_0(\vartheta_r - k^2\vartheta_i) + kr_0]A' + s_t r_1[bk^2 r_0\omega_r + 2b\omega_i + bkr_0(\vartheta_i + k^2\vartheta_r) + k^5 r_0^2]B'}{\Delta' k^2 r_0^2 a},$$

$$S_r = \frac{s_t r_1[(kr_0 - b)(\omega_i\vartheta_i - \omega_r\vartheta_r) + bkr_0(\vartheta_r^2 - \vartheta_i^2) + 3kr_0(\omega_i + k\vartheta_i) + 2(\omega_r + k\vartheta_r)]A}{\Delta k^3 r_0^2 a}$$
$$+ \frac{s_t r_1[(b - kr_0)(\omega_i\vartheta_r + \omega_r\vartheta_i) + 2bkr_0\vartheta_r\vartheta_i - 3kr_0(\omega_r + k\vartheta_r) + 2(\omega_i + k\vartheta_i)]B}{\Delta k^3 r_0^2 a},$$

$$S'_r = -\frac{s_t r_1[(kr_0 - b)(\omega_i\vartheta_i - \omega_r\vartheta_r) + bkr_0(\vartheta_r^2 - \vartheta_i^2) + kr_0(\omega_i + 3k\vartheta_i) + 2k\vartheta_r]A'}{\Delta' k^3 r_0^2 a}$$
$$+ \frac{s_t r_1[(b - kr_0)(\omega_i\vartheta_r + \omega_r\vartheta_i) + 2bkr_0\vartheta_r\vartheta_i - kr_0(\omega_r + 3k\vartheta_r) + 2k\vartheta_i]B'}{\Delta' k^3 r_0^2 a},$$

$$S_i = \frac{s_t r_1[(b - kr_0)(\omega_i\vartheta_r + \omega_r\vartheta_i) + 2bkr_0\vartheta_r\vartheta_i - 3kr_0(\omega_r + k\vartheta_r) + 2(\omega_i + k\vartheta_i)]A}{\Delta k^3 r_0^2 a},$$

$$+ \frac{s_t r_1[(kr_0 - b)(\omega_i \vartheta_i - \omega_r \vartheta_r) + bkr_0(\vartheta_r^2 - \vartheta_i^2) + 3kr_0(\omega_i + k\vartheta_i) + 2(\omega_r + k\vartheta_r)]B}{\Delta k^3 r_0^2 a}$$

$$S_i' = \frac{s_t r_1[(b - kr_0)(\omega_i \vartheta_r + \omega_r \vartheta_i) + 2bkr_0 \vartheta_r \vartheta_i - kr_0(\omega_r + 3k\vartheta_r) + 2k\vartheta_i]A'}{\Delta' k^3 r_0^2 a}$$

$$- \frac{s_t r_1[(kr_0 - b)(\omega_i \vartheta_i - \omega_r \vartheta_r) + bkr_0(\vartheta_r^2 - \vartheta_i^2) + kr_0(\omega_i + 3k\vartheta_i) + 2k\vartheta_r]B'}{\Delta' k^3 r_0^2 a},$$

$$T_r = - \frac{s_t r_1[2kr_0(\omega_r \vartheta_i - \omega_i \vartheta_r) + s_t(\omega_r \vartheta_r - \omega_i \vartheta_i) + ks_t(\vartheta_r^2 - \vartheta_i^2) + 2k^2 r_0 \vartheta_r \vartheta_i]A}{\Delta k^3 r_0^2 a}$$

$$+ \frac{s_t r_1[2kr_0(\omega_r \vartheta_r - \omega_i \vartheta_i) - s_t(\omega_r \vartheta_i + \omega_i \vartheta_r) + k^2 r_0^2(\vartheta_r^2 - \vartheta_i^2) - 2ks_t \vartheta_r \vartheta_i]B}{\Delta k^3 r_0^2 a},$$

$$T_r' = \frac{s_t r_1[kr_0(\omega_r \vartheta_i + \omega_i \vartheta_r) + kr_0(\omega_i \vartheta_i - \omega_r \vartheta_r) + 2k^2 r_0^2 \vartheta_r \vartheta_i - \omega_r + ks_t \vartheta_r]A'}{\Delta' k^3 r_0^2 a}$$

$$+ \frac{s_t r_1[kr_0(\omega_r \vartheta_i + \omega_i \vartheta_r) - kr_0(\omega_i \vartheta_i - \omega_r \vartheta_r) + k^2 r_0^2(\vartheta_r^2 - \vartheta_i^2) + \omega_i - ks_t \vartheta_i]B'}{\Delta' k^3 r_0^2 a},$$

$$T_i = \frac{s_t r_1[2kr_0(\omega_r \vartheta_r - \omega_i \vartheta_i) - s_t(\omega_r \vartheta_i + \omega_i \vartheta_r) + k^2 r_0^2(\vartheta_r^2 - \vartheta_i^2) - 2ks_t \vartheta_r \vartheta_i]A}{\Delta k^3 r_0^2 a}$$

$$- \frac{s_t r_1[2kr_0(\omega_r \vartheta_i - \omega_i \vartheta_r) + s_t(\omega_r \vartheta_r - \omega_i \vartheta_i) + ks_t(\vartheta_r^2 - \vartheta_i^2) + 2k^2 r_0 \vartheta_r \vartheta_i]B}{\Delta k^3 r_0^2 a},$$

$$T_i' = - \frac{s_t r_1[kr_0(\omega_r \vartheta_i + \omega_i \vartheta_r) - kr_0(\omega_i \vartheta_i - \omega_r \vartheta_r) + k^2 r_0^2(\vartheta_r^2 - \vartheta_i^2) + \omega_i - ks_t \vartheta_i]A'}{\Delta' k^3 r_0^2 a}$$

$$- \frac{s_t r_1[kr_0(\omega_r \vartheta_i + \omega_i \vartheta_r) + kr_0(\omega_i \vartheta_i - \omega_r \vartheta_r) + 2k^2 r_0^2 \vartheta_r \vartheta_i - \omega_r + ks_t \vartheta_r]B'}{\Delta' k^3 r_0^2 a},$$

$$M_r = \frac{-bs_t r_1^2[(\vartheta_r^2 - \vartheta_i^2)A - 2\vartheta_r \vartheta_i B]}{\Delta k^2 r_0^2 a}, \quad M_i = \frac{-bs_t r_1^2[(\vartheta_r^2 - \vartheta_i^2)B - 2\vartheta_r \vartheta_i A]}{\Delta k^2 r_0^2 a},$$

$$M_r' = \frac{-bs_t r_1^2[(\vartheta_r^2 - \vartheta_i^2)A' - 2\vartheta_r \vartheta_i B']}{\Delta' k^2 r_0^2 a}, \quad M_i' = \frac{-bs_t r_1^2[(\vartheta_r^2 - \vartheta_i^2)B' - 2\vartheta_r \vartheta_i A']}{\Delta' k^2 r_0^2 a}. \tag{25}$$

References

1. C. Julien, Cardiovasc. Res. **70**, 12 (2006)
2. R. Fatouleh, V.G. Macefield, Exp. Physiol. **98**, 1327 (2013)
3. C. Finucane, G. Boyle, C.W. Fan, D. Hade, L. Byrne, R.A. Kenny, Eurospace **12**, 247 (2010)
4. G. Cakmak, F.A. Alkan, K. Korkmaz, Z.A. Saglam, D. Karis, M. Yenigun, M. Ercan, Transl. Resp. Med. **1**, 3 (2013)
5. K. Wolfgang, S. Malte, F. Birgit, D. Angela, L. Hannelore, E. Edzard, Arterioscler. Thomb. Vasc. Biol. **18**, 768 (1998)
6. L. Dintenfass, Angiology **25**, 365 (1974)
7. R.L. Letcher, S. Chien, T.G. Pickering, J.H. Laragh, Hypertension **5**, 757 (1983)
8. G.D. Lowe, Clin. Sci. **71**, 137 (1986)
9. S. Yomosa, J. Phys. Soc. Jpn. **56**, 506 (1987)
10. Y. Hashimuze, J. Phys. Soc. Jpn. **54**, 3305 (1985)
11. H. Demiray, Eur. J. Mech. **24**, 337 (2005)
12. H. Demiray, Chaos Solit. Fract. **42**, 358 (2009)
13. J.C. Misra, M.K. Patra, Comput. Math. Appl. **54**, 242 (2007)
14. J.F. Paquerot, M. Remoissenet, Phys. Lett. A **194**, 77 (1994)
15. W.-S. Duan, B.-R. Wang, R.-J. Wein, Phys. Lett. A **225**, 154 (1997)
16. G.A. Truskey, F. Yuan, D.F. Katz, *Transport Phenomena in Biological Systems* (Pearson Education Inc., New Jersey, 2004)
17. J. Hron, J. Malek, S. Turek, Int. J. Numer. Methods Fluids **32**, 863 (2000)
18. S.N. Majhi, V.R. Nair, Int. J. Eng. Sci. **32**, 839 (1994)
19. J. Prakash, A. Ogulu, Int. Commun. Heat Mass Transfer **34**, 762 (2007)
20. N.S. Akbar, S.U. Rahman, R. Ellahi, S. Nadeem, Eur. Phys. J. Plus **129**, 1 (2014)
21. R. Ellahi, S.U. Rahman, S. Nadeem, Phys. Lett. A **378**, 2973 (2014)
22. L. Formaggia, D. Lamponi, A. Quartenori, J. Eng. Math. **47**, 251 (2003)
23. R.A. Ramachandra, Acte Mech. **46**, 155 (1983)

24. B.K. Sharma, C. Kumawat, O.D. Makinde, Biomech. Model. Mechanobiol. **21**, 797 (2022)
25. P.K. Mandal, Int. J. Nonl. Mech. **40**, 151 (2005)
26. K. Vajravelu, S. Sreenadh, P. Lakshminarayana, Comm. Nonlin. Sci. Numer. Simul. **16**, 3107 (2011)
27. N.S. Akbar, S. Nadeem, Commun. Theor. Phys. **57**, 133 (2012)
28. Narayana, C.H.B., Sreenadh, S. Devaki, P, Adv. Appl. Sci. Res. **3**, (2012) 671
29. I.S. Aranson, L. Kramer, Rev. Mod. Phys. **74**, 99 (2002)
30. A. Hasegawa, *Plasma Instabilities and Nonlinear Effects* (Springer-Verlag, Berlin, 1975)
31. R. Conte, M. Musette, Pure Appl. Opt. **4**, 315 (1995)
32. A. Mohamadou, B.E. Ayissi, T.C. Kofané, Phys. Rev. E **74**, 046604 (2006)
33. P.K. Jakobsen, J.V. Maloney, A.C. Newell, R. Indik, Phys. Rev. A **45**, 8128 (1992)
34. G.K. Harkness, W.J. Firth, J.B. Geddes, J.V. Maloney, E.M. Wright, Phys. Rev. A **50**, 4310 (1994)
35. R. Graham, Fluctuations, instabilities, and phase transition, Ed. T. Riste (Berlin: Springer; 1975)
36. D. Yemele, T.C. Kofane, J. Phys. D **39**, 4504 (2006)
37. E. Kengne, K.K. Cletus, Int. J. Mod. Phys. B **19**, 3961 (2005)
38. F II. Ndzana, A. Mohamadou, T. C. Kofané and L. Q. English, Phys. Rev. E **78** (2008) 016606
39. O. Hirayama, K. Ohtsuka, S. Ishiwata, S. Watanabe, Physica D **185**, 97 (2003)
40. T.B. Benjamin, J.E. Feir, J. Fluid Mech. **27**, 417 (1967)
41. C.B. Tabi, A. Mohamadou, T.C. Kofané, Chin. Phys. Lett. **26**, 068703 (2009)
42. C.G.L. Tiofack, A. Mohamadou, T.C. Kofané, Opt. Commun. **283**, 1096 (2010)
43. J.C. Mimshe, C.B. Tabi, H. Edongue, H.P. Ekobena, A. Mohamadou, T.C. Kofanê, Phys. Scr. **87**, 025801 (2013)
44. C.B. Tabi, A.K. Dang, R.O. Doko, H.P.F. Ekobena, T.C. Kofané, Phys. A **442**, 498 (2016)
45. G.R.Y. Mefire, C.B. Tabi, A. Mohamadou, H.P.F. Ekobena, T.C. Kofane, Chaos **23**, 033128 (2013)
46. T. Taniuti, H. Washimi, Phys. Rev. Lett. **21**, 209 (1968)
47. A. Hasegawa, Phys. Rev. Lett. **24**, 1165 (1970)
48. C.D. Bansi Kamdem, C.B. Tabi, A. Mohamadou, Chaos Solit. Fract. **109**, 170 (2018)
49. S. Mayer, Sitzungsber. Akad. Wiss. Wien, Math.-Naturwiss. B3 **74**, 302 (1876)
50. F. I.I. Ndzana, A. Mohamadou, T.C. Kofané, Chaos **18**, 043121 (2008)
51. E. Kengne, R. Vaillancourt, Nonl. Oscil. **9**, 438 (2006)
52. K. Kotani, A. Inata, S. Araga, Arch. Med. Res. **38**, 463 (2007)
53. K. Yufu, N. Takahashi, N. Okada, T. Shinohara, M. Hara, T. Saikawa et al., Circ. J. **73**, 174 (2009)
54. K. Hasegawa, S. Terashima, N. Satoh, M. Inoue, H. Wada, C. Itoh et al., Smoking Cont. Sci. **2**, 23 (2008)